Experimental Investigation of Void Fraction During Horizontal Flow in Larger Diameter Refrigeration Applications

M. J. Wilson, T. A. Newell, and J. C. Chato

ACRC TR-140 July 1998

For additional information:

Air Conditioning and Refrigeration Center
University of Illinois
Mechanical & Industrial Engineering Dept.
1206 West Green Street
1206 West Green Street
Urbana, IL 61801

(217) 333-3115

Prepared as part of ACRC Project 74
Experimental Investigation of Void Fraction
During Refrigerant Condensation and Evaporation
T. A. Newell and J. C. Chato, Principal Investigators

The Air Conditioning and Refrigeration Center was founded in 1988 with a grant from the estate of Richard W. Kritzer, the founder of Peerless of America Inc. A State of Illinois Technology Challenge Grant helped build the laboratory facilities. The ACRC receives continuing support from the Richard W. Kritzer Endowment and the National Science Foundation. The following organizations have also become sponsors of the Center.

Amana Refrigeration, Inc.
Brazeway, Inc.
Carrier Corporation
Caterpillar, Inc.
Copeland Corporation
Dayton Thermal Products
Delphi Harrison Thermal Systems
Eaton Corporation
Ford Motor Company
Frigidaire Company
General Electric Company
Hill PHOENIX
Hydro Aluminum Adrian, Inc.
Indiana Tube Corporation
Lennox International, Inc.
Modine Manufacturing Co.
Peerless of America, Inc.
The Trane Company
Whirlpool Corporation
York International, Inc.

For additional information:

Air Conditioning & Refrigeration Center
Mechanical & Industrial Engineering Dept.
University of Illinois
1206 West Green Street
Urbana IL 61801

217 333 3115

Abstract

EXPERIMENTAL INVESTIGATION OF VOID FRACTION DURING HORIZONTAL FLOW IN LARGER DIAMETER REFRIGERATION APPLICATIONS

Michael Jay Wilson
Department of Mechanical and Industrial Engineering
University of Illinois at Urbana-Champaign, 1998
Ty Newell and John C. Chato, Advisors

Void fractions were measured for R134a and R410A for a smooth tube with inside diameter of 6.12 mm (0.241"), an axially grooved tube of base diameter 8.89 mm (0.350"), and a 18° helically grooved of base diameter 8.93 mm (0.352"). The experiment covered mass fluxes from 75 kg/m^{2}s to 700 kg/m^{2}s (55 - 515 klb$_m$/ft^2-hr) and average test section qualities from 5% to 99% with an inlet temperature of 5°C (41°F). Several existing models are examined for accuracy and a simple adjusted model is presented to accurately predict the data and data presented in a companion study by Yashar[1998]. The experimental apparatus and methodology are also discussed.

Table of Contents

List of Tables

List of Figures

Nomenclature

D_i	Inner Diameter (for grooved tubes D_i = base diameter)		
F_1	Premoli correlation variable 1		Equation 2.19
F_2	Premoli correlation variable 2		Equation 2.20
Fr	Froude number	$=\frac{1}{g_c D_i}\left(\frac{Gx}{\beta\rho_g}\right)^2$	Equation 2.26
Ft	Froude rate		Equation 2.31
F_{TD}	Taitel-Dukler Froude number		
$F(X_{tt})$	Tandon's Lockhart-Martinelli function		Equation 2.18
G	Mass Flux		
g_c	Gravity		
K	Smith's entrainment ratio		Equation 2.9
K_H	Hughmark correction factor		Table 3.3
m	Mass		
$m_?$	Specific mass reading in Chapter 4		
P	Pressure		
$P.I._1$	Property Index 1		Equation 2.6
$P.I._2$	Property Index 2		Equation 2.7
Re_α	Hughmark's Reynolds number		Equation 2.25
Re_L	Liquid Reynolds number	$=\frac{GD_i}{\mu_L}$	Equation 2.17
S	Slip ratio		Equation 2.2
T	Temperature		
v	Specific volume		
$\forall_{ts}$	Test section volume		
We_L	Liquid Weber number	$=\frac{G^2 D_i}{\sigma\rho_l g_c}$	Equation 2.22
x	Quality		

x_s	Static quality		Equation 4.9
X_{tt}	Lockhart-Martinelli parameter		Equation 2.11
y	Premoli's volumetric quality ratio		Equation 2.21
y_L	Hughmark liquid volume fraction		Equation 2.27
Z	Hughmark flow parameter		Equation 2.24
α	Void Fraction		
β	Volumetric quality	$= \frac{1}{1+\left(\frac{1-x}{x}\right)\left(\frac{\rho_g}{\rho_l}\right)}$	Equation 2.23
Δm	Change in mass		Equation 4.1
γ	Thom's slip factor		Equation 2.8
μ	Viscosity		
μ_l	Viscosity of saturated liquid		
μ_g	Viscosity of saturated vapor (gas)		
ρ	Density		
ρ_l	Density of saturated liquid		
ρ_g	Density of saturated vapor (gas)		
σ	Surface tension		

Chapter 1

Introduction

Since the second world war, two-phase flow has been studied by several researchers. This research has found void fraction to be an integral to part to models of pressure-drop, heat transfer, and overall system simulation. Most void fraction correlations were built upon air-water or steam-water data in smooth tubes. Little is known about how well these correlations work for refrigerants or in micro-finned tubes. This study will discuss refrigerant void fraction in smooth and micro-finned tubes.

This paper was created to present and correlate experimental void fraction data. Chapter 2 first presents background information on void fraction. Several existing models are discussed. Chapter 3 discloses the experimental setup and the measuring techniques used. In Chapter 4 the experimental methodology is discussed. Void fraction data for smooth, axially grooved, and helically grooved tubes is presented in Chapters 5,6 and 7, respectively. These chapters also discuss the accuracy of the correlations discussed in Chapter 2. Chapter 8 concludes all of the work and suggests a void fraction model which correlates the data.

Chapter 2

Literature Review

Over the last half-century many researchers have studied void fraction and derived models to predict void fraction. The study of void fraction is important for many applications such as pressure drop correlations, heat transfer predictions, and overall system simulation. Many of these models were reviewed by Rice [1987] who separated the models into four categories: homogenous, slip-ratio, Lockhart-Martinelli, and mass flux dependent. The purpose of this literature review is to explain the history, intended use, and accuracy of each model.

2.1- Homogenous

The homogenous relation considers the liquid and gaseous phases to be traveling as a homogenous mixture. The relation can be derived by simplification of fundamental thermodynamic property relations and relates the void fraction to average quality by

$$\alpha = \frac{1}{1+\left(\frac{1-x}{x}\right)\left(\frac{\rho_g}{\rho_l}\right)} \tag{2.1}$$

2.2- Slip Ratio

Five correlations are of the form

$$\alpha = \frac{1}{1+\left(\frac{1-x}{x}\right)\left(\frac{\rho_g}{\rho_l}\right)\bullet S} \tag{2.2}$$

where S is the slip ratio. In a physical sense the slip ratio is the ratio of vapor velocity to liquid velocity. The homogenous correlation is a special case where the slip ratio is unity.

2.2.1- Rigot Correlation

Rigot [1973] correlation is one of the simplest correlations in which he suggests a constant slip ratio of

$$S=2 \tag{2.3}$$

2.2.2- Zivi Correlation

Zivi [1964] derived a model based on the assumption that in a steady state thermodynamic process the rate of entropy production is minimized. Zivi assumed that the flow was steady and annular, wall friction was negligible, and he did not account for liquid entrainment. Using these assumptions, Zivi derived the slip ratio S to be

$$S=\left(\frac{\rho_l}{\rho_g}\right)^{\frac{1}{3}} \tag{2.4}$$

and thus void fraction can be calculated by

$$\alpha=\frac{1}{1+\left(\frac{1-x}{x}\right)\left(\frac{\rho_g}{\rho_l}\right)^{\frac{2}{3}}} \tag{2.5}$$

Using the data from Martinelli and Nelson [1948], Larson [1957], and Maurer [1960] to evaluate his model, Zivi concluded that his model provided the lower bound while the homogenous model provided the upper bound. Zivi also noted that these two

models approach each other as pressure is increased. Zivi proposed that liquid entrainment was needed to interpolate between the two models. He suggested that further experiments and theoretical modeling be done to explore liquid entrainment.

2.2.3- Smith Correlation

Smith [1969] derived a model based on equal velocity heads. Smith's assumptions were that the flow is annular with a liquid phase and a homogenous mixture phase, the homogenous and liquid phase have the same velocity heads ($\rho_l V_l^2=\rho_m V_m^2$), the homogenous mixture behaves as a single fluid with variable density, and that thermal equilibrium exists.

Smith then established the variable K defined as the mass ratio of water flowing in a homogenous mixture to the total mass of water flowing. This ratio simply describes the amount of water entrained in the homogenous mixture. From these assumptions the slip ratio was found to be

$$S = K + (1-K)\left[\frac{\frac{1}{\frac{\rho_g}{\rho_l}} + K\left(\frac{1-x}{x}\right)}{1+K\left(\frac{1-x}{x}\right)}\right]^{\frac{1}{2}} \tag{2.9}$$

Smith found that an entrainment ratio of 40% (K=.4) correlated the data quite well. He compared his correlation to steam-water and air-water data and found his correlation to be accurate within 10%.

2.2.4- Ahrens-Thom

Before discussing the Ahrens-Thom correlation it is useful to define property index 1 ($P.I_1$) and property index 2 ($P.I._2$). The property indexes were given in Rice's [1987] analysis and are used in other correlations.

$$P.I._1 = \frac{\rho_g}{\rho_l} \tag{2.6}$$

$$P.I._2 = \left(\frac{\mu_l}{\mu_g}\right)^{0.2} \bullet \frac{\rho_g}{\rho_l} = \left(\frac{\mu_l}{\mu_g}\right)^{0.2} \bullet P.I._1 \tag{2.7}$$

Ahrens [1983] suggested the steam/water data presented by Thom [1964] generalized by $P.I._2$ to be a suitable void fraction model. Thom proposed a void fraction model of the form

$$\alpha = \frac{\gamma \bullet x}{1 + x \bullet (\gamma - 1)} \tag{2.8}$$

in which the slip factor γ is a constant at any given pressure. Ahrens redefined the independent variable as $P.I._2$ instead of pressure. Rice presents the Ahrens-Thom correlation in Table 2.1.

Table 2.1 Ahrens-Thom Correlation

$P.I._2$	S
0.00116	6.45
0.0154	2.48
0.0375	1.92
0.0878	1.57
0.187	1.35
0.466	1.15
1.0	1

2.2.5- Levy Correlation

Levy's [1960] correlation was derived from a momentum exchange model which assumes equal friction and head losses between the fluid and gaseous phases.

$$x = \frac{\alpha(1-2\alpha) + \alpha\sqrt{(1-2\alpha)^2 + \alpha\left[2\left(\frac{\rho_l}{\rho_g}\right)(1-\alpha)^2 + \alpha(1-2\alpha)\right]}}{2\left(\frac{\rho_l}{\rho_g}\right)(1-\alpha)^2 + \alpha(1-2\alpha)} \tag{2.10}$$

Levy found his correlation to hold well at high pressures and high steam qualities, but otherwise his correlation under-predicted the void fraction by at least 20%. Levy concluded that his correlation formed the lower bound. Since Levy's correlation shows such deviation it will not be used to compare against our experimental data, but this discussion was added for completion purposes.

2.3- Lockhart-Martinelli

This set of correlations employ the Lockhart-Martinelli parameter [1949] for two phase flow. The Lockhart-Martinelli parameter (X_{tt}) is defined as

$$X_{tt} = \left(\frac{1-x}{x}\right)^{0.9}\left(\frac{\rho_g}{\rho_l}\right)^{0.5}\left(\frac{\mu_l}{\mu_g}\right)^{0.1} \tag{2.11}$$

This parameter was formed using experimental data for air with various liquids including benzene, kerosene, water, and various oils.

2.3.1- Baroczy Correlation

Baroczy [1965] developed a correlation based on X_{tt} and $P.I._2$. Baroczy's correlation was based on liquid-mercury nitrogen and air-water data. Baroczy made his correlation in tabular form for calculating the liquid fraction. To find the void fraction, subtract the liquid fraction from 1.

Table 2.2 Baroczy Correlation

	X_{tt}										
P.I.2	0.01	0.04	0.1	0.2	0.5	1	3	5	10	30	100
	Liquid Fraction (1-α)										
0.00002				0.0012	0.009	0.068	0.17	0.22	0.30	0.47	0.71
0.0001			0.0015	0.0054	0.030	0.104	0.23	0.29	0.38	0.57	0.79
0.0004		0.0022	0.0072	0.180	0.066	0.142	0.28	0.35	0.45	0.67	0.85
0.001	0.0018	0.0066	0.0170	0.0345	0.091	0.170	0.32	0.40	0.50	0.72	0.88
0.004	0.0043	0.0165	0.0370	0.0650	0.134	0.222	0.39	0.48	0.58	0.80	0.92
0.01	0.0050	0.0210	0.0475	0.0840	0.165	0.262	0.44	0.53	0.63	0.84	0.94
0.04	0.0056	0.0250	0.0590	0.1050	0.215	0.330	0.53	0.63	0.72	0.90	0.96
0.1	0.0058	0.0268	0.0640	0.1170	0.242	0.380	0.60	0.70	0.78	0.92	0.98
1	0.0060	0.0280	0.0720	0.1400	0.320	.500	0.75	0.85	0.90	0.94	0.99

Baroczy noted that his correlation gave good correspondence to experimental data for steam and Santowax R, a coolant.

2.3.2- Wallis Correlation

Lockhart-Martinelli's pressure drop work also presented void fraction data. This data was later correlated by Wallis [1969] as a function of X_{tt}

$$\alpha = \left(1 + X_{tt}^{0.8}\right)^{-0.378} \tag{2.12}$$

Wallis states that the Lockhart-Martinelli parameter balances frictional shear stress with pressure drop, thus increasing error as the frictional portion of the pressure drop decreases with respect to other terms.

Domanski [1983] adjusted the Wallis correlation. Domanski stated that the Wallis correlation was to be followed for X_{tt} less than 10, and a new correlation be used for X_{tt} greater than 10.

$$\alpha = \left(1 + X_{tt}^{0.8}\right)^{-0.378} \qquad X_{tt}<10$$

$$\alpha = .823 - .157 \bullet \ln\left(X_{tt}\right) \qquad 10<X_{tt}<189 \tag{2.13}$$

2.4- Mass Flux Dependent

This set of correlations predict void fraction as a function of mass flux as well as properties of the fluid and the pipe.

2.4.1 Tandon Correlation

Tandon [1985] assumes the flow to be steady, one dimensional, and annular with an axisymmetric liquid annulus and a vapor core with no liquid entrainment. Both the liquid and vapor flows are assumed to be turbulent and follow the von Karman velocity profile. Using established correlations for film thickness, shear stress and pressure drop, Tandon was able to derive an expression for void fraction based on the Lockhart-Martinelli parameter and the Reynolds number.

$$\alpha = 1 - 1.928\frac{Re_L^{-0.315}}{F(X_{tt})} + 0.9293\frac{Re_L^{-0.63}}{F(X_{tt})^2} \qquad \text{for } 50<Re_L<1125 \tag{2.14}$$

$$\alpha = 1 - 0.38\frac{Re_L^{-0.088}}{F(X_{tt})} + 0.0361\frac{Re_L^{-0.176}}{F(X_{tt})^2} \qquad \text{for } Re_L>1125 \tag{2.15}$$

where

$$F(X_{tt}) = .015 \bullet \left(\frac{1}{X_{tt}} + \frac{2.85}{X_{tt}^{0.476}} \right) \tag{2.16}$$

$$Re_L = \frac{GD_i}{\mu_l} \qquad \text{Liquid Reynolds Number} \tag{2.17}$$

Tandon's correlation does include mass flux effects but only slightly. Tandon found his correlation to be valid within 10% at pressures below 2100 kPa, but only satisfactory performance at higher pressures. Tandon concluded that his model was more accurate than Zivi's and Wallis's, but that Smith's correlation was just as good.

2.4.2- Premoli Correlation

Premoli [1971] developed a correlation to predict void fraction for two-phase mixtures flowing upward in adiabatic channels. The correlation was empirically formed by doing a large number of experiments and varying mixture velocities, fluid properties, and channel geometries. Premoli developed the correlation by comparing slip-ratios and governing parameters, then optimized the correlation by minimizing density calculation errors. The correlation follows the slip ratio form of Equation 2.2 and is defined as follows

$$S = 1 + F_1 \left(\frac{y}{1 + F_2 y} - F_2 y \right)^{\frac{1}{2}} \tag{2.18}$$

$$F_1 = 1.578 \bullet Re_L^{-0.19} \left(\frac{\rho_l}{\rho_g} \right)^{0.22} \tag{2.19}$$

$$F_2 = 0.0273 \bullet We_L \, Re_L^{-0.51} \left(\frac{\rho_l}{\rho_g} \right)^{-0.08} \tag{2.20}$$

$$y = \frac{\beta}{1 - \beta} \tag{2.21}$$

$$We_L = \frac{G^2 D_i}{\sigma \rho_l g_c} \qquad \text{Liquid Weber Number} \tag{2.22}$$

$$\beta = \frac{1}{1 + \left(\frac{1-x}{x}\right)\left(\frac{\rho_g}{\rho_l}\right)} \tag{2.23}$$

Where g_c is gravity (9.81 m/s^2) and σ is the surface tension. Premoli found his correlation to hold within 5% of experimental results.

2.4.3- Hughmark Correlation

Hughmark [1962] developed a correlation for void fraction that was an expansion on the earlier work of Bankoff [1960]. Bankoff suggested a model in which the mixture flows as a suspension of bubbles in the liquid. The concentration of bubbles is highest in the center and decreases in the radial direction. Bankoff's correlation holds well for a steam-water system, but is flawed for an air-liquid system.

Bankoff's work influenced Hughmark to assume void fraction was dependent on the Reynolds, Froude, and Weber numbers (Hughmark later found the Weber number to be insignificant). Hughmark's correlation is as follows:

$$Z = \frac{Re_\alpha^{\frac{1}{6}} Fr^{\frac{1}{8}}}{y_L^{\frac{1}{4}}} \tag{2.24}$$

$$Re_\alpha = \frac{D_i G}{\mu_l + \alpha(\mu_g - \mu_l)} \tag{2.25}$$

$$Fr = \frac{1}{g_c D_i}\left(\frac{Gx}{\beta \rho_g}\right)^2 \tag{2.26}$$

$$y_L = \frac{1}{1 + \left(\frac{x}{1-x}\right)\frac{\rho_l}{\rho_g}} = 1 - \beta \tag{2.27}$$

Table 2.3 Hughmark flow parameter K_H as a function of Z

Z	K_H
1.3	0.185
1.5	0.225
2.0	0.325
3.0	0.49
4.0	0.605
5.0	0.675
6.0	0.72
8.0	0.767
10	0.78
15	0.808
20	0.83
40	0.88
70	0.93
130	0.98

$$\alpha = \frac{K_H}{1+\left(\frac{1-x}{x}\right)\left(\frac{\rho_g}{\rho_l}\right)} \tag{2.28}$$

The difficulty in using the Hughmark correlation is that it is iterative. First the void fraction must be guessed. Then all of the parameters (Re_α, Fr, y_L) can be calculated. Next Z is calculated, K_H is looked up, the new void fraction is calculated, and then the void fraction guess can be checked. This procedure is repeated until the guessed void fraction matches the calculated void fraction.

2.4.4- Graham's Condenser Correlation

Graham [1998] provides a correlation based on work done with R134a and R410A in a condensing apparatus. Graham tested the mentioned refrigerants in a horizontal smooth tube while varying the inlet quality and mass flux. Graham found that his data

correlated with a Froude Rate parameter derived by Hulbert and Newell [1997]. Graham's correlation is a follows:

$$\alpha = 1 - \exp\left[-1 - 0.3 \bullet \ln(Ft) - 0.0328 \bullet (\ln(Ft))^2)\right] \quad Ft>0.01032 \tag{2.29}$$

$$\alpha = 0 \quad Ft<0.01032 \tag{2.30}$$

$$Ft = \left[\frac{x^3 G^2}{\rho_g{}^2 g_c D_i (1-x)}\right]^{\frac{1}{2}} \tag{2.31}$$

Graham stated that his correlation predicted the experimental data within 10%.

Chapter 3

Experimental Facilities and Measurement Techniques

The purpose of this chapter is to describe the apparatus, test sections, data acquisition system, and methodology used to experimentally determine the void fraction. The experimental apparatus is located in the Mechanical Engineering Laboratory at the University of Illinois. It was designed and built by Wattelet in 1989 to determine two-phase heat transfer coefficients for alternative refrigerants. Modifications made were to measure void fraction. A detailed description of the apparatus is recorded in Panic[1991], Christoffersen[1993], Wattelet[1994], and De Guzman [1997], therefore only a brief overview will be given here.

3.1- Experimental Test Facility

The experimental facility consists of a refrigerant loop, a commercial chiller system, and a test section. In the following sections each part of the test facility will be described.

3.1.1- Refrigerant Loop

The purpose of the refrigerant loop is to provide pure, uncontaminated refrigerant to the test section at the desired test section inlet conditions. The conditions controlled are the inlet temperature, mass flux, inlet quality and the test section heat flux.

A schematic of the refrigerant loop appears in Figure 3.1. Subcooled liquid is drawn from the condenser into a variable speed gear pump which forces the refrigerant flow. The mass flow rate can be set by adjusting the speed of the pump. A system of bypass lines near the pump controls the mass flow rate. A pump is used instead of a compressor to eliminate the possibility of oil entering the flow. The refrigerants flow through a Coriolis-type mass flow meter manufactured by Micro-Motion®.

Next the refrigerant flows through a pre-heater which conditions the flow to the desired inlet quality. Physically, the pre-heater is three 1.8 meter passes of 3/8" outer diameter copper tube in a serpentine shape. The outside of the tube is wrapped with twelve electrical heating strips of various resistances. Ten of the strips are controlled by four switches and deliver a constant amount of power to the pre-heater. The other two strips are controlled by a 115 Volt variac which offers control of the power delivered to those two strips.

The refrigerant then flows into the test section and then into the condenser. When the test section is closed for void fraction measurements a bypass loop allows the refrigerant to continue circulating.

3.1.2- Chiller

The refrigerant is condensed after exiting the test section. The refrigerant condensation is achieved by use of two counter-flow heat exchangers in which one loop uses a 50/50 mix of ethylene glycol and the other R502 as coolants. A schematic of the chiller system appears in Figure 3.2.

The first loop requires approximately 50 lbm. (23 kg) of ethylene glycol. The ethylene glycol is held in a storage tank where the temperature could be monitored. From a chiller control board, a "set point temperature" can be set, and two pumps in the antifreeze loop are cycled on and off to maintain the tank temperature within 2°F (1°C) of the set point temperature.

The second chiller loop, using R502 as the coolant, extracts heat from the ethylene glycol loop. This loop is a standard refrigeration loop, but with two expansion valves. The high temperature expansion valve is for high tank temperatures (above 0°F), and the low temperature expansion valve is for low tank temperatures (below 0°F).

Controlling the capacity of the chiller system allows steady-state conditions to be maintained in the refrigerant loop. A "false-load heater" is used to control the chiller capacity. The "false-load heater" is an electrical heating system that can deliver power to the ethylene glycol loop.

These steps must be followed to reach steady-state conditions in the refrigerant loop. First, the chiller system is turned on and a low set point temperature for the ethylene glycol tank is entered into the chiller control board. When the tank temperature approaches the set point temperature the false load heater is turned on to counteract the cooling provided by the ethylene glycol loop. From trial and error the refrigerant loop can be adjusted to reach steady-state at the desired inlet conditions.

3.1.3- Test Section

The test sections used in this study are single pass cylindrical tubes. Each test section has either a different diameter or different inside geometry. The dimensions are 6.12 mm and 4.26 mm inner diameter smooth tubes, 8.93 mm and 7.25 mm base diameter tubes with axial grooves, and 8.93 mm and 7.25 mm base diameter tubes with helical grooves and a 18° helix angle. A diagram of the inside geometries for the 60 fin tubes appears in Figure 3.3 which is taken from Ponchner [1993]. A table of the dimensions for each tube appears in Table 3.1.

Table 3.1 Dimensions of grooved tubes

Base Dia.	Helix Angle	# of Fins	Outside Dia.	Cross Sec Area	Perimeter
7.25 mm	0°	50	7.94 mm	40.20 mm^2	36.44 mm
8.89 mm	0°	60	9.53 mm	60.90 mm^2	45.26 mm
7.25 mm	18°	50	7.94 mm	39.39 mm^2	35.12 mm
8.93 mm	18°	60	9.53 mm	60.64 mm^2	46.85 mm

A schematic of the test section showing all relevant dimensions and fittings appears in Figure 3.4. At the end of each test section, two ball valves are used to close off the test section for void fraction tests. These valves are connected by a four-bar mechanism to ensure simultaneous closing of the valves. Slightly inside each ball valve are pressure taps. The pressure taps are 48 inches apart and signify the start and end of the test section (neglecting the distance between the valve and pressure taps). Close to one of the pressure taps exists another tap, this is the void fraction tap which allows for the test

section to be evacuated. A diagram of the taps used on the test section appear in Figure 3.5 (from Graham [1998]) and Figure 3.6.

Each test section is equipped with 16 type T thermocouples. These thermocouples are stationed in groups of four every 12" along the test section. In each group a thermocouple is placed every 90°. When using the smooth tubes the wall is thick so that grooves can be cut into the pipe and the thermocouples can be soldered into the grooves. The walls of the grooved tube are quite thin not allowing grooves to be cut into it. Instead, the thermocouples are placed on the outside of the tube using shims. Refer to Figures 3.7 and 3.8 to view how the thermocouples were attached.

Electrical heater strips are attached to the outside of the tube. Four to six strips of equal resistance were applied to the outside of the test section to ensure equal heating. The strips, manufactured by the Minco company, were 8" x 1" and had a resistance of 82 ohms. The heater strips were then connected to a 115V Variac which could control the power input into the test section.

3.2- Data Acquisition System

A computerized data acquisition system is used to control, monitor, and log data. A Macintosh II computer and a Strawberry Tree ™ data acquisition system consisting of six terminal panels, four data acquisition boards, and software Analog Connection Workbench™ are the primary data acquisition components.

Four of the data acquisition boards are used for temperature measurements by type T thermocouples. Two other boards are used for pressure transducers, power transducers, flow rate transducers, and controlling the false load heaters.

The terminal panels are linked to the data acquisition boards with a 50 pin ribbon connector. Two of the data acquisition boards are 16 channel boards of model number ACM2-16-16. The other two data acquisition boards are 8 channel boards of model numbers ACM2-16-8A and ACM2-12-8A (the 12 and 16 denoting bit precision). These two 8 channel boards also had the capability to output a signal. In all, the system can

accept 48 analog inputs and output 4 analog signals. The sampling frequency is set at 1 Hz.

The software used is an icon driven program consisting of signal output, calculation, control, and metering blocks. The input voltage or current would be read, a correlation would be performed, then the output would be metered on a real time display. The false load heater is also controlled by use of the analog output by changing the setting in a control block. The software also has the capability to log data and save it in a file.

3.3 Instrumentation and Measurements

This section will discuss instruments and techniques used in measuring different parameters in the experiment. The parameters that were measured include temperature, pressure, mass flow rate, power, and calculated quantities such as quality.

3.3.1- Temperature Measurements

Type T thermocouples are used for temperature measurements. These thermocouples are calibrated using an ice bath reference and are considered valid from 10°C to 100°C with an uncertainty of ± 0.2°C.

One thermocouple on each data acquisition terminal is designated as the reference. The reference thermocouple is placed in a ice-water bath at 0°C. The voltages recorded at the ice bath are subtracted from the voltage recorded by the reference thermocouple. A curve fit supplied by the thermocouple manufacturer is then used to determine the temperature.

3.3.2- Pressure Measurements

Four pressure transducers are installed on the refrigeration loop and test section. Three of the transducers are absolute pressure transducers and are located at the inlet to the pump, pre-heater, and test section. The other transducer is a differential transducer

which measures the pressure drop across the test section. The pre-heater inlet and test section inlet transducers are BEC strain-gage type transducers with ranges of 0-300 psi (0-2100 kPa). The pump inlet pressure transducer is manufactured by Sentra with a range of 0-1000 psi (0-6900 kPa). Lastly, the differential pressure transducer was manufactured by Sensotec, and has a range of 0-5 psi (0-35 kPa). All four transducers were calibrated using a dead weight tester with an uncertainty of 0.3% of the full scale reading.

3.3.3- Mass Flow Measurements

The mass flow meter used is a model D12 manufactured by Micromotion®. The meter measures the flow rate by the vibration frequency of a U-tube located inside. The meter delivers a specific current depending on the vibrational frequency of the U-tube. The data acquisition program reads the current and a curve fit is used to determine the mass flow rate.

A second flow meter is used in the chiller system to measure the ethylene glycol flow rate. This flow meter was manufactured by Flow Technology and is used by the chiller control board to regulate the "set point temperature".

3.3.4- Power Measurements

Three power transducers manufactured by the Ohio Semitronics company are used on the experimental facility. The heat flux to the test section is measured by a PC5-49D92 power transducer. The heat input to the pre-heater is measured by two different transducers. One of the transducers is used to measure the power delivered by the circuits that were switch controlled. The other is used to measure the power delivered by the variac controlled circuit. Each of these power transducers was tested at the factory to have an uncertainty of 0.2% full scale reading.

3.3.5- Calculated Parameters

Several quantities cannot be measured directly and these must be calculated within the data acquisition program. These include test section heat flux, mass flux, the amount of subcooling, and test section inlet quality,

The mass flux is determined by dividing the mass flow rate by the test section cross sectional area. This can be done in the data acquisition program. The test section heat flux is calculated in much the same way using the surface area of the test section.

To determine the amount of subcooling at a point both the temperature and pressure must be known. If the pressure is known the saturation temperature can be found by a using a curve fit in the data acquisition program. Next, the real temperature can be subtracted from the saturation temperature to find the amount of subcooling.

To determine the inlet quality, the pre-heater inlet temperature and pressure must be known. The enthalpy at that point can be calculated by a curve fit. Next, the enthalpy at the test section inlet can be found by adding the heat input by the pre-heater. The saturated liquid and saturated vapor enthalpies at the test section inlet temperature are calculated using curve fits. Lastly, the inlet quality can be calculated by comparing the inlet enthalpy to the test section to the saturated liquid and saturated vapor enthalpies. Refprop version 4.01, a software program developed by NIST [1993], was used to develop the property curve fits for both R134a and R410A.

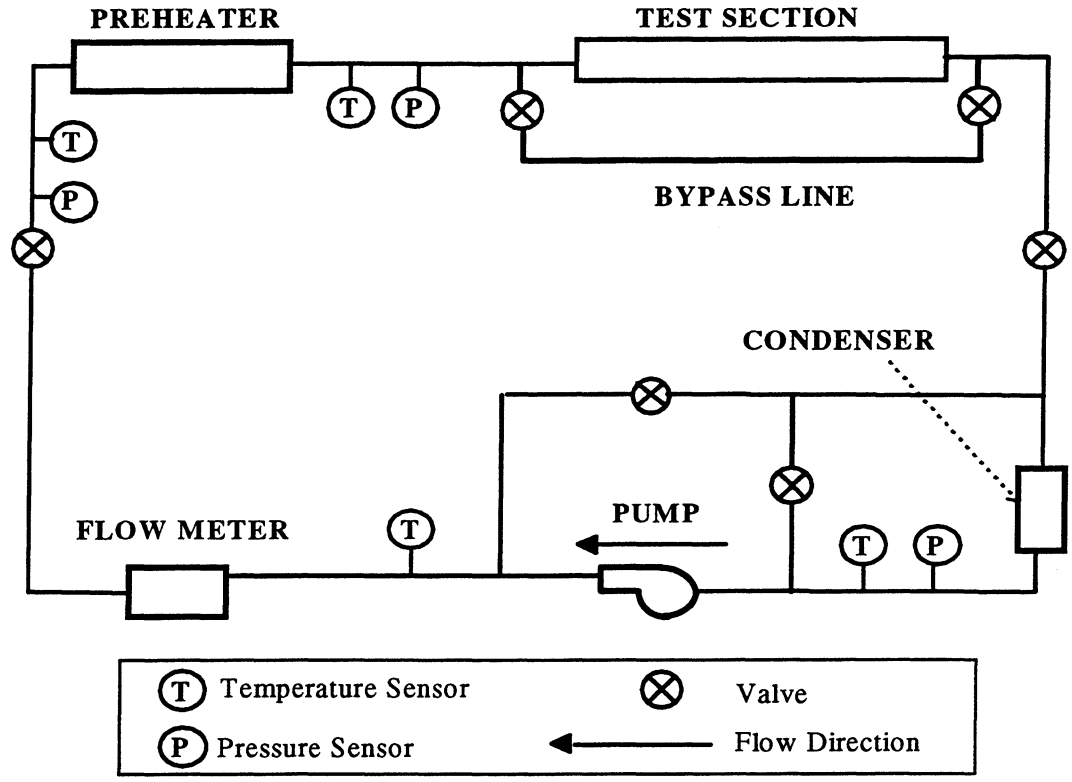

Figure 3.1 Schematic of refrigerant loop

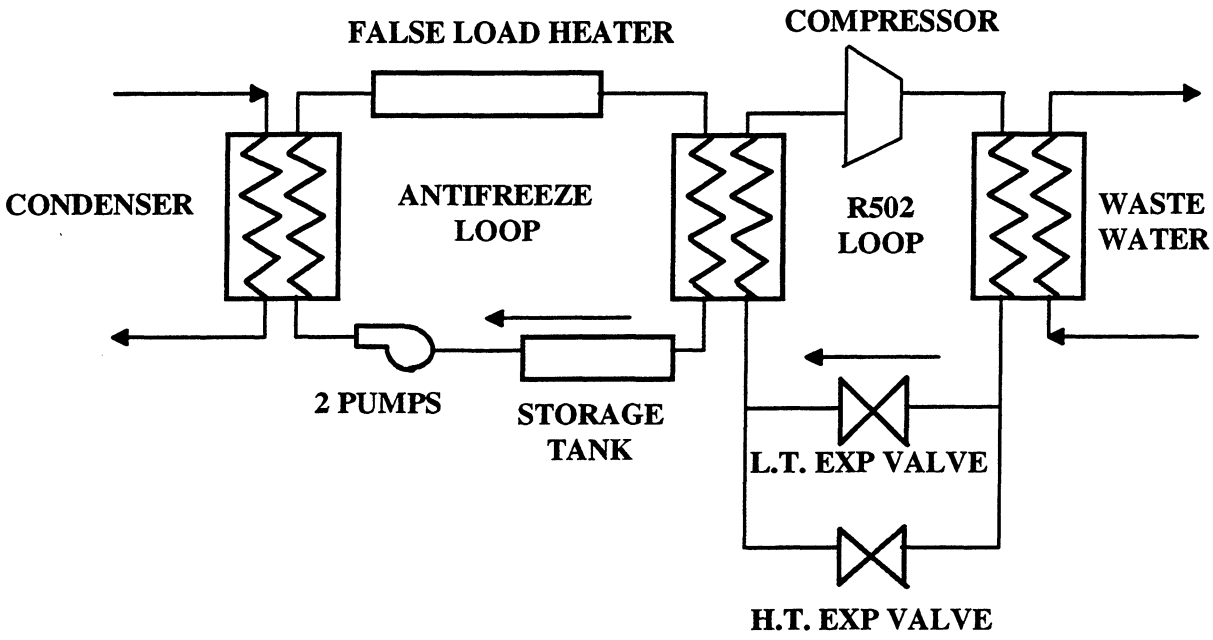

Figure 3.2 Chiller system

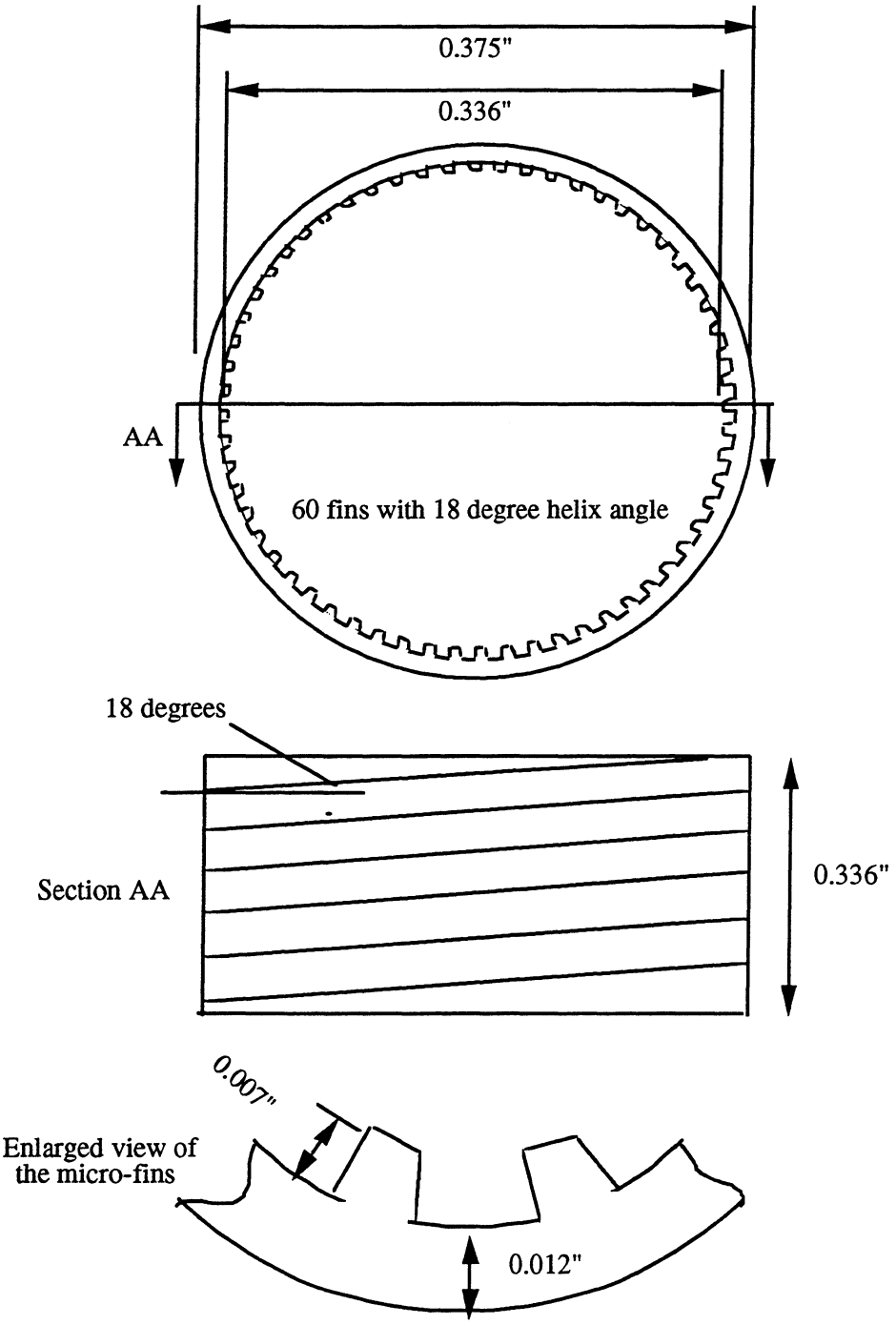

Figure 3.3 Micro-fin tubes dimensions and features for 8.93 mm inner diameter micro-finned test section

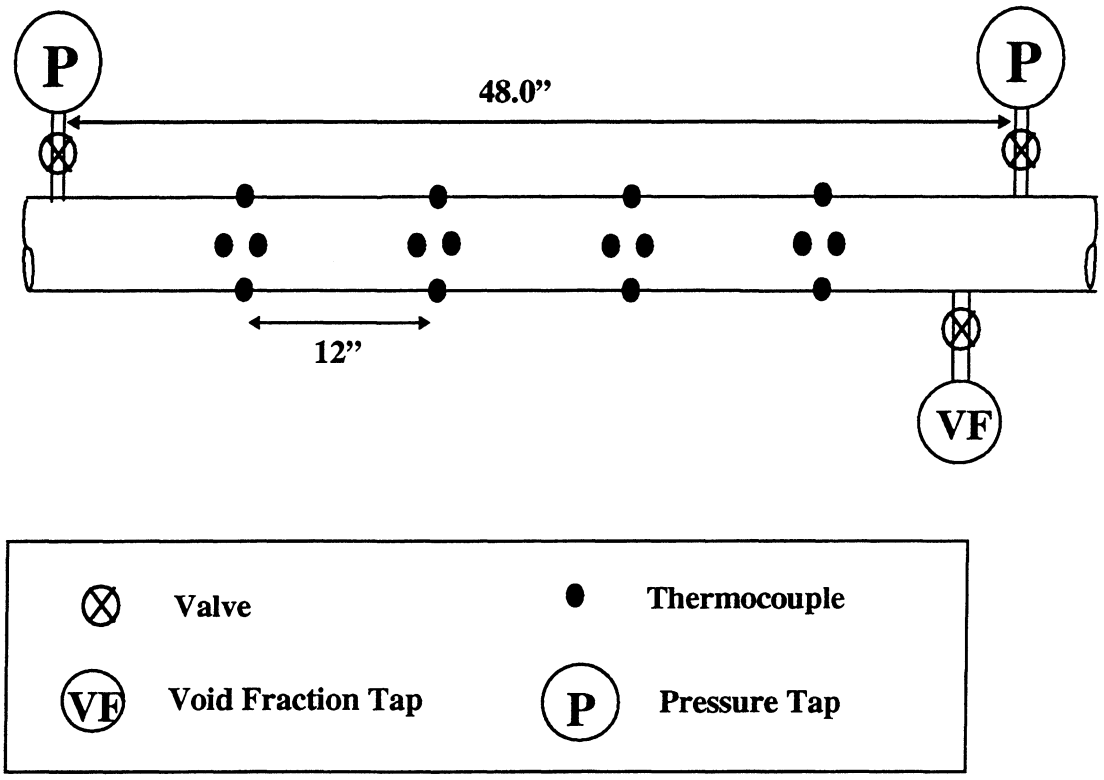

Figure 3.4 Test section dimensions and features

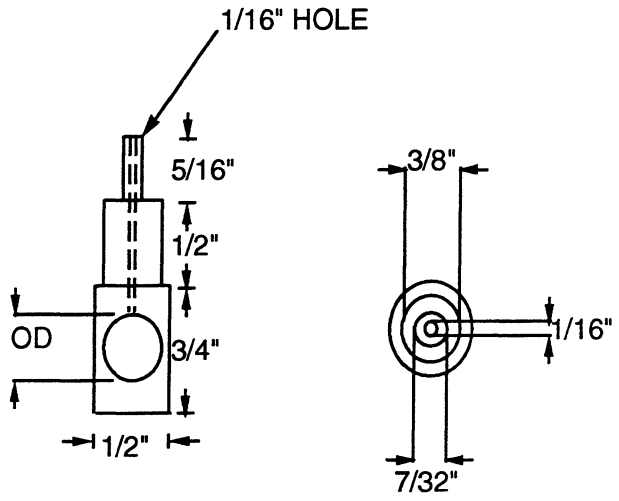

Figure 3.5 Void fraction tap where OD is the outside diameter of the test section the tap will fit on to.

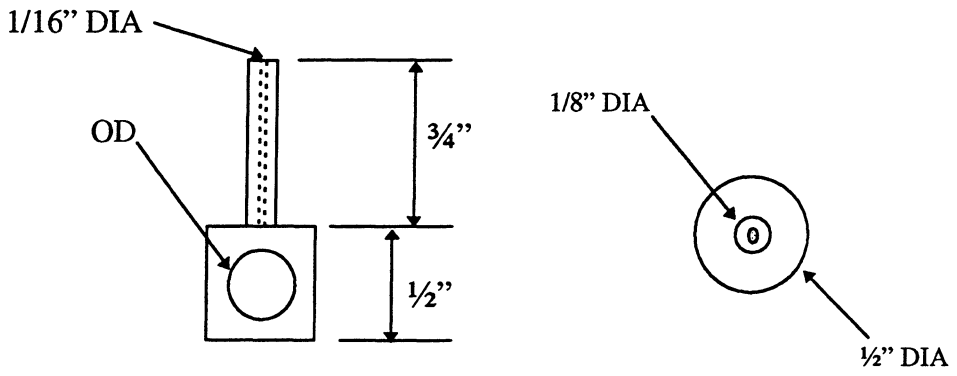

Figure 3.6 Pressure tap where OD is the outside diameter of the test section the tap will fit on to

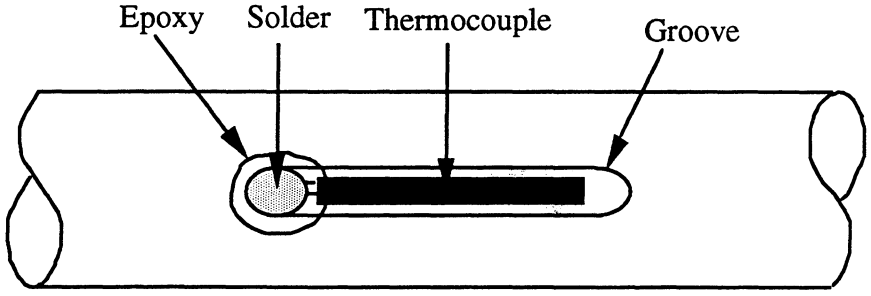

Figure 3.7 Thermocouple placement in thick walled tubes

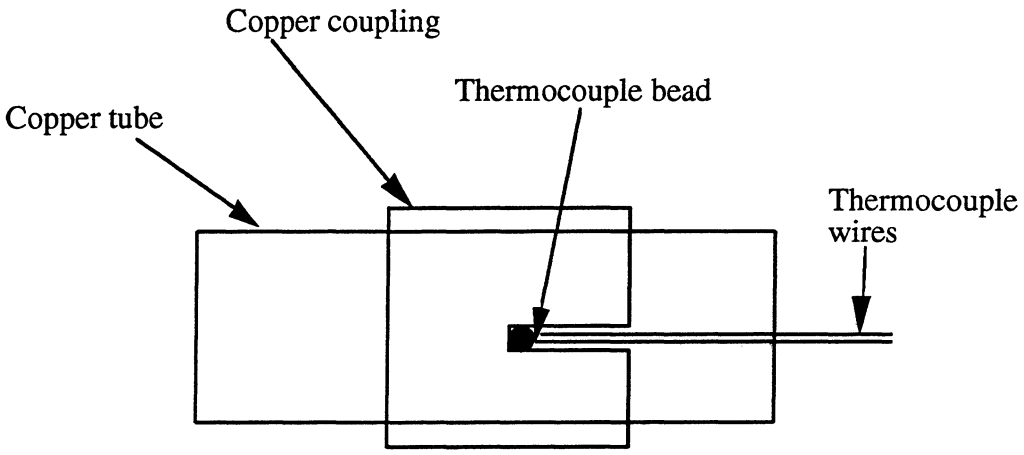

Figure 3.8 Thermocouple placement in thin walled tubes

Chapter 4

Experimental Procedure and Data Reduction

This chapter discusses the methods to find the test section volume, properly condition the system to the desired state, and to take a sample to determine the test section void fraction. One of the key tools not yet introduced is the use of a receiving tank. The receiving tank is an approximately 1 liter tank with an attached pressure tap and fittings to connect to the void fraction tap. Graham [1998] developed the void fraction determination technique and gives an additional description of the method.

4.1- Test Section Volumes

The first task is to find the volume of the test section. This is done by first evacuating the refrigerant loop then closing all of the valves to the test section. Next one of the receiving tanks is filled with an known gas usually R134a vapor, R22 vapor, or nitrogen. The receiving tank is then weighed to find the total mass of tank plus the vapor in the tank (m_1). The tank is then attached to the test section, and the vapor is allowed to flow freely from the receiving tank into the test section. After letting the system equilibrate, the pressure of the system (P) is recorded from the pressure gage attached to the receiver, and the ambient temperature (T) is recorded. The receiving tank is now detached from the system and weighed again (m_2). From the two scale readings the mass released into the test section can be determined (Δm) and the specific volume of the vapor can be found. This test is usually done up to a dozen times with three different fluids and an average taken as sample calculations appear below.

$$\Delta m = m_1 - m_2 \tag{4.1}$$

$$v = f(P,T) \tag{4.2}$$

$$\forall_{ts} = \Delta m * v \tag{4.3}$$

where f can be the ideal gas law or other property data such as Refprop or EES.

4.2- Void Fraction Calculations

The system is conditioned to desired inlet conditions to begin sample collection. First the mass flux is set, and then the overall system temperature is lowered by the chiller. Once the inlet temperature is much lower than 5°C, the pre-heater is used to establish the desired inlet quality. When the quality and mass flux are set, the false load heater (FLH) is turned on until a steady state inlet temperature of 5°C is reached. The mass flux and quality may need to be slightly adjusted as the inlet temperature changes.

After the refrigerant loop reaches steady state, the four-bar mechanism that controls the test section valves is closed and the bypass loop is opened. An evacuated receiver is weighed (m_e) and attached to the test section. The void fraction tap valve is then opened allowing refrigerant to flow into the receiver. The receiver is kept in an ice bath to keep the pressure inside the receiver low. The test section heaters are turned on to evaporate any liquid left in the test section. When it is believed that all of the liquid has been evaporated, the receiver is taken off of the test section and weighed. The pressure of the system (from the gage on the receiving tank) and the estimated temperature in the test section (from the thermocouples outside of the test section) are recorded. The amount of mass in the receiver and the specific volume of the refrigerant left in the test section allow the void fraction to be found.

Calculation of the void fraction requires knowing the amount of mass trapped in the test section when the test section shut off valves are closed. First, the mass in the receiver (m_r) is calculated by subtracting the final scale reading mass (m_f) from the evacuated receiving tank mass (m_e).

$$m_r = m_f - m_e \tag{4.4}$$

Next, the specific volume of the vapor left in the test section is found using equation 4.2 which leads to the amount of mass left in the test section (m_l) .

$$m_l = \forall_{ts} / v \tag{4.5}$$

These two masses are then added together to get the total test section mass (m_{ts}) . By dividing the test section volume by the total mass in the test section a static specific volume of the test section can be found (v_{ts}).

$$m_{ts} = m_r + m_l \tag{4.6}$$

$$v_{ts} = \frac{\forall_{ts}}{m_{ts}} \tag{4.7}$$

The static quality (x_s) can be found by comparing the static specific volume of the test section to the specific volume of saturated vapor and saturated liquid of the refrigerant at the temperature of the inlet to the test section (usually 5°C).

$$x_s = \frac{v_{ts} - v_l}{v_{lg}} \tag{4.8}$$

The void fraction can be related to the static quality by inversion of the homogenous relation.

$$x_s = \left[\frac{1-\alpha}{\alpha} * \frac{v_g}{v_l} + 1 \right]^{-1} \tag{4.9}$$

Where v_g and v_l are the specific volumes of saturated liquid and saturated vapor at the inlet temperature of the test section.

4.3- Uncertainty Analysis

Table 4.1 is a table of the average quality of test section and the uncertainty associated with void fraction measurements at that quality for that tube.

Table 4.1 Void fraction uncertainty for given quality range and tube

Quality Range	Smooth	Axially Grooved	Helically Grooved
0-10%	5.0%	5.0%	3.2%
10-20%	4.8%	2.4%	2.0%
20-30%	2.0%	1.3%	1.6%
30-40%	1.5%	1.2%	1.3%
40-50%	1.4%	1.1%	1.0%
50-60%	1.0%	1.0%	0.7%
60-70%	0.8%	0.9%	0.6%
70-80%	0.7%	0.8%	0.4%
80-100%	0.6%	0.7%	0.3%

This table was constructed by plotting the average uncertainty for each data point, then using a hand drawn curve which would be higher than 95% of the errors, (see Figure 4.1). As quality increases error decreases. This is expected since the highest mass measurements were in the low quality range leaving more room for error.

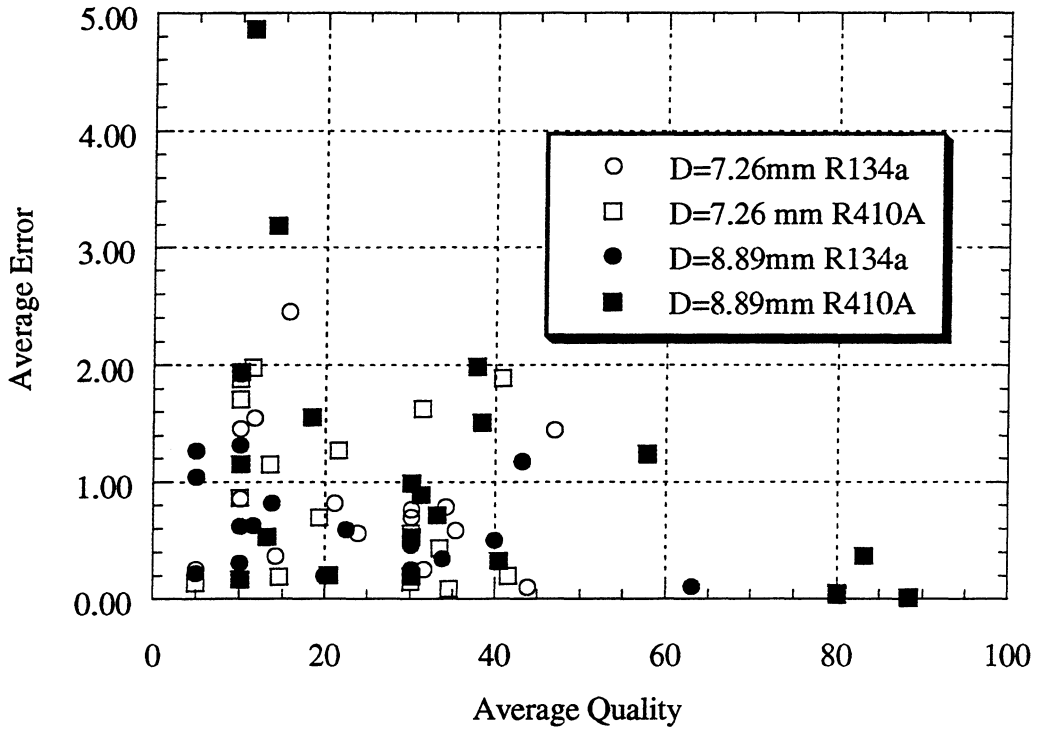

Figure 4.1 Example error analysis plot for the helically grooved tube.

Chapter 5

Smooth Tube Experimental Results

This chapter will present and discuss void fraction results for evaporation in a 6.12 mm inner diameter smooth tube. The results to be discussed in this chapter have been determined using the equipment and methods discussed in Chapters 3 and 4. The results will also be compared with existing models. In Chapter 8 all of the void fraction data from the smooth and enhanced tubes will be presented and a model will be given to predict void fraction.

5.1- Void Fraction Results

The experimental void fraction results are presented in this section. Void fraction dependence on refrigerant, mass flux, heat flux, and diameter are discussed.

5.1.1- Effect of Refrigerant on Void Fraction

Figure 5.1 is a plot of measured void fraction for R134a and R410A with respect to average quality. The plot shows R134a to have a slightly higher void fraction (~5% on average) than R410A at the same average quality. This was expected because R410A has a higher vapor pressure and thus higher vapor density causing the vapor to flow at a lower velocity.

5.1.2- Effect of Mass Flux on Void Fraction

Figure 5.2 plots the measured void fraction with respect to average quality in the test section at different mass fluxes with R134a as the refrigerant. Additionally, Figure 5.3 plots the measured void fraction with respect to average quality in the test section at different mass fluxes with R410A as the refrigerant. The three different experimental mass

fluxes are 75 kg/m^{2}s, 200 kg/m^{2}s, and 500 kg/m^{2}s. Figure 5.2 depicts void fraction being independent of mass flux. Figure 5.3 shows the higher mass fluxes having lower void fractions at low qualities, but for the most part all of the data points are mixed showing a trend of mass flux independence. Appendix A contains more detailed plots of the data and trends discussed here.

5.1.3- Effect of Heat Flux on Void Fraction

Figures 5.4 and 5.5 display plots of void fraction with respect to average quality in the test section with three different heat fluxes into the test section. Figure 5.4 represents the void fraction for R134a and Figure 5.5 represents R410A. The three different heat fluxes are 0 W/m^2 (adiabatic) , 3 W/m^2, and 10 W/m^2. Both figures show that void fraction is independent of heat flux. Figures in Appendix A show more detailed plots of the heat flux effects.

An important point to be brought out is that the aforementioned plots were made average quality and not inlet quality as the independent variable. The average quality takes into account the heat flux into the test section. Thus in reality heat flux does bear some effect on the void fraction.

5.1.4- Effect of Diameter on Void Fraction

Data was also taken using the same experimental apparatus in a companion study by Yashar [1998]. His work concentrated on smaller diameter smooth tubes. Yashar's data for a 4.26 mm inner diameter tuber is plotted with the 6.12 mm smooth tube data and appears in Figure 5.6. No size trends are seen in this plot indicating that void fraction has no dependence on diameter within this range of operation.

5.2- Correlation Comparison

This section will present and discuss the accuracy of the void fraction correlations presented in Chapter 2 with respect to the 6.12 mm inner diameter smooth tube data. Each of the figures is enhanced to show any mass flux dependencies or refrigerant dependencies of the correlation.

5.2.1- Slip Ratio Correlations

The experimental data is plotted against the Homogenous, Rigot, Zivi , Ahrens-Thom, and Smith correlations in Figures 5.7 - 5.11, respectively. The Ahrens-Thom, Rigot, and Zivi plots are very similar to the Homogenous plot except they are rotated upward about the pure vapor point. These correlations over-predict the void fraction at high qualities, but then the correlations swing and under-predict the void fraction at lower qualities. The Smith correlation does a good job of predicting void fractions above 0.70. Below a void fraction of 0.70, the Smith correlation also starts to swing upward like the other slip-ratio correlations. No mass flux or refrigerant preferences were seen in any of the correlations.

The Homogenous correlation drastically over-predicts the void fraction by up to 38%; on average it is 10.2% in error. The Rigot correlation also over predicts the void fraction until it's swing point at a void fraction of about 0.75. The Rigot correlation will predict the void fraction within 12.3% with an average deviation of 5.2% from the experimental data. Zivi's correlation is extremely accurate for void fractions of 0.80, but errors up to 50% for void fractions lower than 0.55. Zivi's correlation deviates from the experimental void fraction by an average of 4.5%. The Ahrens-Thom correlation predicts the void fraction to within 15% with an average deviation of 4.5%. The Smith correlation is extremely accurate for void fractions above 0.70, predicting the void fraction within 4.5% with an average deviation of 1.5%. Smith's correlation correctly predicts all of the larger smooth tube data within 14% with an average deviation of 2.2%.

5.2.2- Lockhart-Martinelli Correlations

Experimental void fraction data is plotted against the Wallis and Baroczy correlations in Figures 5.12-5.13, respectively. The Baroczy correlation results are similar to the slip ratio figures. The Baroczy correlation holds well for void fractions above 0.85, but then takes a swing where it under predicts the void fraction. For the larger smooth tube the Baroczy correlation is in error by up to 25%. No mass flux or refrigerant preferences were seen.

The Wallis correlation accurately predicts the void fraction to within 11%. Though the majority of the data lies slightly below the 45° line the predicted void fraction only differs by 2% on average. The Wallis correlation does show a slight refrigerant preference as the data representing R134a is usually above the R410A data. No mass flux preferences were seen with respect to the Wallis correlation.

5.2.3- Flux Dependent Correlations

The experimentally determined void fraction is plotted against the Tandon, Premoli, Hughmark, and Graham condenser correlations in Figures 5.14-5.17, respectively.

The Tandon correlation predicts the void fraction to within 11% with an average deviation of 2.5%. No mass flux or refrigerant preferences are seen and the correlation centers the data. The Premoli correlation predicts the data to within 16% with an average deviation of 3.2%. No refrigerant of mass flux preferences are seen, but the Premoli correlation does systematically over-predict the data by 3%.

The Hughmark correlation over predicts the void fraction up to 16% with an average deviation from the experimental data of 7%. It is also apparent that as the mass flux increases the Hughmark correlation becomes more accurate. At a mass flux of 75 kg/m^2s the average deviation is 10.7%, but at 200 kg/m^2s the average deviation is 6.6%, and at 500 kg/m^2s the average deviation is only 4.2%.

Graham's correlation does not represent the data well. This correlation has a strong mass flux dependence, and the plot shows how insensitive the void fraction data is to mass flux. For mass flux's of 500 kg/m^{2}s, Graham's correlation does a fair job of predicting the void fraction with a maximum deviation of 11%. For the lower mass fluxes, Graham's correlation over predicts the void fraction by up to 29%.

5.2.4- Diameter Effects on the Correlations

Appendix A contains detailed figures which depict the correlations with both the 4.26 mm and 6.12 mm inner diameter smooth tubes. The data does not show significant diameter effects, except for the Tandon correlation. The Tandon correlation depicts void fractions in smaller tubes being higher than for larger tubes.

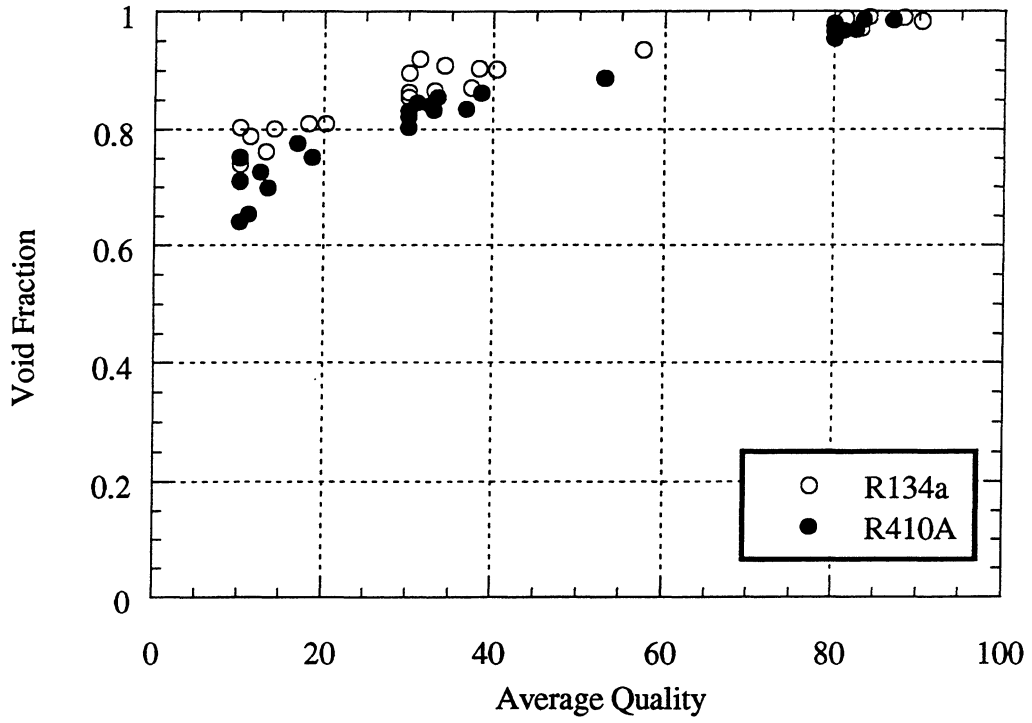

Figure 5.1 Void fraction vs. average quality 6.12 mm inner diameter smooth tube.

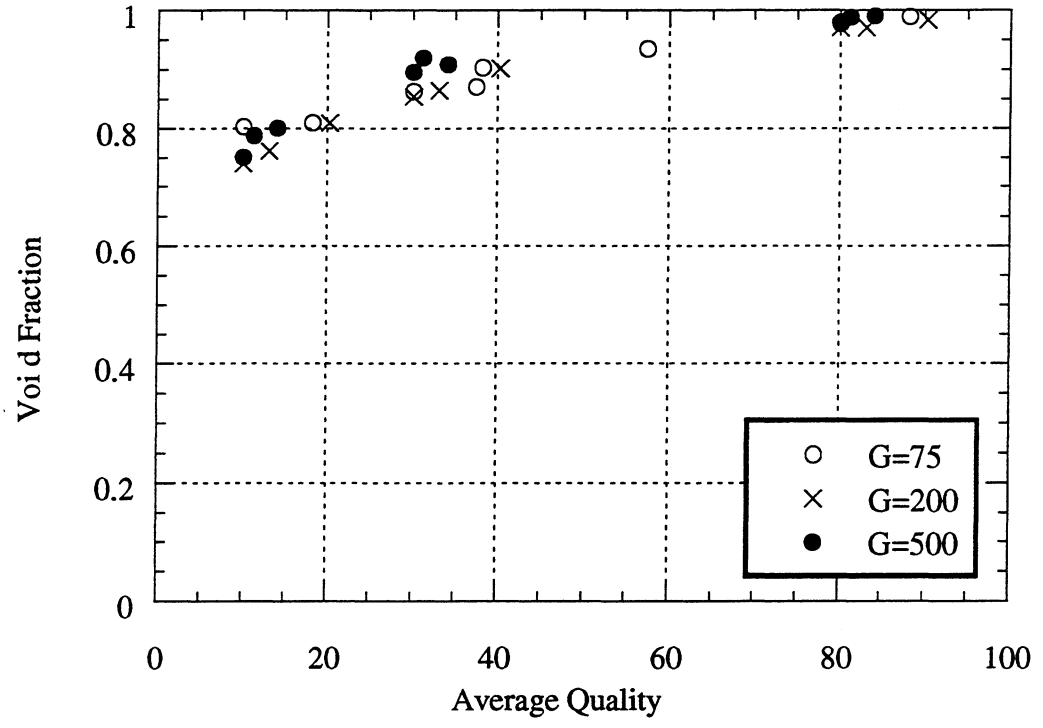

Figure 5.2 Void fraction vs. average quality using R134a in 6.12 mm inner diameter smooth tube. Mass flux (G) given in kg/m^2s.

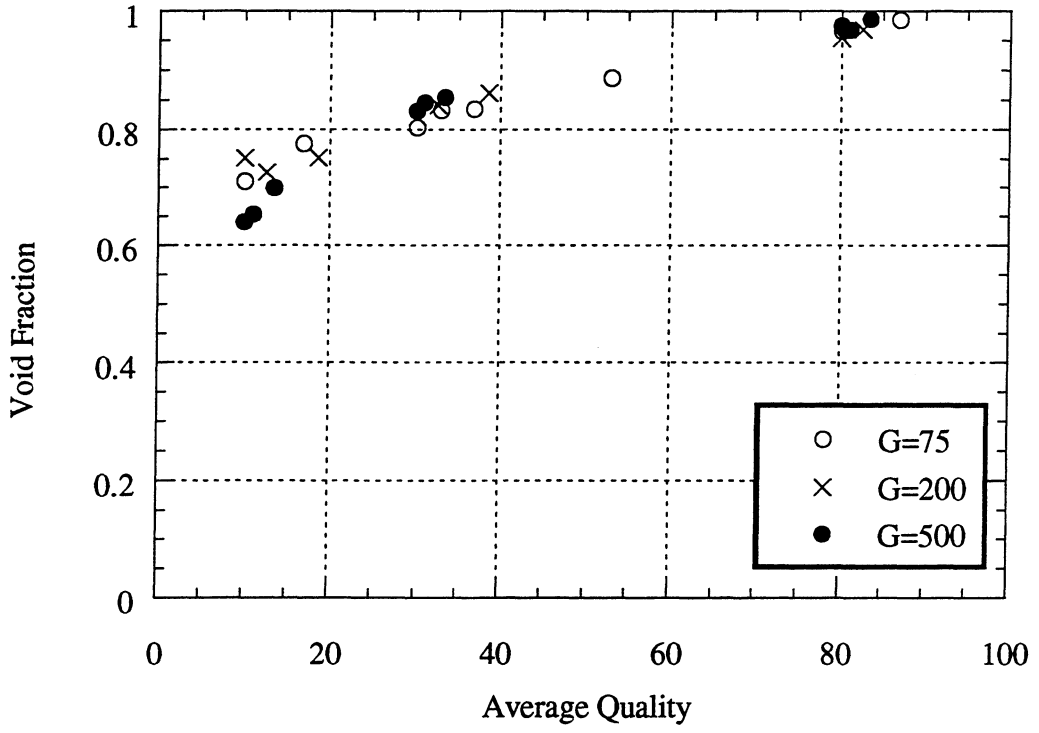

Figure 5.3 Void fraction vs. average quality using R410A in 6.12 mm inner diameter smooth tube. Mass flux (G) in kg/m^{2}s.

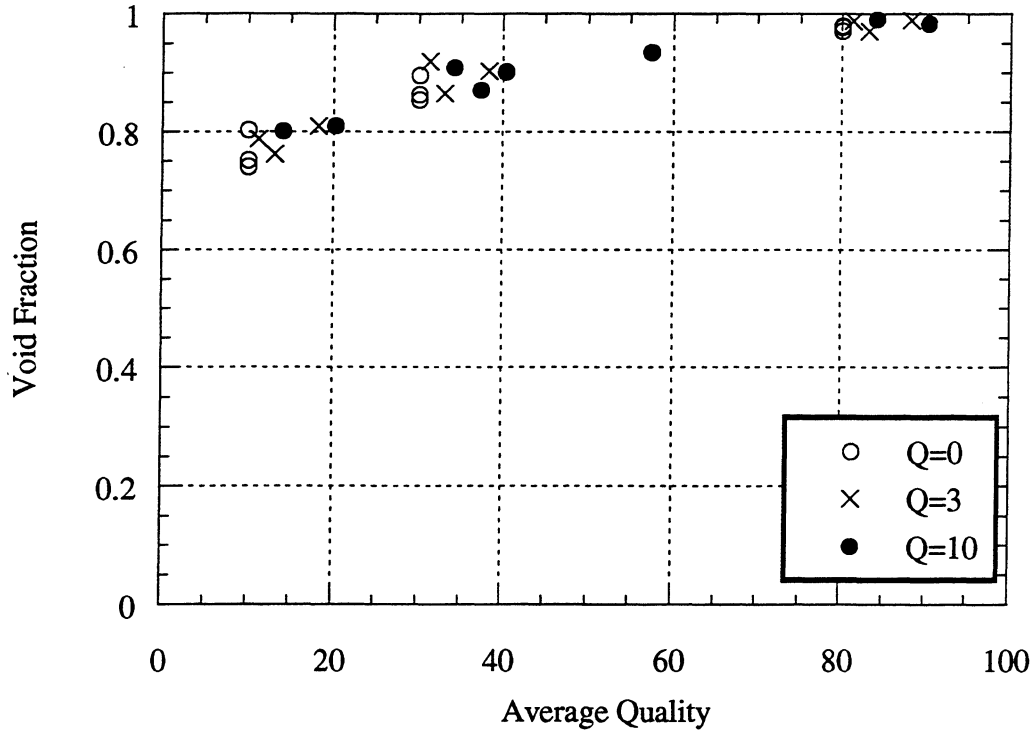

Figure 5.4 Void fraction vs. average quality in test section using R134a in a 6.12 mm inner diameter smooth tube. Test section heat flux (Q) given in W/m^2.

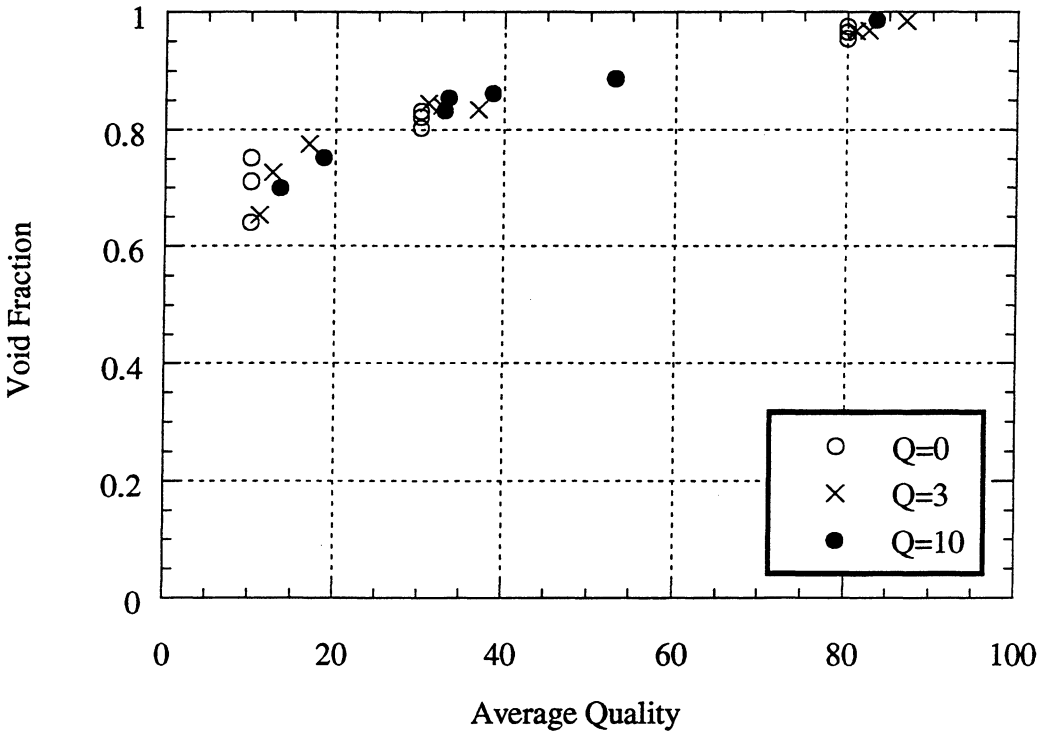

Figure 5.5 Void fraction vs. average quality using R410A in a 6.12 mm inner diameter smooth tube. Test section heat flux (Q) given in W/m^2.

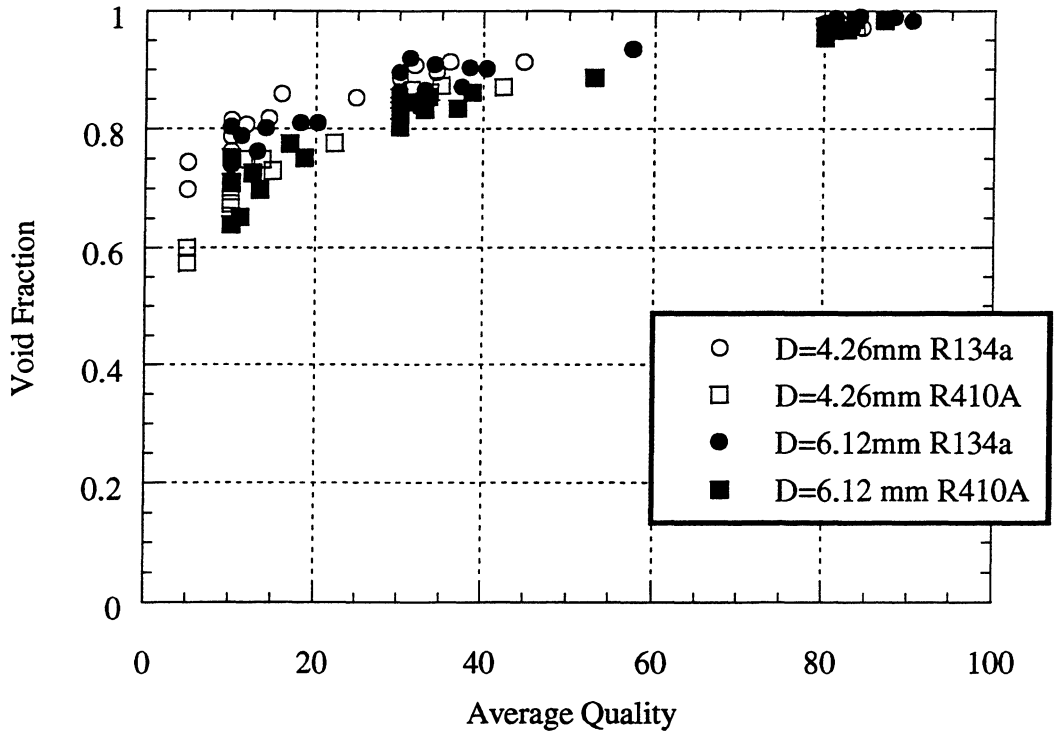

Figure 5.6 Void fraction vs. average quality for a 4.26mm and 6.12mm inner diameter smooth tube using R134a and R410A.

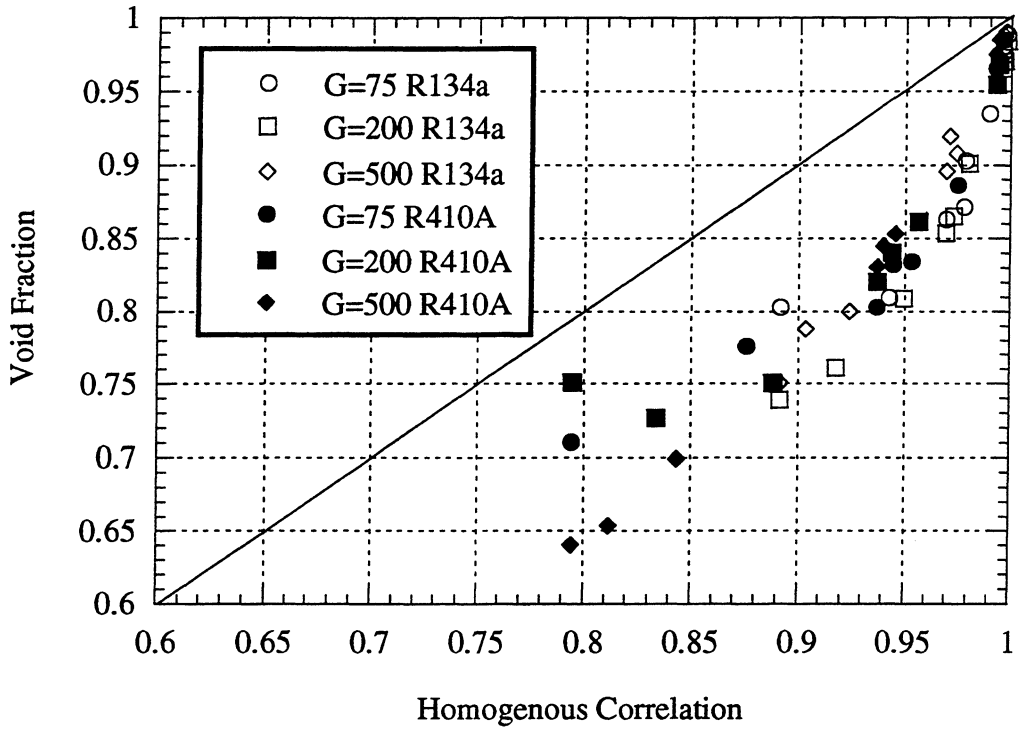

Figure 5.7 Void fraction vs. Homogenous correlation for 6.12mm inner diameter smooth tube using R134a and R410A. Mass flux (G) is in kg/m^{2}s.

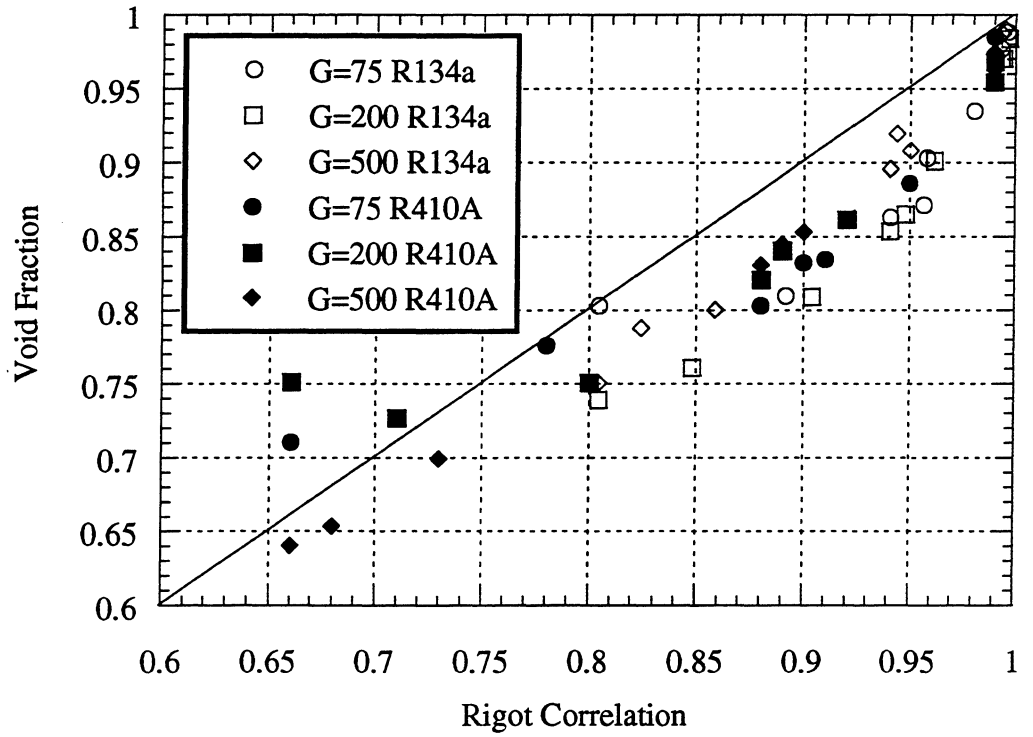

Figure 5.8 Void fraction vs. Rigot correlation for 6.12mm inner diameter smooth tube using R134a and R410A. Mass flux (G) is in kg/m^{2}s.

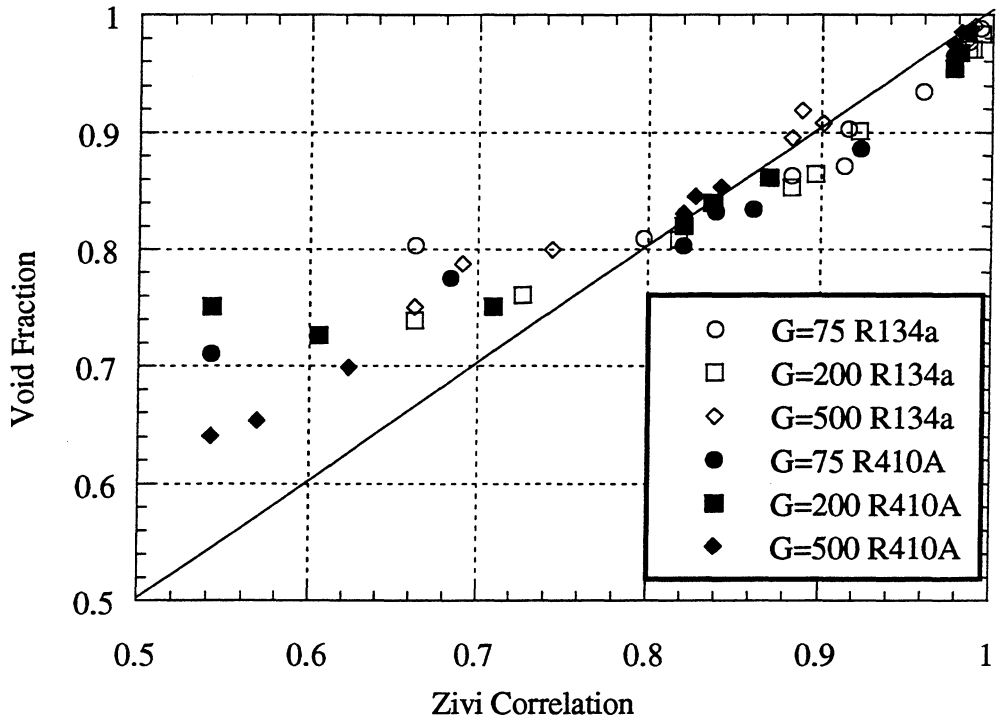

Figure 5.9 Void fraction vs. Zivi correlation for 6.12mm inner diameter smooth tube using R134a and R410A. Mass flux (G) is in kg/m^{2}s.

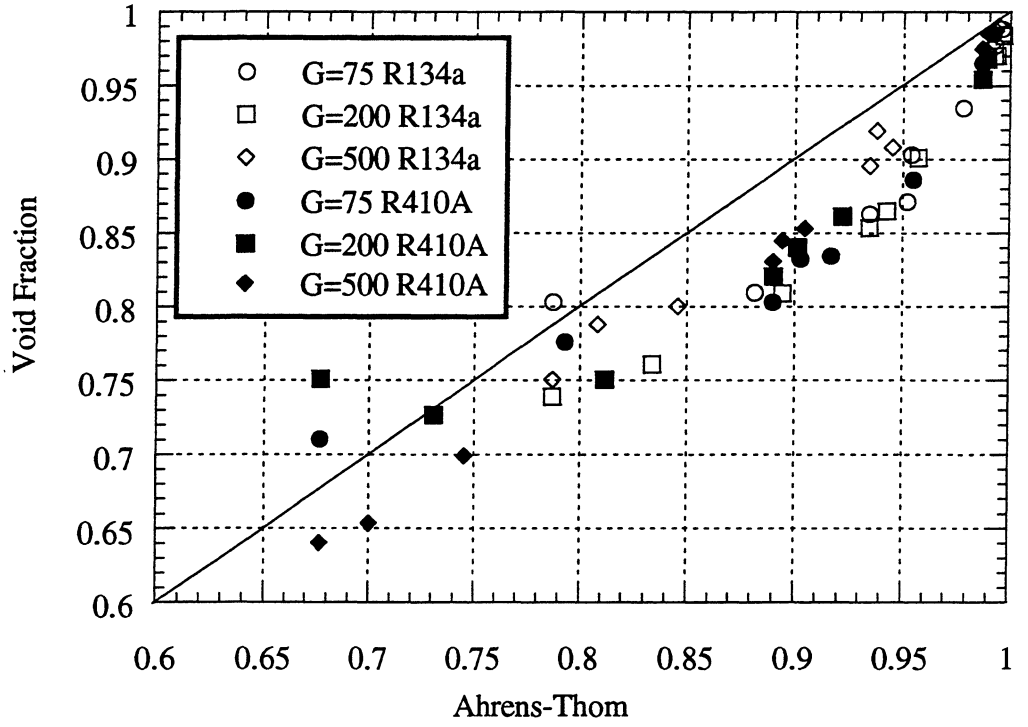

Figure 5.10 Void fraction vs. Ahrens-Thom correlation for 6.12mm inner diameter smooth tube using R134a and R410A. Mass flux (G) is in kg/m^{2}s.

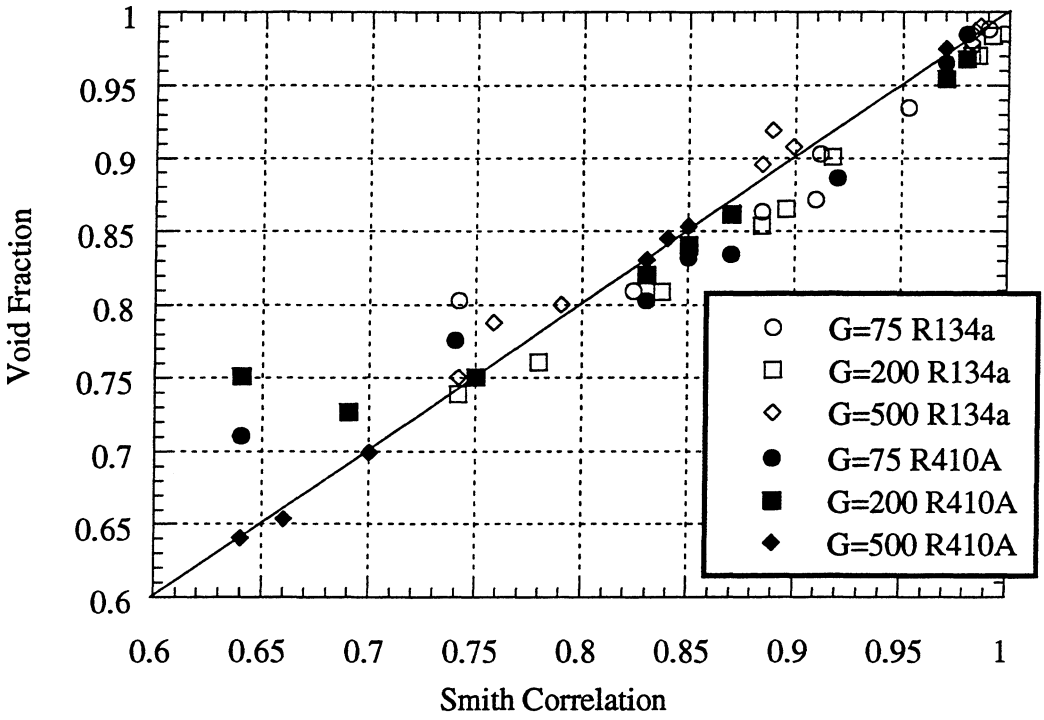

Figure 5.11 Void fraction vs. Smith correlation for 6.12mm inner diameter smooth tube using R134a and R410A. Mass flux (G) is in kg/m^{2}s.

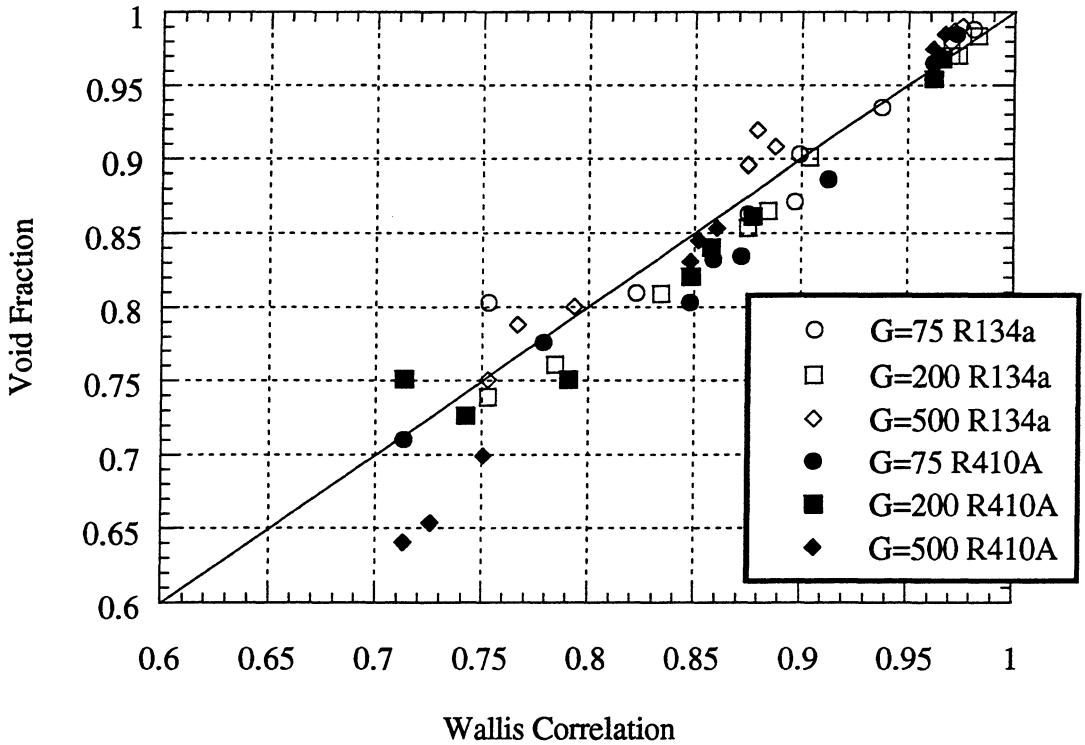

Figure 5.12 Void fraction vs. Wallis correlation for 6.12mm inner diameter smooth tube using R134a and R410A. Mass flux (G) is in kg/m^{2}s.

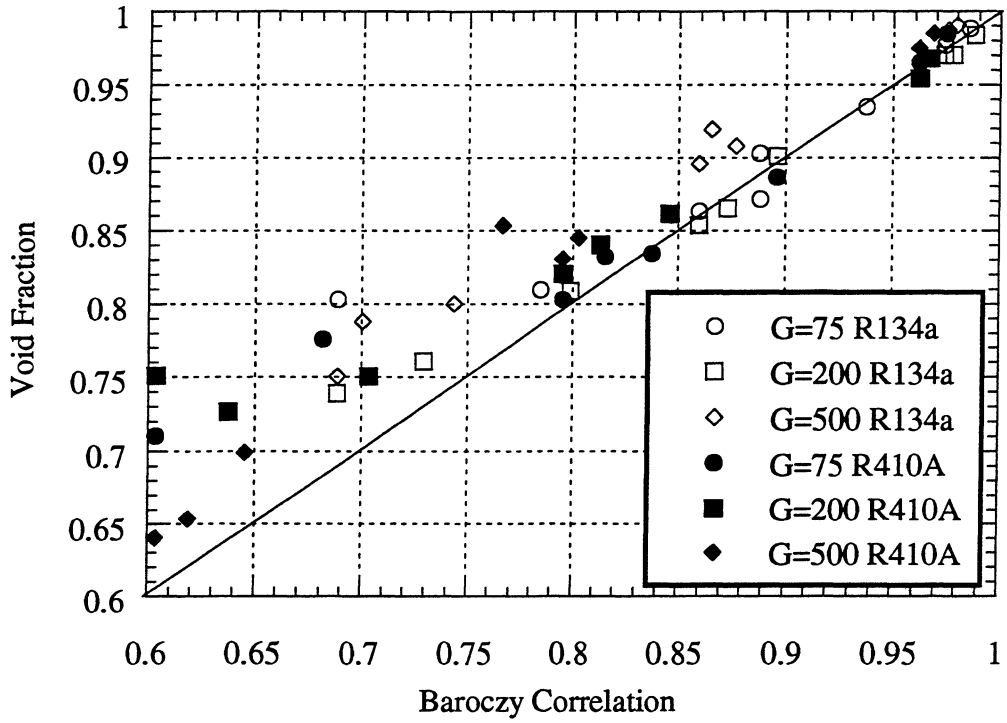

Figure 5.13 Void fraction vs. Baroczy correlation for 6.12mm inner diameter smooth tube using R134a and R410A. Mass flux (G) is in kg/m^{2}s.

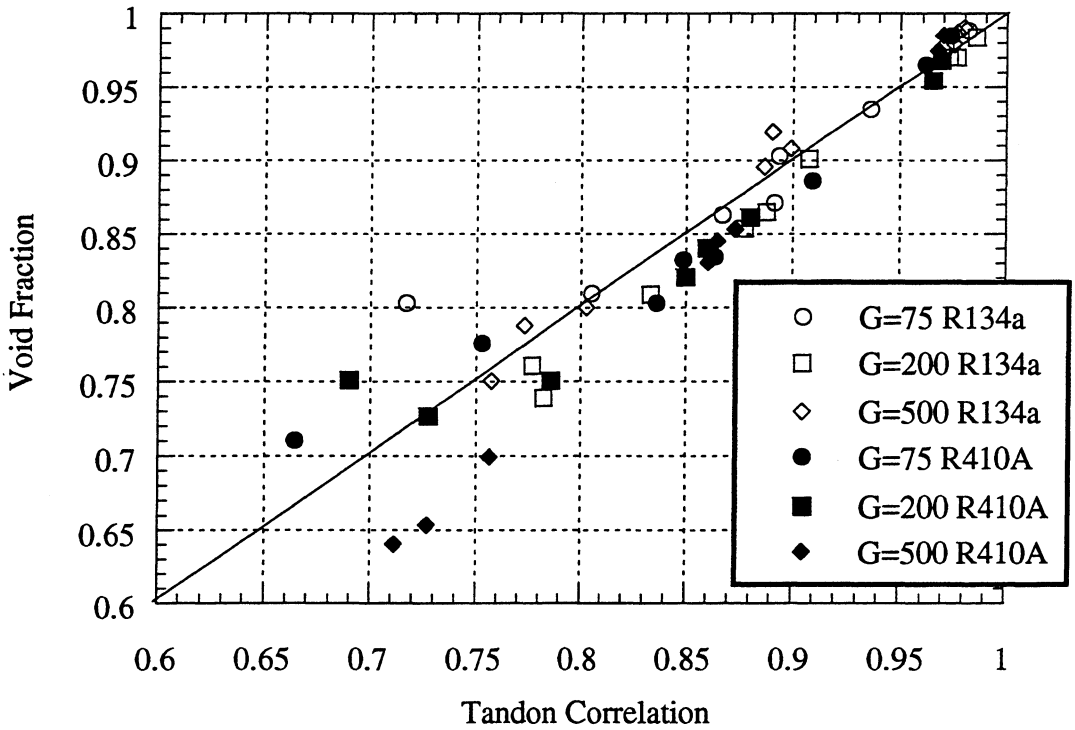

Figure 5.14 Void fraction vs. Tandon correlation for 6.12mm inner diameter smooth tube using R134a and R410A. Mass flux (G) is in kg/m^{2}s.

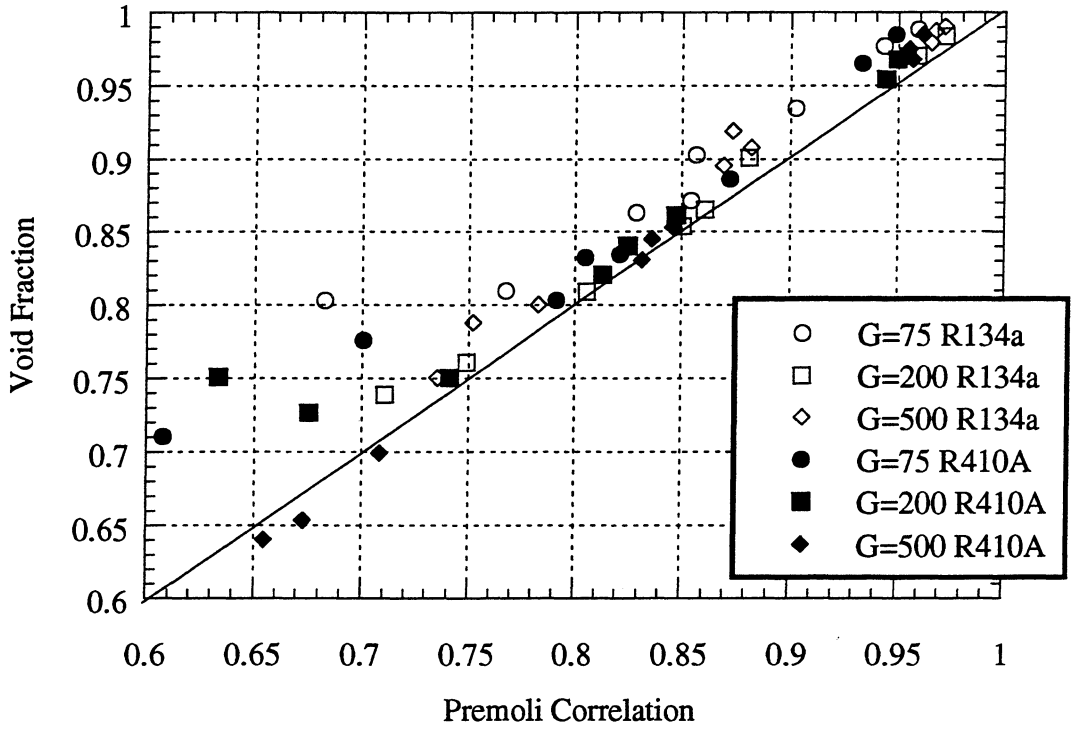

Figure 5.15 Void fraction vs. Premoli correlation for 6.12mm inner diameter smooth tube using R134a and R410A. Mass flux (G) is in kg/m^{2}s.

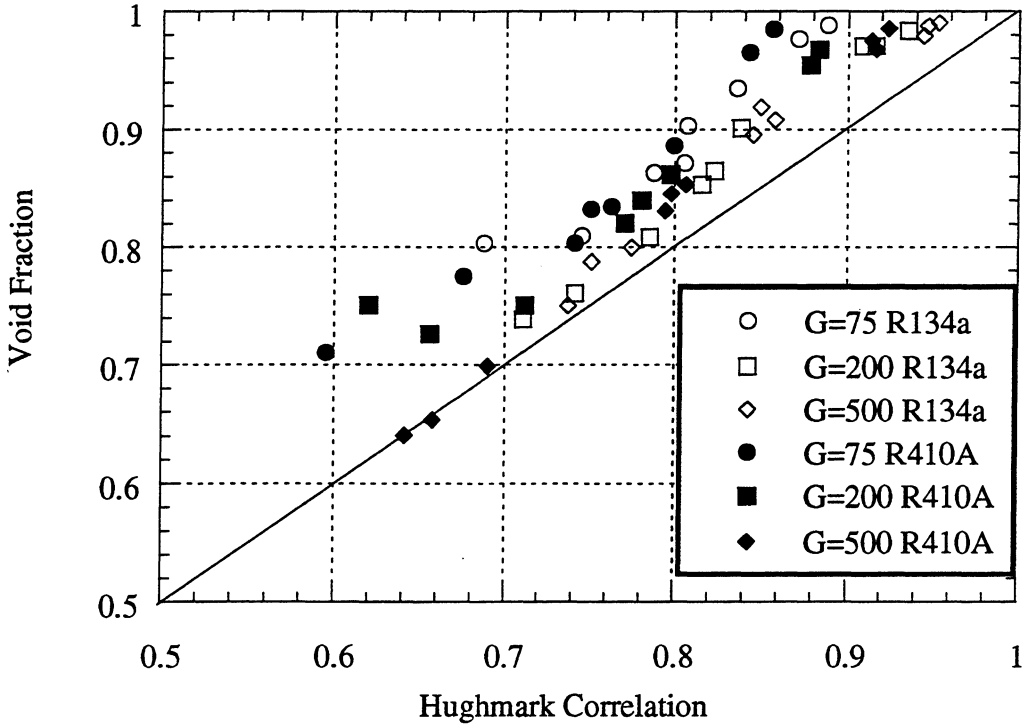

Figure 5.16 Void fraction vs. Hughmark correlation for 6.12mm inner diameter smooth tube using R134a and R410A. Mass flux (G) is in kg/m^{2}s.

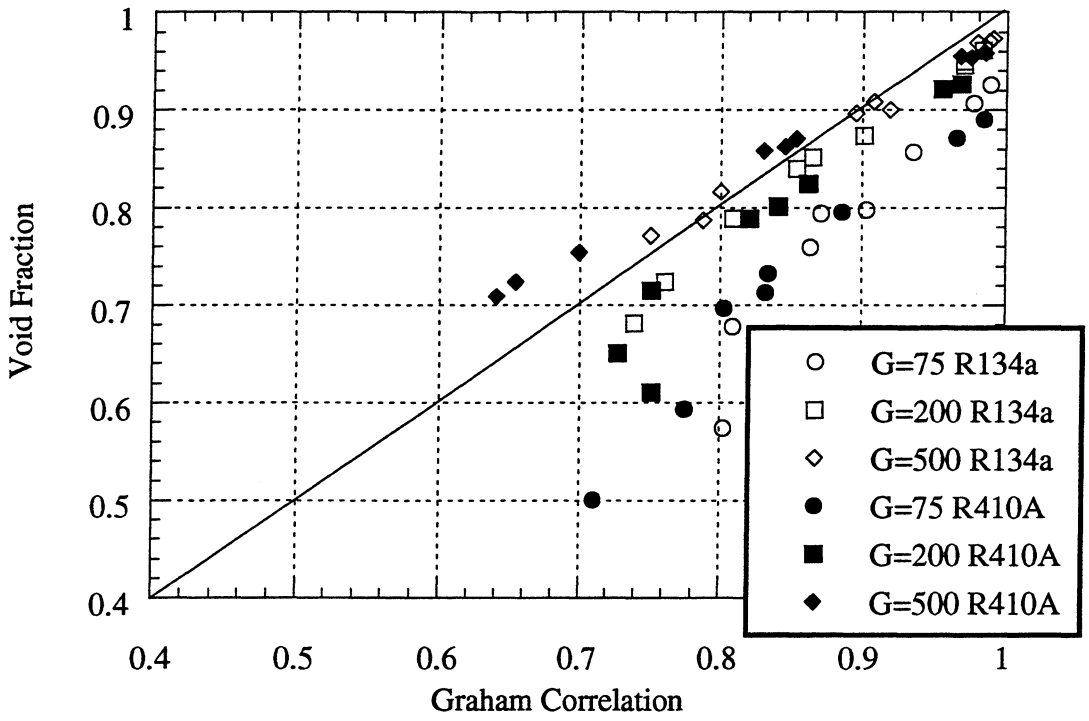

Figure 5.17 Void fraction vs. Graham's condenser correlation for 6.12mm inner diameter smooth tube using R134a and R410A. Mass flux (G) is in kg/m^{2}s.

Chapter 6

Axially Grooved Experimental Results

This chapter provides the void fraction results for experimentation on a 8.93 mm base diameter axially grooved tube for R134a and R410A. The characteristics of the tube and experimental setup were discussed in Chapters 3 and 4. The results will also be compared with existing void fraction models. In Chapter 8 a model to determine void fractions in smooth, axially grooved, and helically grooved tubes will be presented.

6.1- Void Fraction Results

The experimentally determined void fraction will be presented and the effects of refrigerant, mass flux, heat flux, diameter, and internal grooves on void fraction will be discussed.

6.1.1- Effect of Refrigerant on Void Fraction

Figure 6.1 is a plot of measured void fraction for both R134a and R410A with respect to the average quality in the test section. The plot shows that the void fraction for R134a tends to be slightly higher (~7%) than the void fraction for R410A at the same quality. This was the expected trend because R410A has the higher vapor pressure and therefore a higher vapor density causing the vapor to flow at a lower velocity.

6.1.2- Effect of Mass Flux on Void Fraction

Figures 6.2 and 6.3 are plots of void fraction vs. average quality for R134a and R410A, respectively. The mass fluxes used are 75 kg/m^{2}s, 200 kg/m^{2}s, and 500 kg/m^{2}s. Each figure shows a slight mass flux dependence as higher mass fluxes give higher void

fractions for the same average quality. Appendix B contains additional figures of more detailed plots showing the effects of mass flux.

6.1.3- Effect of Heat Flux on Void Fraction

The effect of heat flux on the test section is depicted in Figures 6.4 and 6.5 for both R134a and R410A, respectively. Each figure plots void fraction against average quality and contrasts heat fluxes of 0 W/m^2, 3 W/m^2, and 10 W/m^2. Both figures indicate that void fraction is independent of heat flux. Figures in Appendix B are of more detailed plots showing the effects of heat flux.

It is important to note here, as in the last chapter, that the above mentioned plots are made against average quality and not inlet quality. In calculating the average quality the test section heat flux must be taken into account.

6.1.4- Effect of Diameter on Void Fraction

A companion study by Yashar [1998] was done on the same experimental apparatus using a 7.25 mm base diameter axially grooved tube. Figure 6.6 is a plot of void fraction vs. average quality for the axially grooved tubes distinguishing the two different diameters. A slight deviation appears between the two diameters. For axially grooved tubes larger diameters tends toward higher void fractions.

6.1.5- Effect of Micro-fins on Void Fraction

Figure 6.7 is a plot of void fraction vs. average quality for the 6.12 mm inner diameter smooth tube and 8.93 inner diameter axially grooved tube. In the axially grooved tube the void fractions appear to be slightly less (1-2%) at the same average quality. This suggests that enhancing the tube lowers the void fraction.

6.2- Correlation Comparison

This section will discuss the accuracy of the correlations for the axially grooved tube data. The only correlations that will be compared are the ones that performed reasonably well for the smooth tube data which are the Smith, Wallis, Tandon, and Premoli correlations. The correlations not discussed here are presented in graphical form in Appendix B.

Figure 6.8 is a plot of void fraction versus the Smith correlation for the 8.89 mm inner diameter axially grooved tube. The Smith correlation predicts the void fraction within 7.3% with an average deviation of 2.4% with the experimental data. Looking closer at the Smith correlation a mass flux preference appears as the data is layered by mass flux. At a mass flux of 500 kg/m^{2}s, the Smith correlation under predicts the void fraction, but at the lower mass flow rates the Smith correlation over predicts the void fraction. The Smith correlation does an excellent job of centering the data giving no preference of over predicting or under predicting the void fraction.

The accuracy of the Wallis correlation appears in Figure 6.9. The experimental void fraction is accurately predicted to within 14.3% within an average deviation from the Wallis correlation of 3.4%. The majority of the data points lie below the 45° line indicating the Wallis correlation over predicts the void fraction. A mass flux preference is also depicted as the data points for the 500 kg/m^{2}s mass flux lie above the lower mass flux data points.

A plot showing the accuracy of the Tandon correlation appears in Figure 6.10. The Tandon correlation is accurate to within 7.8% with an average deviation of 2.3% from the experimental data. The data is centered and no mass flux preference is seen, but a refrigerant preference is depicted. The data points for the R134a data lie above the data points for the R410A data.

Figure 6.11 is a plot of the experimental void fraction against the Premoli correlation. The Premoli correlation is accurate to 5.6% with an average deviation of

1.9% to the experimental data. The Premoli correlation centers the data well and shows no preference to mass flux or refrigerant.

Figure 6.12 through Figure 6.15 are plots of void fraction with respect to the Smith, Wallis, Tandon, and Premoli correlations, respectively. Yashar's data was added to these figures to display the effect of diameter on each correlation. These figures indicate no dependence on diameter for any of the correlations.

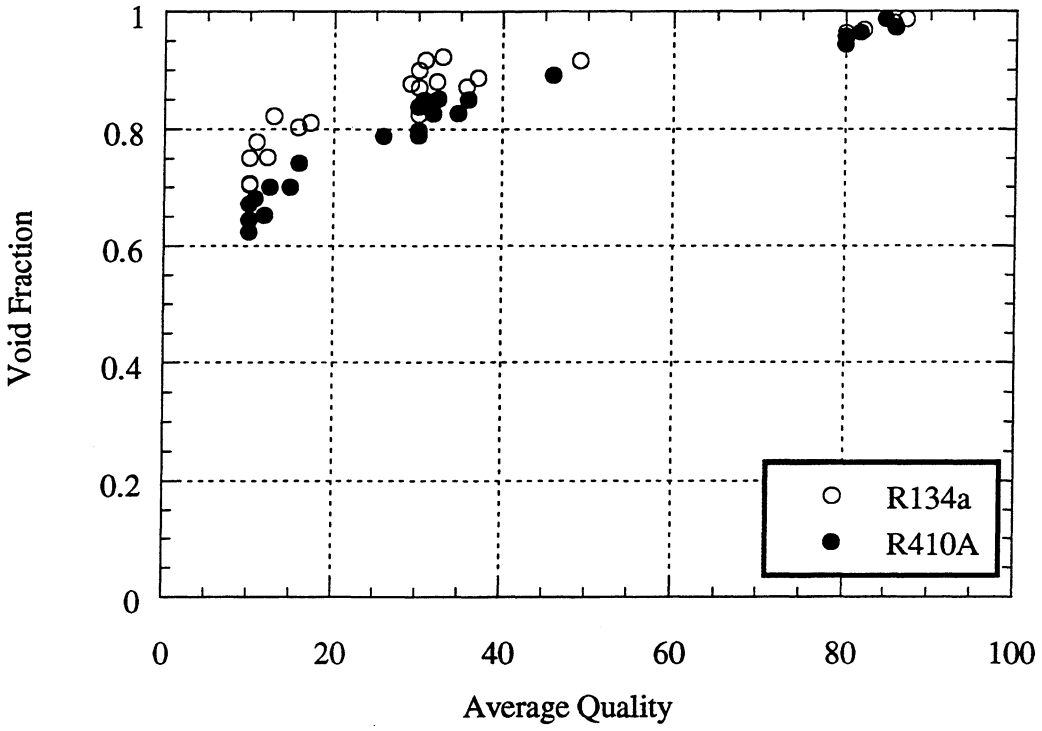

Figure 6.1 Void fraction vs. average quality for a 8.89 mm base diameter axially grooved tube.

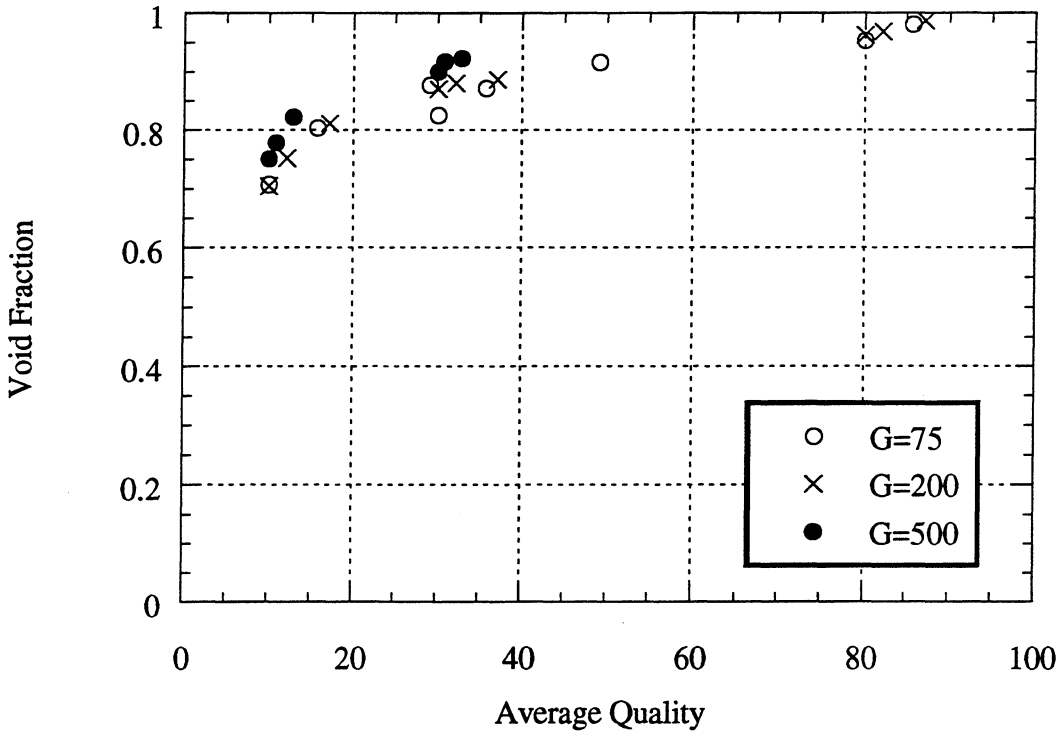

Figure 6.2 Void fraction vs. average quality using R134a in a 8.89 mm base diameter axially grooved tube. Mass flux (G) given in kg/m^{2}s.

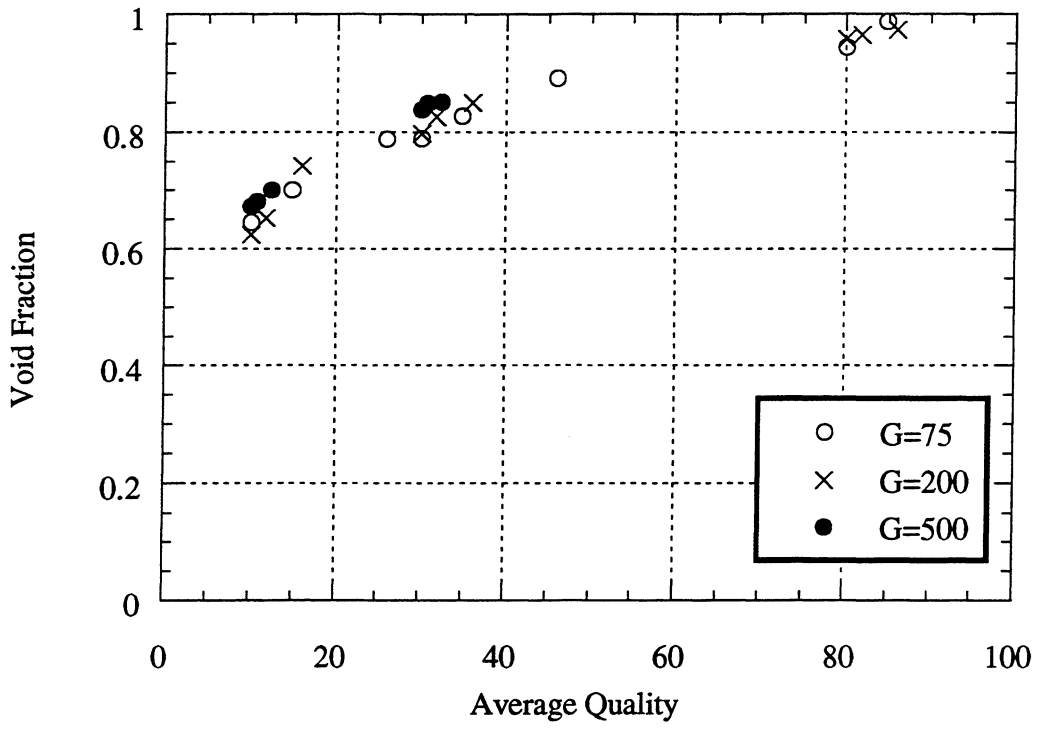

Figure 6.3 Void fraction vs. average quality using R410A in a 8.89 mm base diameter axially grooved tube. Mass flux (G) given in kg/m^{2}s.

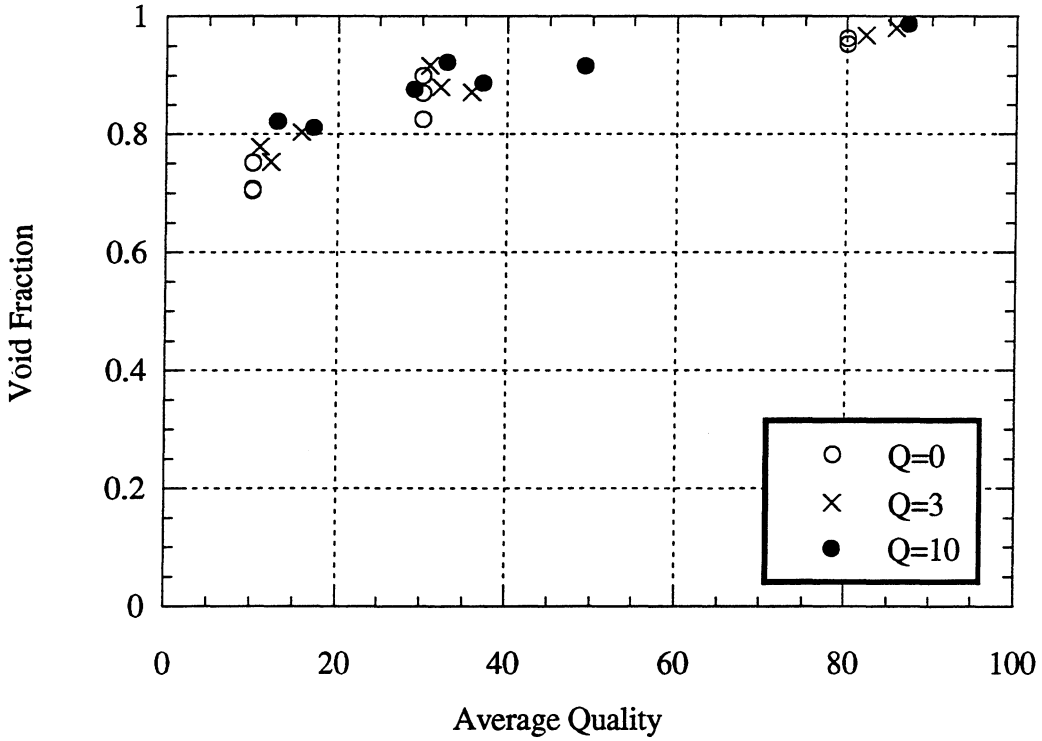

Figure 6.4 Void fraction vs. average quality using R134a in a 8.89 mm base diameter axially grooved tube. Test section heat flux (Q) given in W/m^2.

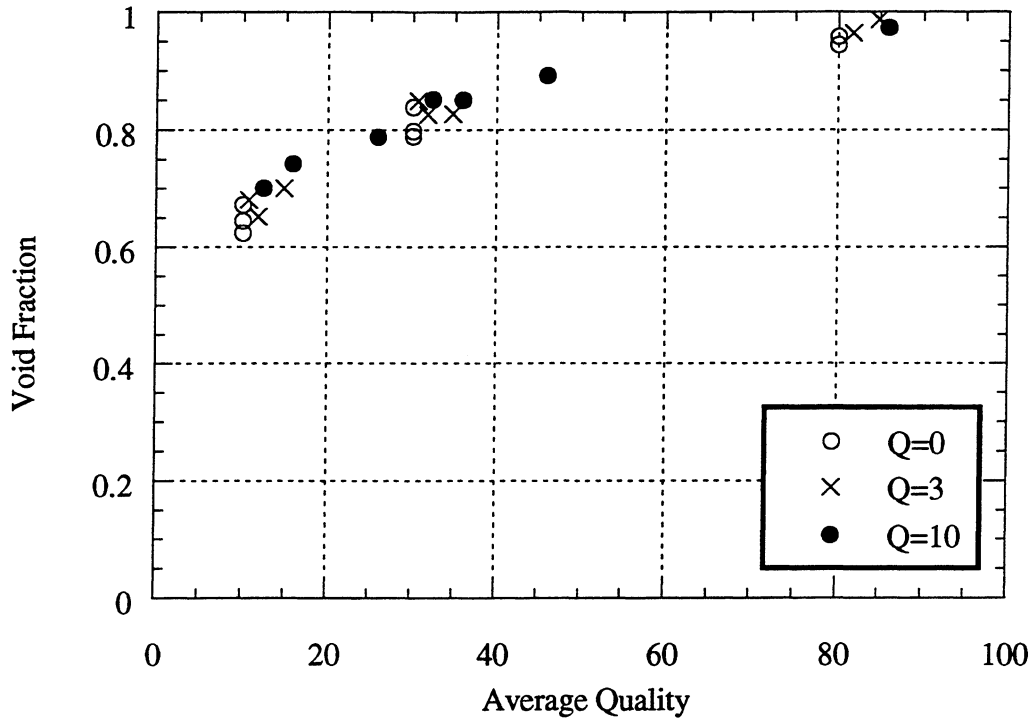

Figure 6.5 Void fraction vs. average quality using R410A in a 8.89 mm base diameter axially grooved tube. Test section heat flux (Q) given in W/m^2.

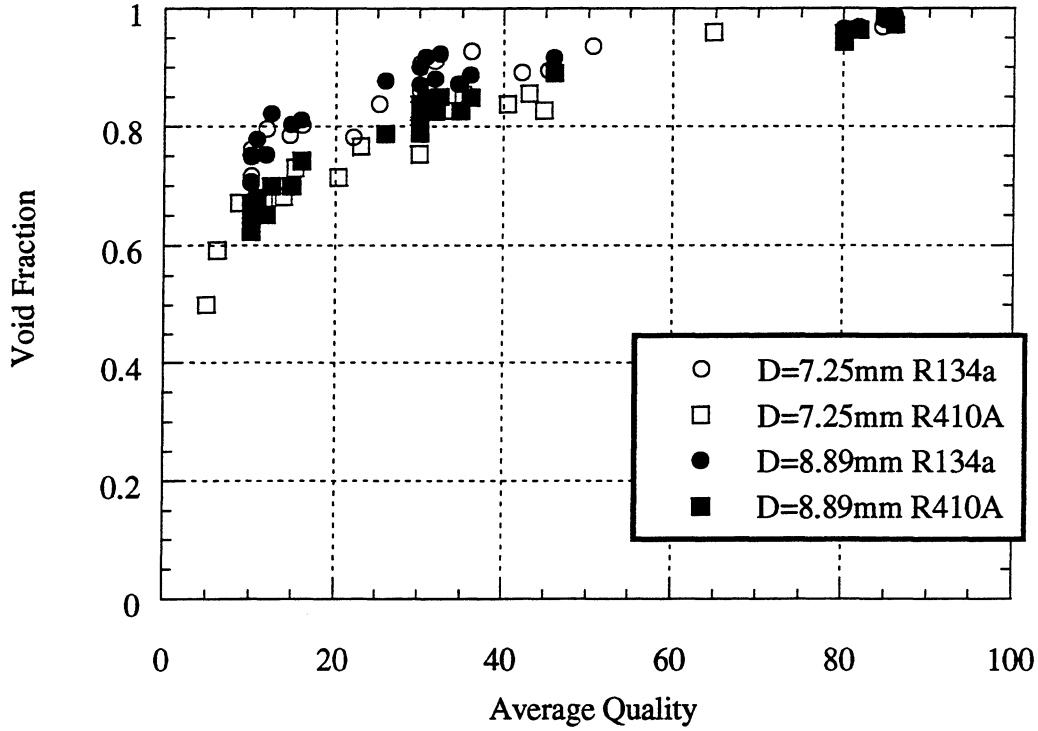

Figure 6.6 Void fraction vs. average quality for 8.89 mm and 7.25 mm base diameter axially grooved tube using R134a and R410A.

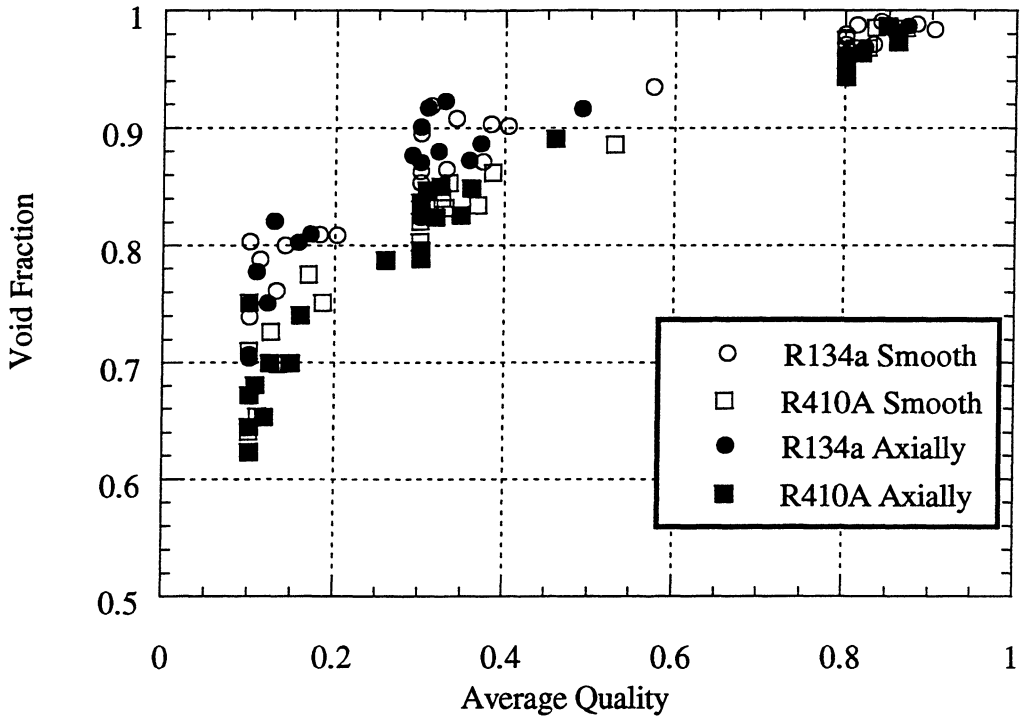

Figure 6.7 Void fraction vs. average quality for 6.12 mm inner diameter smooth tube and 8.89 mm base diameter grooved tube using R134a and R410A.

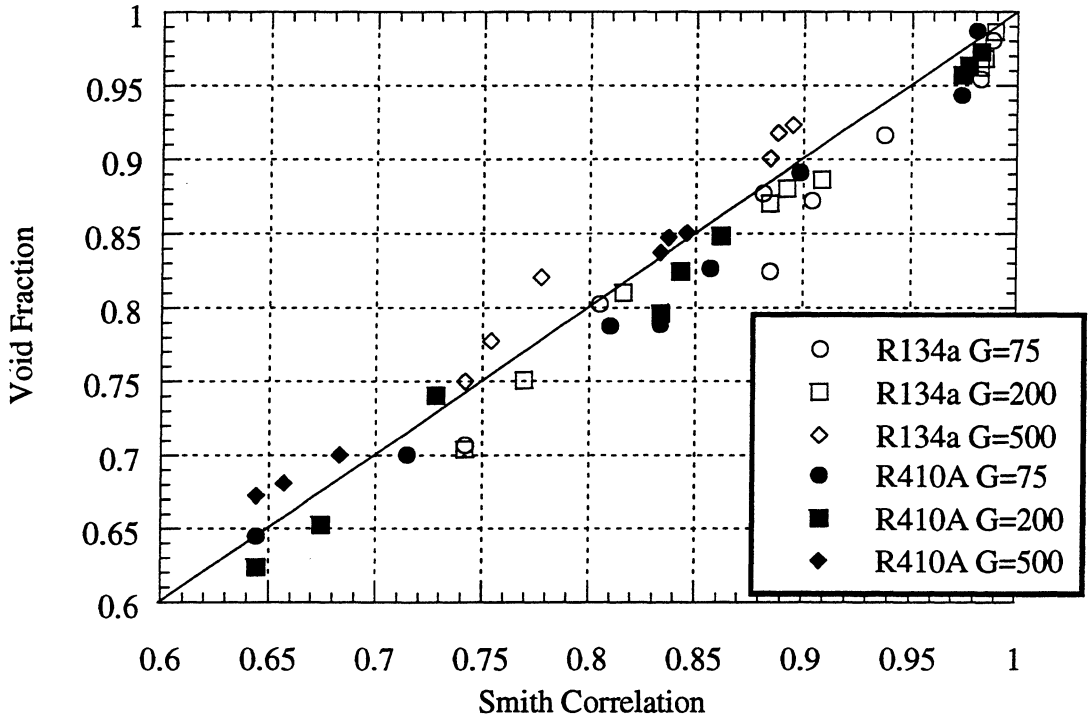

Figure 6.8 Void fraction vs. Smith correlation for 8.93 mm base diameter axially grooved tube using R134a and R410A. Mass Flux (G) in kg/m^2s.

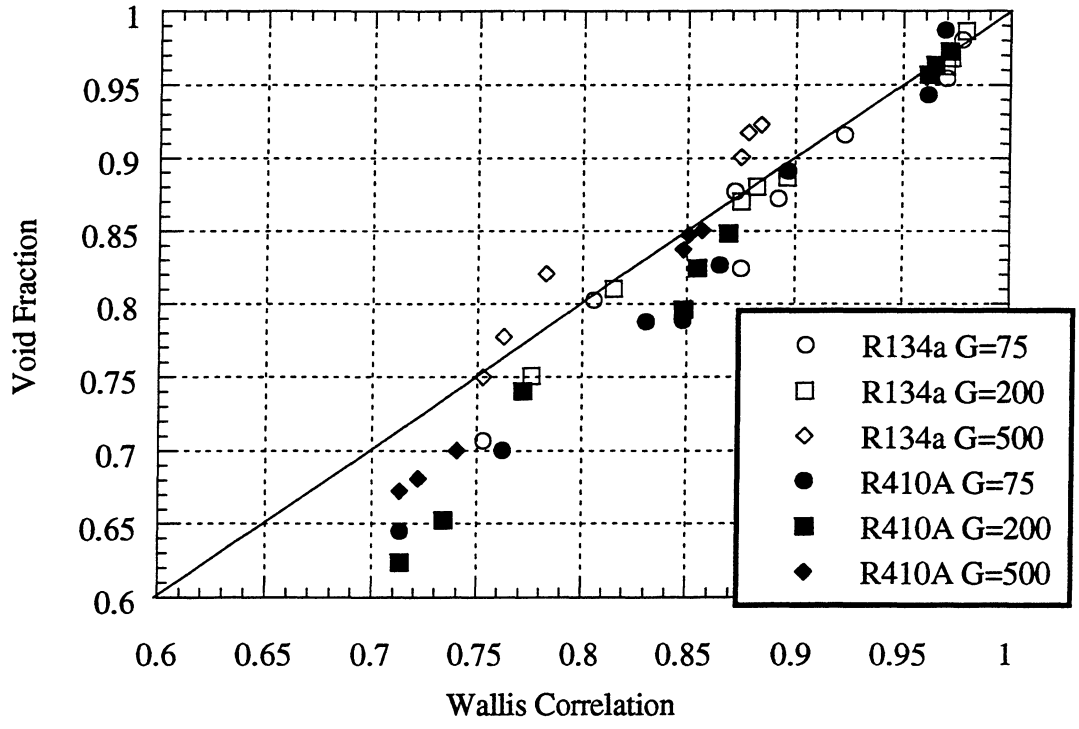

Figure 6.9 Void fraction vs. Wallis correlation for 8.93 mm base diameter axially grooved tube using R134a and R410A. Mass Flux (G) in kg/m^{2}s.

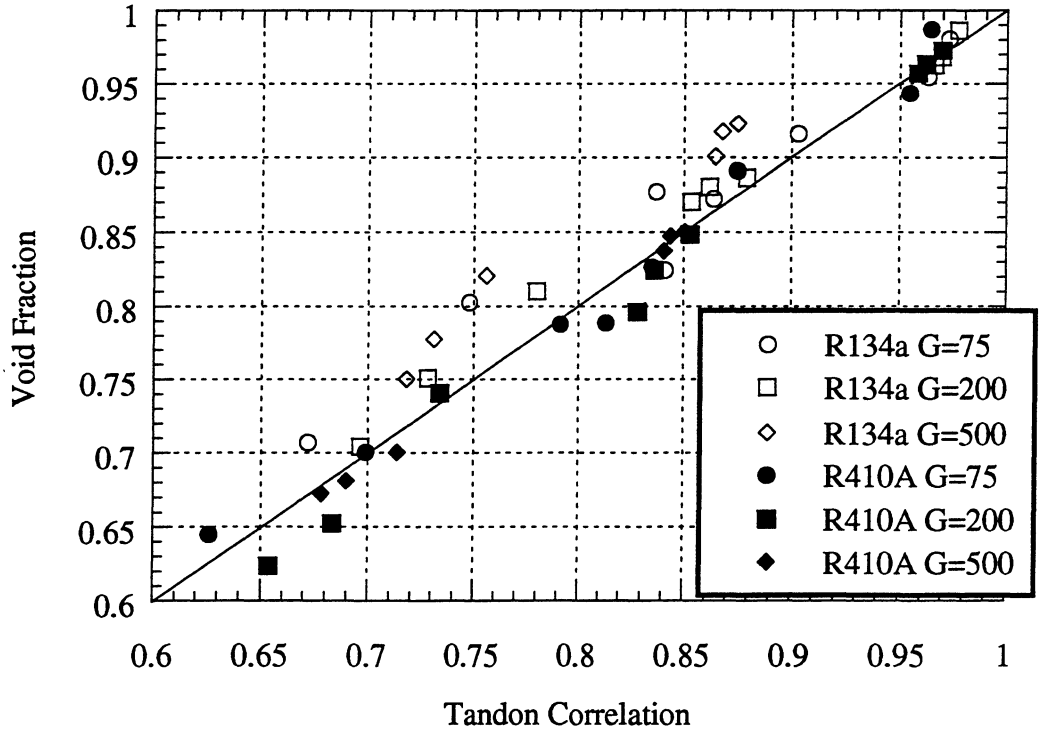

Figure 6.10 Void fraction vs. Tandon correlation for 8.93 mm base diameter axially tube using R134a and R410A. Mass Flux (G) in kg/m^{2}s.

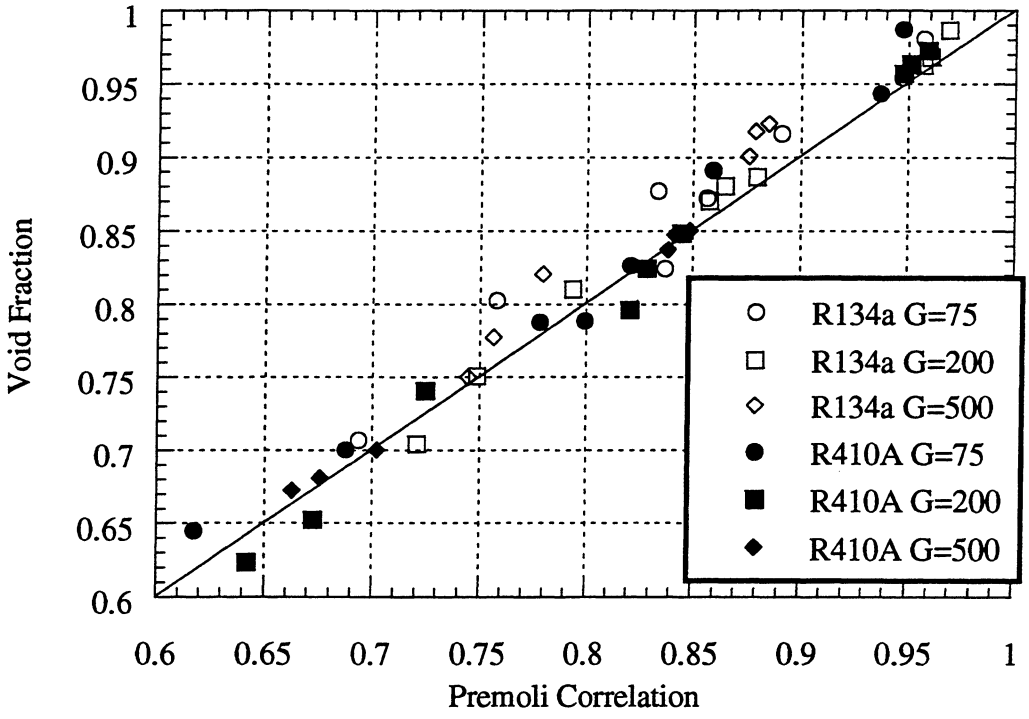

Figure 6.11 Void fraction vs. Premoli correlation for 8.93 mm base diameter axially tube using R134a and R410A. Mass Flux (G) in kg/m^{2}s.

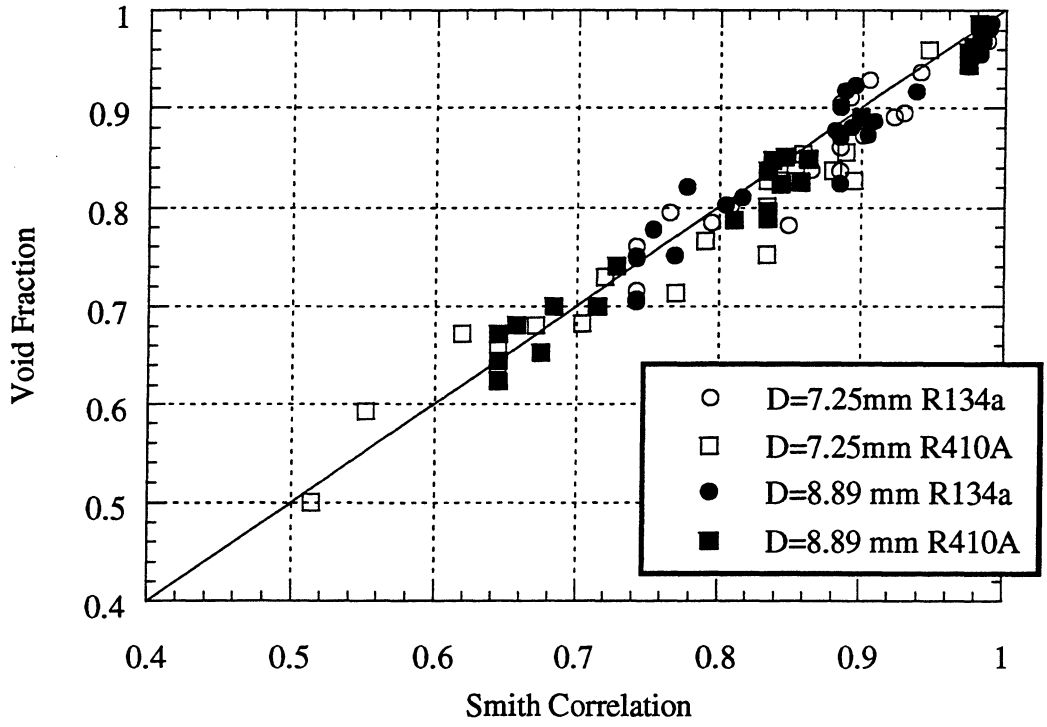

Figure 6.12 Void fraction vs. Smith correlation for 7.25 mm and 8.93 mm base diameter axially grooved tube using R134a and R410A.

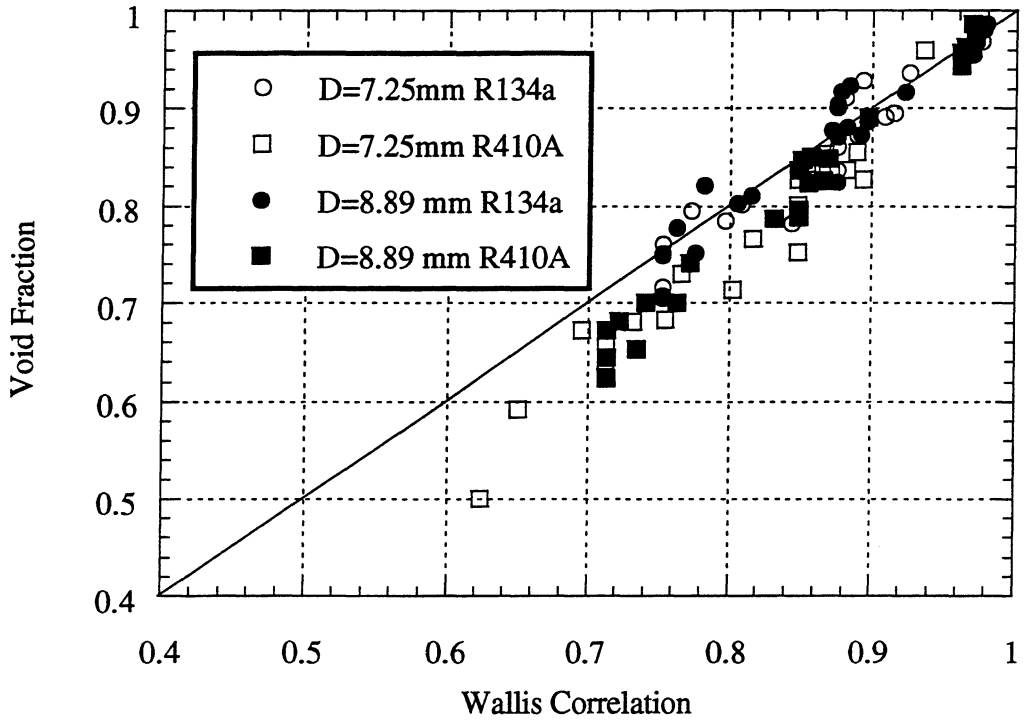

Figure 6.13 Void fraction vs. Wallis correlation for 7.25 mm and 8.93 mm base diameter axially grooved tube using R134a and R410A.

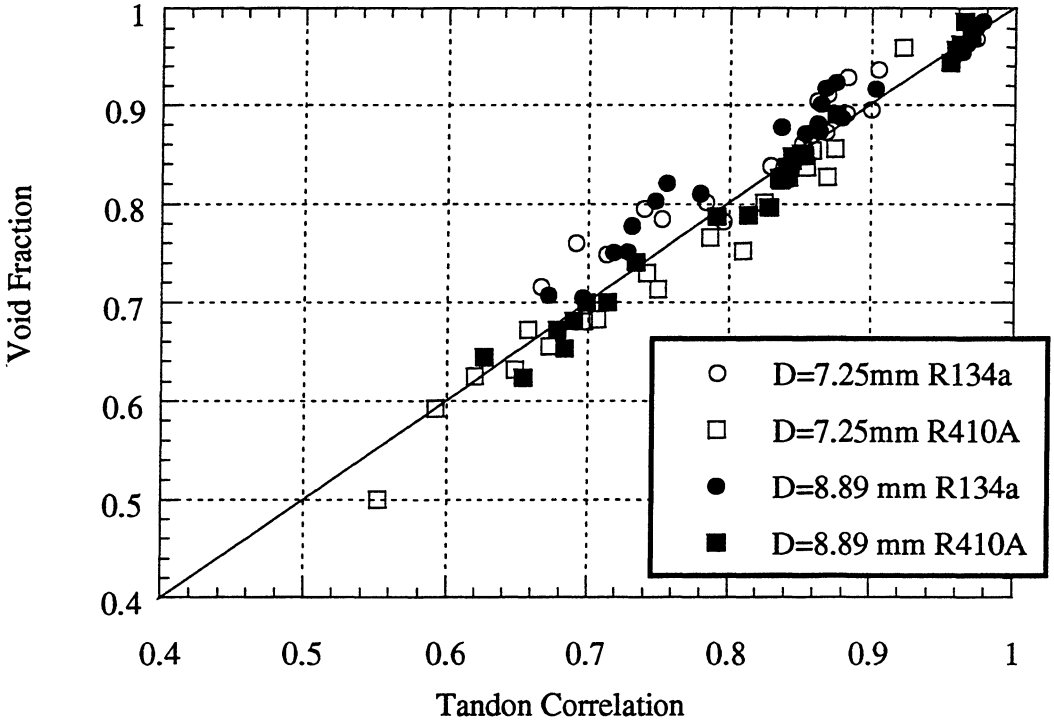

Figure 6.14 Void fraction vs. Tandon correlation for 7.25 mm and 8.93 mm base diameter axially grooved tube using R134a and R410A.

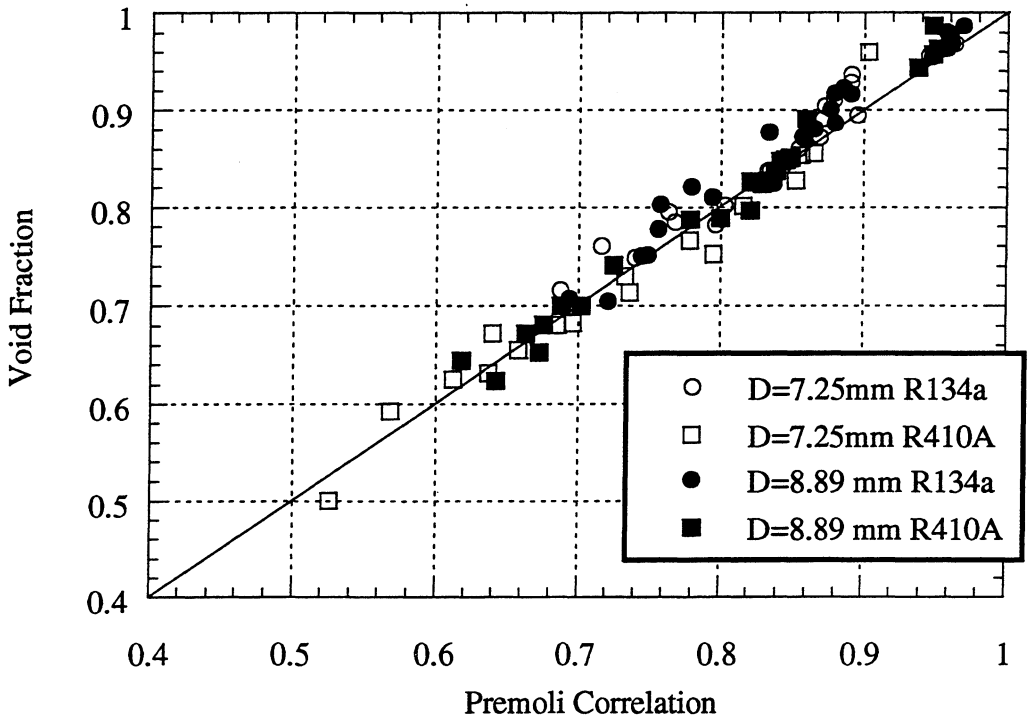

Figure 6.15 Void fraction vs. Premoli correlation for 7.25 mm and 8.93 mm base diameter axially grooved tube using R134a and R410A.

Chapter 7

Helically Grooved Tube Results

This chapter will present and discuss void fraction results obtained with a 8.93 mm base diameter helically grooved tube with an 18° helix angle. These results were found using the equipment and methodology discussed in chapters 3 and 4 using R134a and R410A. Chapter 8 will discuss a void fraction model to correlate all of the smooth and microfinned tube data.

7.1- Void Fraction Results

This section will present the void fractions experimentally obtained on the helical tube. The effects of refrigerant, mass flux, heat flux, diameter, and internal geometry will also be discussed.

7.1.1- Effect of Refrigerant on Void Fraction

Figure 7.1 plots void fraction versus average quality for a 8.93 mm base diameter helically grooved tube using R134a and R410A. The plots shows R134a having a higher void fraction (~7%) that R410A at the same quality. This was expected since 410A has a higher vapor pressure and higher vapor density which allows the vapor to flow slower.

7.1.2- Effect of Mass Flux on Void Fraction

Plots showing the dependence of mass flux on void fraction are show in Figures 7.2 and 7.3 for R134a and R410A respectively. These two figures plot void fraction against average test section quality while the data points distinguish mass flux. Both figures show that higher mass fluxes tend to give slightly higher void fractions at the same quality. Appendix C contains more descriptive plots of the data and trends described here.

7.1.3- Effect of Heat Flux on Void Fraction

Figures 7.4 and 7.5 plot void fraction vs. average quality for a 8.93 mm base diameter helically grooved tube distinguishing different heat fluxes for R134a and R410A respectively. The heat fluxes generated were 0 W/m^2 (adiabatic), 3 W/m^2, and 10 W/m^2. Neither figure depicts void fraction being a function of heat flux. Figures in Appendix C contain more detailed graphs of the trends and data presented in this section.

It is important to note here as well as in previous chapters that all plots are made against average quality and not inlet quality. Heat flux does affect the average quality and thus has an indirect effect on the void fraction.

7.1.4- Effect of Diameter on Void Fraction

Figure 7.6 is a plot of void fraction vs. average quality for 7.25 mm and 8.93 mm base diameter helically grooved tubes. For R134a near a quality of 30% it appears that the smaller tube gives a slightly higher void fraction at the same quality. The rest of the plot shows void fraction being independent of diameter. It is the author's opinion that Figure 7.6 depicts no influence of diameter on void fraction and the aforementioned specific points are within experimental error of supporting this claim.

7.1.5- Effects of Tube Enhancements on Void Fraction

Figure 7.7 is a plot comparing the void fraction in the 8.93 mm base diameter helically grooved tube to the 6.12 mm inner diameter smooth tube. The figure shows the helically grooved tube giving a slightly lower void fraction at the same quality. Figure 7.8 is a plot comparing the void fractions of the 8.93 mm base diameter helically grooved tube to the 8.89 mm base diameter axially grooved tube. This figure depicts the helically grooved tube having a slightly lower void fraction at the same qualities.

7.2- Correlation Comparison

This section will discuss the accuracy of the Smith, Wallis, Tandon, and Premoli correlations for the helically grooved tube. Though the other seven correlations discussed in the literature are not discussed here graphs of the accuracy for those correlations appear in Appendix C.

A plot of the measured void fraction vs. the Smith correlation appears in Figure 7.9. The Smith correlation predicts the void fraction to within 9.2% with an average deviation of 3.25%. The Smith correlation also shows a mass flux preference as the data points representing higher flow rates are above the data points representing slower flow rates. The void fraction is under predicted for a mass flux of 500 kg/m^2s, but over predicted for slower mass fluxes. The Smith correlation also sees the swing representative of the slip ratio correlations (see discussion in Chapter 5). Smith over predicts the void fraction at high qualities, but the curve swings out and begins under predicting the void fraction.

Figure 7.10 depicts the accuracy of the Wallis correlation. The Wallis correlation predicts the void fraction to within 11% with an average deviation of 3.3%. The Wallis correlation appears to over predict as most of the data lies below the 45° line. The Wallis correlation also depicts mass flux and refrigerant segregation.

The accuracy of the Tandon correlation appears in Figure 7.11. The Tandon correlation is accurate within 9.5% with an average deviation of 3.2%. The Tandon correlation centers the data nicely and no mass flux preference can be seen. A refrigerant segregation is depicted as the R134a data lies on top of the R410A data.

Figure 7.12 is a plot showing the accuracy of the Premoli correlation. Premoli's correlation is accurate within 9.1% with an average deviation from the experimental data of 2.5%. A slight mass flux dependence is seen at lower void fractions and the data points depicting R410A do tend to lie below the R134a points. On the whole though the data does look evenly mixed. Most of the data lies above the 45° line indicating that the Premoli correlation slightly under predicts the void fraction.

Figure 7.13-7.16 are plots of void fraction vs. the Smith, Wallis, Tandon and Premoli correlation, respectively. These plots distinguish the two different tube diameters to aid in determining if the correlations have a diameter preference. No diameter preferences are seen in the four plots.

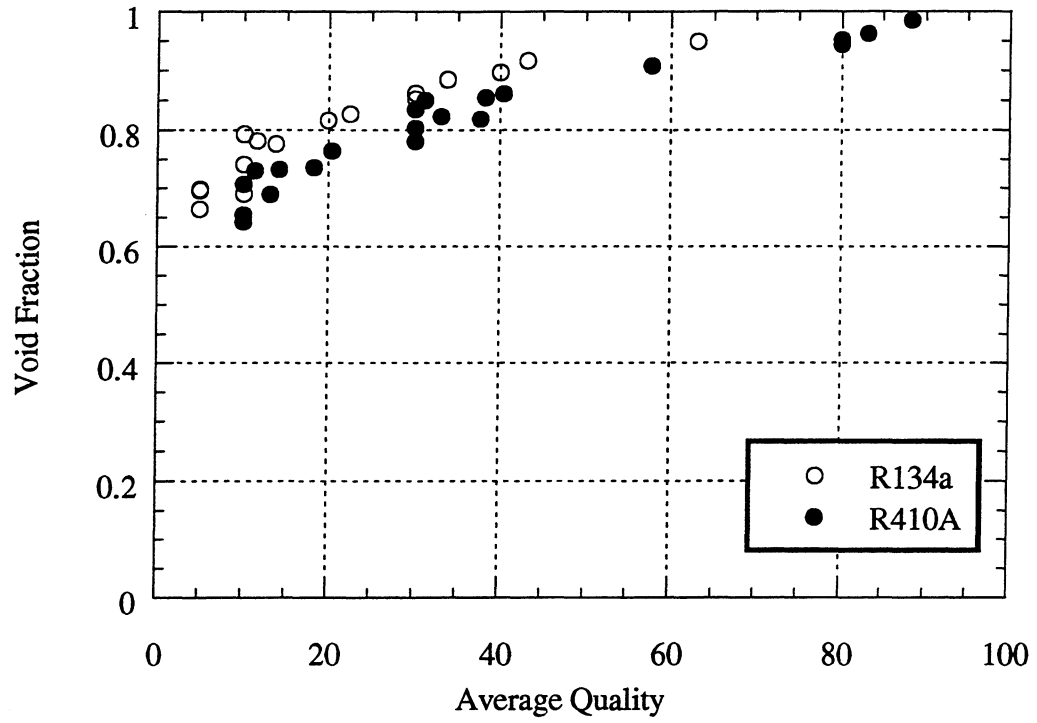

Figure 7.1 Void fraction vs. average quality for a 8.93 mm base diameter 18° helically grooved tube.

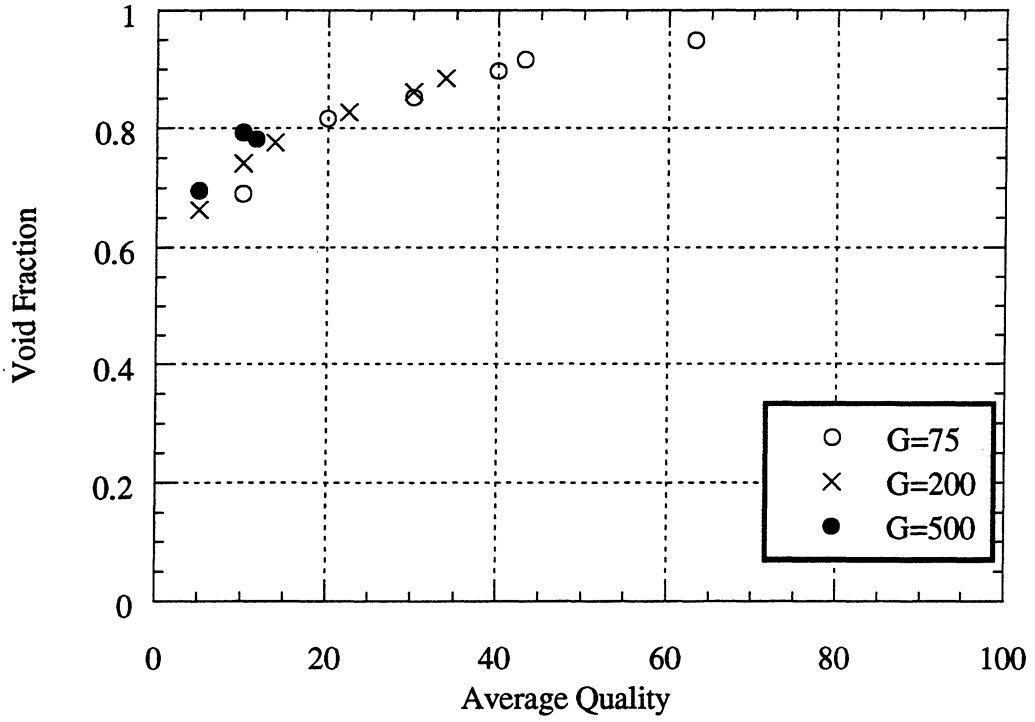

Figure 7.2 Void fraction vs. average quality using R134a in a 8.93 mm base diameter 18° helically grooved tube. Mass Flux (G) given in kg/m^2s.

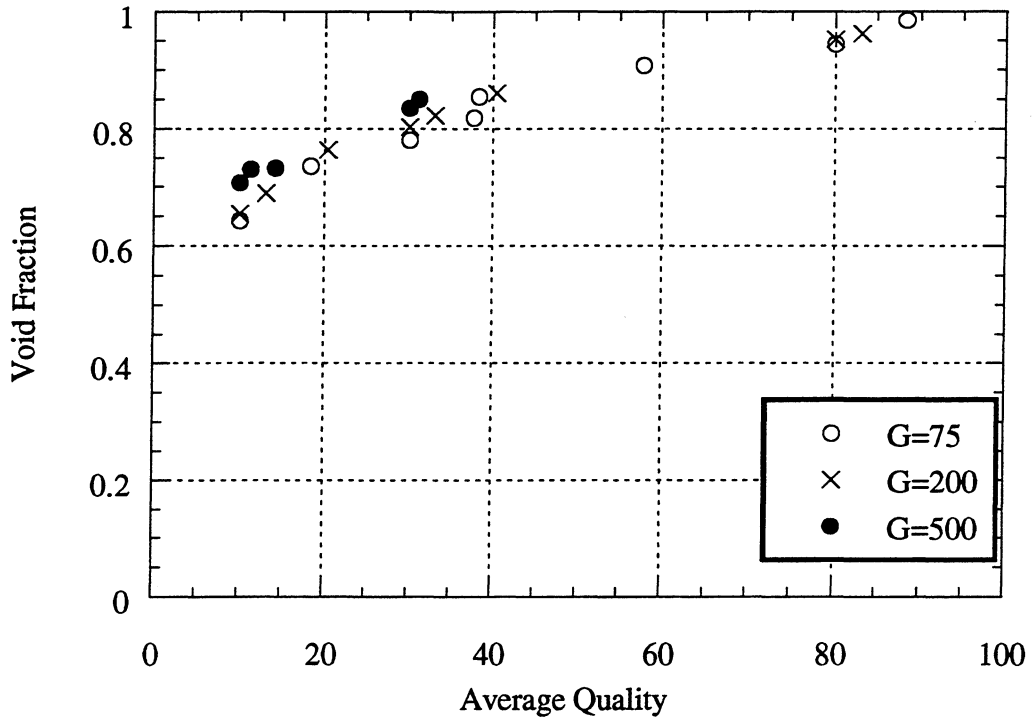

Figure 7.3 Void fraction vs. average quality using R410A in a 8.93 mm base diameter 18° helically grooved tube. Mass flux (G) given in kg/m^{2}s.

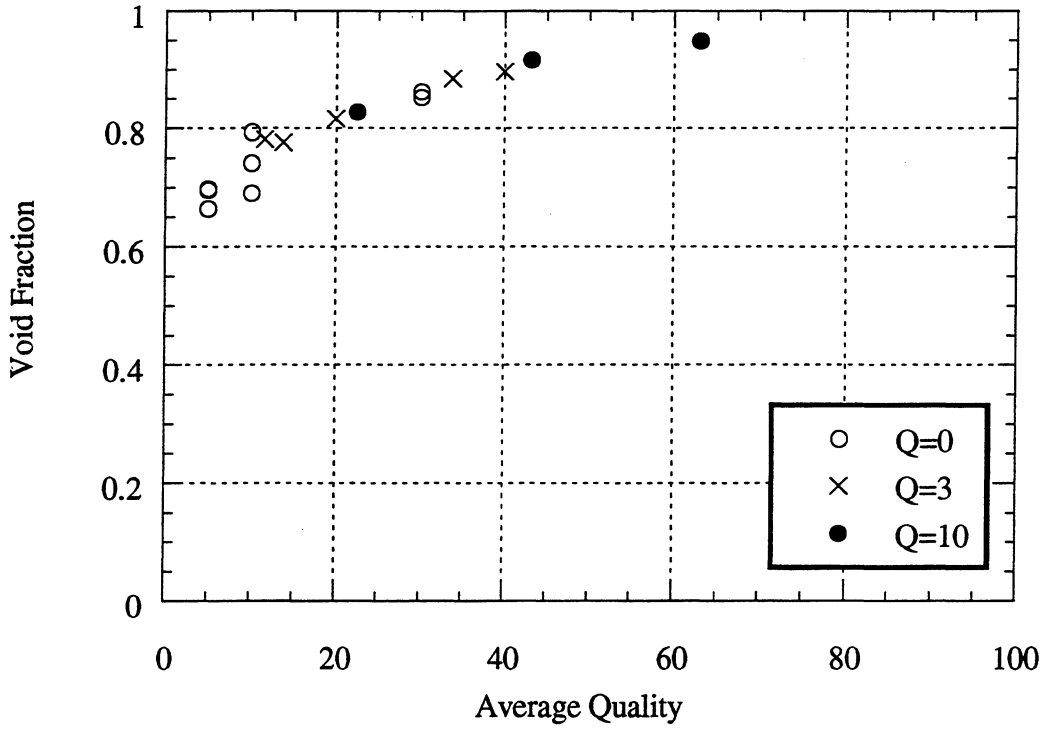

Figure 7.4 Void fraction vs. average quality using R134a in a 8.93 mm base diameter 18° helically grooved tube. Test section heat flux (Q) given in W/m^2.

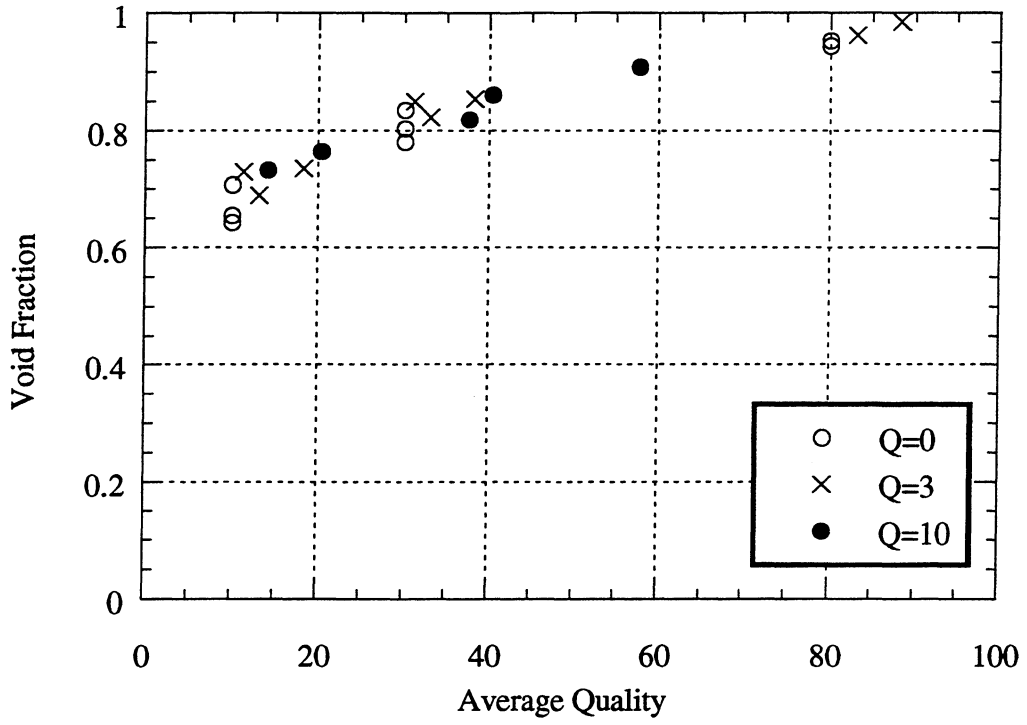

Figure 7.5 Void fraction vs. average quality using R410A in a 8.93 mm base diameter 18° helically grooved tube. Test section heat flux (Q) given in W/m^2.

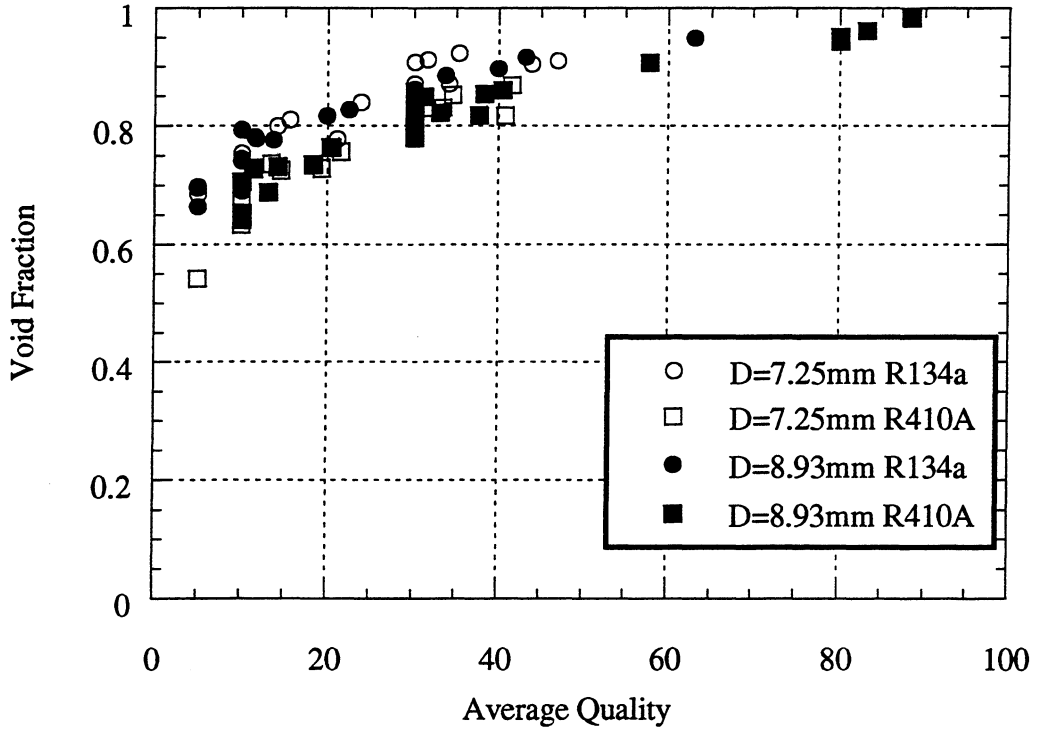

Figure 7.6 Void fraction vs. average quality for 8.93 mm base diameter 18° helically grooved tube using R134a and R410A.

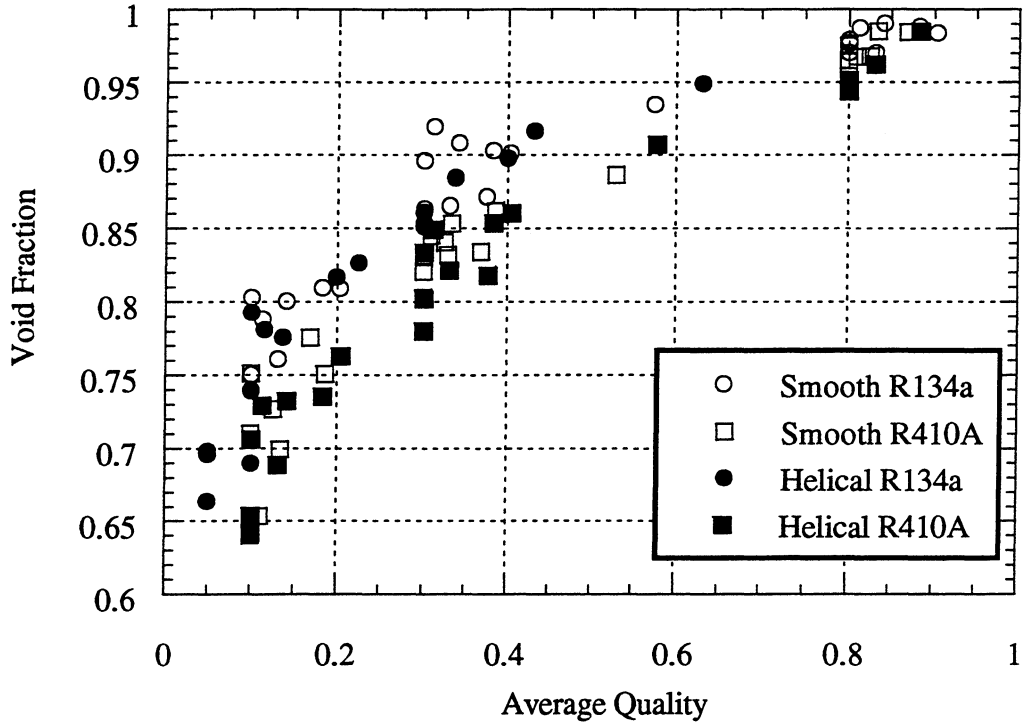

Figure 7.7 Void fraction vs. average quality for 8.93 mm base diameter helically grooved tube and 6.12 mm inner diameter smooth tube.

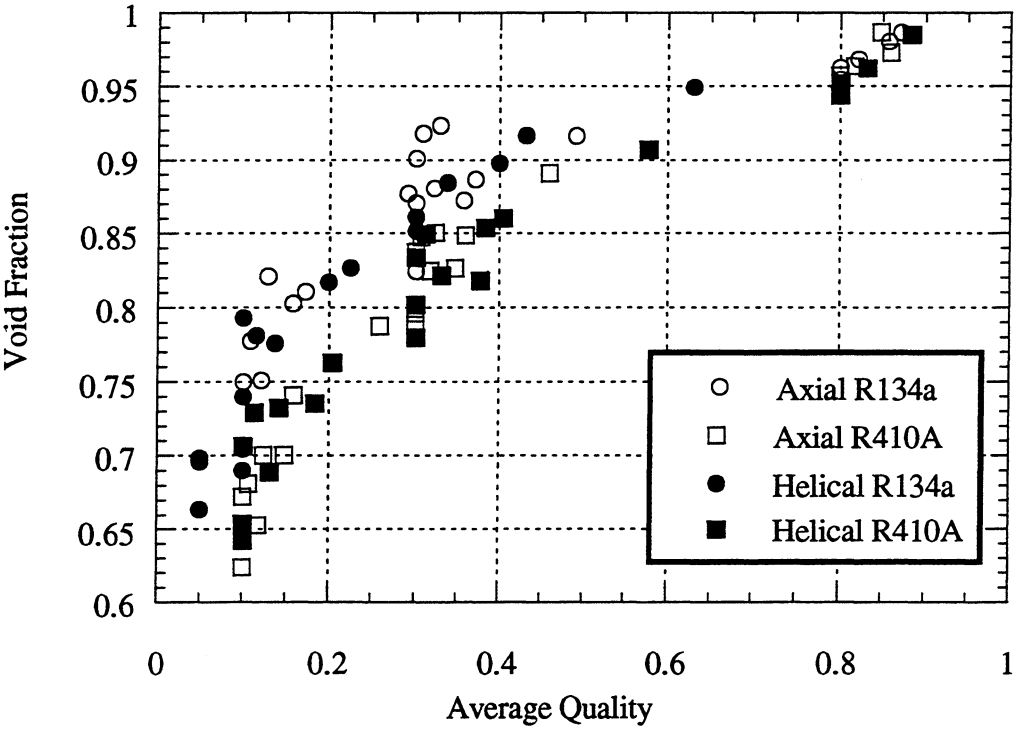

Figure 7.8 Void fraction vs. average quality for 8.93 mm base diameter helically grooved tube and 8.89 mm base diameter axially grooved tube.

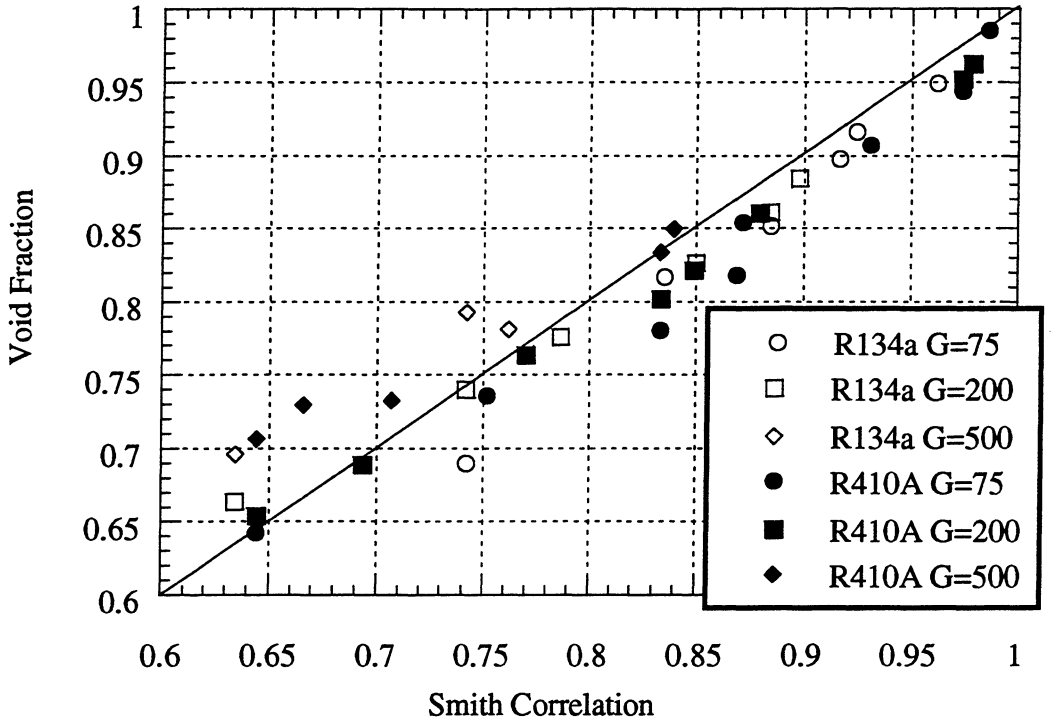

Figure 7.9 Void fraction vs. Smith correlation for 8.93 mm base diameter 18° helically grooved tube using R134a and R410A. Mass flux (G) in kg/m^{2}s.

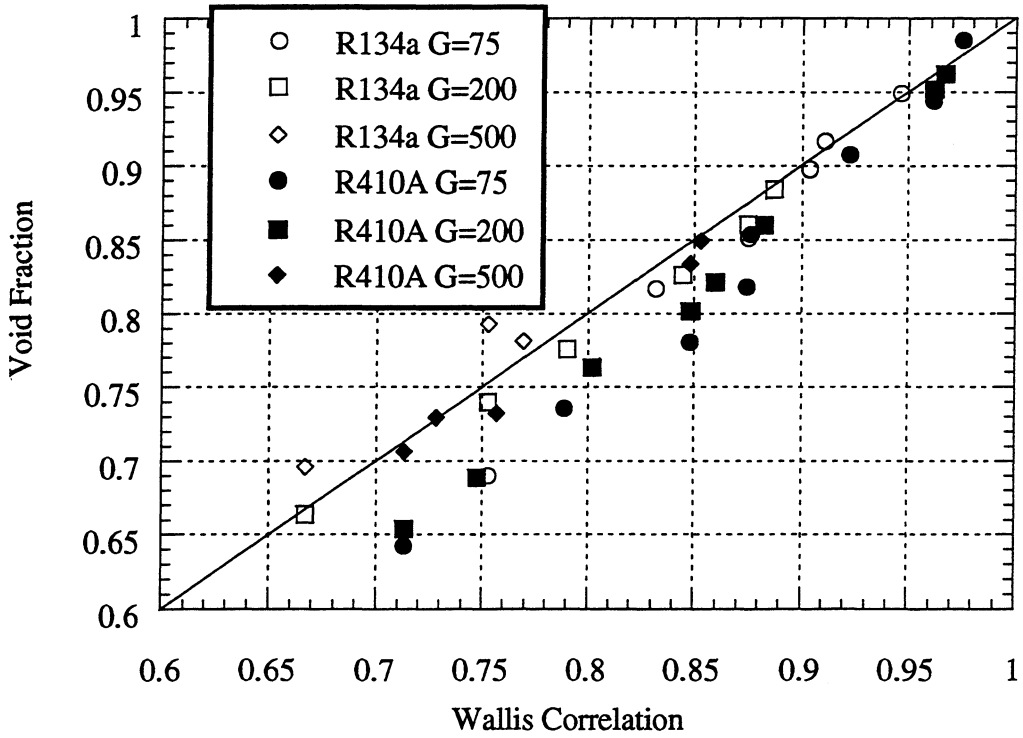

Figure 7.10 Void fraction vs. Wallis correlation for 8.93 mm base diameter 18° helically grooved tube using R134a and R410A. Mass flux (G) in kg/m^{2}s.

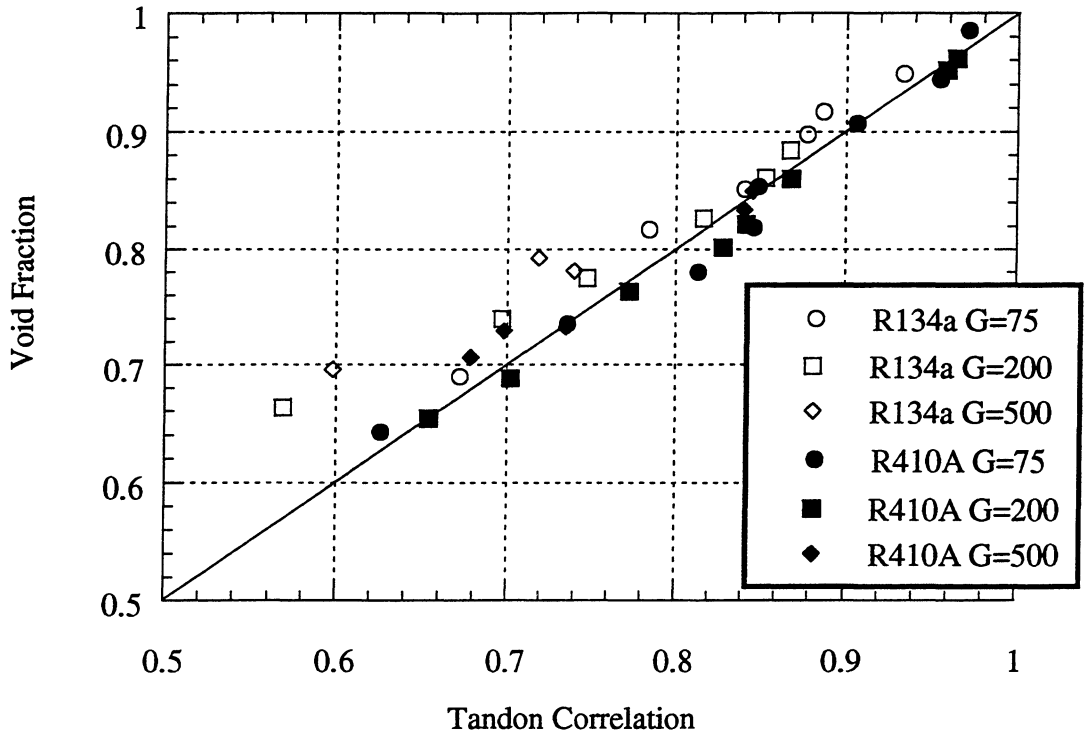

Figure 7.11 Void fraction vs. Tandon correlation for 8.93 mm base diameter 18° helically grooved tube using R134a and R410A. Mass flux (G) in kg/m^{2}s.

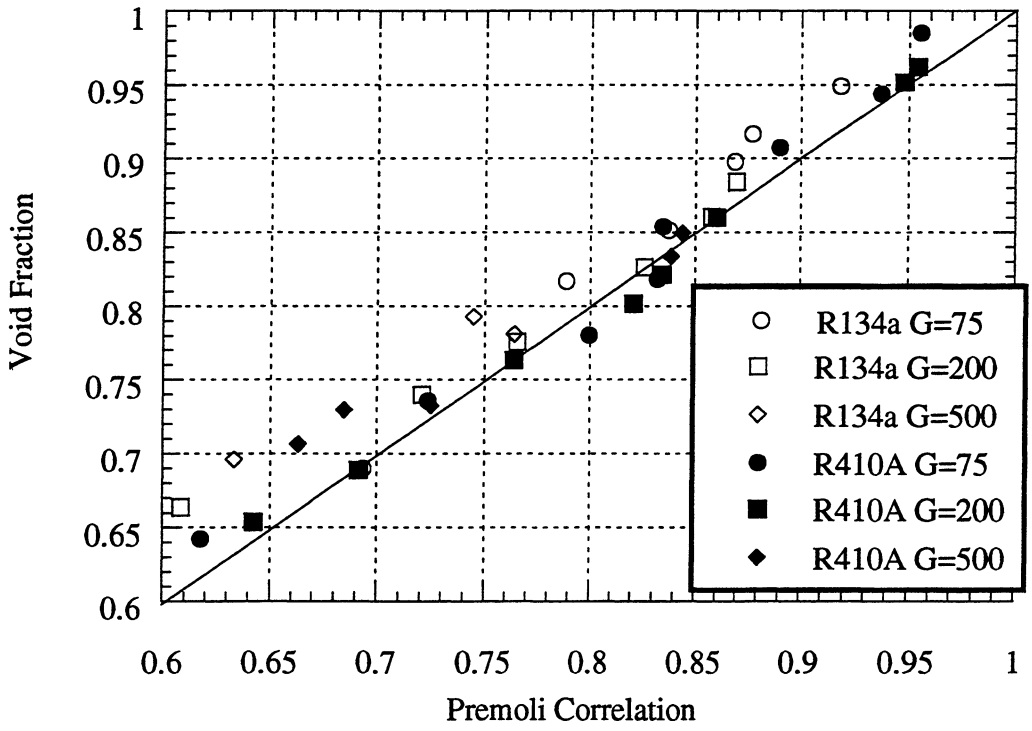

Figure 7.12 Void fraction vs. Premoli correlation for 8.93 mm base diameter 18° helically grooved tube using R134a and R410A. Mass flux (G) in kg/m^{2}s.

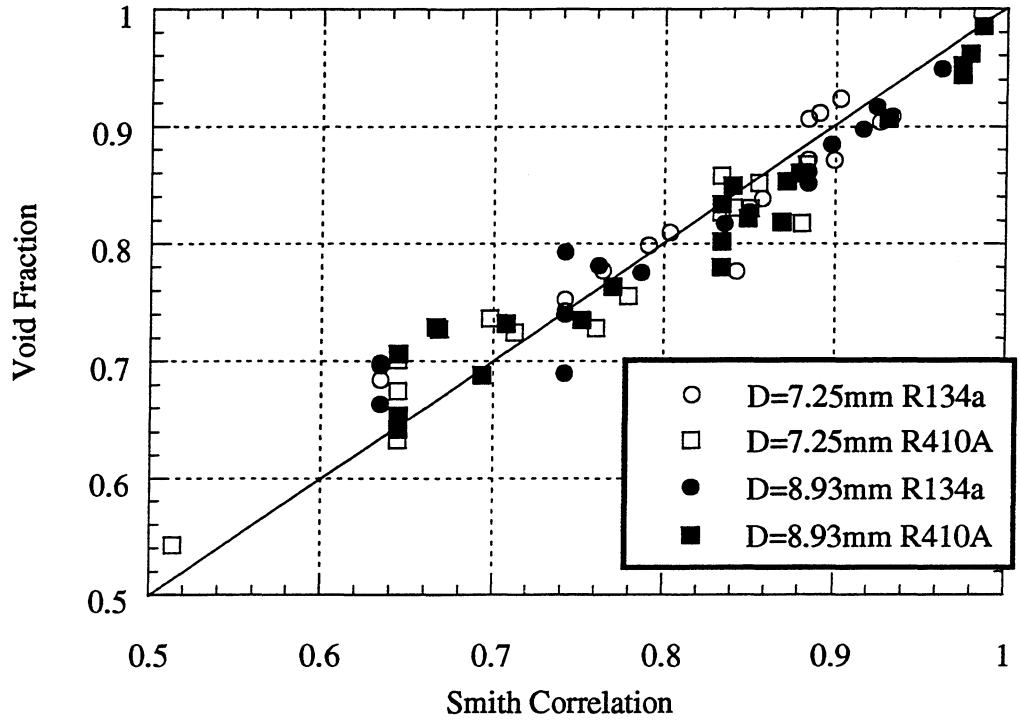

Figure 7.13 Void fraction vs. Smith correlation for 7.26 mm and 8.93 mm base diameter helically grooved tube using R134a and R410A.

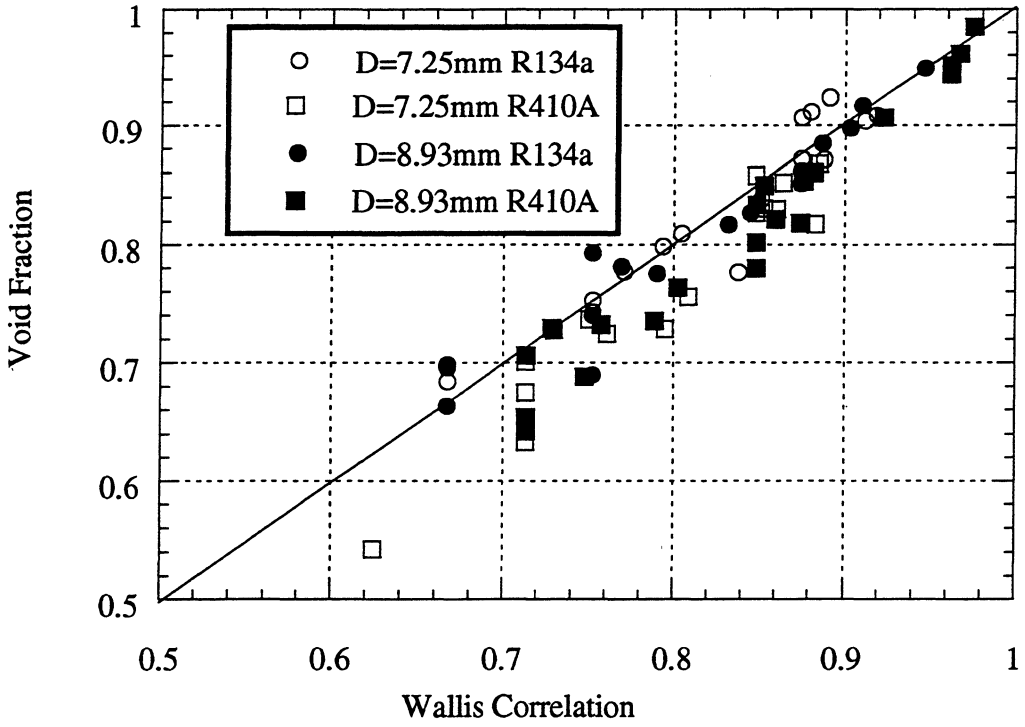

Figure 7.14 Void fraction vs. Wallis correlation for 7.26 mm and 8.93 mm base diameter helically grooved tube using R134a and R410A.

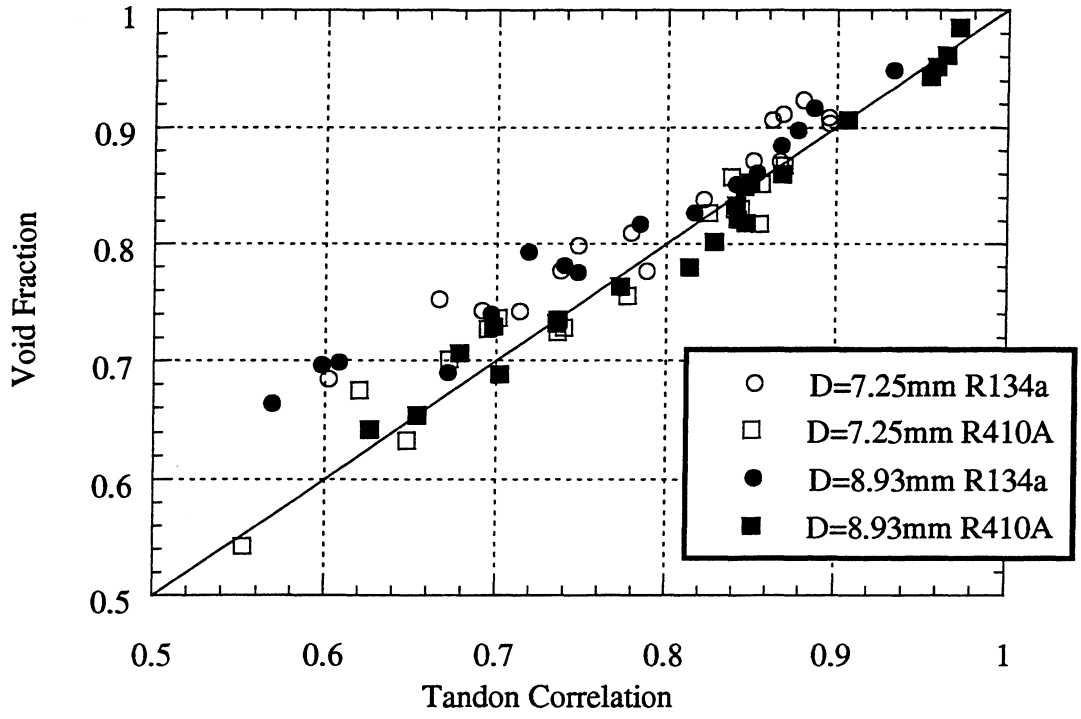

Figure 7.15 Void fraction vs. Tandon correlation for 7.26 mm and 8.93 mm base diameter helically grooved tube using R134a and R410A.

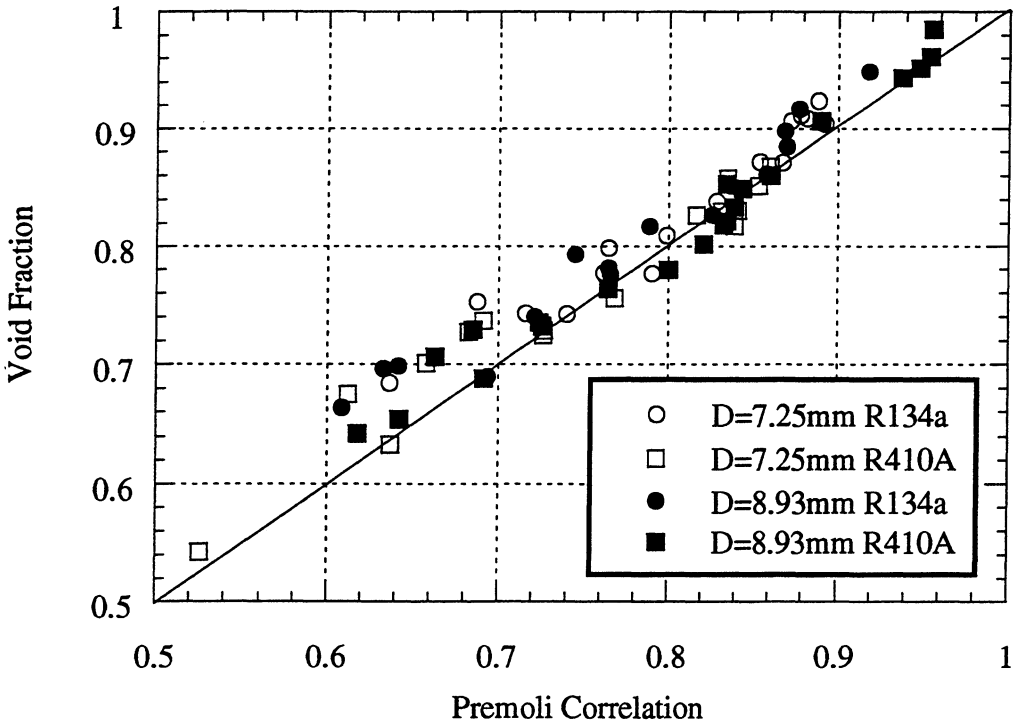

Figure 7.16 Void fraction vs. Premoli correlation for 7.26 mm and 8.93 mm base diameter helically grooved tube using R134a and R410A.

Chapter 8

Conclusions and Recommendations

This final chapter will review all of the void fraction data presented here and in Yashar[1998] and Graham[1998]. A final recommendation of a void fraction model will be given.

8.1- Mass Flux Independence or Dependence

The wide variety of void fraction models emphasize a variety of parameters. Of special interest is the question of void fraction dependence on mass flux. Seven of the correlations model void fraction as being independent of mass flux, four of the correlations state that void fraction is dependent on mass flux. Evaporation data presented here and by Yashar depicts no mass flux dependence except for a slight dependence in the microfinned tubes. Graham, on the other hand, found that during condensation void fraction was dependent on mass flux. Graham's plots shown in Figures 8.1 and 8.2, indicate void fraction is strongly dependent on mass flux for low mass fluxes and low qualities. At higher mass flow rates and higher qualities void fraction is less dependent on mass flux. To further examine the mass flux dependence question, flow regime maps are investigated. The Taitel-Dukler flow map will be used as suggested by Wattelet [1994] and Dobson [1994].

The evaporator data are plotted on the Taitel-Dukler flow map in Figure 8.3 to Figure 8.8. Almost all of the evaporator data lies in the annular flow regime. Some of the lower mass flux data points (G=75 kg/m^{2}s) lie on the border between the annular and stratified regimes. A few of the low quality data points lie on the border of the annular, slug, and bubbly flow regimes.

Graham's condenser data is plotted on the Taitel-Dukler flow regime map in Figure 8.9. All of the low mass flux (G=75 kg/m^{2}s) condenser data points and several of

the low-mid mass flux data points (G=150 kg/m^{2}s) lie in the stratified region. The other data points lie half in the annular regime and half in the slug-plug flow regime.

Flow in the stratified flow regime appears to have a void fraction dependent on mass flux. For flow in the annular flow regime, the void fraction does not appear to be dependent on mass flux. There are not enough points in the slug-plug regime or bubbly regime to state if there is mass flux independence.

Earlier chapters stated that the smooth tube evaporator data did not show a mass flux dependence while the microfinned tubes did show a slight mass flux dependence. It is speculated that the internal grooves move the flow toward the stratified regime and a mass flux dependence. This may explain why the mass flux dependent correlations (Premoli, Tandon) are better predictors of void fraction for the microfinned tubes than for the smooth tubes.

8.2- Correlation Recommendation

Of the four models shown to have good correlation with the experimental data (Wallis, Smith, Premoli, Tandon), all have their own individual problems. The Smith is accurate above 0.70, but shows the systematic curvature of slip-ratio correlations. The Wallis correlation is extremely accurate for R134a, but deviates for R410A. The Tandon correlation performs differently for different refrigerants and tube diameters. The Premoli correlation is accurate, but it is dependent on surface tension which is sometimes difficult to obtain.

The following two sections will suggest models that the author deems valid for predicting refrigerant void fraction. These models are deemed valid for R134a and R410A, with mass fluxes ranging from 75 kg/m^{2}s to 500 kg/m^{2}s, with qualities from 5% to 99%, and heat fluxes of 0 W/m^2 to 10 W/m^2. The following correlations are based on the data here as well as that presented in Yashar. Therefore the correlations are valid for smooth tubes with inner diameters of 4.26 mm to 6.12 mm, axially grooved tubes with base diameters of 7.25 mm to 8.89 mm, and helically grooved tubes with base diameters of 7.26 mm to 8.93 mm.

8.2.1- Adjusted Premoli Correlation

The following recommended correlation is made by adjusting the Premoli correlation. The Premoli correlation does a good job of mixing the data with regard to mass flux, refrigerant, and diameter. The Premoli correlation has a slight mass flux dependence which enables it to accurately model the micro-finned tube data, but it is so slight it does not affect the smooth tube data.

Recalling the Premoli correlation equations from Chapter 2

$$S = 1 + F_1\left(\frac{y}{1+F_2 y} - F_2 y\right)^{\frac{1}{2}} \tag{2.18}$$

$$F_1 = 1.578 \bullet Re_L^{-0.19}\left(\frac{\rho_l}{\rho_g}\right)^{0.22} \tag{2.19}$$

$$F_2 = 0.0273 \bullet We_L\, Re_L^{-0.51}\left(\frac{\rho_l}{\rho_g}\right)^{-0.08} \tag{2.20}$$

$$y = \frac{\beta}{1-\beta} \tag{2.21}$$

$$We_L = \frac{G^2 D_i}{\sigma \rho_l g_c} \qquad \text{Liquid Weber Number} \tag{2.22}$$

$$\beta = \frac{1}{1+\left(\frac{1-x}{x}\right)\left(\frac{\rho_g}{\rho_l}\right)} \tag{2.23}$$

Through a detailed mathematical analysis it was found that the F_2 parameter had little effect on void fraction (<0.5%). Thus the Premoli correlation can be greatly simplified by setting $F_2 = 0$. To properly adjust the data, the constant in front of the F_1 parameter can be adjusted to properly correlate the data.

8.2.1.1- Smooth Tubes

As shown in Figure 5.15, the Premoli correlation consistently under predicts the smooth data. By decreasing the F_1 parameter the smooth tube data can be accurately correlated. The new slip ratio is

$$S = 1 + 1.105 \bullet Re_L^{-0.19} \left(\frac{\rho_l}{\rho_g} \right)^{0.22} y^{\frac{1}{2}} \tag{8.1}$$

Figure 8.10 is a plot of the accuracy of this correlation for the smooth tube data. Above void fractions of 0.75 this correlation is accurate to within 5%, but for lower void fractions the correlation loses accuracy. This correlation predicts all of the data to within 11.5% with an average deviation of 2.5%.

It was stated in Yashar[1998] that for smooth tubes with void fractions below 0.85 all of the correlations showed large amounts of scatter. He went on to state that for lower void fractions in small diameter tubes, the intermittent region is located at a lower value of the Lockhart-Martinelli parameter than suggested by Taitel-Dukler. The data presented here supports that conclusion.

Though this correlation has larger errors at low qualities it holds well for normal evaporator entrance qualities (~20%). Also the errors at the low qualities are not large (<11.5%). Thus this correlation is suitable for modeling evaporators.

8.2.1.2- Axially Grooved Tubes

Referring to Figure 6.11 the Premoli correlation is accurate for the axially grooved tube and requires no adjustment to the F_1 constant. Therefore the slip ratio is

$$S = 1 + 1.578 \bullet Re_L^{-0.19} \left(\frac{\rho_l}{\rho_g} \right)^{0.22} y^{\frac{1}{2}} \tag{8.2}$$

Figure 8.11 is a plot depicting the accuracy of this correlation. The correlation is accurate for all tested diameters, refrigerants, and mass fluxes. The correlation is accurate to within 6% within an average deviation of 2%.

8.2.1.3- Helically Grooved Tubes

Referring to Figure 7.12 the Premoli correlation slightly under predicts the helically grooved tube data. By again slightly adjusting the F_1 constant the accuracy can be greatly improved. The new slip ratio is

$$S = 1 + 1.388 \bullet Re_L^{-0.19} \left(\frac{\rho_l}{\rho_g} \right)^{0.22} y^{\frac{1}{2}} \tag{8.3}$$

Figure 8.12 is a plot showing the accuracy of this correlation. The adjusted correlation is accurate to within 7% within an average deviation of 2.25%.

8.2.2- Froude Rate Correlations

These correlations all are based on an adjusted Froude Rate.

8.2.2.1- Smooth Tubes

When examining the accuracy of Grahams' condenser correlation (see Figure 5.7), three lines appeared on the plot. These three lines represented the three different mass fluxes used. If the void fraction is plotted against Froude Rate divided by mass flux the data collapses as seen in Figure 8.13. Figures in Appendix D depict how this correlation scatters data with respect to mass flux, diameter, and refrigerant. The correlation does show refrigerant segregation for void fractions lower than 0.80, but above void fractions of 0.80 the refrigerant specific data points are well intermixed. This is the same trend seen

by Yashar [1998] and supports his statement about these data points representing a different flow regime.

By simple curve fit of the data in Figure 8.13 the void fraction is related to the Froude Rate by

$$\alpha = -0.0062 * \ln^2\left(\frac{Ft}{G}\right) + 0.0229 * \ln\left(\frac{Ft}{G}\right) + 1.0050 \tag{8.4}$$

If the mass flux was non-dimensionalized by $G_{ref} = 300$ kg/m^{2}s the new fit is

$$\alpha = -0.0062 * \ln^2\left(\frac{Ft}{G/G_{ref}}\right) + 0.0935 * \ln\left(\frac{Ft}{G/G_{ref}}\right) + 0.6726 \tag{8.5}$$

This fit is accurate to within 10% with an average deviation of 2.15%.

8.2.2.2- Axially Grooved Tubes

The micro-finned tubes experimental void fraction appeared to show mass flux dependence, but not as strong as that seen by Graham[1998] for condenser operation in the wavy-stratified range. In order to account for this dependence the Froude rate must be adjusted accordingly to have a small dependence on mass flux.

When trying to correlate the axially grooved tube data against Ft/G three curves appeared for the three different mass fluxes used. Recalling Figure 6.3 and 6.4 the axial tubes showed void fraction to vary with mass flux. The data is re-correlated with $Ft/G^{2/3}$ as the governing parameter to leave some mass flux dependence in the correlating parameter. This collapses the data nicely, but a diameter dependence appears. This diameter dependence is also shown in Figure 6.6. Rearranging the correlating parameter the new parameter is $Ft*D/G^{2/3}$. A plot of void fraction versus this new parameter is in Figure 8.14 and the corresponding curve fit is

$$\alpha = -0.0105 * \ln^2\left(\frac{Ft * D}{G^{2/3}}\right) - .0606 * \ln\left(\frac{Ft * D}{G^{2/3}}\right) + .9035 \qquad (8.6)$$

Non-dimensionalizing with respect to G_{ref} and adding a reference diameter D_{ref} = 8.00 mm, the new correlation is

$$\alpha = -0.0105 * \ln^2\left(\frac{Ft * \frac{D}{D_{ref}}}{\left(\frac{G}{G_{ref}}\right)^{\frac{2}{3}}}\right) + 0.1200 * \ln\left(\frac{Ft * \frac{D}{D_{ref}}}{\left(\frac{G}{G_{ref}}\right)^{\frac{2}{3}}}\right) + .6473 \qquad (8.7)$$

It is found that this correlation is accurate within 10% with an average deviation of 2%. Plots in Appendix D show that the data is well scattered with respect to refrigerant, diameter, and mass flux.

8.2.2.3- Helically Grooved Tubes

The helically grooved tube when plotted against Ft/G showed three lines with respect to each mass flux used in the experiment. When reducing the strength of the denominator the void faction is found to correlate well with respect to $Ft/G^{2/3}$. A plot of void fraction versus $Ft/G^{2/3}$ appears in Figure 8.15 and the corresponding curve fit is

$$\alpha = -0.0035 * \ln^2\left(\frac{Ft}{G^{2/3}}\right) + 0.0619 * \ln\left(\frac{Ft}{G^{2/3}}\right) + 0.9662 \qquad (8.8)$$

If the reference mass flux is used the correlation becomes

$$\alpha = -0.0035 * \ln^2\left(\frac{Ft}{\left(\frac{G}{G_{ref}}\right)^{2/3}}\right) + 0.0883 * \ln\left(\frac{Ft}{\left(\frac{G}{G_{ref}}\right)^{2/3}}\right) + .6808 \qquad (8.9)$$

This correlation correctly predicts the data to within 14.6% with an average deviation of 2%. If the most outlying data point is removed the correlation is accurate to within 8%.

8.3- Conclusions

Many observations were made during this study of void fraction in evaporation. In smooth tubes it was found that void fraction was not dependent on mass flux. In axially grooved tubes void fraction is dependent on both mass flux, and diameter. In helically grooved tubes void fraction is dependent on mass flux, but not diameter. The correlations described above can be used to determine the void fraction to within 10%.

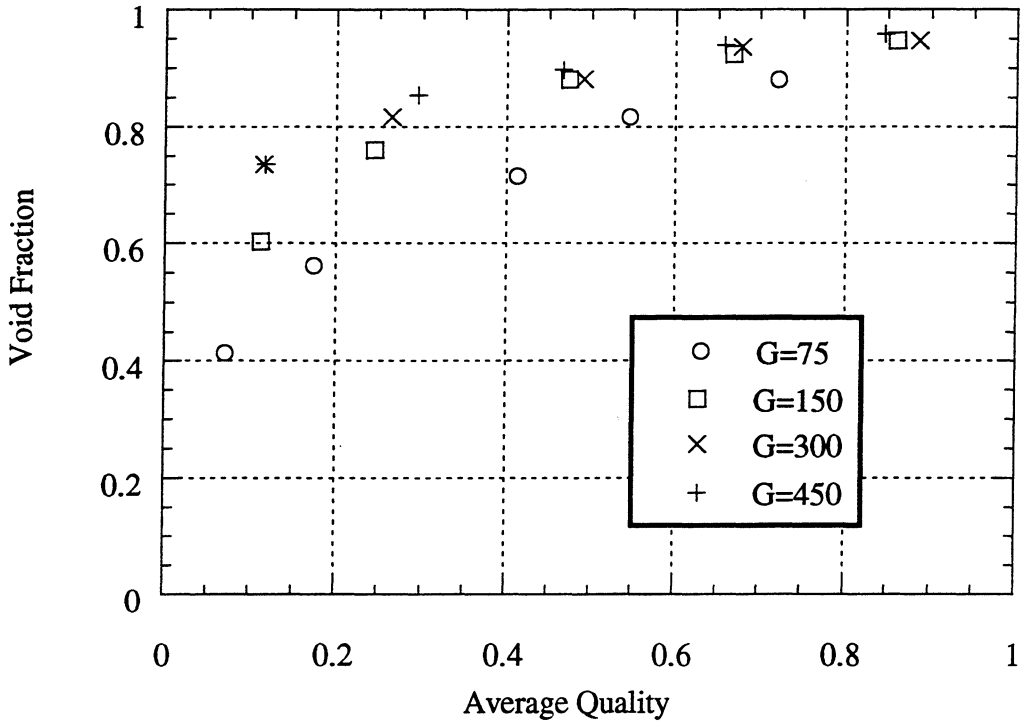

Figure 8.1 Void fraction vs. average quality for Graham's R134a condenser data.

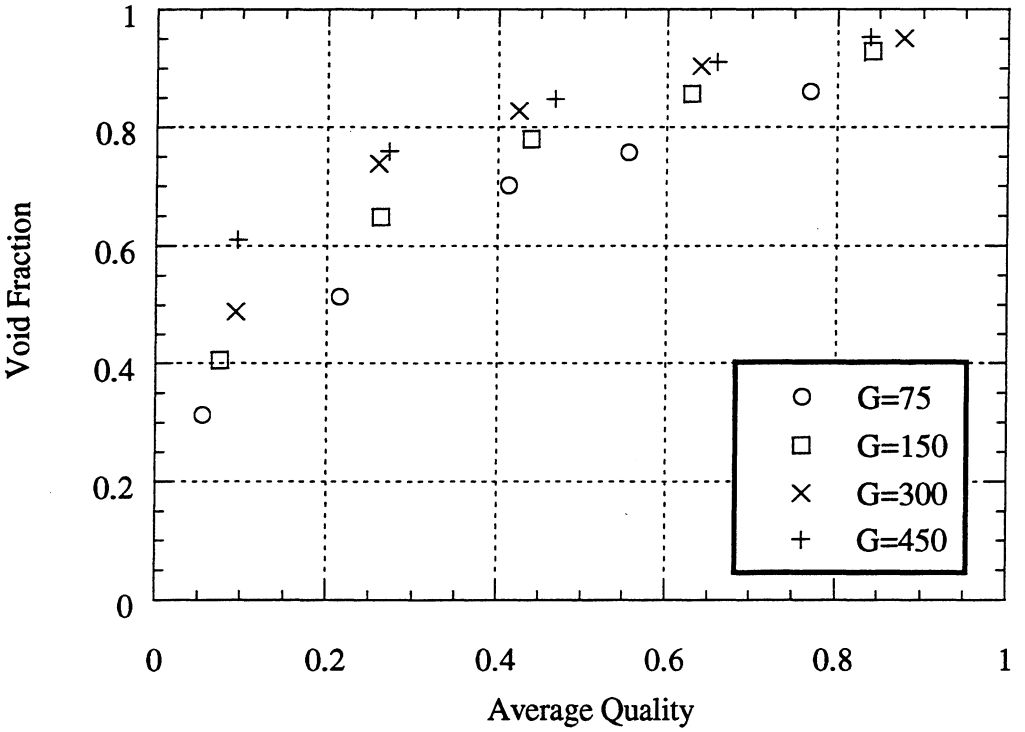

Figure 8.2 Void fraction vs. average quality for Graham's R410A condenser data.

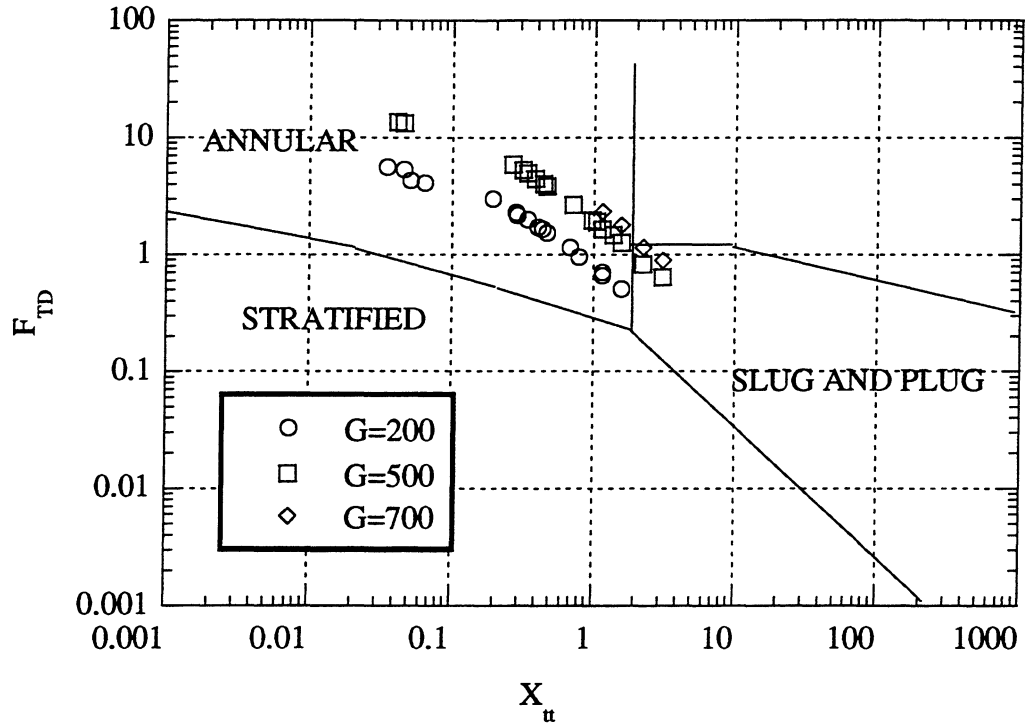

Figure 8.3 Taitel-Dukler Map for 4.26 mm inner diameter smooth tube.

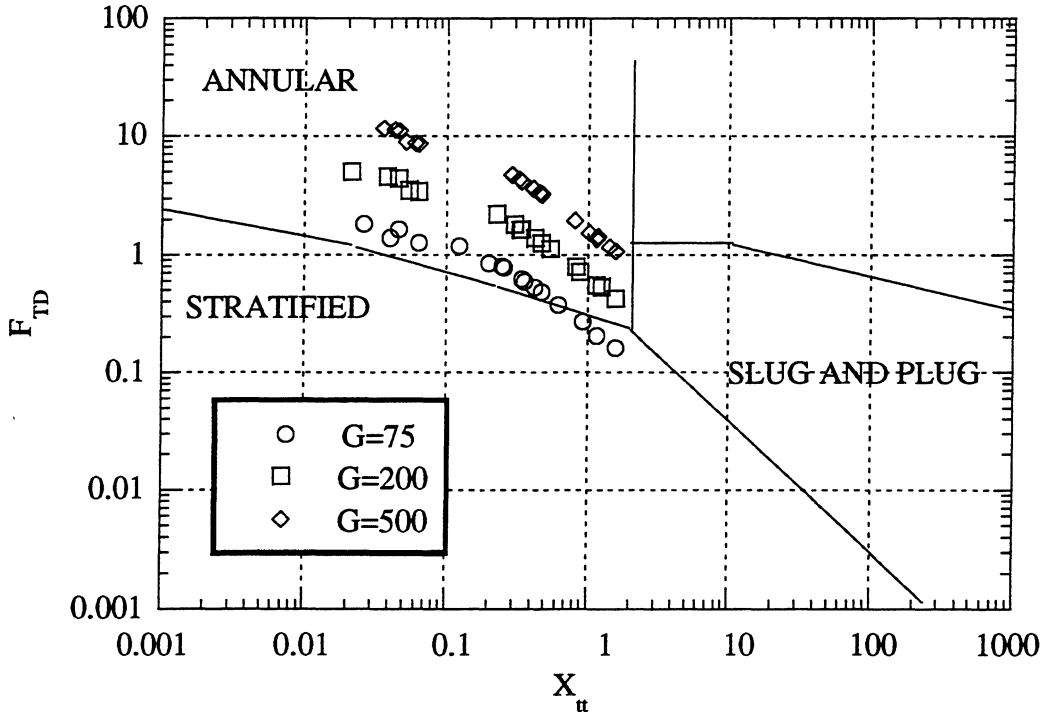

Figure 8.4 Taitel-Dukler Map for 6.12 mm inner diameter smooth tube.

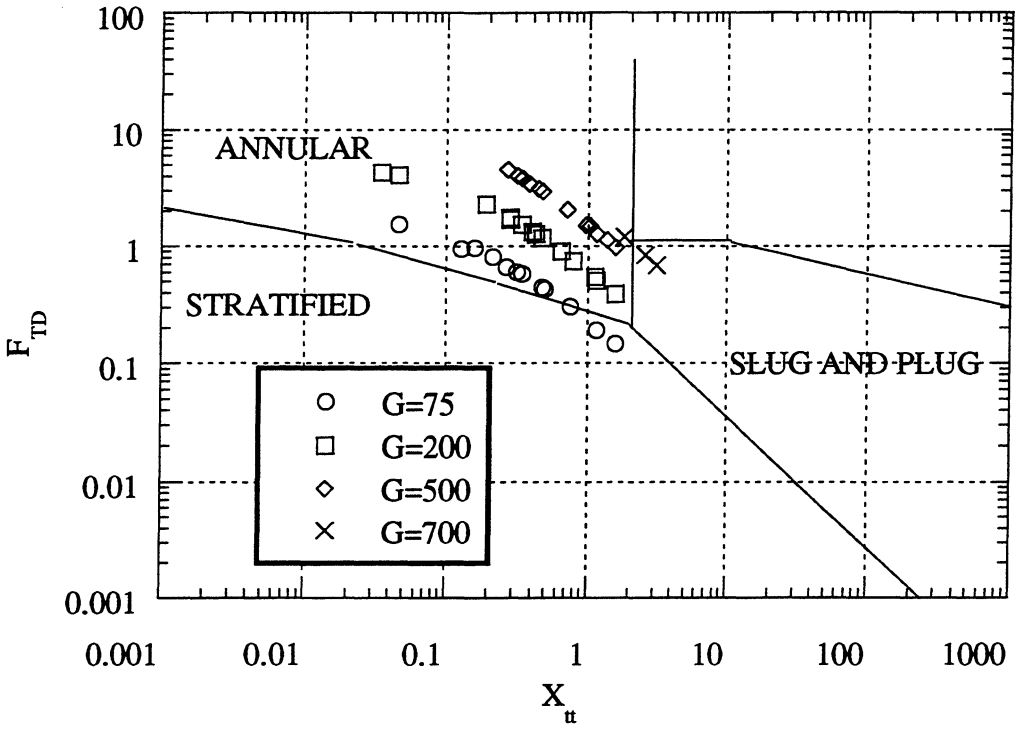

Figure 8.5 Taitel-Dukler Map for 7.25 mm base diameter axially grooved tube.

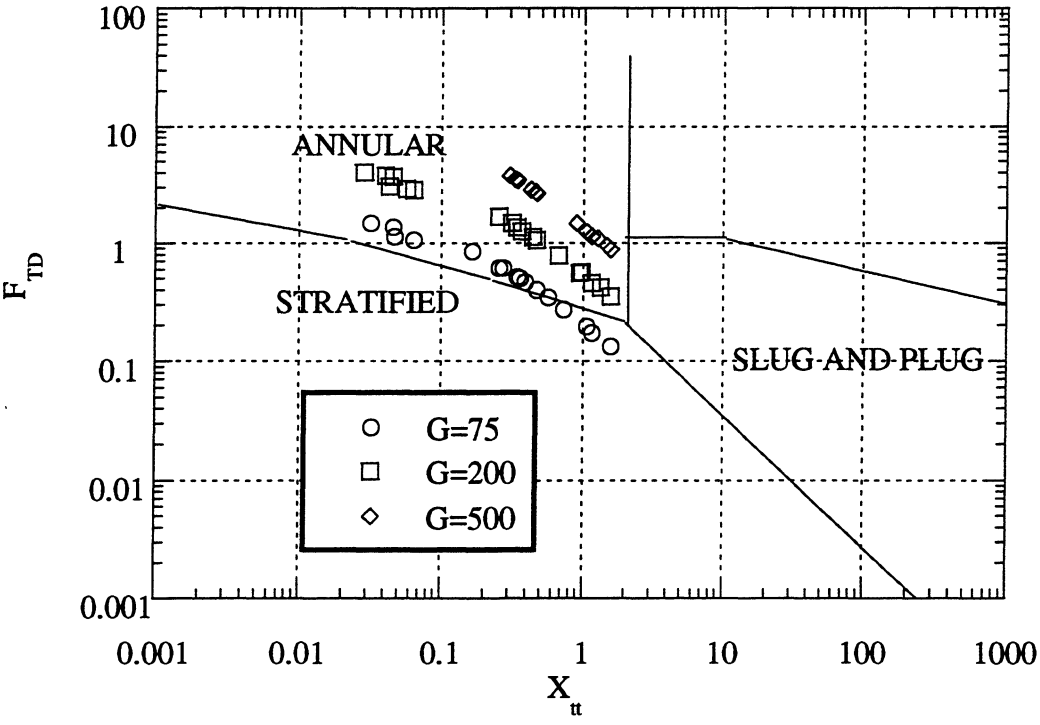

Figure 8.6 Taitel-Dukler Map for 8.89 mm base diameter axially grooved tube.

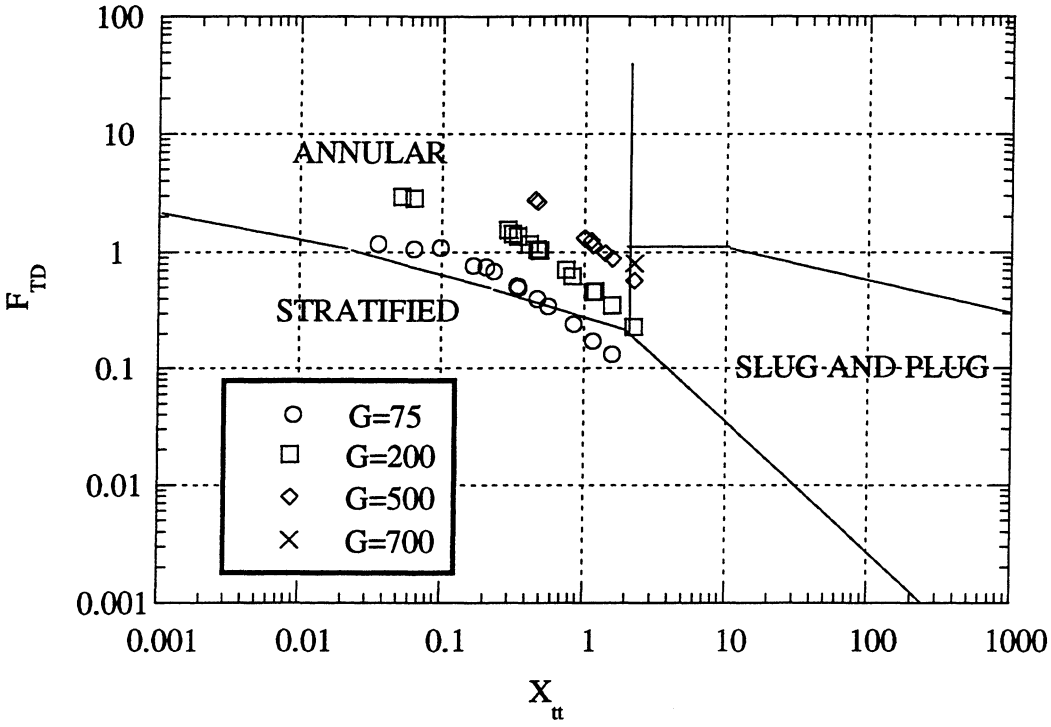

Figure 8.7 Taitel-Dukler Map for 7.25 mm base diameter helically grooved tube.

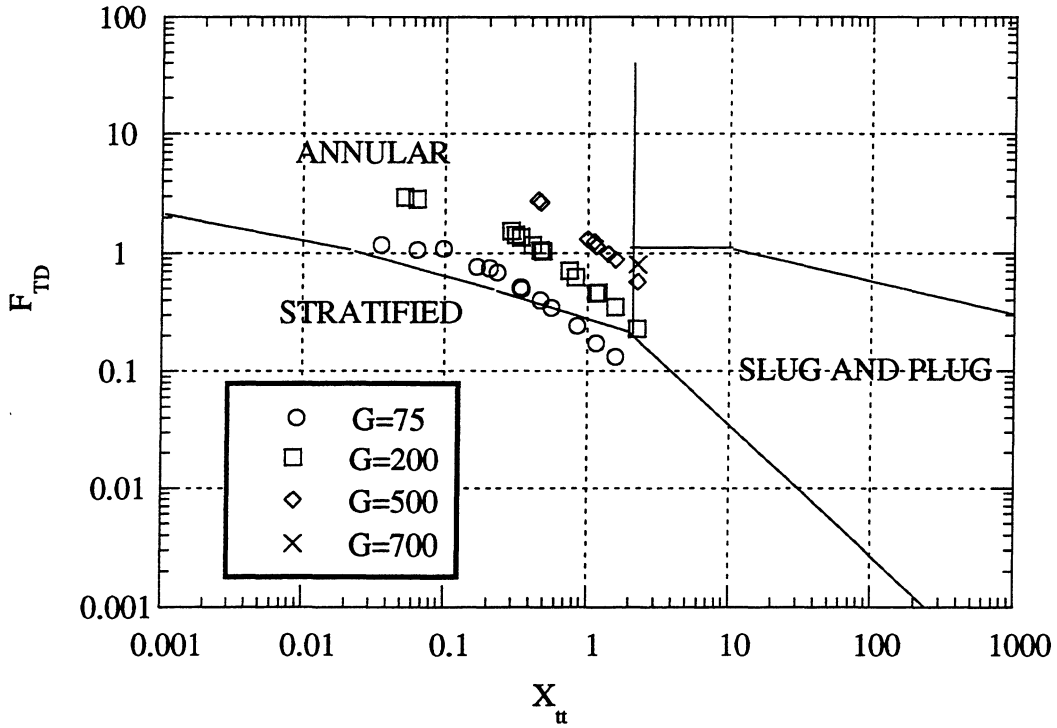

Figure 8.8 Taitel-Dukler Map for 8.93 mm base diameter helically grooved tube.

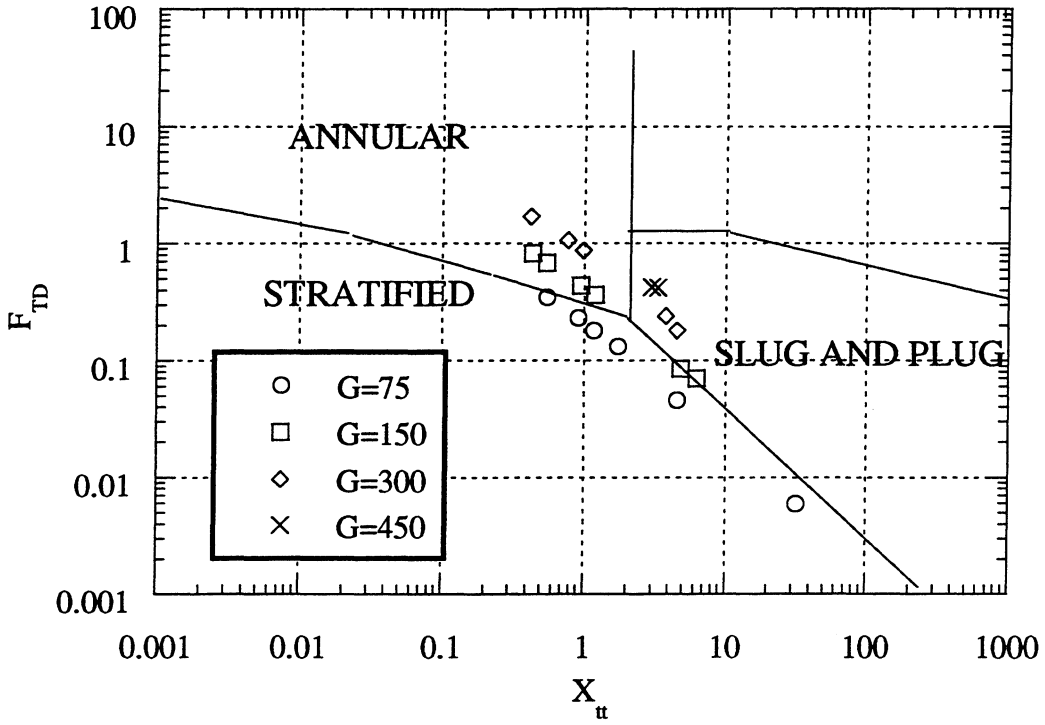

Figure 8.9 Taitel-Dukler Map for Graham's data.

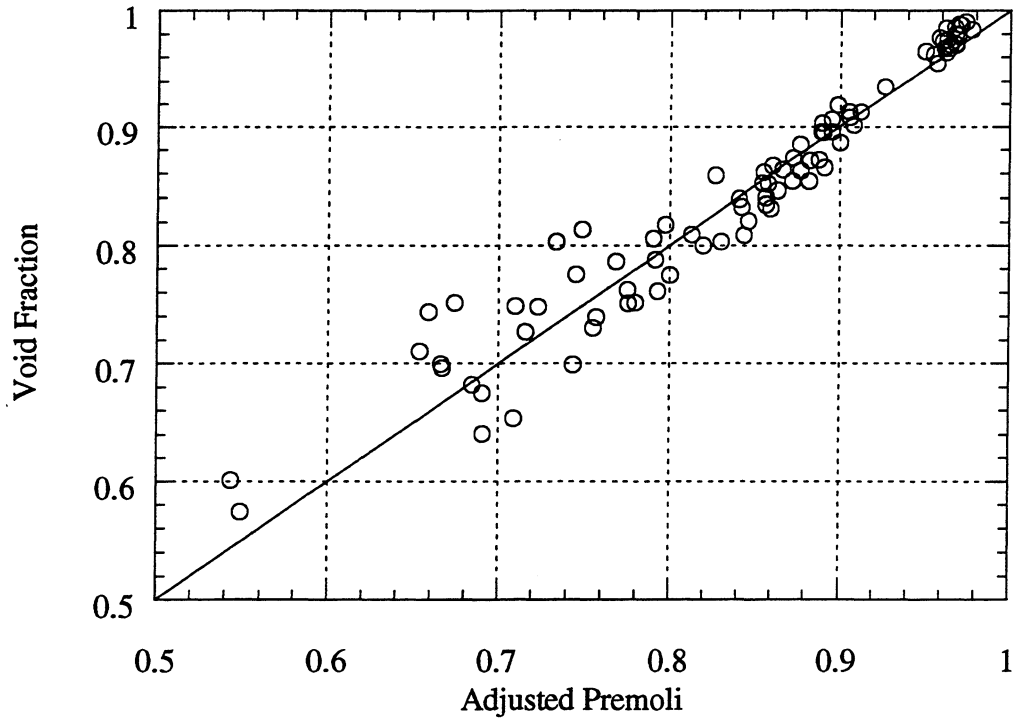

Figure 8.10 Void fraction vs. adjusted Premoli for smooth tubes

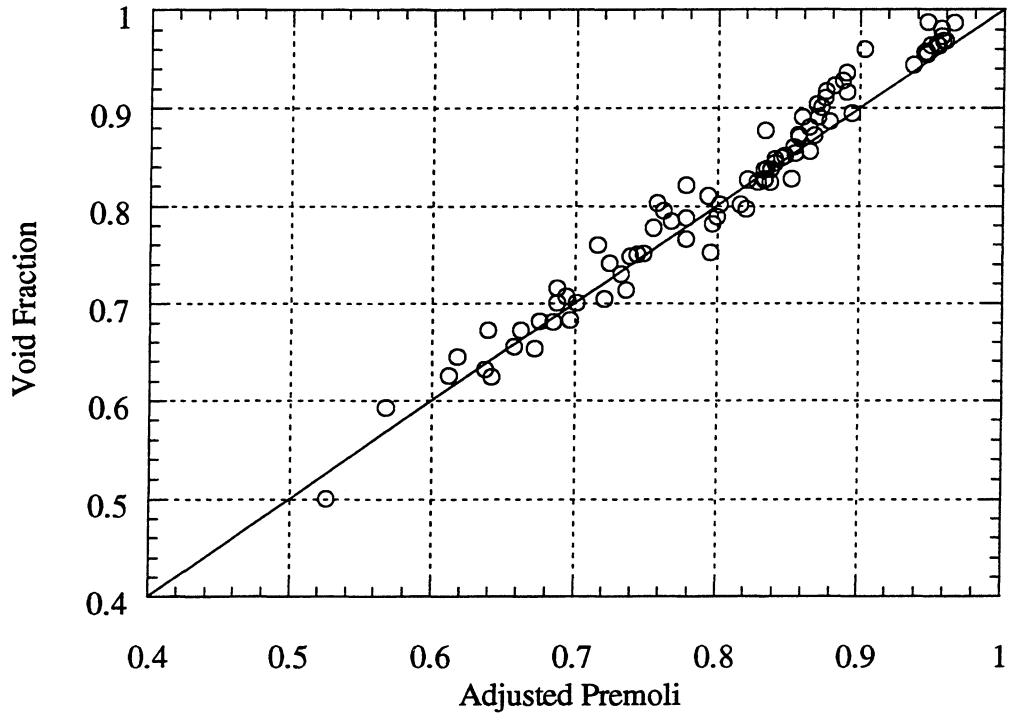

Figure 8.11 Void fraction vs. adjusted Premoli correlation for axially grooved tubes

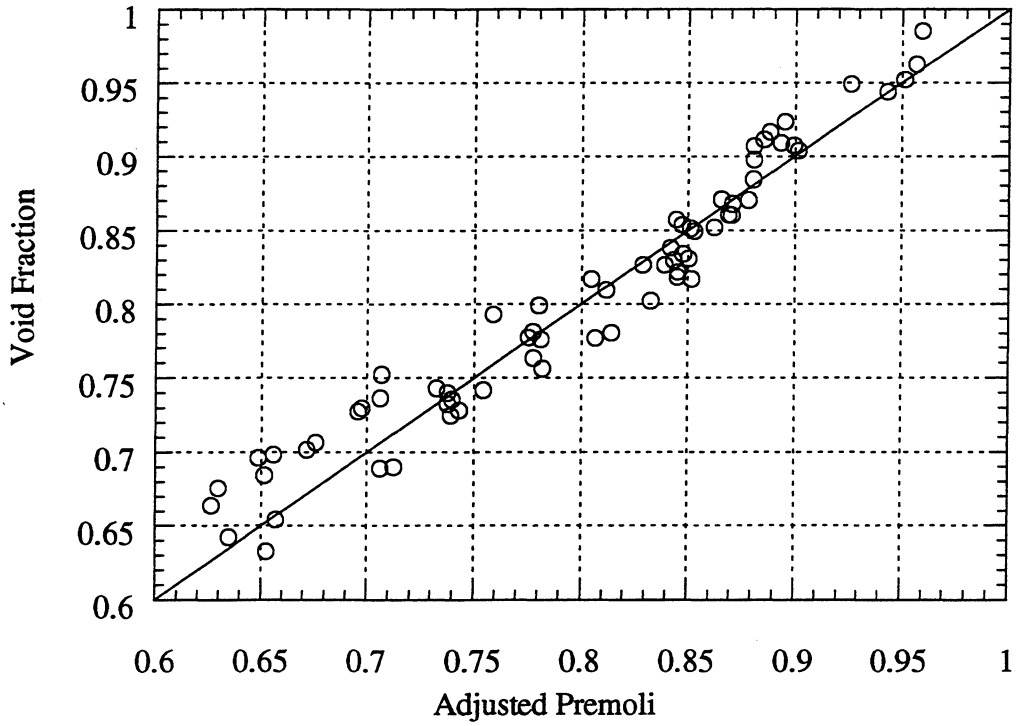

Figure 8.12 Void fraction vs. adjusted Premoli correlation for helically grooved tubes

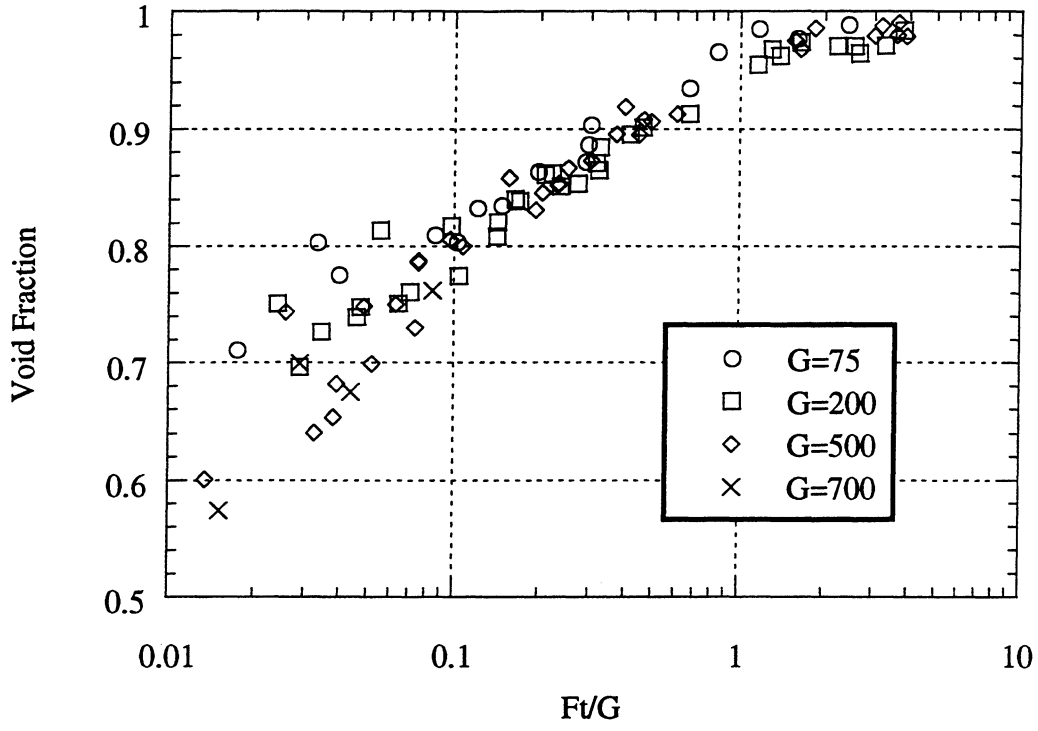

Figure 8.13 Void fraction vs. Ft/G for smooth tube data.

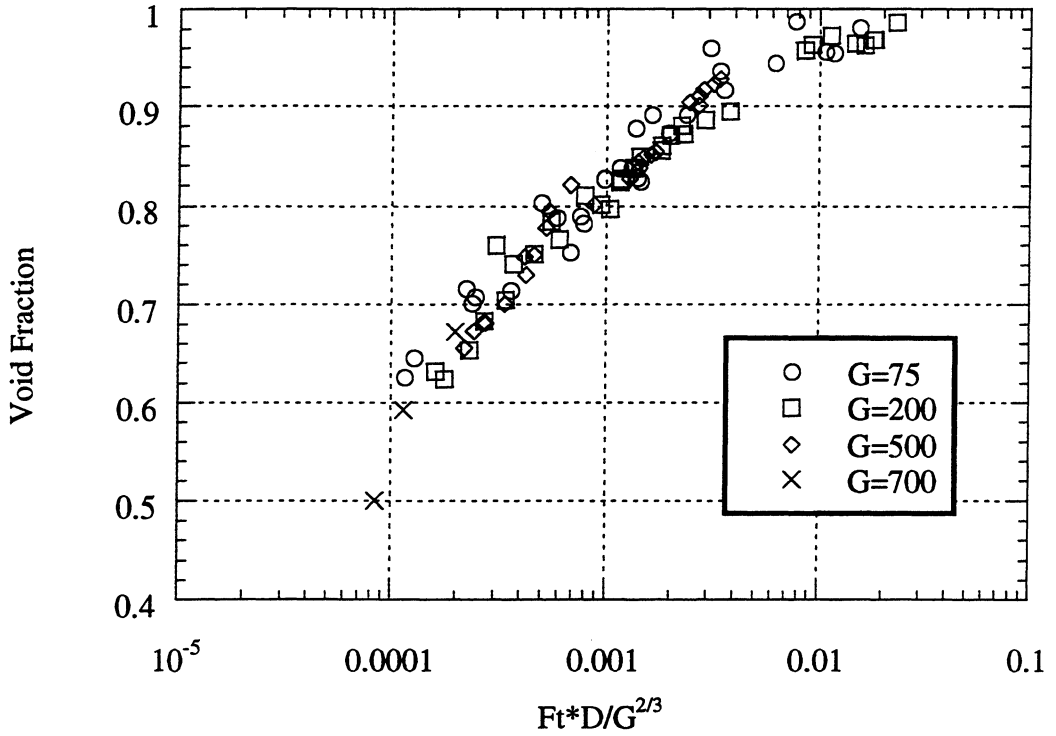

Figure 8.14 Void fraction vs. $Ft*D/G^{2/3}$ for axially grooved tube.

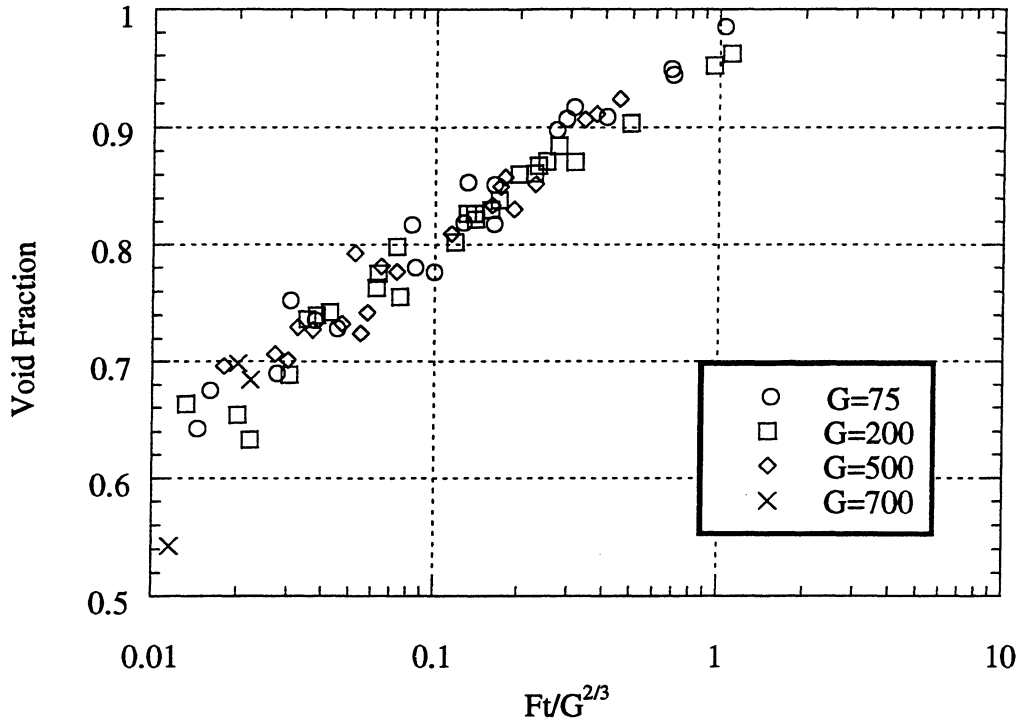

Figure 8.15 Void fraction vs. $Ft/G^{2/3}$ for helically grooved tube.

Bibliography

Ahrens, F.W. 1983. "Heat pump modeling, simulation, and design." *Heat Pump Fundamentals. Proceedings of the NATO Advanced Study Institute on Heat Pump Fundamentals, Espinho, Spain, 1980.* J. Berghmans, ed. The Hague, Netherlands: Martinus Nijhoff Publishers.

Bankoff, S. G. 1960. "A variable density single-fluid model for two-phase flow with particular reference to steam-water flow." *Transactions ASME, Journal of Heat Transfer,* Vol. 82, pp. 265-272.

Baroczy, C. J. 1965. "Correlation of liquid fraction in two-phase flow with application to liquid metals." *Chemical Engineering Progress Symposium Series,* Vol. 61, No. 57, pp. 179-191.

Christoffersen B.C. 1993. "Heat transfer and flow characteristics of R-22, R-32/R-125, and R-134a in smooth and micro-finned tubes." M.S. Thesis, University of Illinois.

De Guzman N.M. 1997. "Evaporative heat transfer characteristics in a vertical channel with obstructions." M.S. Thesis, University of Illinois.

Dobson, M.K. 1994. "Heat transfer and flow regimes during condensation in a horizontal tube." Ph.D. Dissertation, University of Illinois.

Domanski, P., and D. Didion. 1983. *Computer Modeling of the Vapor Compression Cycle with Constant Flow Area Expansion Device.* NBS Building Science Series 155.

Graham, D.M. 1998. "Experimental investigation of void fraction during refrigerant condensation." M.S. Thesis, University of Illinois.

Hughmark, G. A. 1962. "Holdup in gas-liquid flow." *Chemical Engineering Progress,* Vol. 58, No. 4, pp. 62-65.

Hurlburt, E.T. and T.A. Newell. 1997. "Prediction of the circumferential film thickness distribution in horizontal annular gas-liquid flow." Submitted to Int. J. Multiphase Flow.

Larson, H. C. 1957. "Void fractions of two-phase steam water mixtures." M.S. Thesis, University of Minnesota.

Levy, S. 1960. "Steam slip- theoretical prediction from momentum model." *Transactions ASME, Journal of Heat Transfer*, Series C, Vol. 82, pp. 113-124.

Lockhart, R. W. and R. C. Martinelli. 1949. "Proposed correlation of data for isothermal two-phase, two-component flow in pipes." *Chemical Engineering Progress*, Vol. 45, No. 1, pp. 39-48.

Maurer, G. 1960. "A method for predicting steady-state boiling vapor fractions in reactor coolant channels." Bettis Technical Review, WAPD-BT-19.

Martinelli, R. C., and D. B. Nelson 1948. "Prediction of pressure drop during forced-circulation boiling of water." *Transactions ASME*, Vol. 70, pp. 695-702.

NIST 1993. "NIST Thermodynamic properties of refrigerants and refrigerant mixtures", version 4.01. Computer software. National Institute of Standards and Technology.

Panek J.S. 1992. "Evaporation heat transfer and pressure drop in ozone-safe refrigerants and refrigerant oil mixtures." M.S. Thesis, University of Illinois.

Ponchner, M. 1995. "Condensation of HFC-134a in an 18_ helix angle micro-finned tube." M.S. Thesis, University of Illinois.

Premoli, A., D. Francesco, and A. Prina. 1971. "A dimensional correlation for evaluating two-phase mixture density." *La Termotecnica*, Vol. 25, No. 1, pp. 17-26.

Rice, C.K. 1987. "The effect of void fraction correlation and heat flux assumption on refrigerant charge inventory predictions." *ASHRAE Transactions*, Vol. 93, Part 1, pp. 341-367.

Smith, S. L. 1969. "Void fractions in two-phase flow: a correlation based upon an equal velocity head model." *Proc. Instn. Mech Engrs.*, London, Vol. 184, Pt. 1, No. 36, pp. 647-664.

Tandon, T. N., H. K. Varma, and C. P. Gupta. 1985. "A void fraction model for annular two-phase flow." *International Journal of Heat and Mass Transfer*, Vol. 28, No. 1, pp. 191-198.

Thom, J. R. S. 1964. "Prediction of pressure drop during forced circulation boiling of water." *International Journal of Heat and Mass Transfer*, Vol. 7, pp. 709-724.

Wallis, G. B. 1969. *One-Dimensional Two-Phase Flow*. New York: McGraw-Hill, pp. 51-54.

Wattlet, J.P. 1994. "Heat transfer flow regimes of refrigerants in a horizontal-tube evaporator." Ph.D. Dissertation, University of Illinois.

Yashar D.A 1998. "Experimental investigation of void fraction during horizontal flow in smaller diameter refrigerant applications." M.S. Thesis, University of Illinois.

Zivi, S. M. 1964. "Estimation of steady-state steam void-fraction by means of the principle of minimum entropy production." *Transactions ASME, Journal of Heat Transfer*, Series C, Vol. 86, May, pp. 247-252.

Appendix A

Smooth Tubes

This appendix presents raw data taken for the 6.12 mm smooth tube. The 4.26 mm smooth tube data appears in Yashar. Data will be presented first in tabular format, and second in graphical forms.

Table A.1 Raw data for 6.12 mm inner diameter smooth tube.

Refrigerant	Heat Flux	Mass Flux	Inlet Qual(%)	Ave Qual(%)	Void Fraction
R134a	0	200	10	10.00	0.7392
R134a	0	200	30	30.00	0.8537
R134a	0	200	80	80.00	0.9705
R134a	0	500	10	10.00	0.7505
R134a	0	500	30	30.00	0.8953
R134a	0	500	80	80.00	0.9793
R134a	0	75	10	10.00	0.8028
R134a	0	75	30	30.00	0.863
R134a	0	75	80	80.00	0.977
R134a	3	200	10	13.09	0.761
R134a	3	200	30	33.09	0.865
R134a	3	200	80	83.09	0.9705
R134a	3	500	10	11.23	0.7878
R134a	3	500	30	31.23	0.919
R134a	3	500	80	81.23	0.9873
R134a	3	75	10	18.23	0.8092
R134a	3	75	30	38.23	0.903
R134a	3	75	80	88.23	0.9883
R134a	10	200	10	20.29	0.8089
R134a	10	200	30	40.29	0.9009
R134a	10	200	80	90.29	0.9835
R134a	10	500	10	14.12	0.7999
R134a	10	500	30	34.12	0.9077
R134a	10	500	80	84.12	0.9904
R134a	10	75	10	37.44	0.8712
R134a	10	75	30	57.44	0.9347
R410A	0	200	10	10.00	0.7514
R410A	0	200	30	30.00	0.8206
R410A	0	200	80	80.00	0.9546
R410A	0	500	10	10.00	0.6403
R410A	0	500	30	30.00	0.8306
R410A	0	500	80	80.00	0.9751
R410A	0	75	10	10.00	0.7103
R410A	0	75	30	30.00	0.8029
R410A	0	75	80	80.00	0.9652
R410A	3	200	10	12.58	0.7268
R410A	3	200	30	32.58	0.8406
R410A	3	200	80	82.58	0.968
R410A	3	500	10	11.03	0.6538
R410A	3	500	30	31.03	0.8453

R410A	3	500	80	81.03	0.9678
R410A	3	75	10	16.88	0.7753
R410A	3	75	30	36.88	0.8341
R410A	3	75	80	86.88	0.9845
R410A	10	200	10	18.60	0.7511
R410A	10	200	30	38.60	0.8619
R410A	10	500	10	13.44	0.6991
R410A	10	500	30	33.44	0.8534
R410A	10	500	80	83.44	0.985
R410A	10	75	10	32.94	0.8321
R410A	10	75	30	52.94	0.8861

Heat flux is in W/m^2 and mass flux is in kg/m^2s.

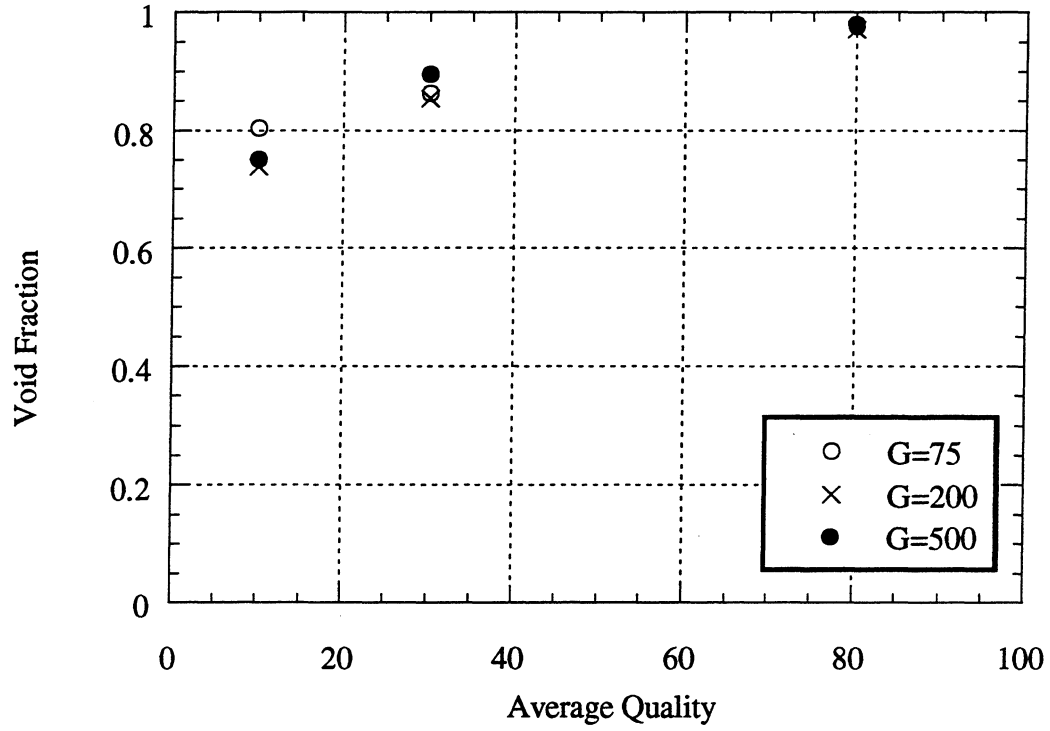

Figure A.1 Void fraction vs. average quality with a heat flux of 0 W/m^2 using R134a in a 6.12 mm inner diameter smooth tube. Mass flux (G) given in kg/m^{2}s.

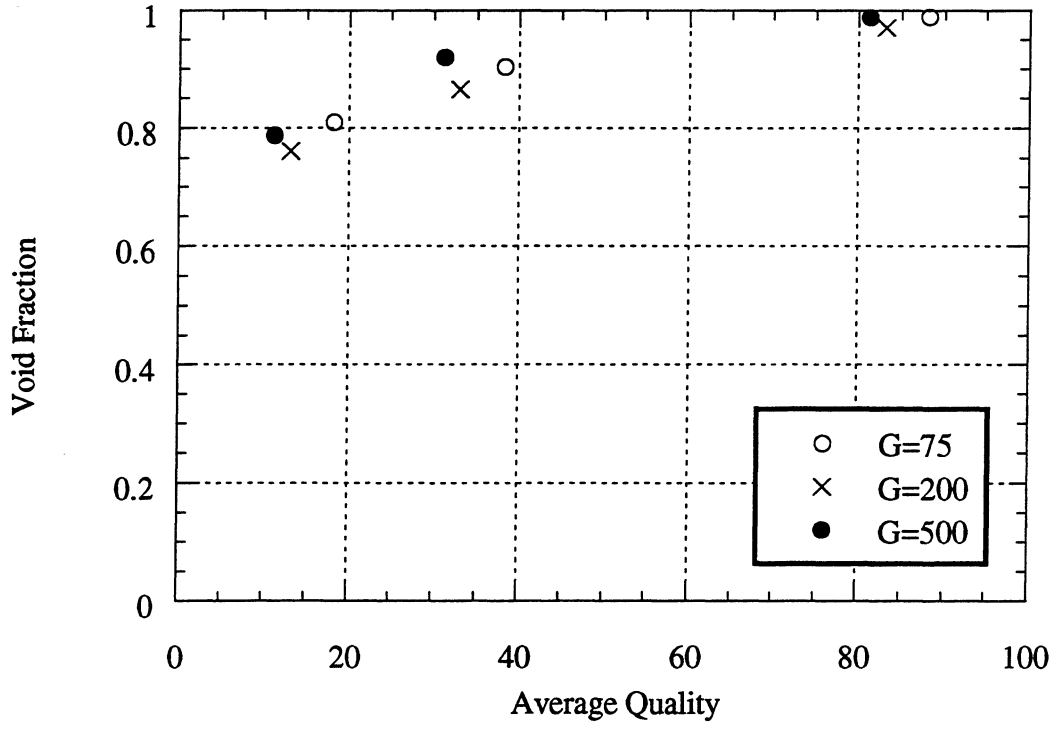

Figure A.2 Void fraction vs. average quality with a heat flux of 3 W/m^2 using R134a in a 6.12 mm inner diameter smooth tube. Mass flux (G) given in kg/m^{2}s.

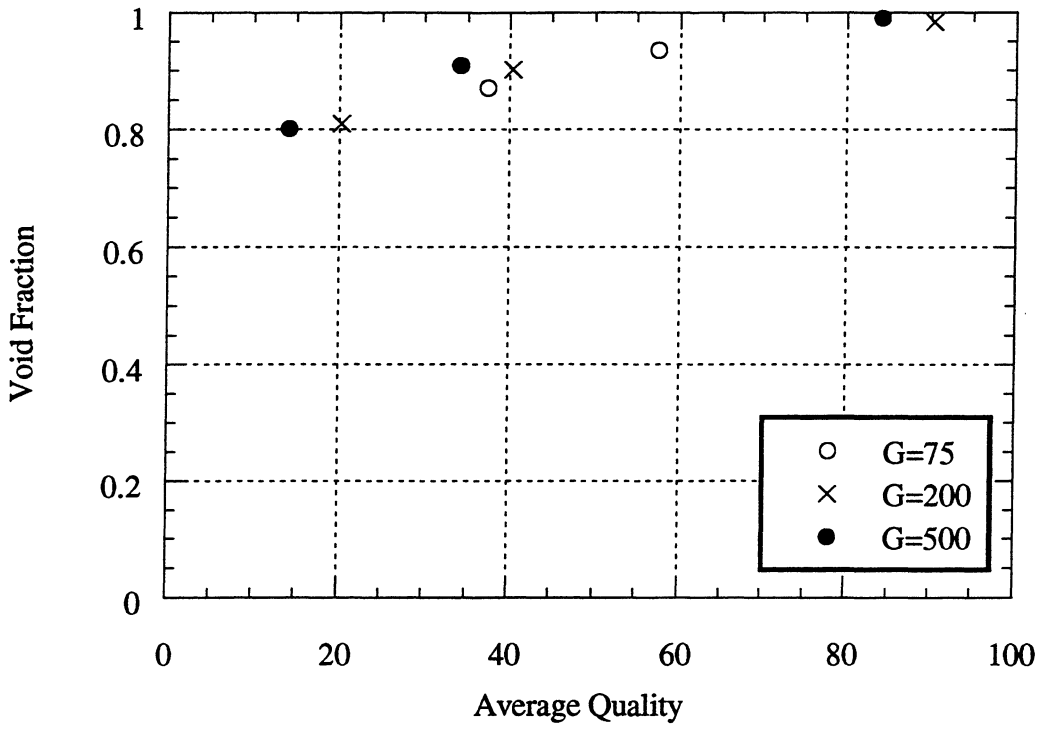

Figure A.3 Void fraction vs. average quality with a heat flux of 10 W/m^2 using R134a in a 6.12 mm inner diameter smooth tube. Mass flux (G) given in kg/m^{2}s.

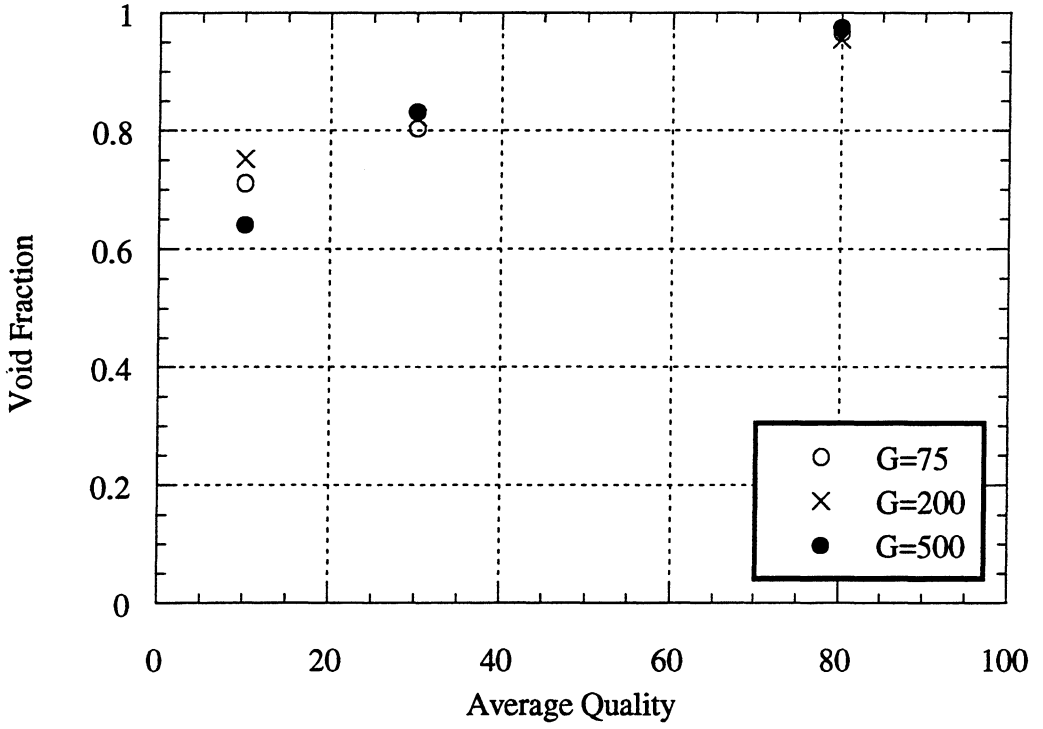

Figure A.4 Void fraction vs. average quality with a heat flux of 0 W/m^2 using R410A in a 6.12 mm inner diameter smooth tube. Mass flux (G) given in kg/m^{2}s.

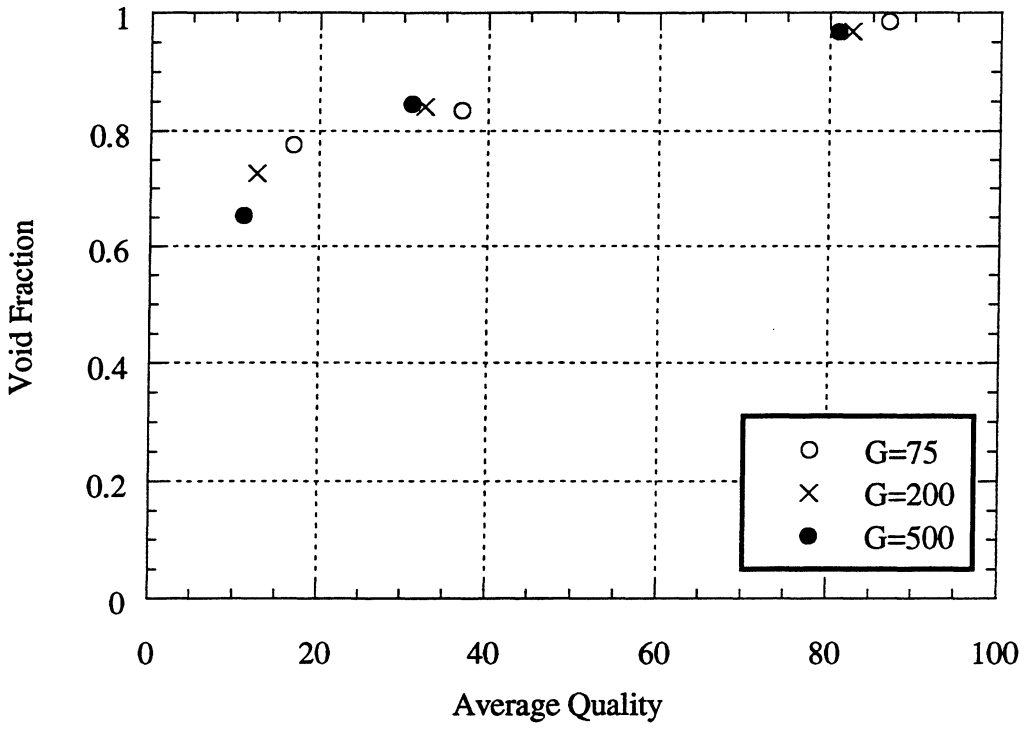

Figure A.5 Void fraction vs. average quality with a heat flux of 3 W/m^2 using R410A in a 6.12 mm inner diameter smooth tube. Mass flux (G) given in kg/m^{2}s.

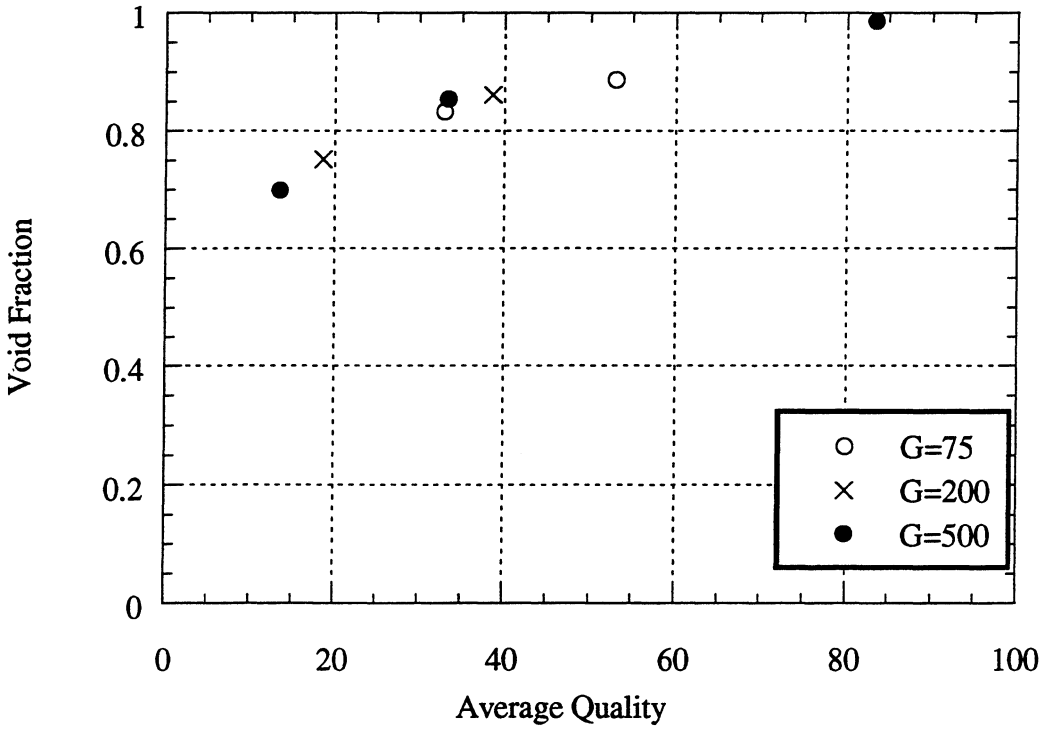

Figure A.6 Void Fraction vs. average quality with a heat flux of 10 W/m^2 using R410A in a 6.12 mm inner diameter smooth tube. Mass flux (G) given in kg/m^{2}s.

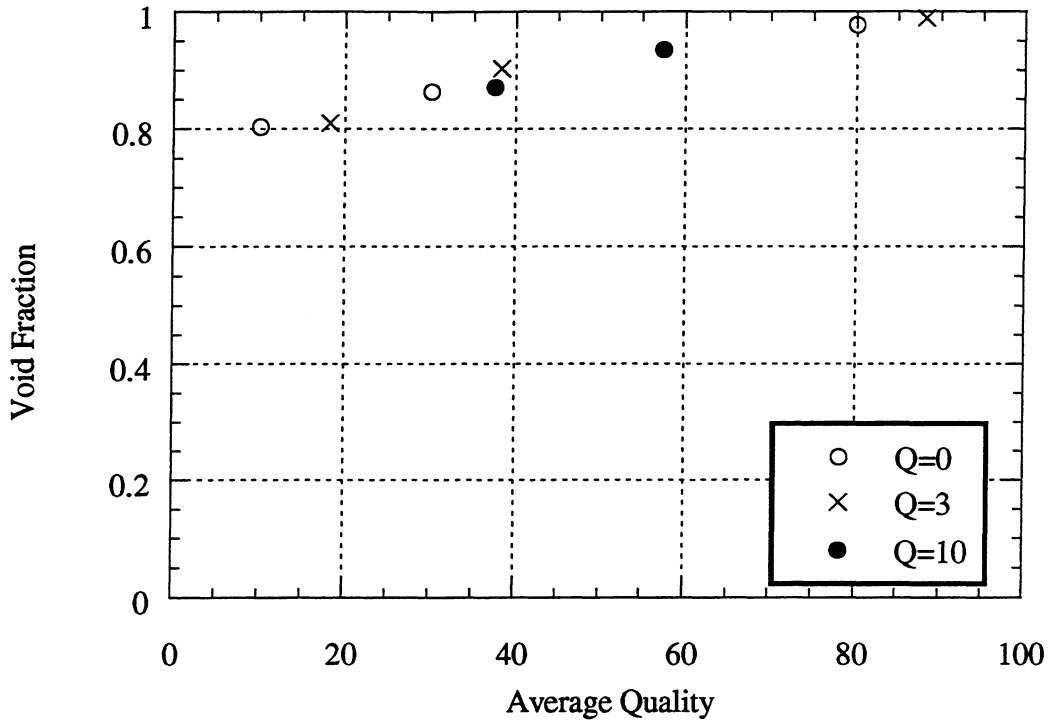

Figure A.7 Void fraction vs. average quality with a mass flux of 75 kg/m^{2}s using R134a in a 6.12 mm inner diameter tube. Heat flux (Q) in W/m^2.

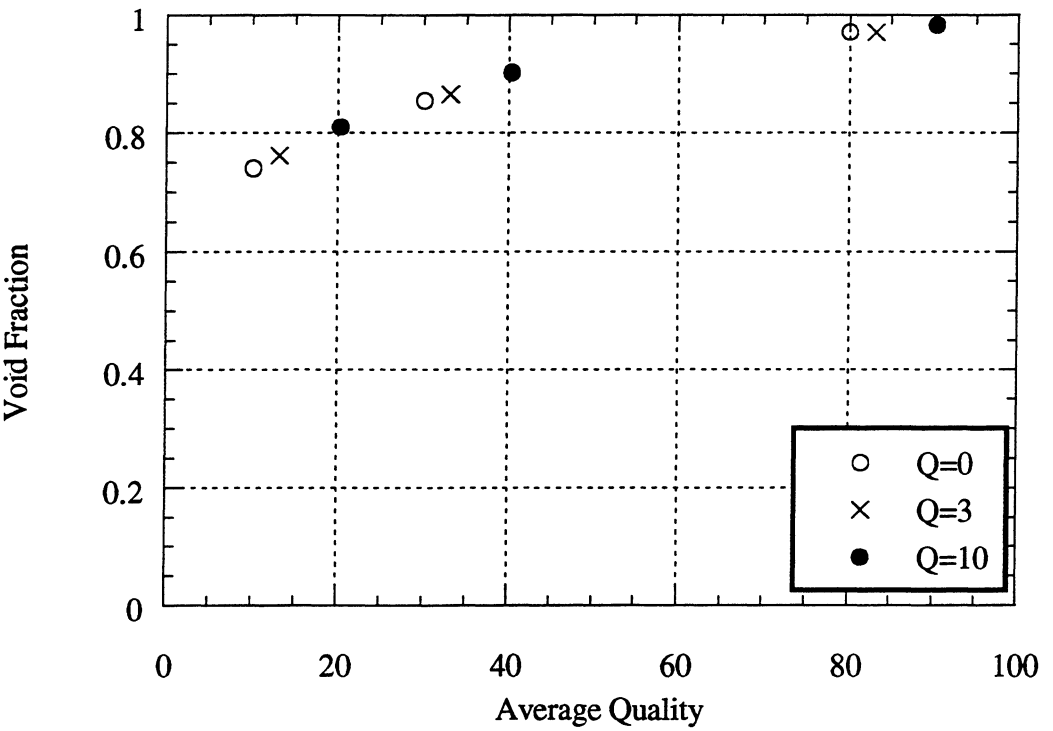

Figure A.8 Void fraction vs. average quality with a mass flux of 200 kg/m^{2}s using R134a in a 6.12 mm inner diameter tube. Heat flux (Q) in W/m^2.

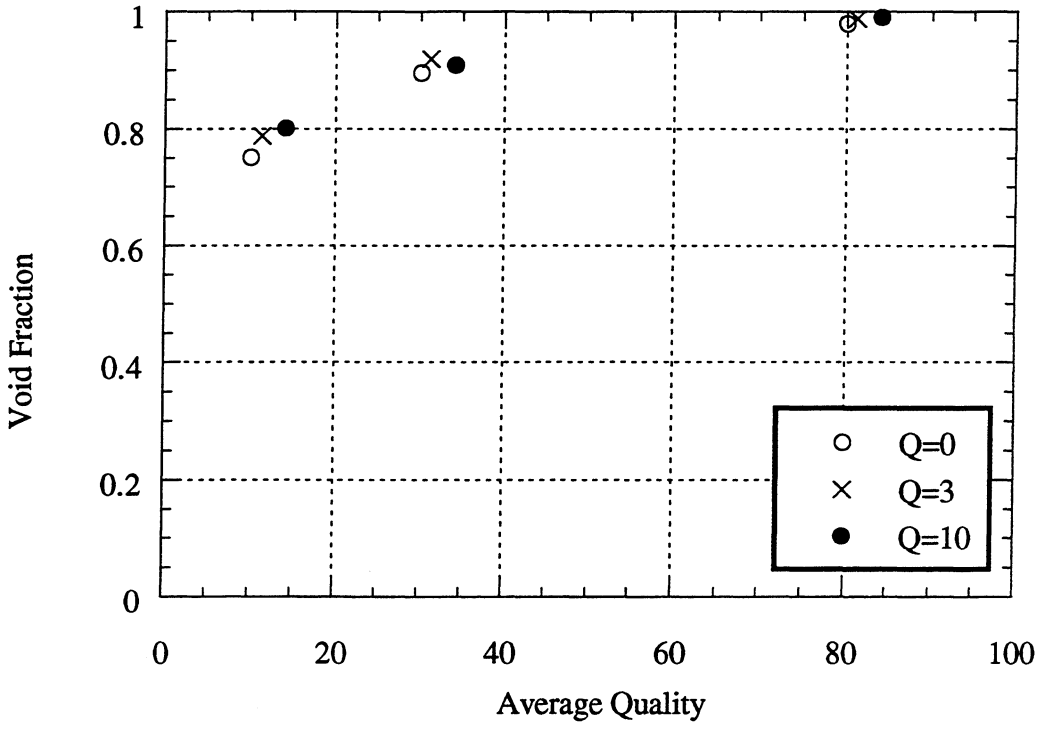

Figure A.9 Void Fraction vs. average quality with a mass flux of 500 kg/m^{2}s using R134a in a 6.12 mm inner diameter tube. Heat flux (Q) in W/m^2.

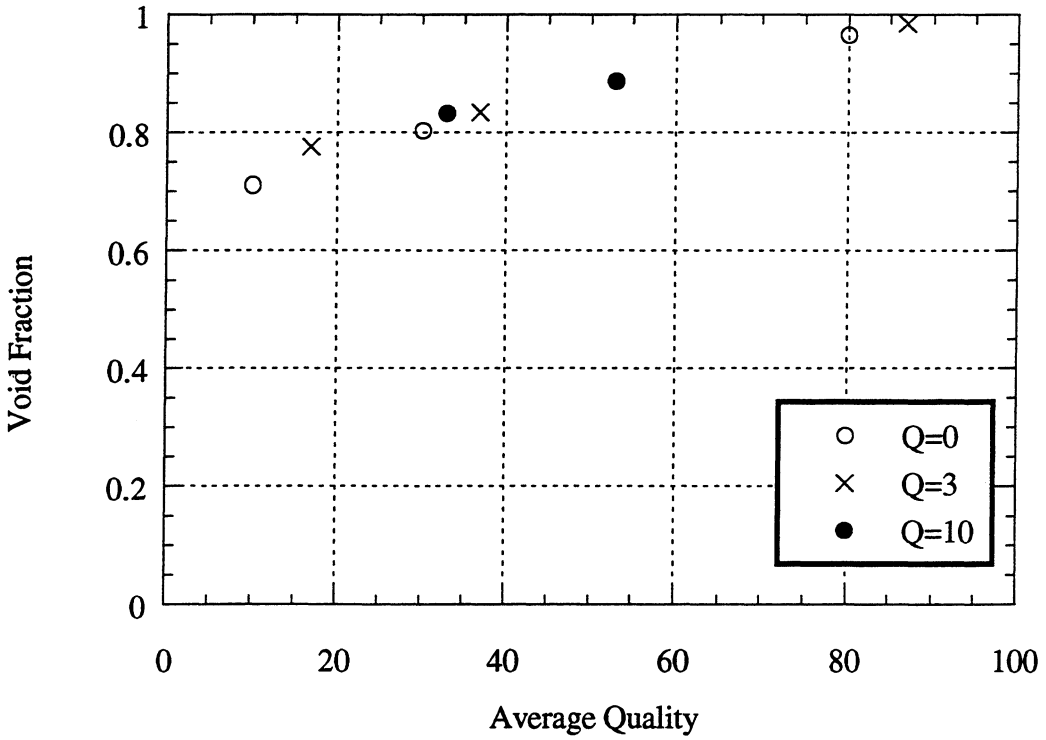

Figure A.10 Void fraction vs. average quality with a mass flux of 75 kg/m^{2}s using R410A in a 6.12 mm inner diameter tube. Heat flux (Q) in W/m^2.

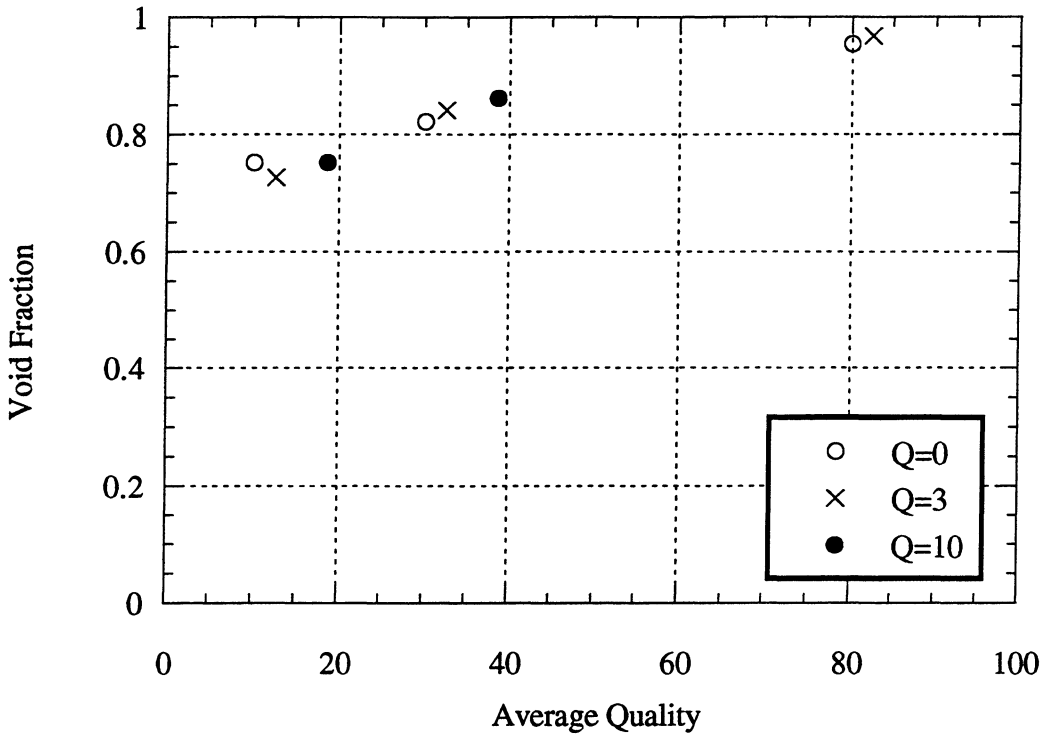

Figure A.11 Void fraction vs. average quality with a mass flux of 200 kg/m^{2}s using R410A in a 6.12 mm inner diameter tube. Heat flux (Q) in W/m^2.

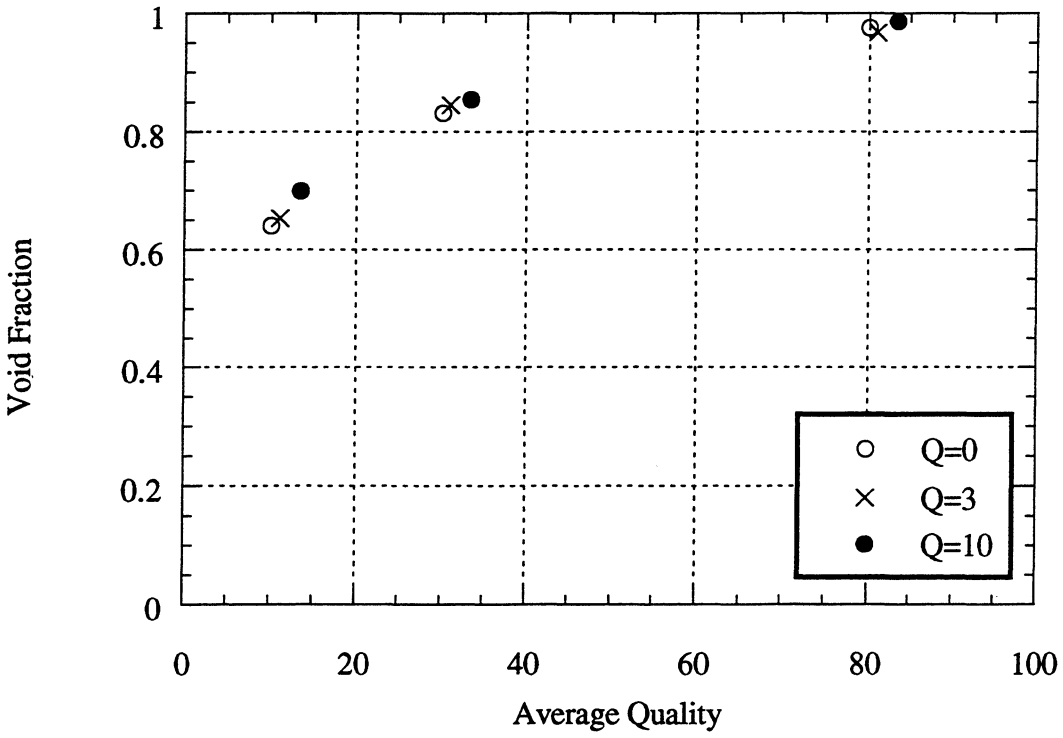

Figure A.12 Void fraction vs. average quality with a mass flux of 500 kg/m^{2}s using R410A in a 6.12 mm inner diameter tube. Heat flux (Q) in W/m^2.

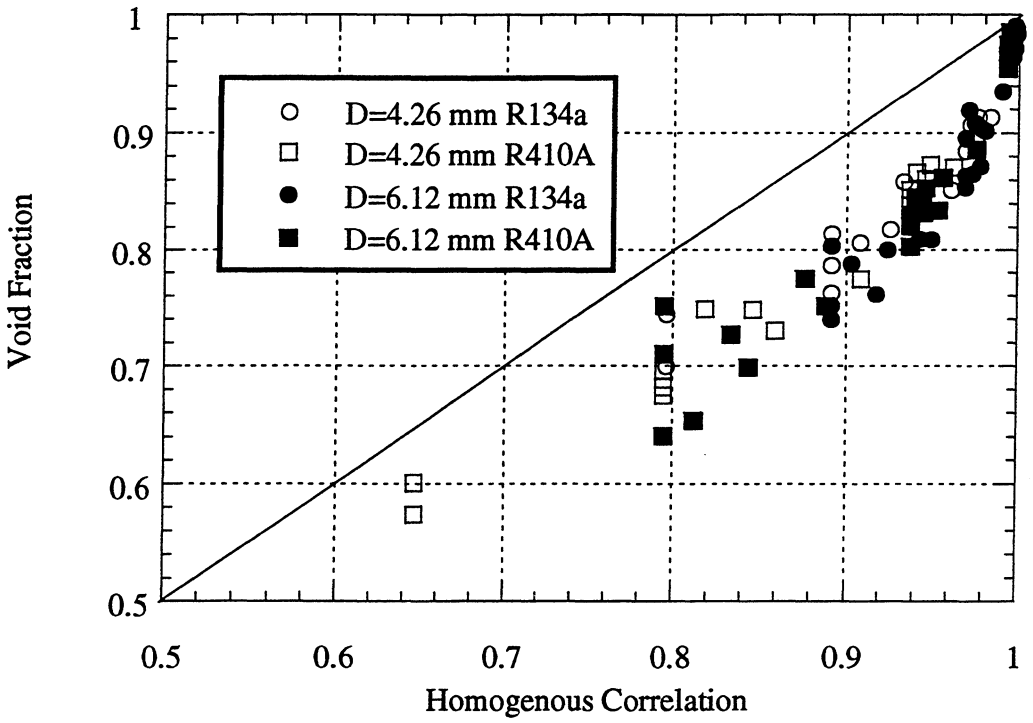

Figure A.13 Void Fraction vs. homogenous correlation showing diameter effects for 4.26 mm and 6.12 mm inner diameter smooth tube.

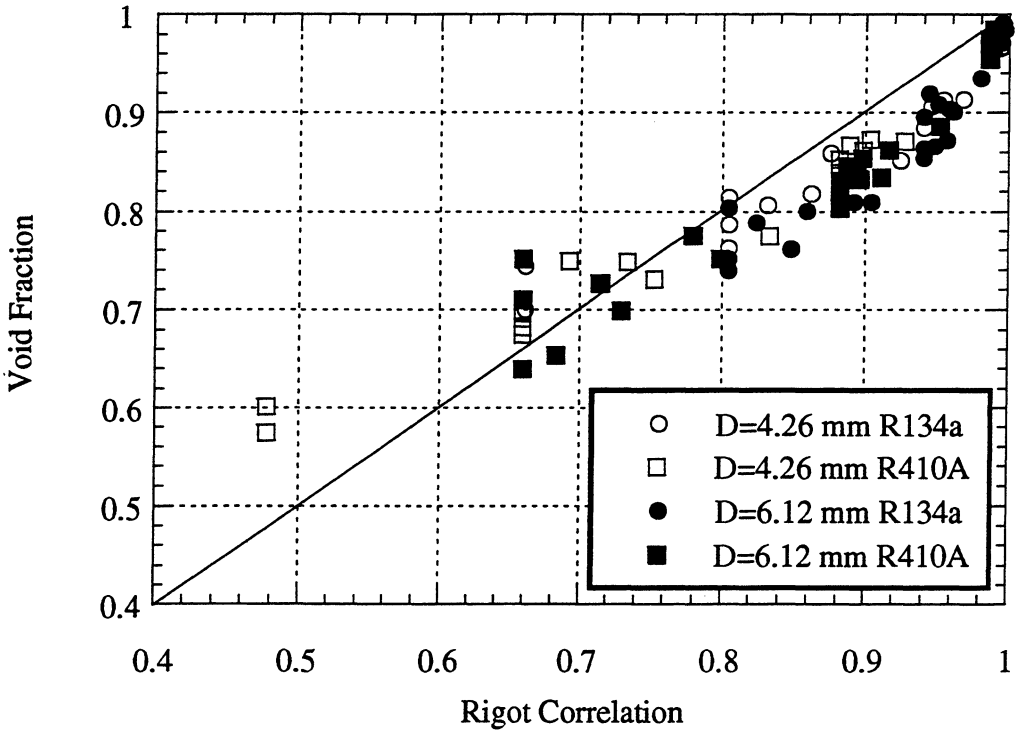

Figure A.14 Void Fraction vs. Rigot correlation showing diameter effects for 4.26 mm and 6.12 mm inner diameter smooth tube.

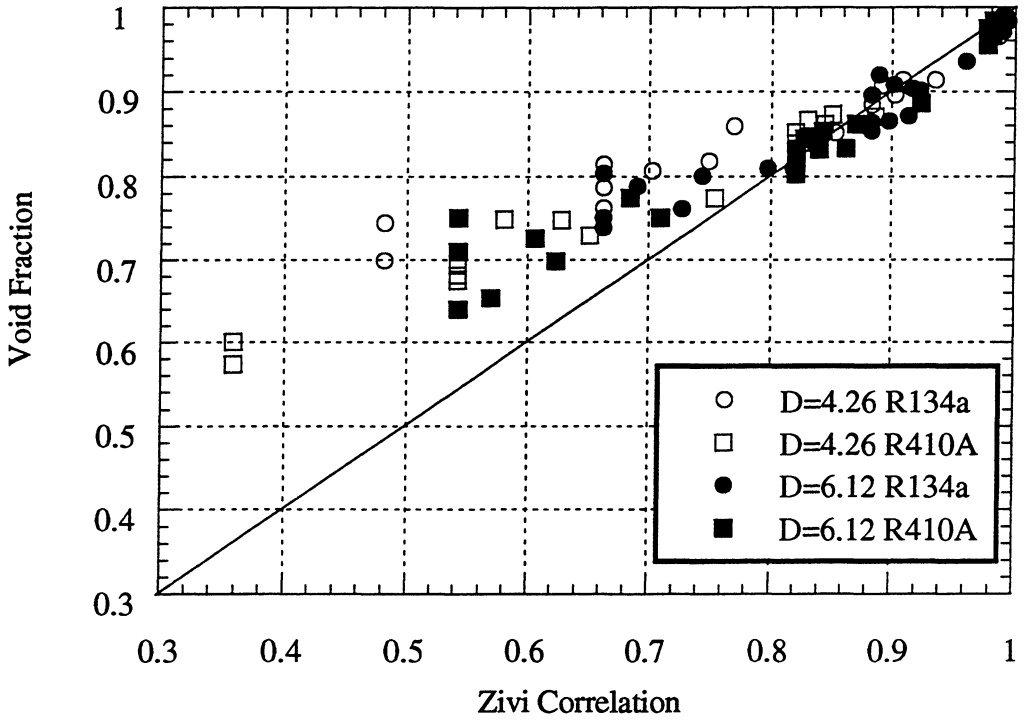

Figure A.15 Void Fraction vs. Zivi correlation showing diameter effects for 4.26 mm and 6.12 mm inner diameter smooth tube.

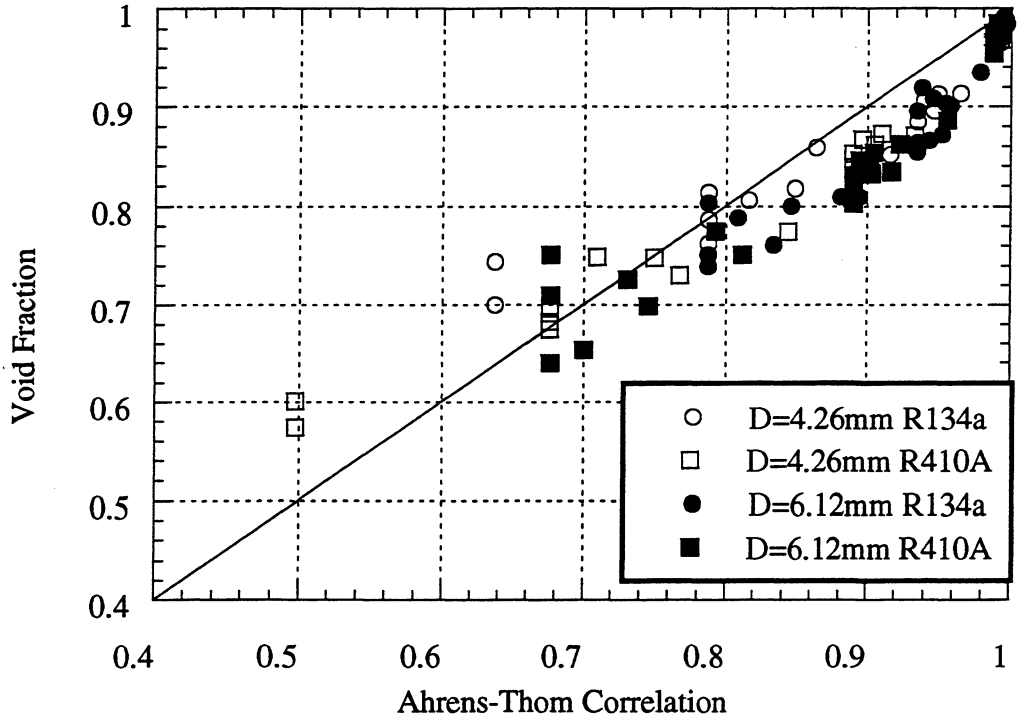

Figure A.16 Void Fraction vs. Ahrens-Thom correlation showing diameter effects for 4.26 mm and 6.12 mm inner diameter smooth tube.

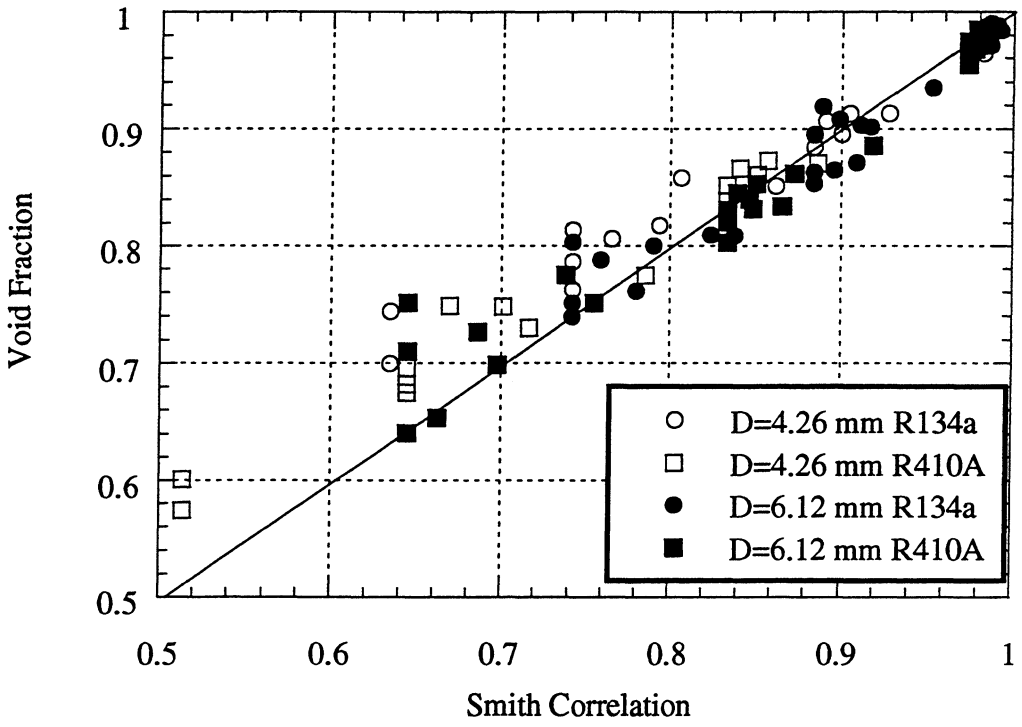

Figure A.17 Void Fraction vs. Smith correlation showing diameter effects for 4.26 mm and 6.12 mm inner diameter smooth tube.

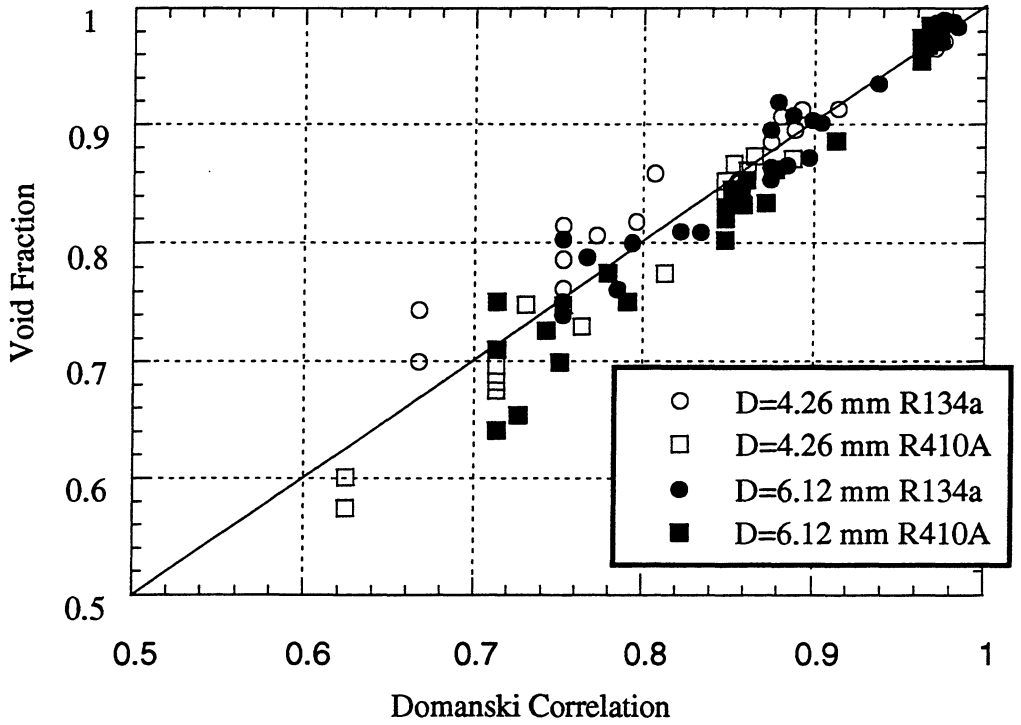

Figure A.18 Void Fraction vs. Wallis correlation showing diameter effects for 4.26 mm and 6.12 mm inner diameter smooth tube.

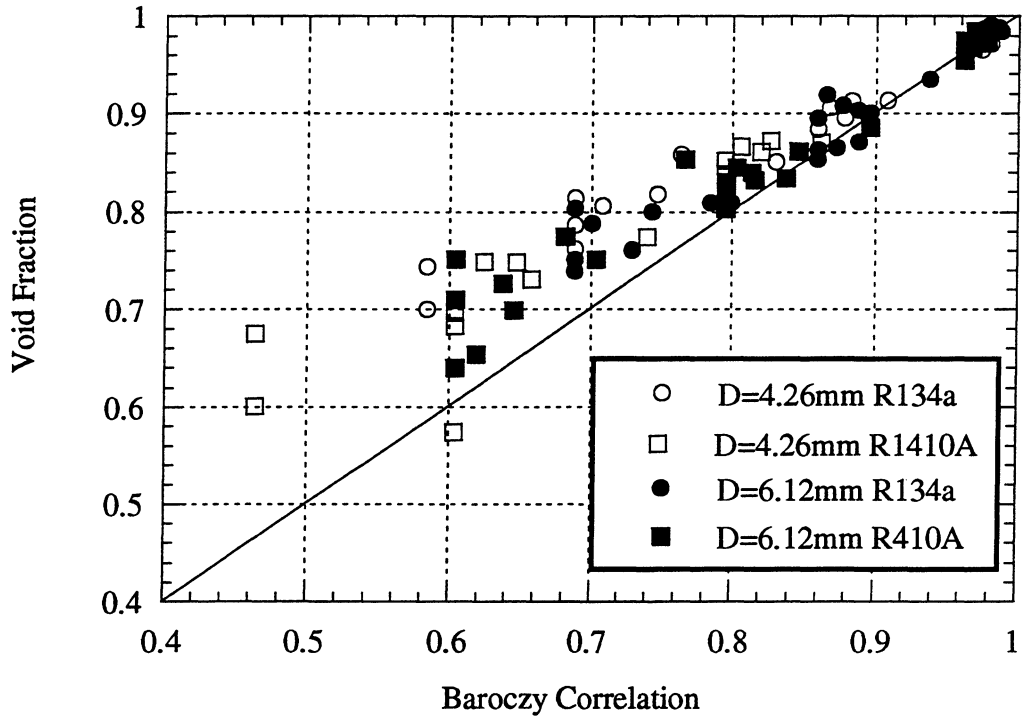

Figure A.19 Void Fraction vs. Baroczy correlation showing diameter effects for 4.26 mm and 6.12 mm inner diameter smooth tube.

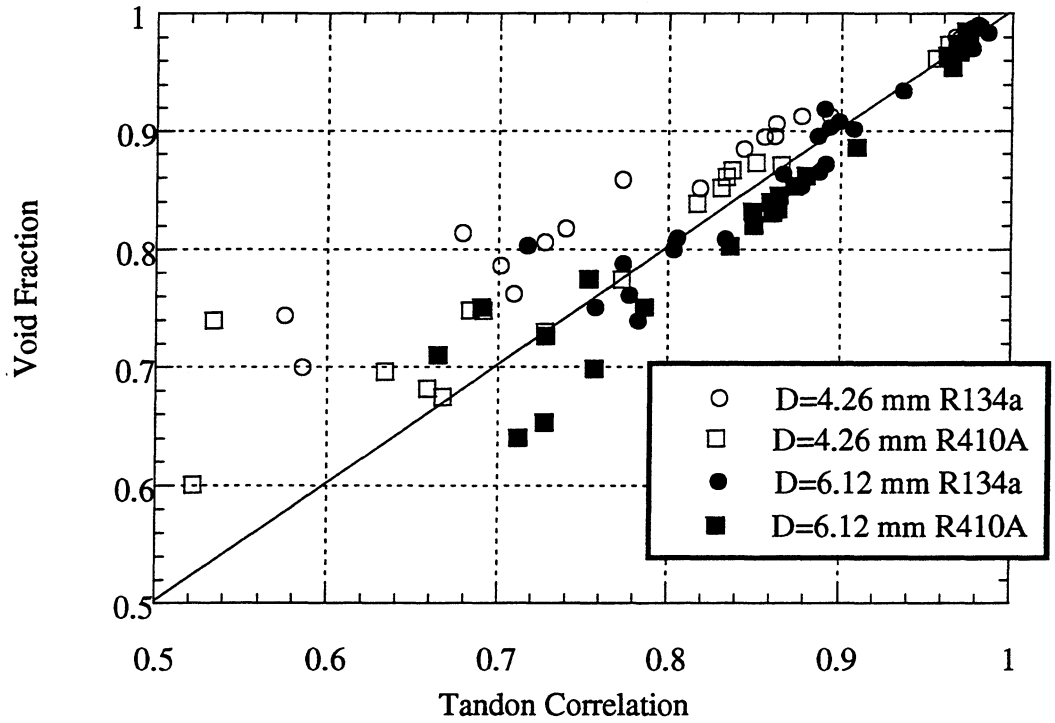

Figure A.20 Void Fraction vs. Tandon correlation showing diameter effects for 4.26 mm and 6.12 mm inner diameter smooth tube.

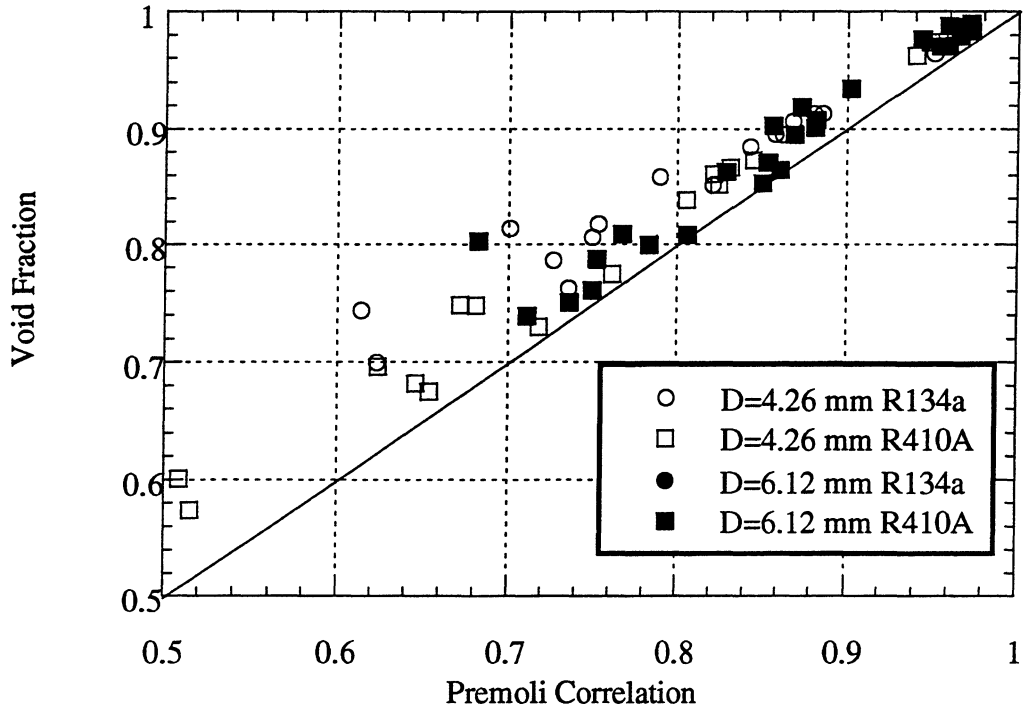

Figure A.21 Void Fraction vs. Premoli correlation showing diameter effects for 4.26 mm and 6.12 mm inner diameter smooth tube.

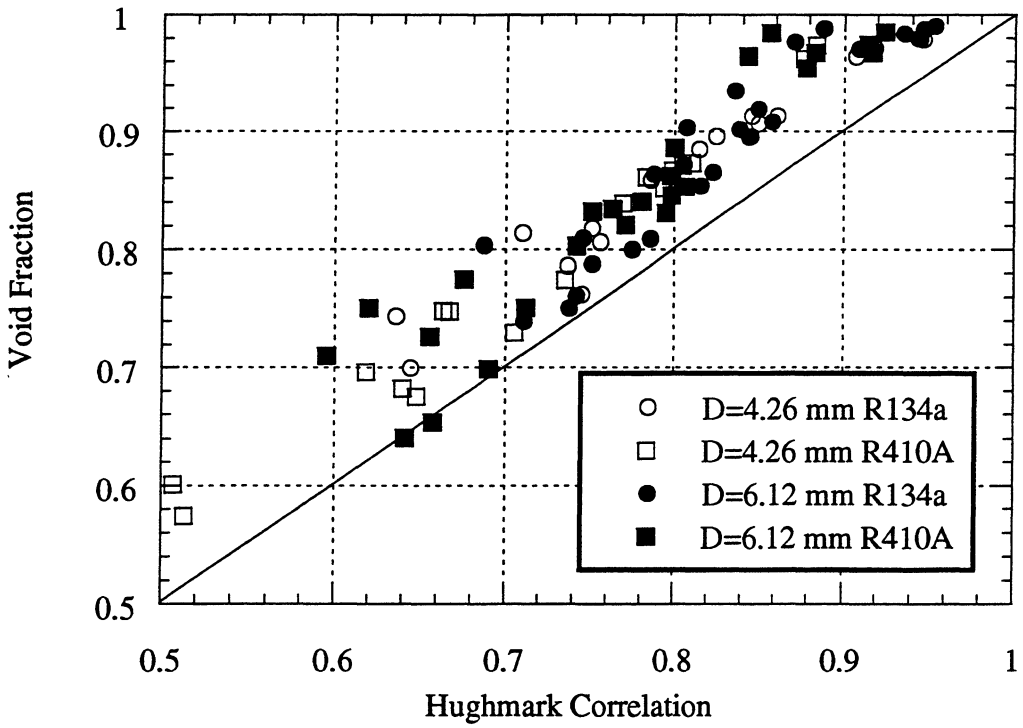

Figure A.22 Void Fraction vs. Hughmark correlation showing diameter effects for 4.26 mm and 6.12 mm inner diameter smooth tube.

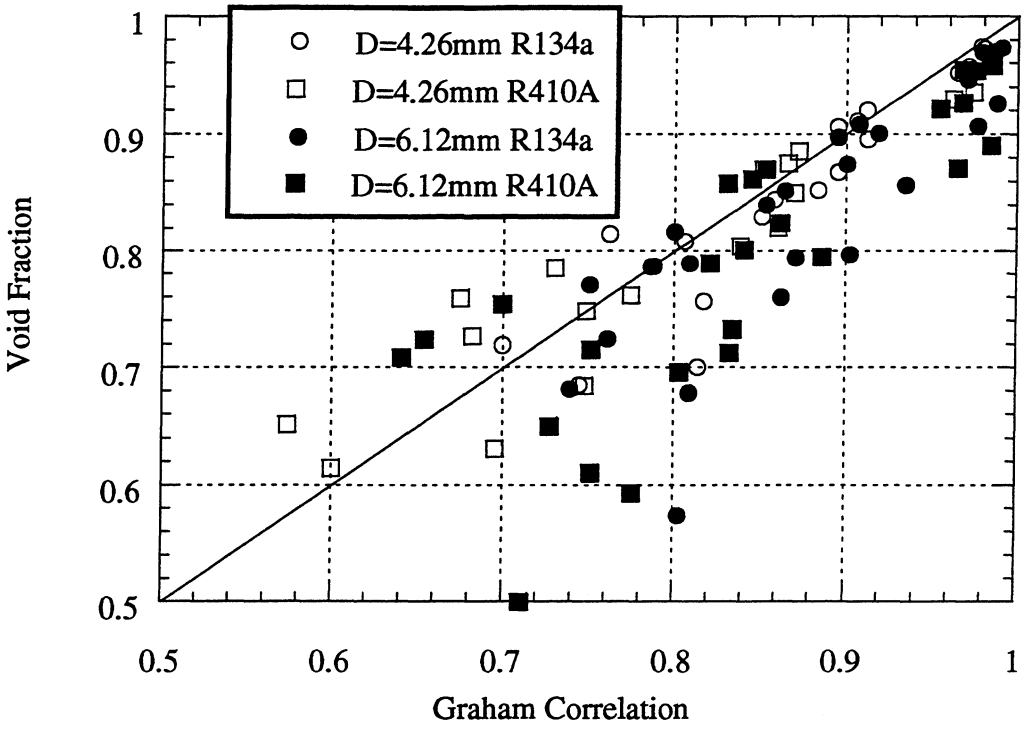

Figure A.23 Void Fraction vs. Graham's condenser correlation showing diameter effects for 4.26 mm and 6.12 mm inner diameter smooth tube.

Appendix B

Axially Grooved Tube

This appendix presents raw data taken for the 8.89 mm base diameter axially grooved tube. The 7.25 mm base diameter axially grooved tube data appears in Yashar. Data will be presented first in tabular format, and second in graphical forms.

Table B.1 Raw data for 8.89 mm base diameter axially grooved tube

Fluid	Heat Flux	Mass Flux	Inlet Qual(%)	Ave Qual(%)	Void Fraction
R134a	0	200	10	10.00	0.7042
R134a	0	200	30	30.00	0.8706
R134a	0	200	80	80.00	0.9623
R134a	0	500	10	10.00	0.7501
R134a	0	500	30	30.00	0.9006
R134a	0	75	10	10.00	0.7070
R134a	0	75	30	30.00	0.8242
R134a	0	75	80	80.00	0.9541
R134a	3	200	10	12.15	0.7508
R134a	3	200	30	32.15	0.8803
R134a	3	200	80	82.15	0.9680
R134a	3	500	10	10.86	0.7774
R134a	3	500	30	30.86	0.9173
R134a	3	75	10	15.72	0.8025
R134a	3	75	30	35.72	0.8723
R134a	3	75	80	85.72	0.9805
R134a	10	200	10	17.15	0.8099
R134a	10	200	30	37.15	0.8862
R134a	10	200	80	87.15	0.9867
R134a	10	500	10	12.86	0.8206
R134a	10	500	30	32.86	0.9229
R134a	10	75	10	29.07	0.8768
R134a	10	75	30	49.07	0.9160
R410A	0	200	10	10.00	0.6236
R410A	0	200	30	30.00	0.7963
R410A	0	200	80	80.00	0.9574
R410A	0	500	10	10.00	0.6723
R410A	0	500	30	30.00	0.8371
R410A	0	75	10	10.00	0.6448
R410A	0	75	30	30.00	0.7885
R410A	0	75	80	80.00	0.9432
R410A	3	200	10	11.79	0.6528
R410A	3	200	30	31.79	0.8246
R410A	3	200	80	81.79	0.9636
R410A	3	500	10	10.72	0.6808
R410A	3	500	30	30.72	0.8474
R410A	3	75	10	14.78	0.7000
R410A	3	75	30	34.78	0.8264

R410A	3	75	80	84.78	0.9870
R410A	10	200	10	15.94	0.7409
R410A	10	200	30	35.94	0.8488
R410A	10	200	80	85.94	0.9730
R410A	10	500	10	12.39	0.7002
R410A	10	500	30	32.39	0.8505
R410A	10	75	10	25.94	0.7873
R410A	10	75	30	45.94	0.8909

Heat flux in W/m^2 and mass flux in kg/m^2s.

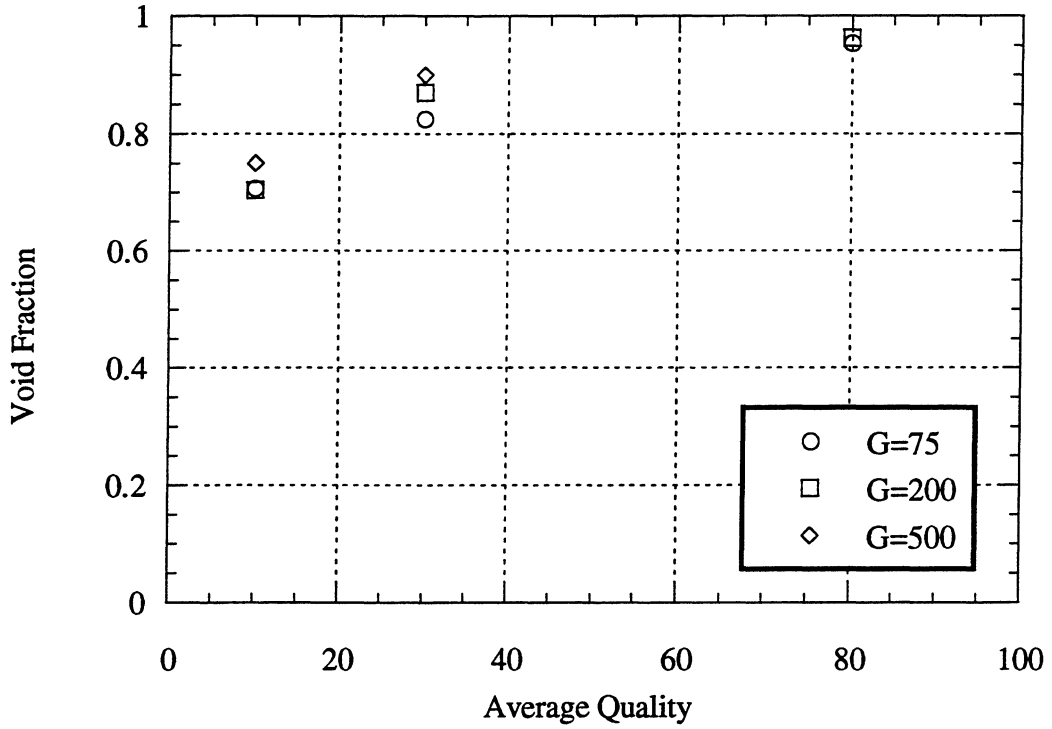

Figure B.1 Void fraction vs. average quality with a heat flux of 0 W/m^2 using R134a in a 8.89 mm base diameter axially grooved tube. Mass flux (G) given in kg/m^{2}s.

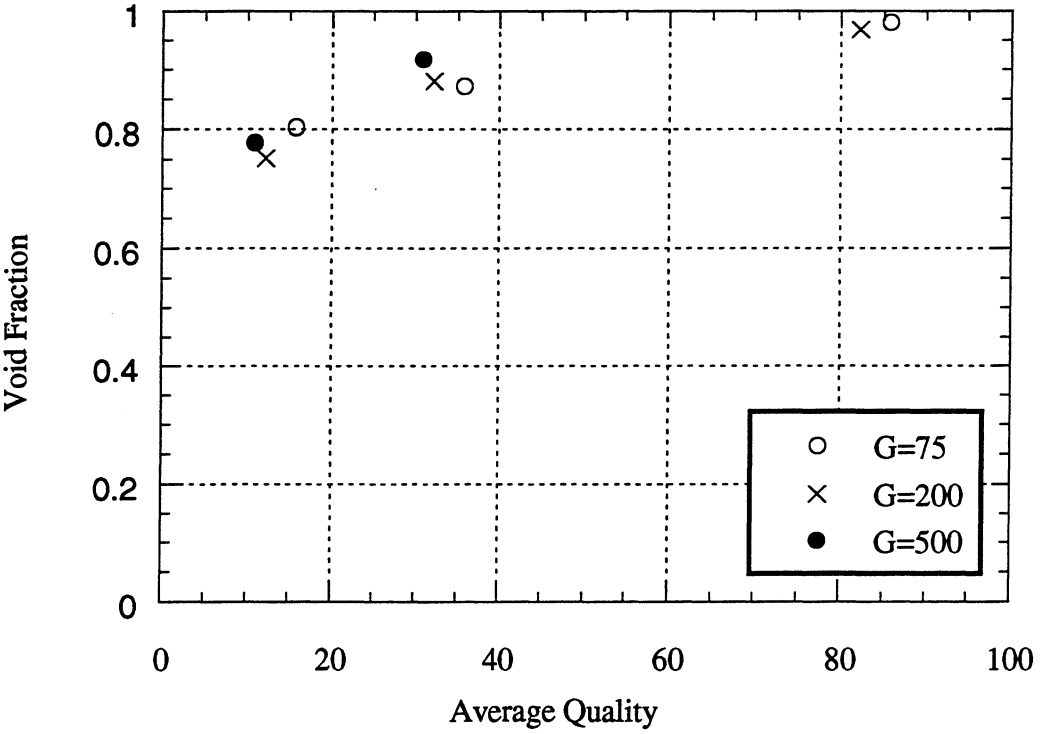

Figure B.2 Void fraction vs. average quality with a heat flux of 3 W/m^2 using R134a in a 8.89 mm base diameter axially grooved tube. Mass flux (G) given in kg/m^{2}s.

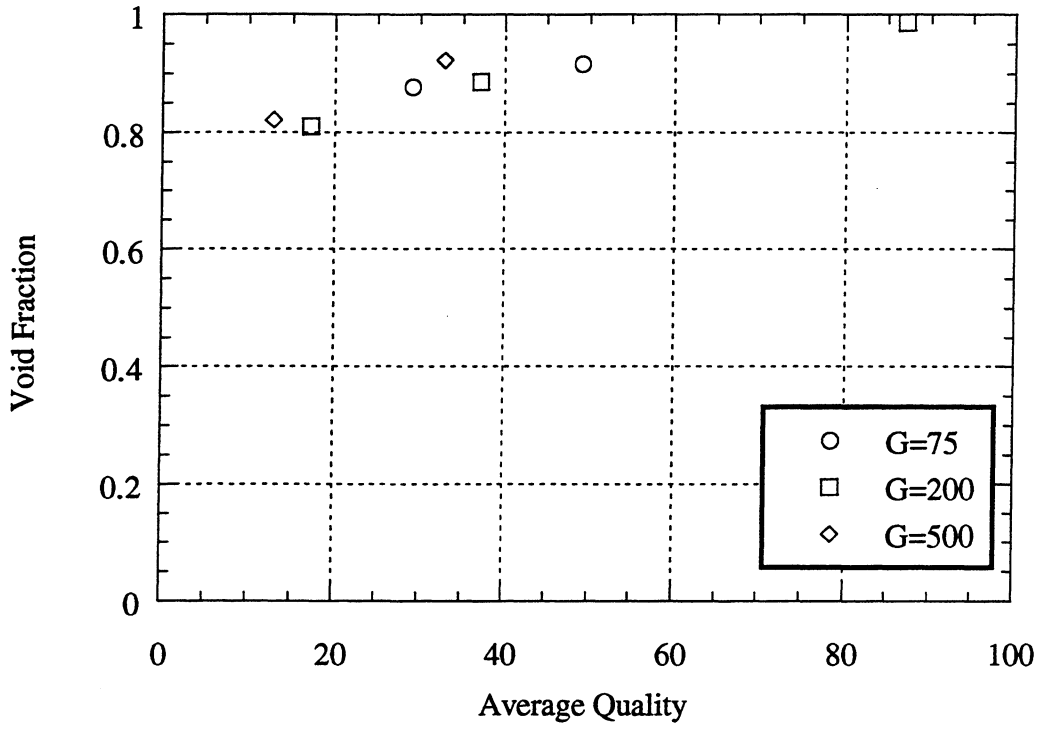

Figure B.3 Void fraction vs. average quality with a heat flux of 10 W/m^2 using R134a in 8.89 mm base diameter axially grooved tube. Mass flux (G) given in kg/m^{2}s.

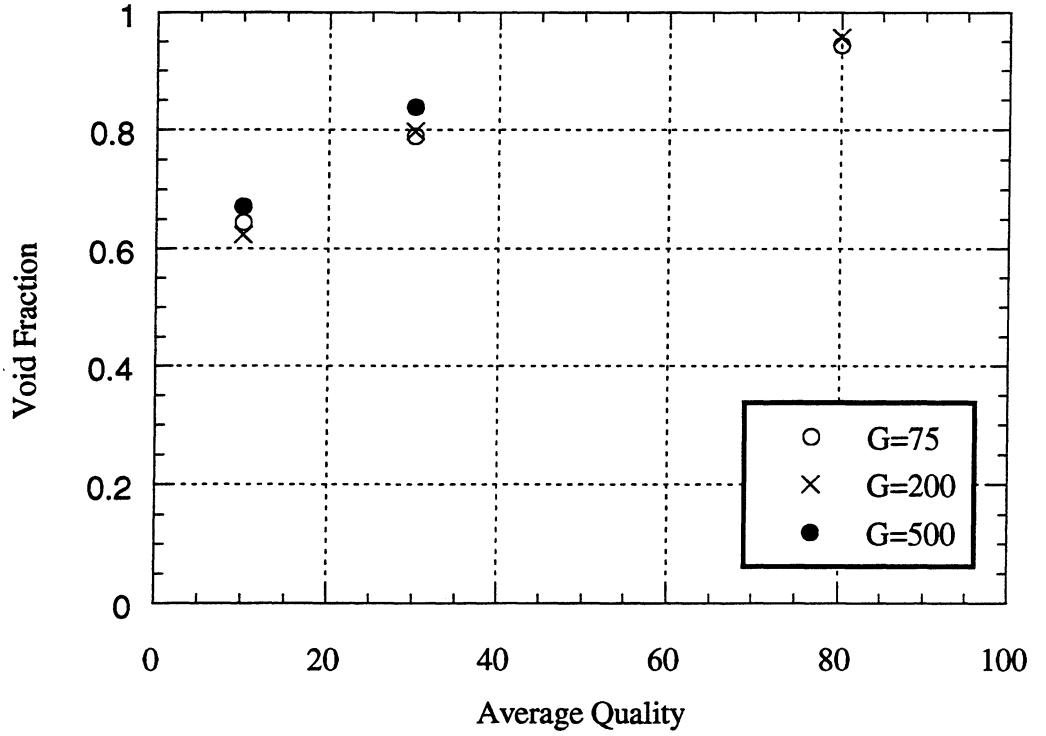

Figure B.4 Void fraction vs. average quality with a heat flux of 0 W/m^2 using R410A in a 8.89 mm base diameter axially grooved tube. Mass flux (G) given in kg/m^{2}s.

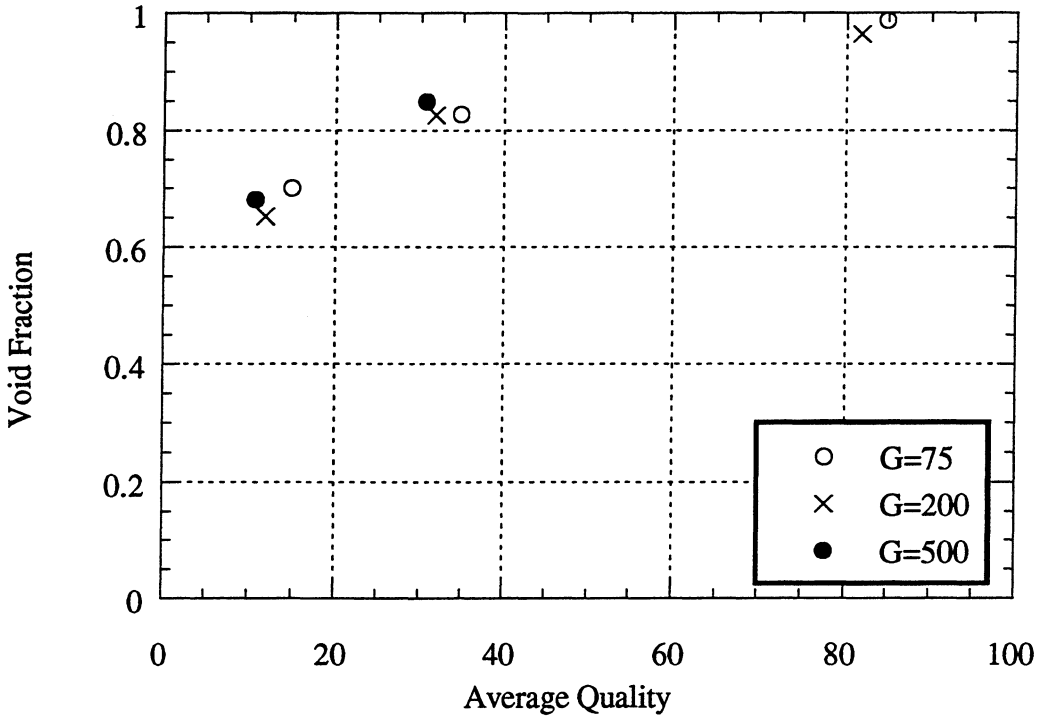

Figure B.5 Void fraction vs. average quality with a heat flux of 3 W/m^2 using R410A in a 8.89 mm base diameter axially grooved tube. Mass flux (G) given in kg/m^{2}s.

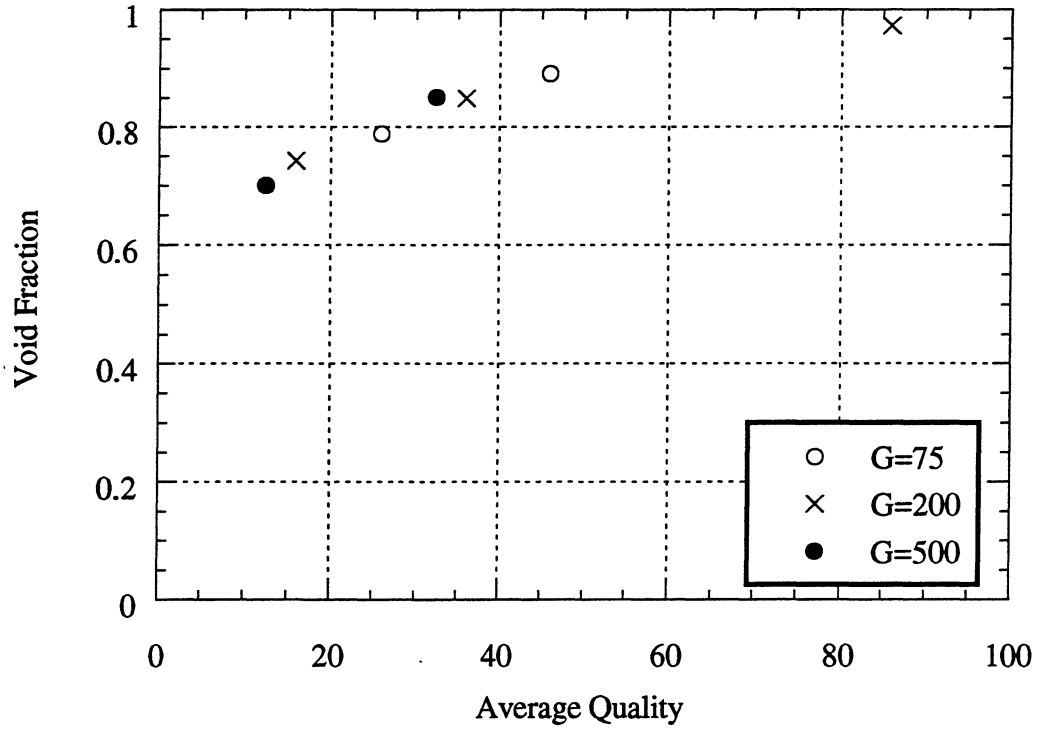

Figure B.6 Void fraction vs. average quality with a heat flux of 10 W/m^2 using R410A in a 8.89 mm base diameter axially grooved tube. Mass flux (G) given in kg/m^{2}s.

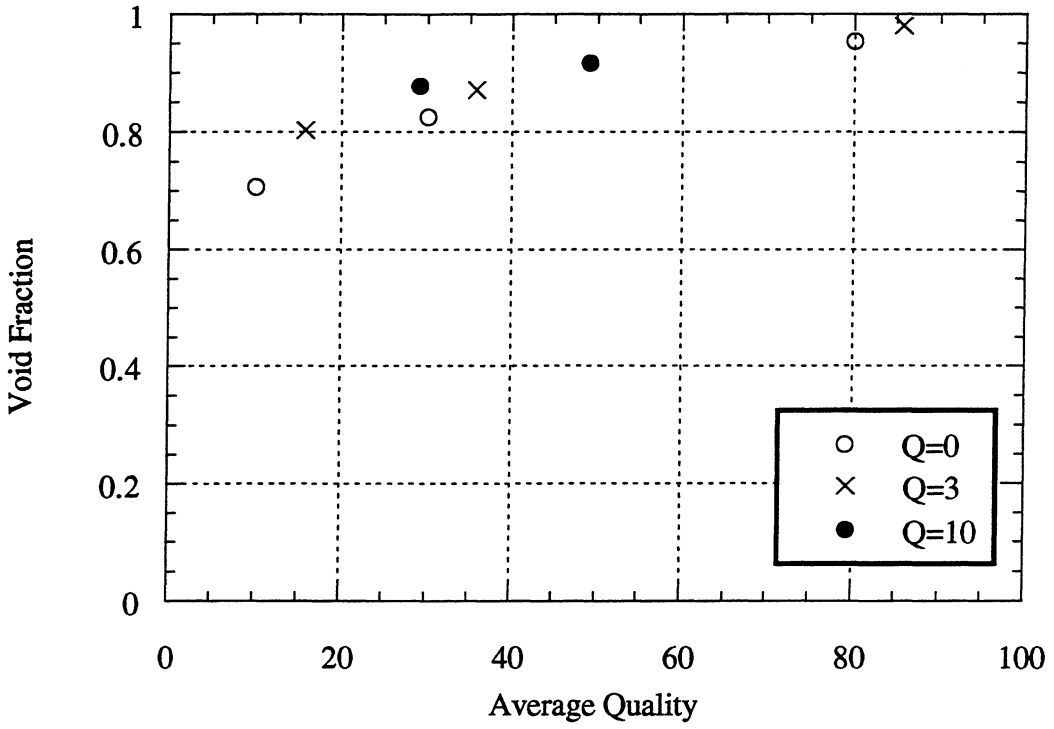

Figure B.7 Void fraction vs. average quality with a mass flux of 75 kg/m^{2}s using R134a in a 8.89 mm base diameter axially grooved tube. Heat flux (Q) in W/m^2.

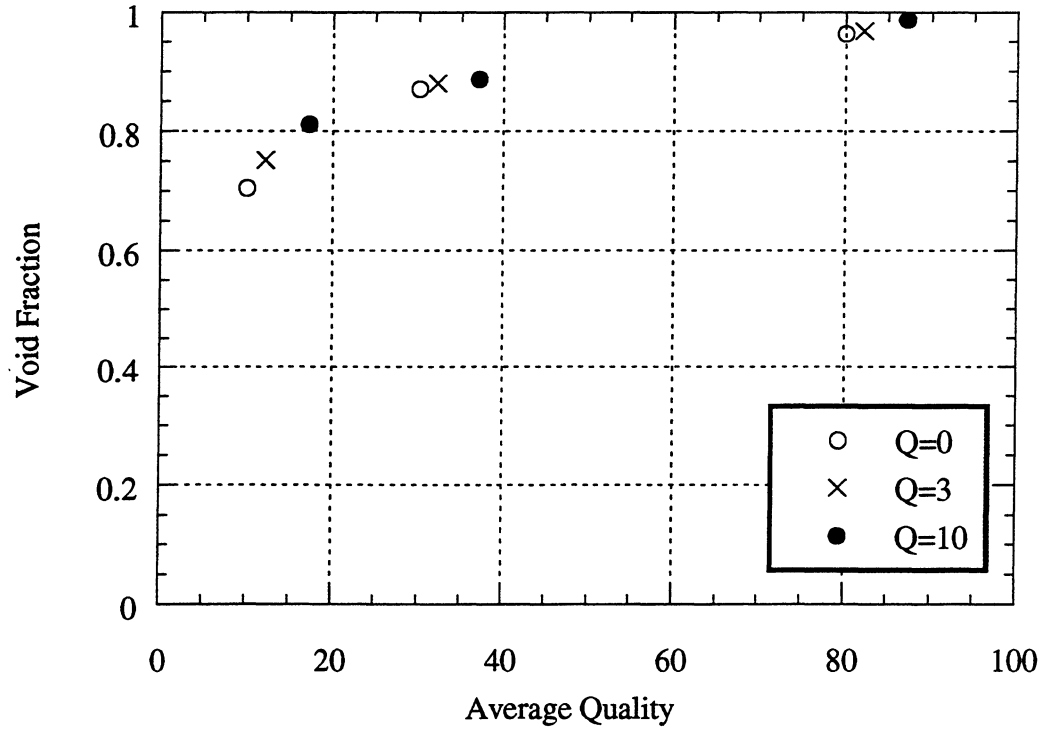

Figure B.8 Void fraction vs. average quality with a mass flux of 200 kg/m^{2}s using R134a a 8.89 mm base diameter axially grooved tube. Heat flux (Q) in W/m^2.

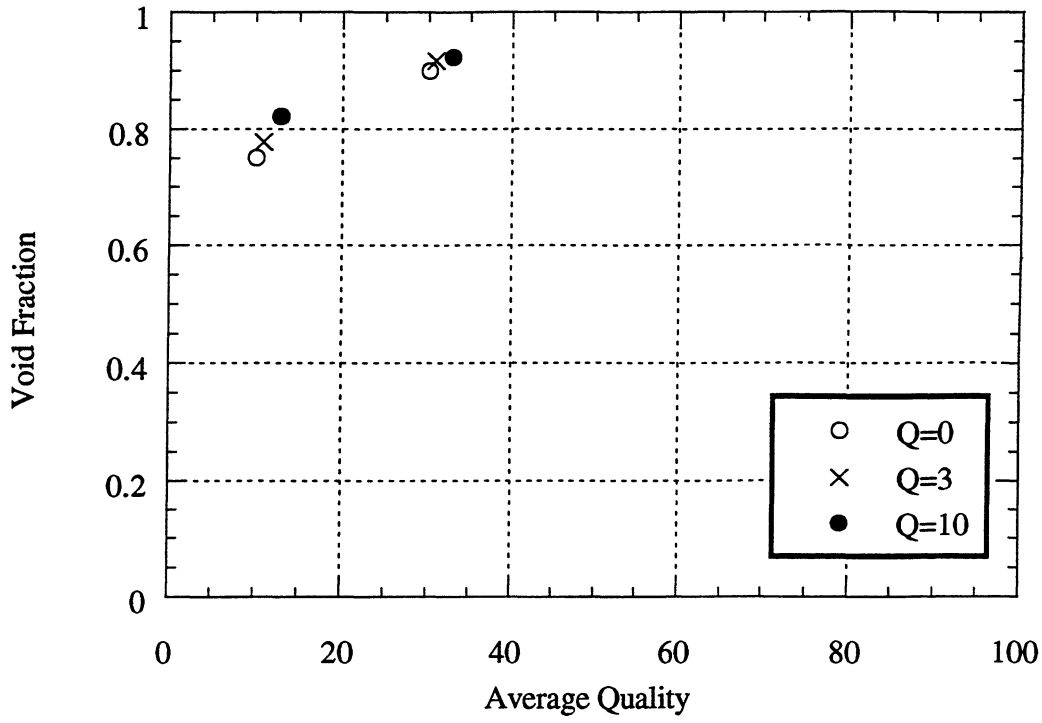

Figure B.9 Void fraction vs. average quality with a mass flux of 500 kg/m^{2}s using R134a in a 8.89 mm base diameter axially grooved tube. Heat flux (Q) in W/m^2.

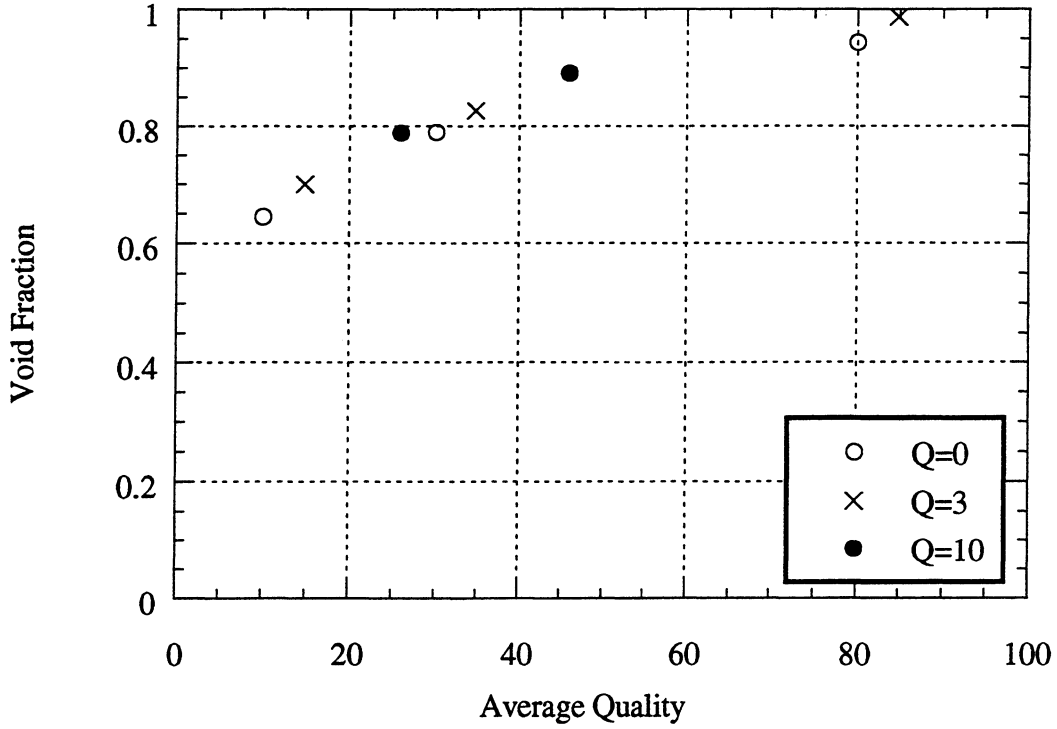

Figure B.10 Void fraction vs. average quality with a mass flux of 75 kg/m^{2}s using R410A in a 8.89 mm base diameter axially grooved tube. Heat flux (Q) in W/m^2.

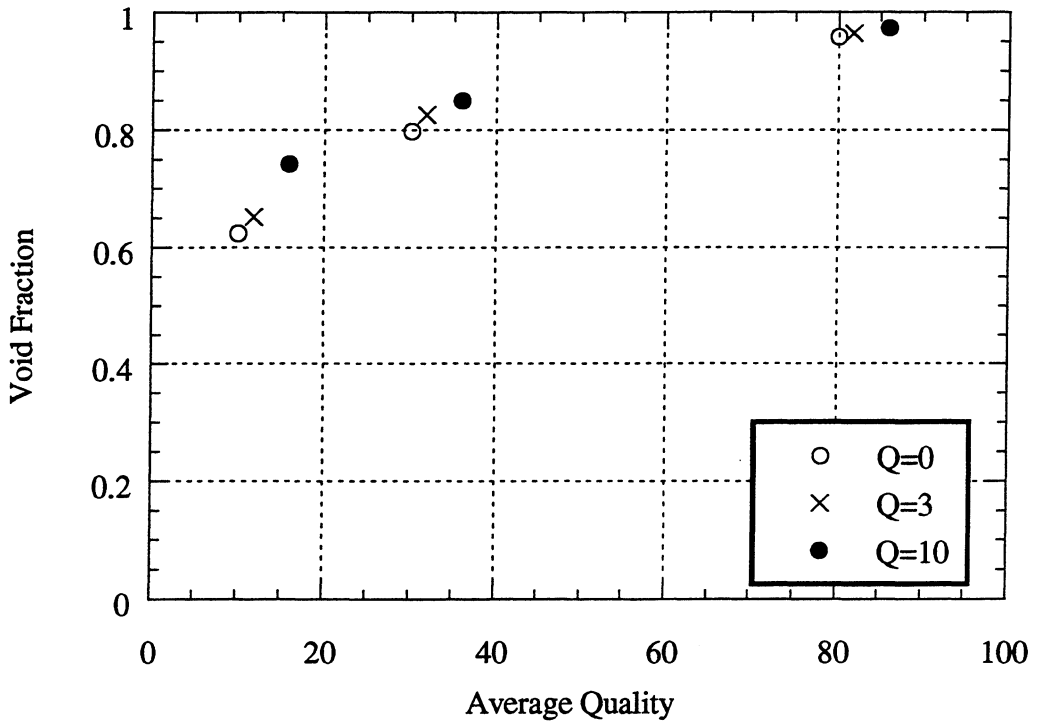

Figure B.11 Void fraction vs. average quality with a mass flux of 200 kg/m^{2}s using R410A in a 8.89 mm base diameter axially grooved tube. Heat flux (Q) in W/m^2.

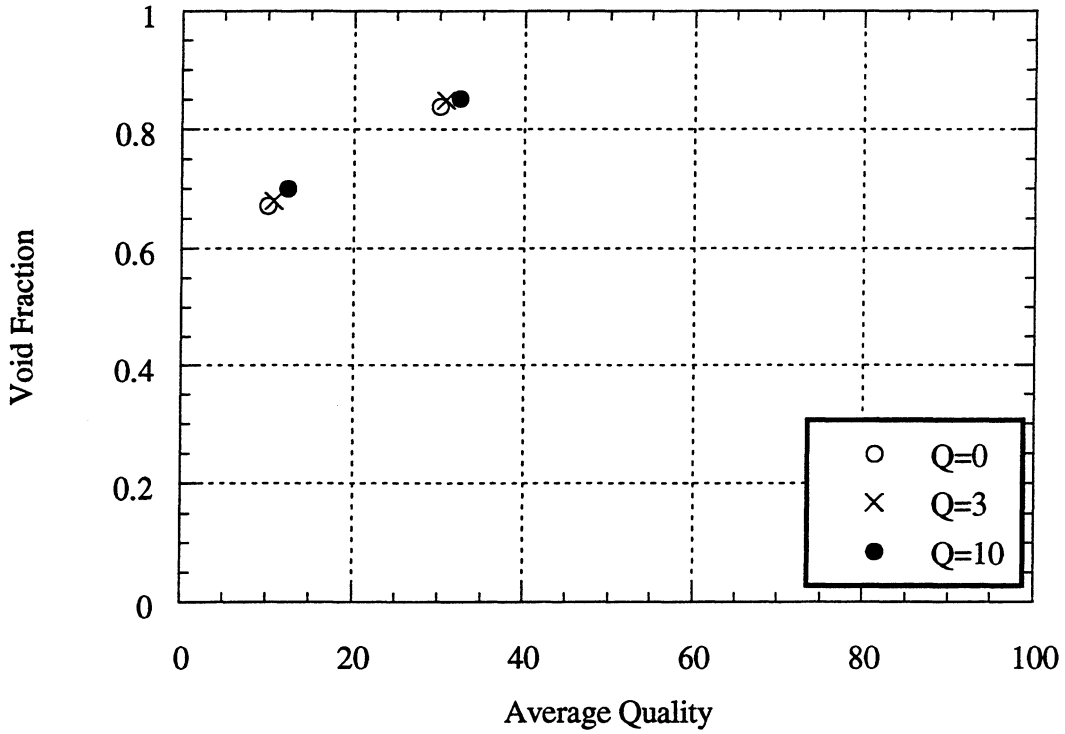

Figure B.12 Void fraction vs. average quality with a mass flux of 500 kg/m^{2}s using R410A in a 8.89 mm base diameter axially grooved tube. Heat flux (Q) in W/m^2.

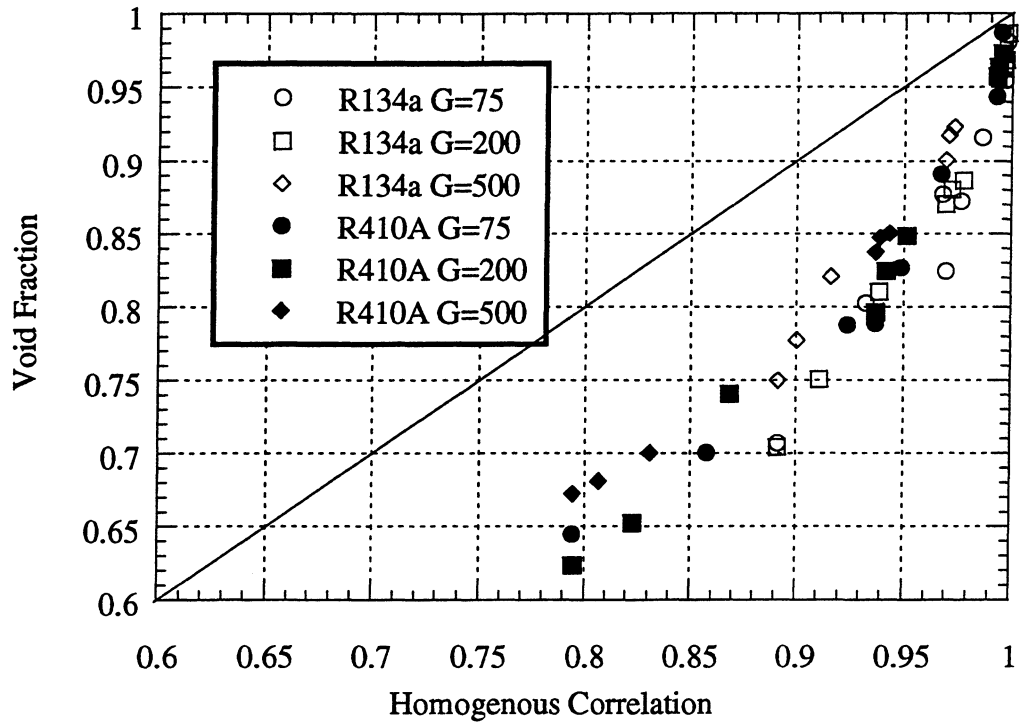

Figure B.13 Void fraction vs. homogenous correlation for 8.89 mm base diameter axially grooved tube using R134a and R410A. Mass flux (G) in kg/m^{2}s.

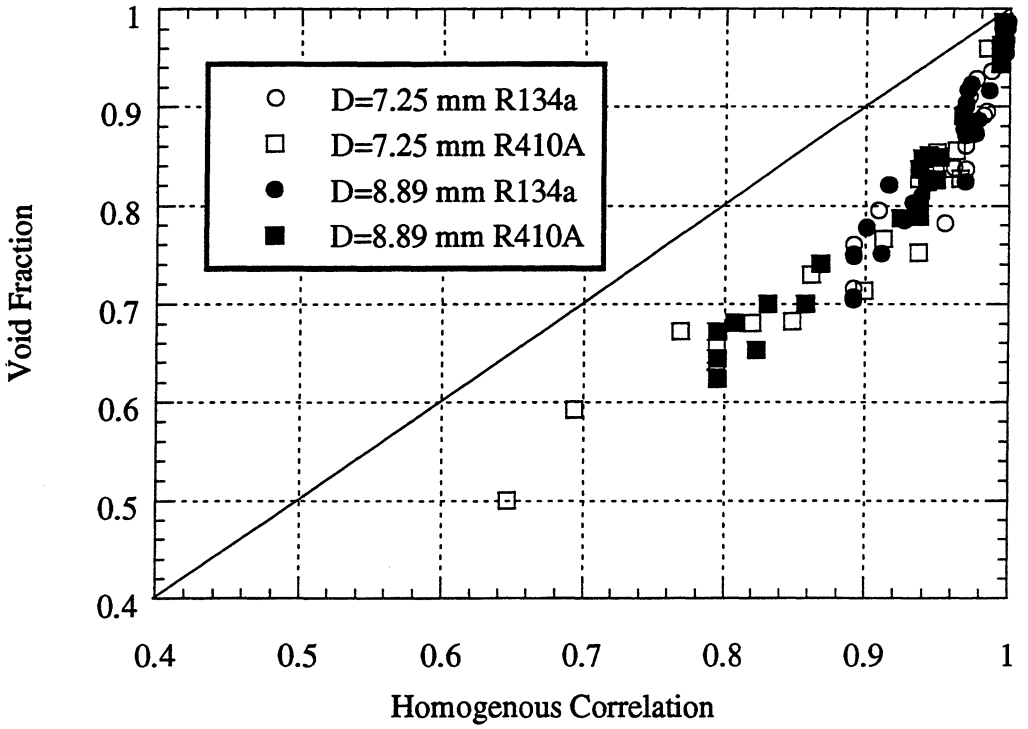

Figure B.14 Void fraction vs. homogenous correlation for 7.25 mm and 8.89 mm base diameter axially grooved tubes using R134a and R410A.

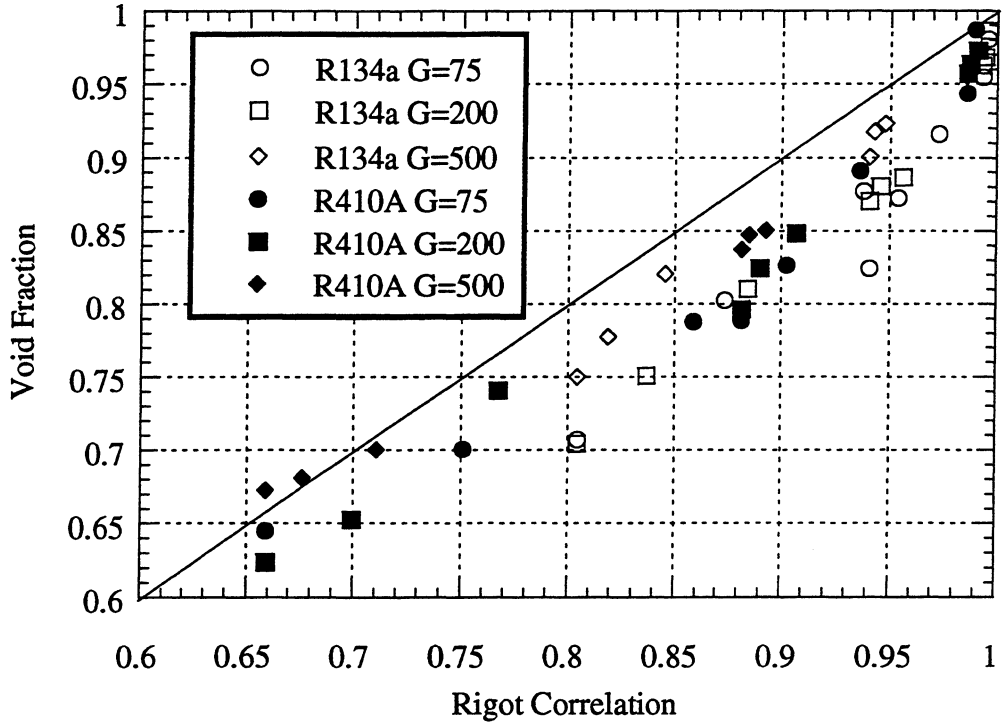

Figure B.15 Void fraction vs. Rigot correlation for 8.89 mm base diameter axially grooved tube using R134a and R410A. Mass flux (G) in kg/m^{2}s.

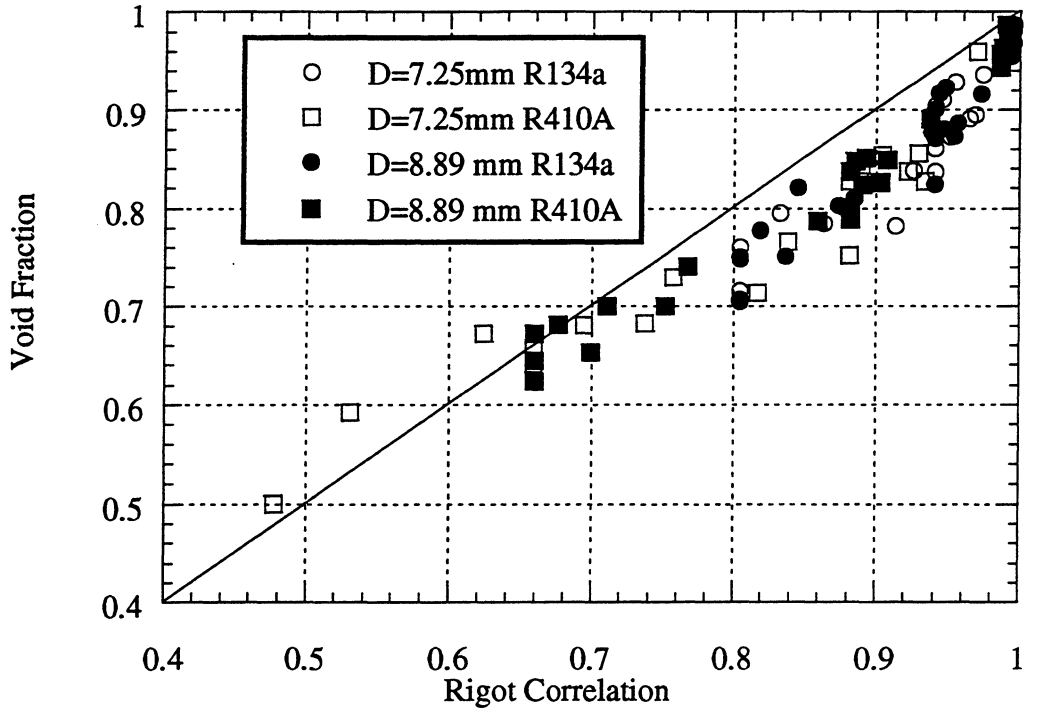

Figure B.16 Void fraction vs. Rigot correlation for 7.25 mm and 8.89 mm base diameter axially grooved tubes using R134a and R410A.

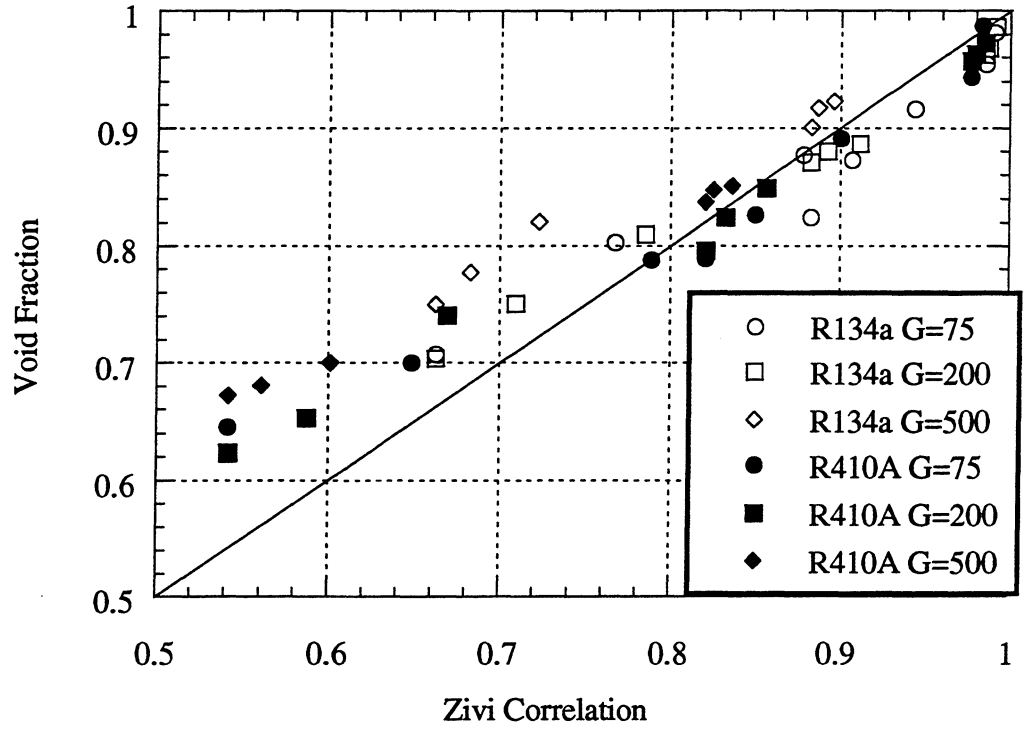

Figure B.17 Void fraction vs. Zivi correlation for 8.89 mm base diameter axially grooved tube using R134a and R410A. Mass flux (G) in kg/m^{2}s.

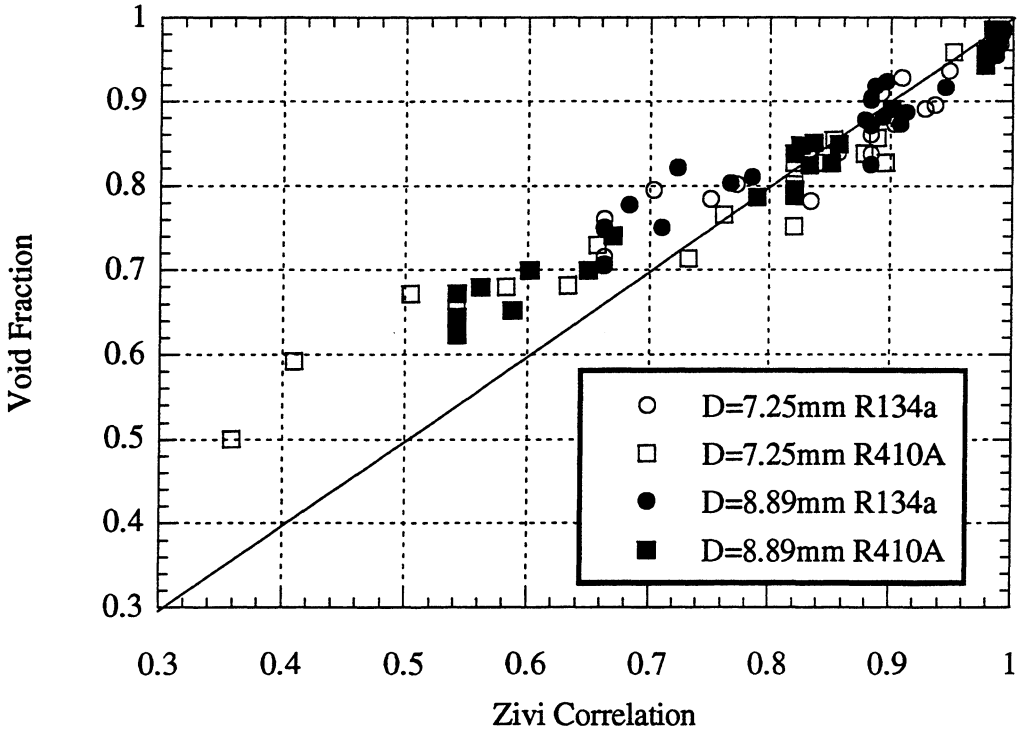

Figure B.18 Void fraction vs. Zivi correlation for 7.25 mm and 8.89 mm base diameter axially grooved tubes using R134a and R410A.

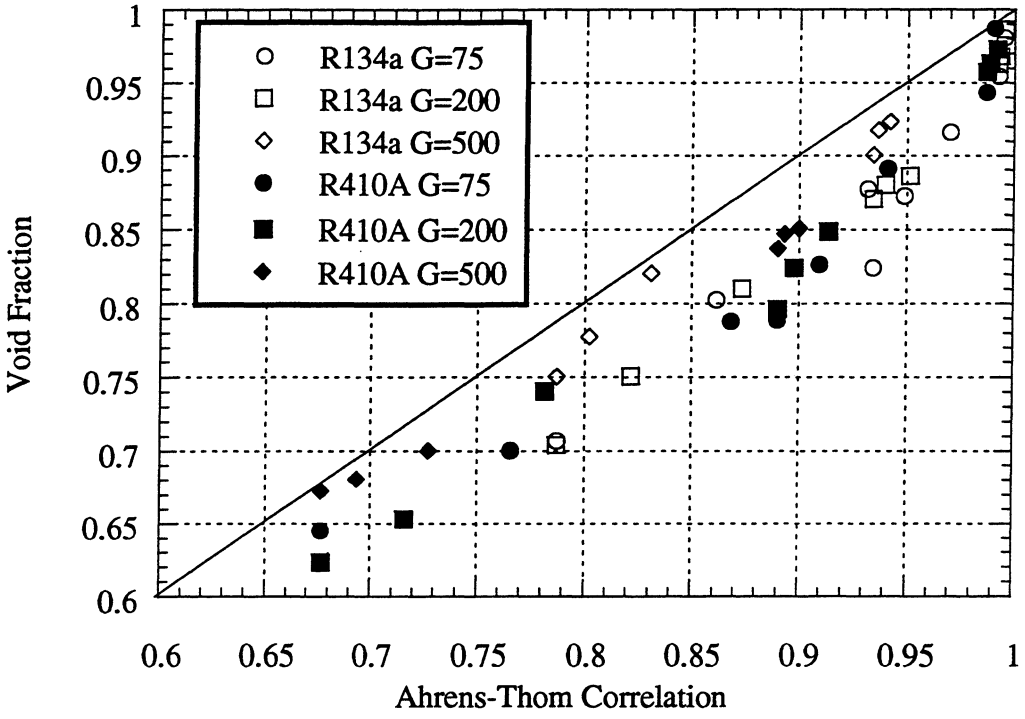

Figure B.19 Void fraction vs. Ahrens-Thom correlation for 8.89 mm base diameter axially grooved tube using R134a and R410A. Mass flux (G) in kg/m^{2}s.

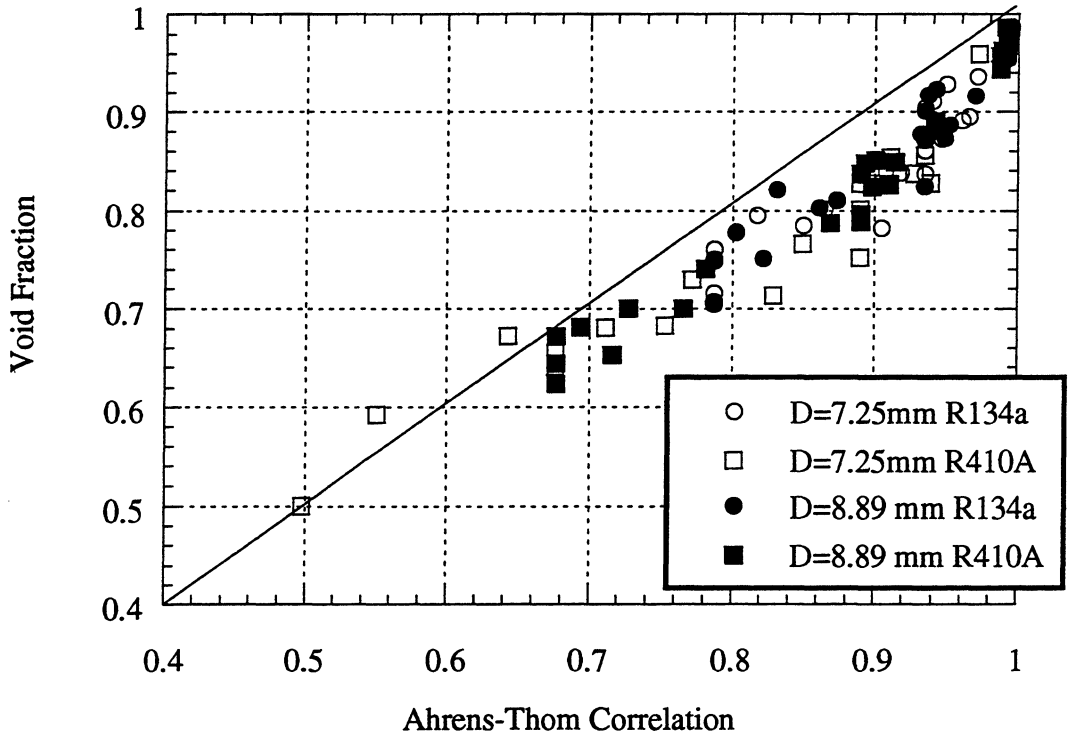

Figure B.20 Void fraction vs. Ahrens-Thom correlation for 7.25 mm and 8.89 mm base diameter axially grooved tubes using R134a and R410A.

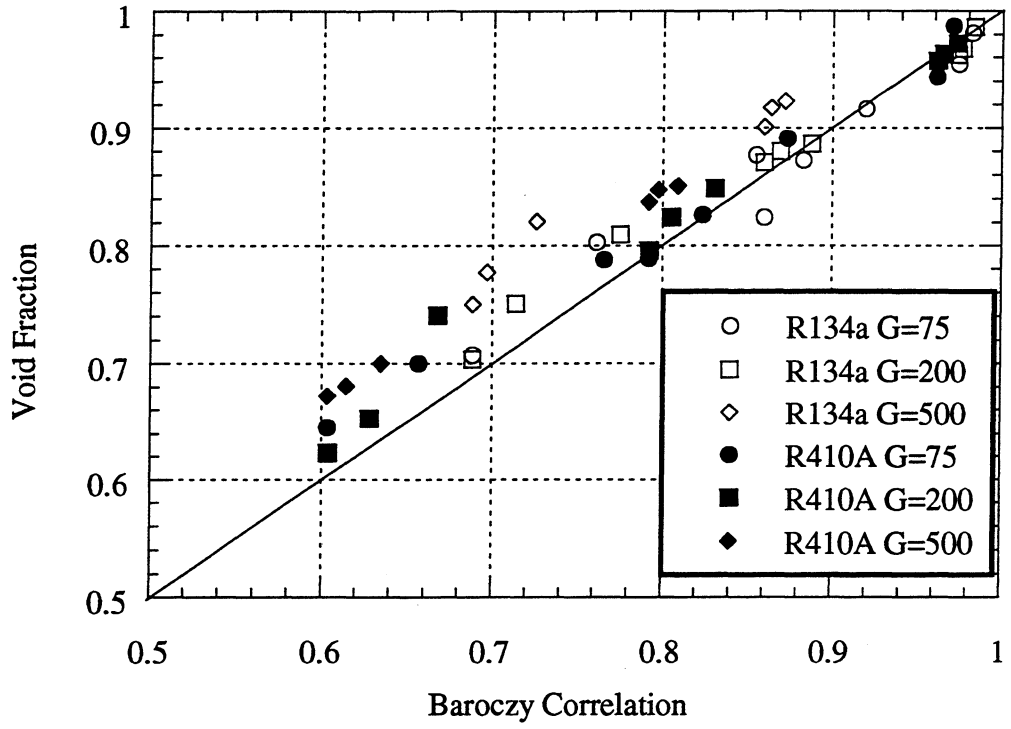

Figure B.21 Void fraction vs. Baroczy correlation for 8.89 mm base diameter axially grooved tube using R134a and R410A. Mass flux (G) in kg/m^{2}s.

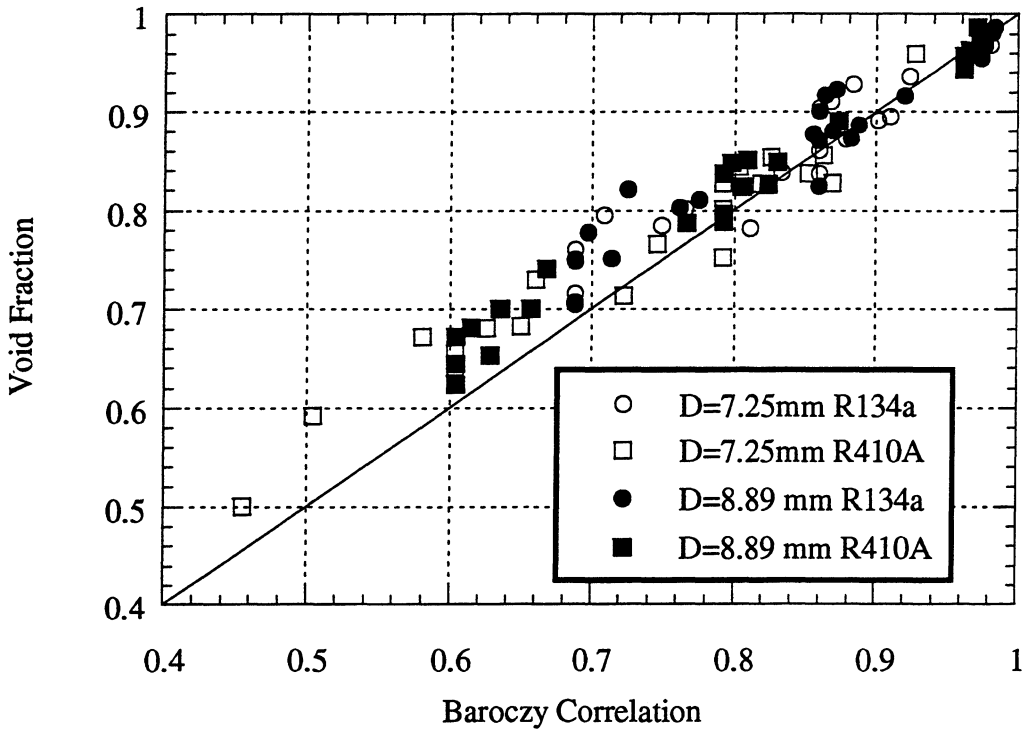

Figure B.22 Void fraction vs. Baroczy correlation for 7.25 mm and 8.89 mm base diameter axially grooved tubes using R134a and R410A.

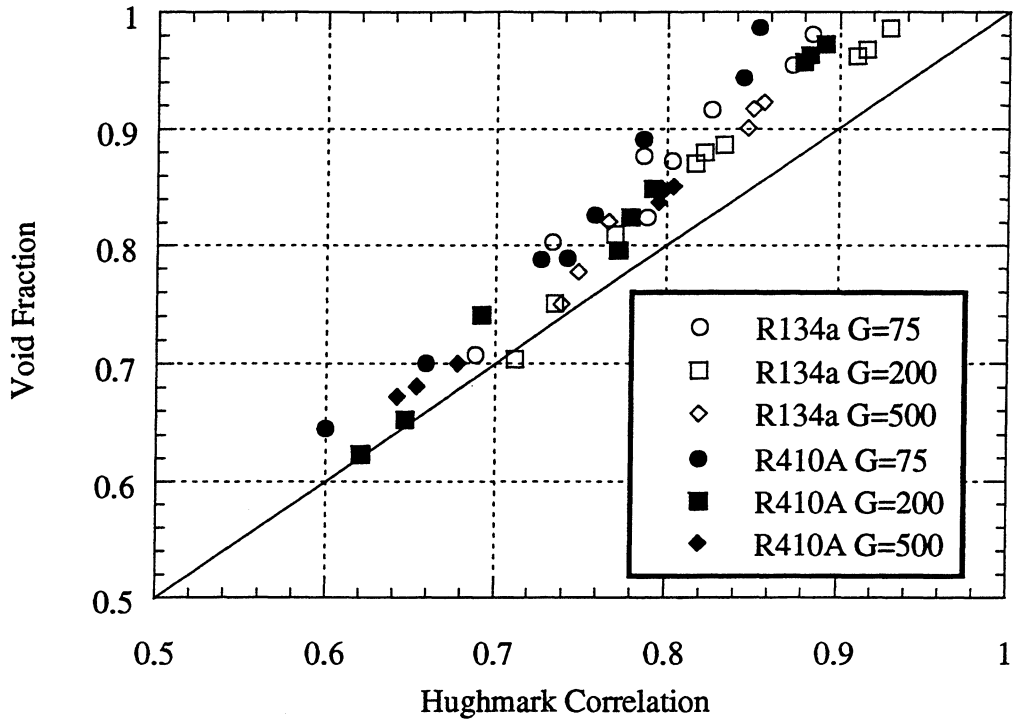

Figure B.23 Void fraction vs. Hughmark correlation for 8.89 mm base diameter axially grooved tube using R134a and R410A. Mass flux (G) in kg/m^{2}s.

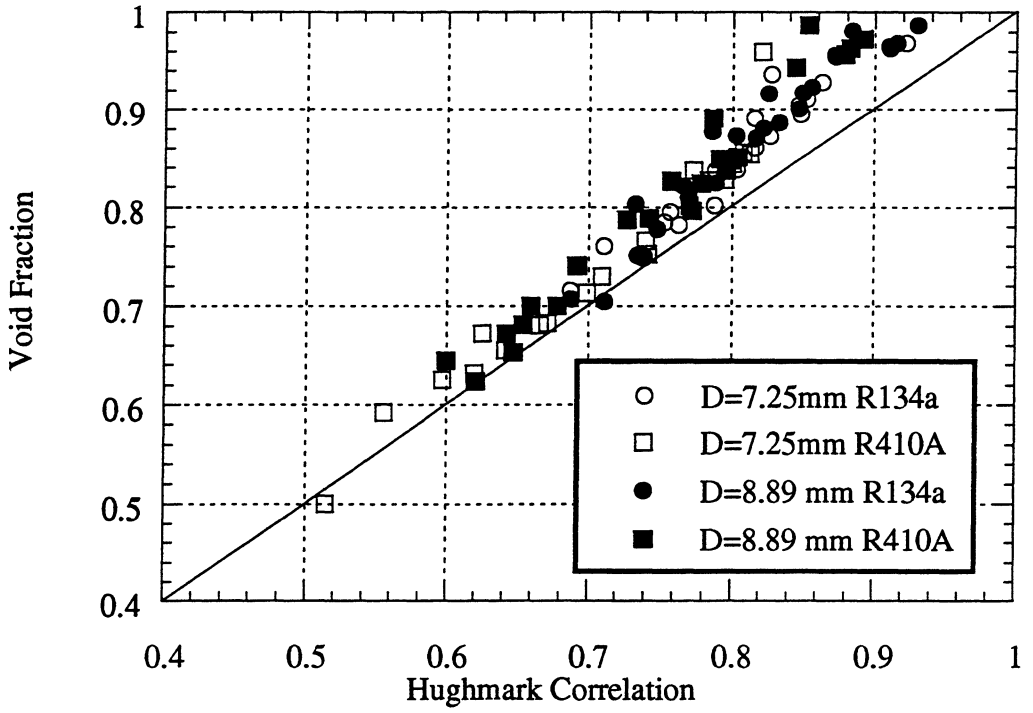

Figure B.24 Void fraction vs. Hughmark correlation for 7.25 mm and 8.89 mm base diameter axially grooved tubes using R134a and R410A.

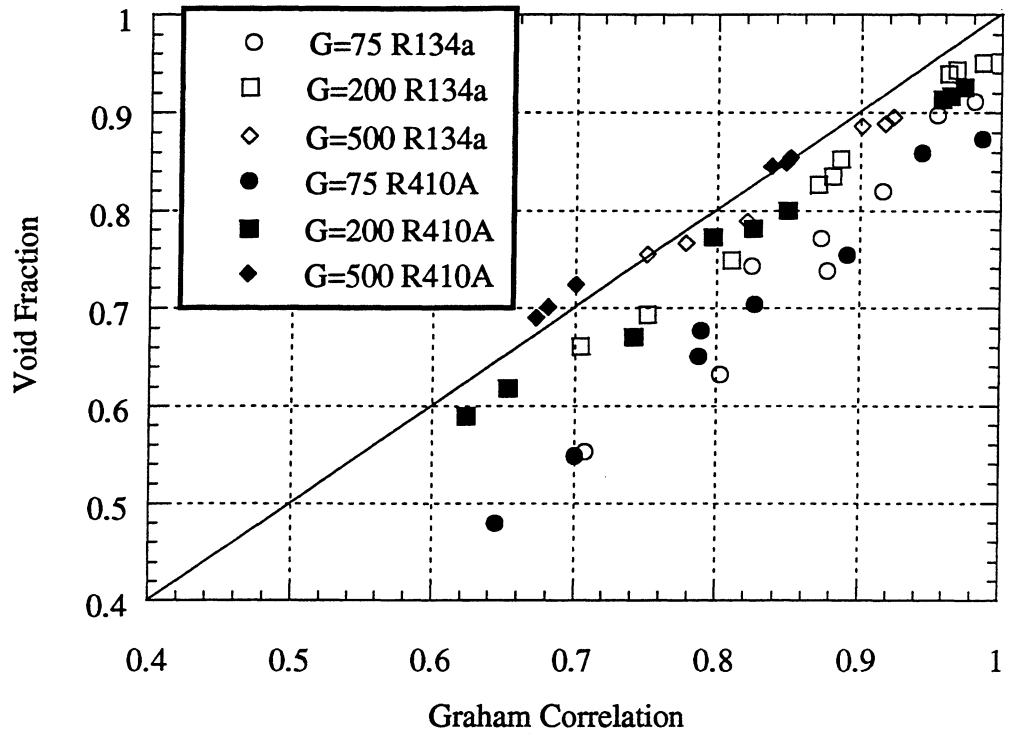

Figure B.25 Void fraction vs. Graham's condenser correlation for 8.89 mm base diameter axially grooved tube using R134a and R410A. Mass flux (G) in kg/m^{2}s.

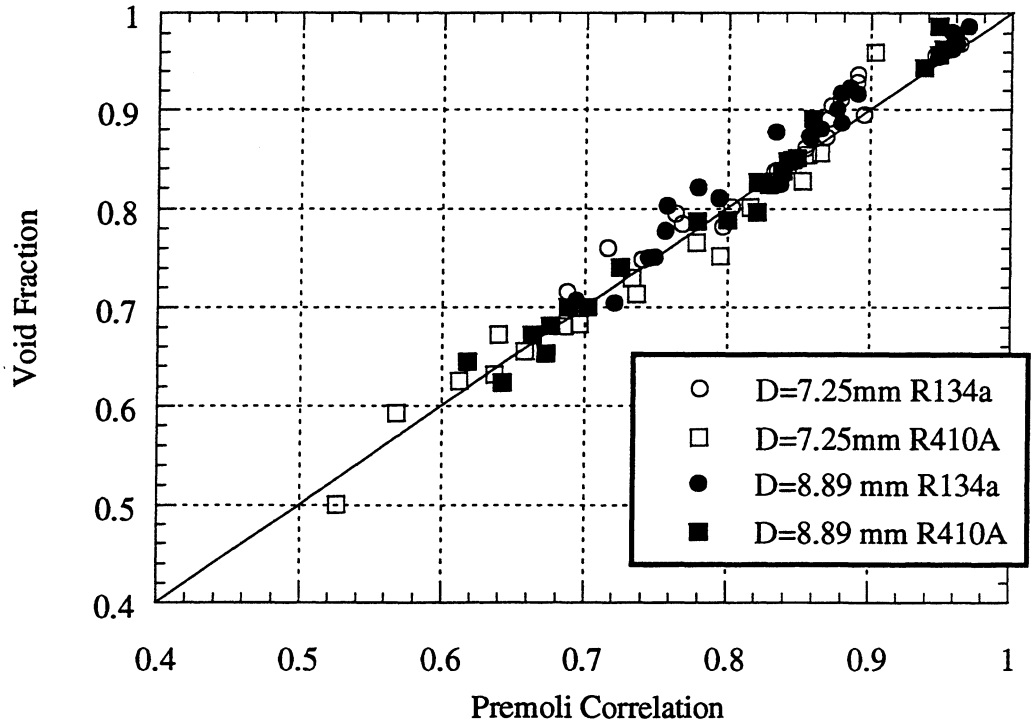

Figure B.26 Void fraction vs. Premoli correlation for 7.25 mm and 8.89 mm base diameter axially grooved tubes using R134a and R410A.

Appendix C

Helically Grooved Tubes

This appendix presents raw data taken for the 8.93 base diameter helically grooved tube. The 7.26 mm base diameter helically grooved tube data appears in Yashar. Data will be presented first in tabular format, and second in graphical forms.

Table C.1 Raw data for 8.93 mm base diameter helically grooved tube

Fluid	Heat Flux	Mass Flux	Inlet Qual(%)	Ave Qual(%)	Void Fraction
R134a	0	75	10	10	0.6897
R134a	3	75	10	19.93	0.8167
R134a	10	75	10	43.11	0.9165
R134a	0	75	30	30	0.8514
R134a	3	75	30	39.93	0.8972
R134a	10	75	30	63.11	0.9492
R134a	0	200	10	10	0.7399
R134a	3	200	10	13.73	0.7753
R134a	10	200	10	22.42	0.8267
R134a	0	200	30	30	0.8610
R134a	3	200	30	33.73	0.8842
R134a	0	500	10	10	0.7926
R134a	3	500	10	11.49	0.7812
R134a	0	200	5	5	0.6639
R134a	0	500	5	5	0.6962
R134a	0	700	5	5	0.6982
R410A	0	75	10	10	0.6422
R410A	3	75	10	18.3	0.7354
R410A	10	75	10	37.68	0.8182
R410A	0	75	30	30	0.7801
R410A	3	75	30	38.3	0.8536
R410A	10	75	30	57.68	0.9069
R410A	0	75	80	80	0.9438
R410A	3	75	80	88.3	0.9850
R410A	0	200	10	10	0.6543
R410A	3	200	10	13.11	0.6886
R410A	10	200	10	20.38	0.7635
R410A	0	200	30	30	0.8020
R410A	3	200	30	33.11	0.8215
R410A	10	200	30	40.38	0.8603
R410A	0	200	80	80	0.9518
R410A	3	200	80	83.11	0.9622
R410A	0	500	10	10	0.7066

R410A	3	500	10	11.25	0.7297
R410A	10	500	10	14.15	0.7322
R410A	0	500	30	30	0.8338
R410A	3	500	30	31.25	0.8494

Heat flux given in W/m^2 and mass flux in kg/m^2s.

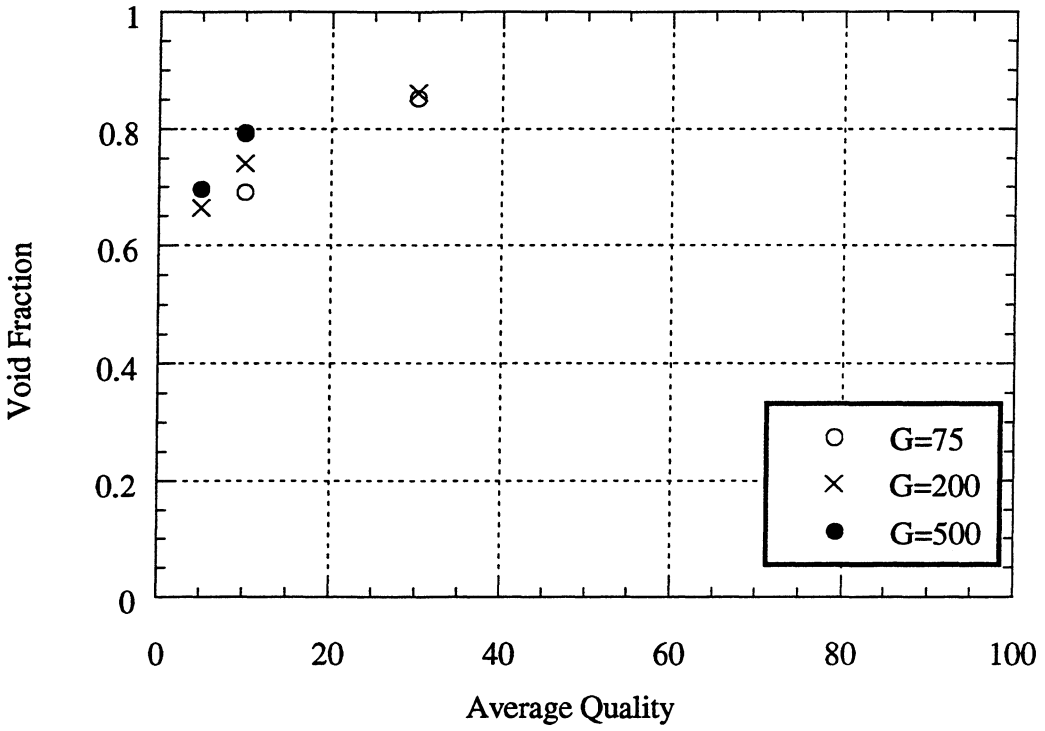

Figure C.1 Void fraction vs. average quality with a heat flux of 0 W/m^2 using R134a in a 8.93 mm base diameter axially grooved tube. Mass flux (G) given in kg/m^{2}s.

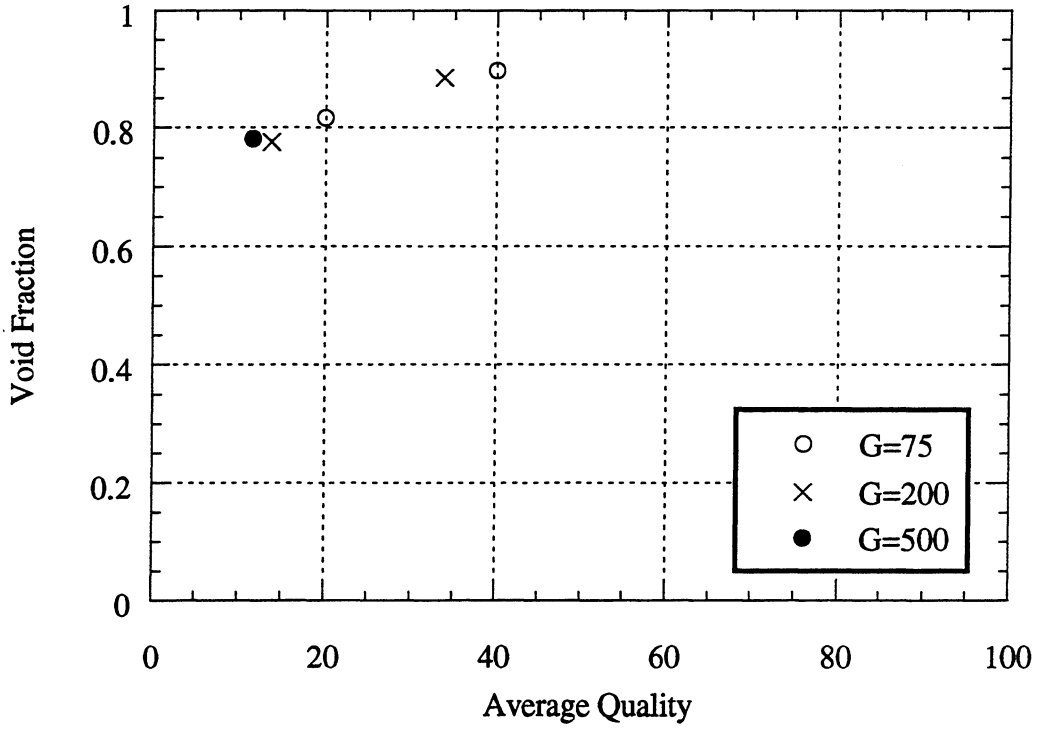

Figure C.2 Void fraction vs. average quality with a heat flux of 3 W/m^2 using R134a in a 8.93 mm base diameter axially grooved tube. Mass flux (G) given in kg/m^{2}s.

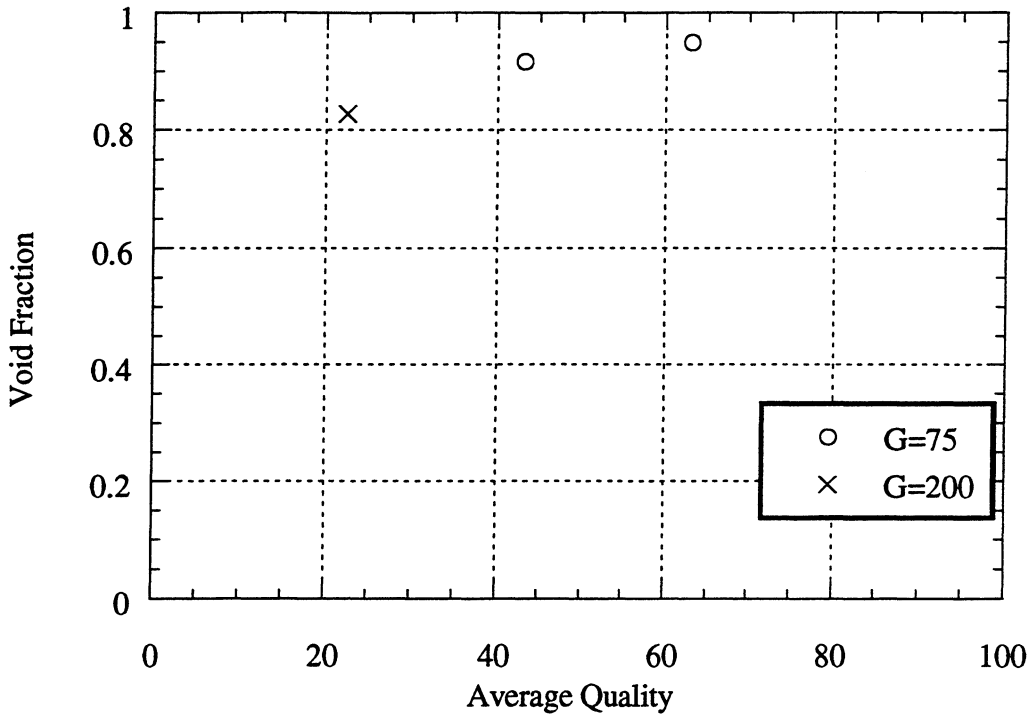

Figure C.3 Void fraction vs. average quality with a heat flux of 10 W/m^2 using R134a in 8.93 mm base diameter axially grooved tube. Mass flux (G) given in kg/m^{2}s.

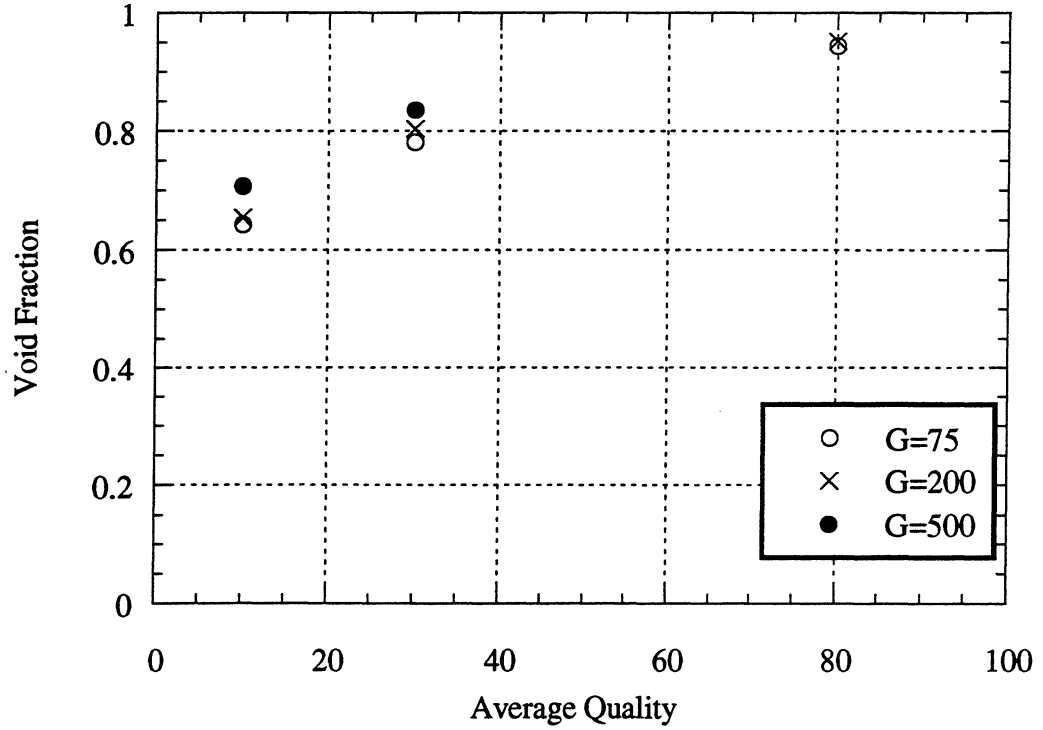

Figure C.4 Void fraction vs. average quality with a heat flux of 0 W/m^2 using R410A in a 8.93 mm base diameter axially grooved tube. Mass flux (G) given in kg/m^{2}s.

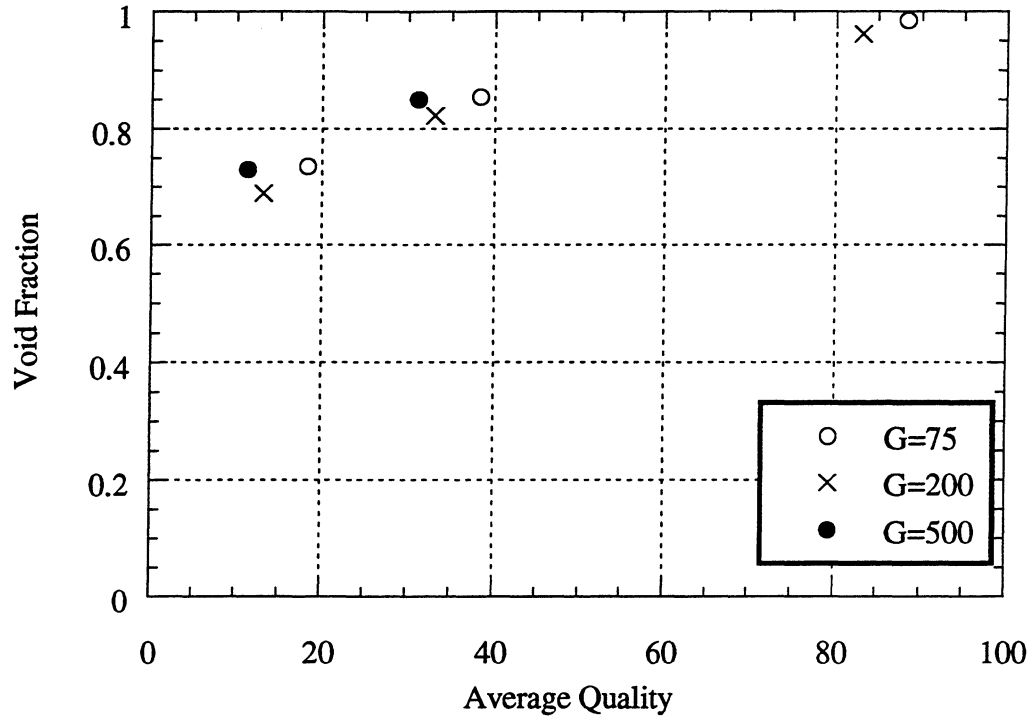

Figure C.5 Void fraction vs. average quality with a heat flux of 3 W/m^2 using R410A in a 8.93 mm base diameter axially grooved tube. Mass flux (G) given in kg/m^{2}s.

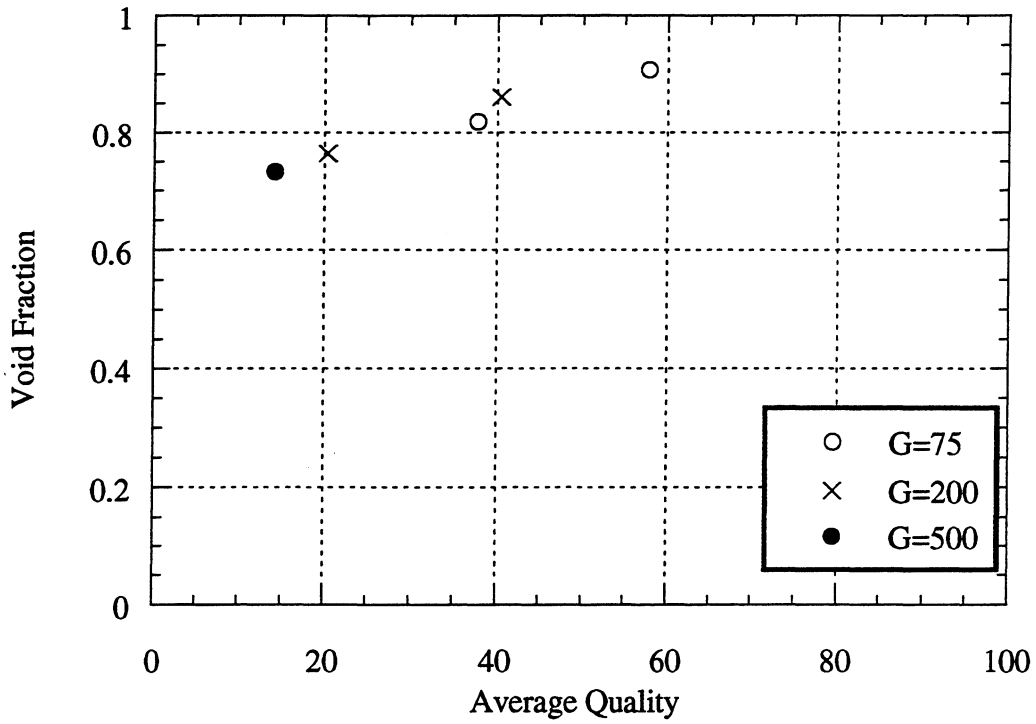

Figure C.6 Void fraction vs. average quality with a heat flux of 10 W/m^2 using R410A in a 8.93 mm base diameter axially grooved tube. Mass flux (G) given in kg/m^{2}s.

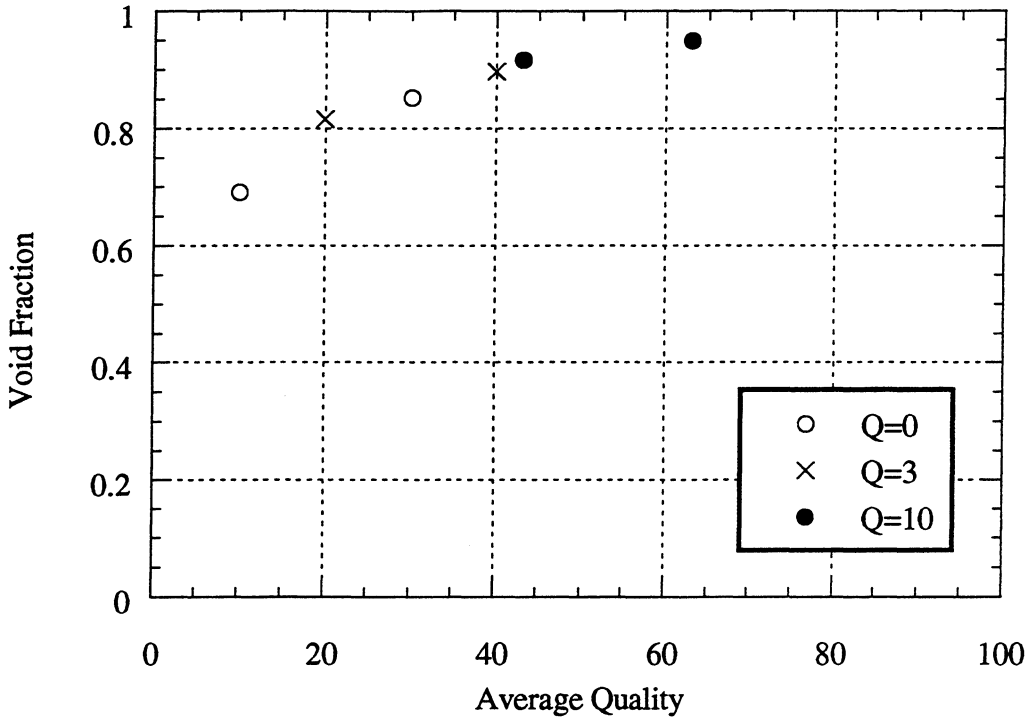

Figure C.7 Void fraction vs. average quality with a mass flux of 75 kg/m^{2}s using R134a in a 8.93 mm base diameter axially grooved tube. Heat flux (Q) in W/m^2.

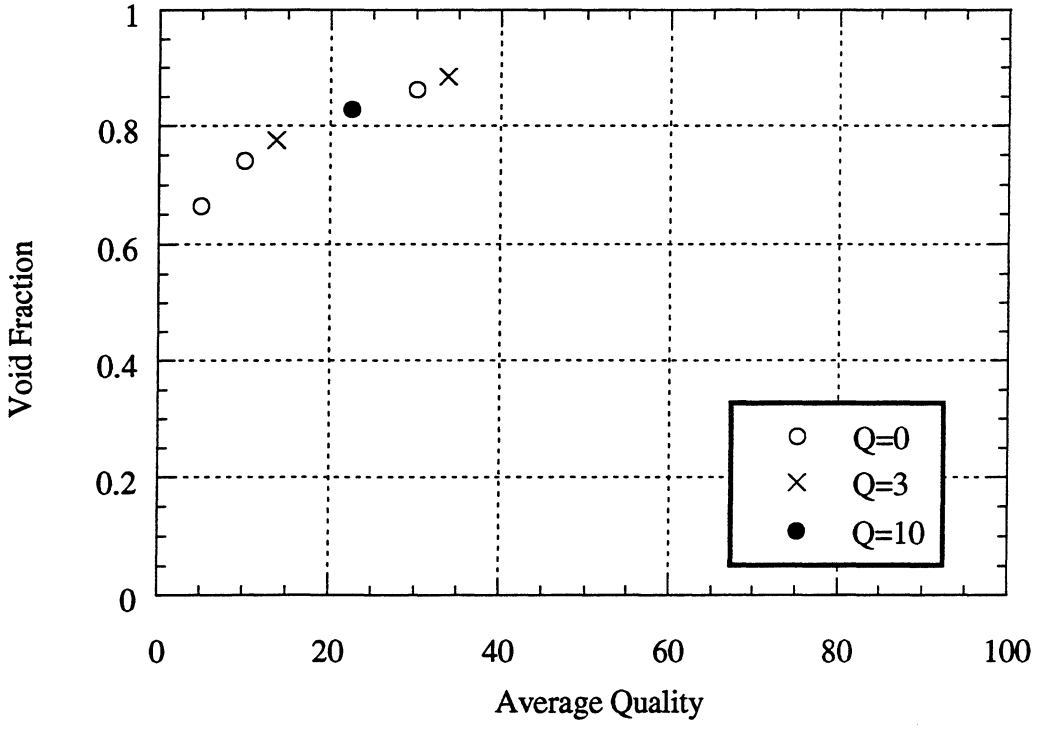

Figure C.8 Void fraction vs. average quality with a mass flux of 200 kg/m^{2}s using R134a a 8.93 mm base diameter axially grooved tube. Heat flux (Q) in W/m^2.

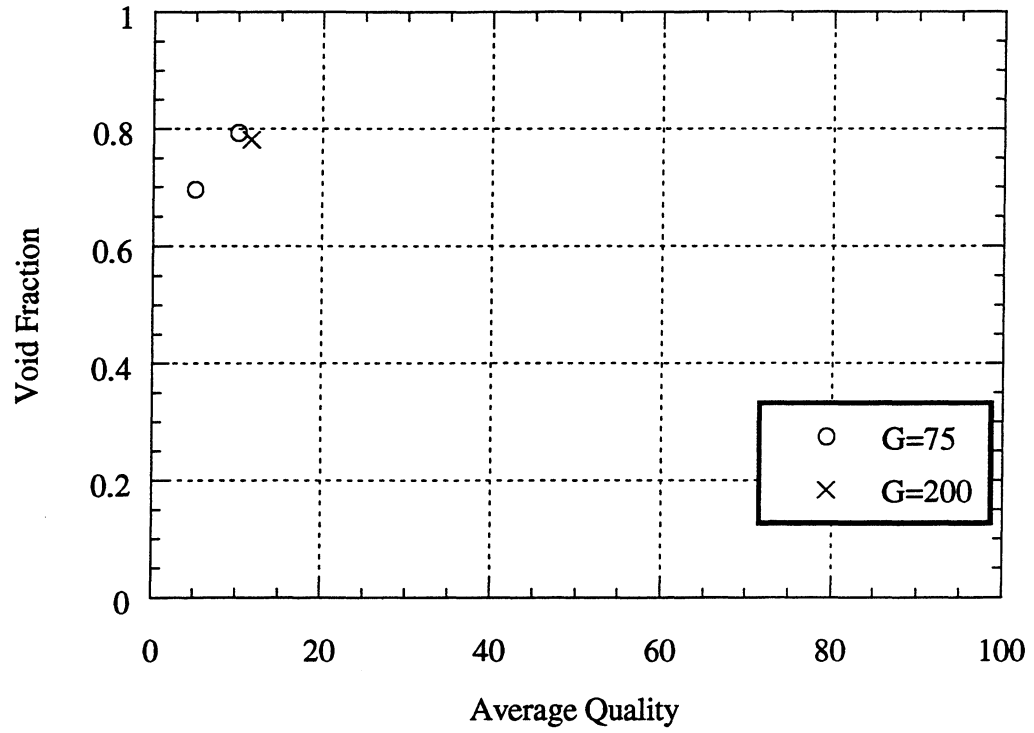

Figure C.9 Void fraction vs. average quality with a mass flux of 500 kg/m^{2}s using R134a in a 8.93 mm base diameter axially grooved tube. Heat flux (Q) in W/m^2.

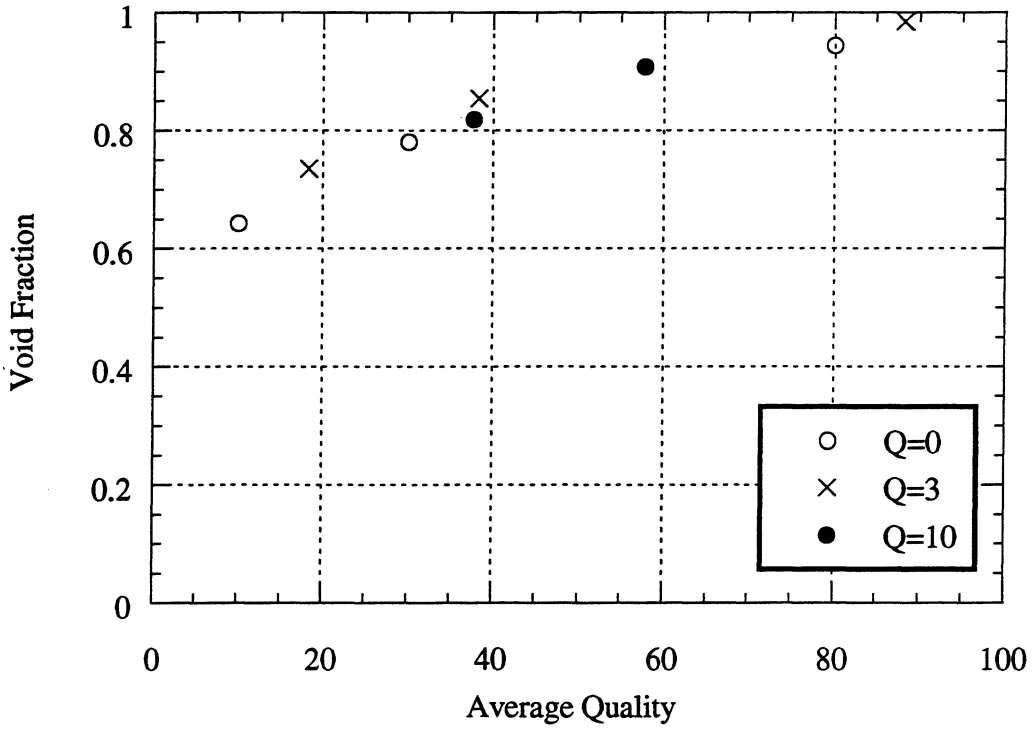

Figure C.10 Void fraction vs. average quality with a mass flux of 75 kg/m^{2}s using R410A in a 8.93 mm base diameter axially grooved tube. Heat flux (Q) in W/m^2.

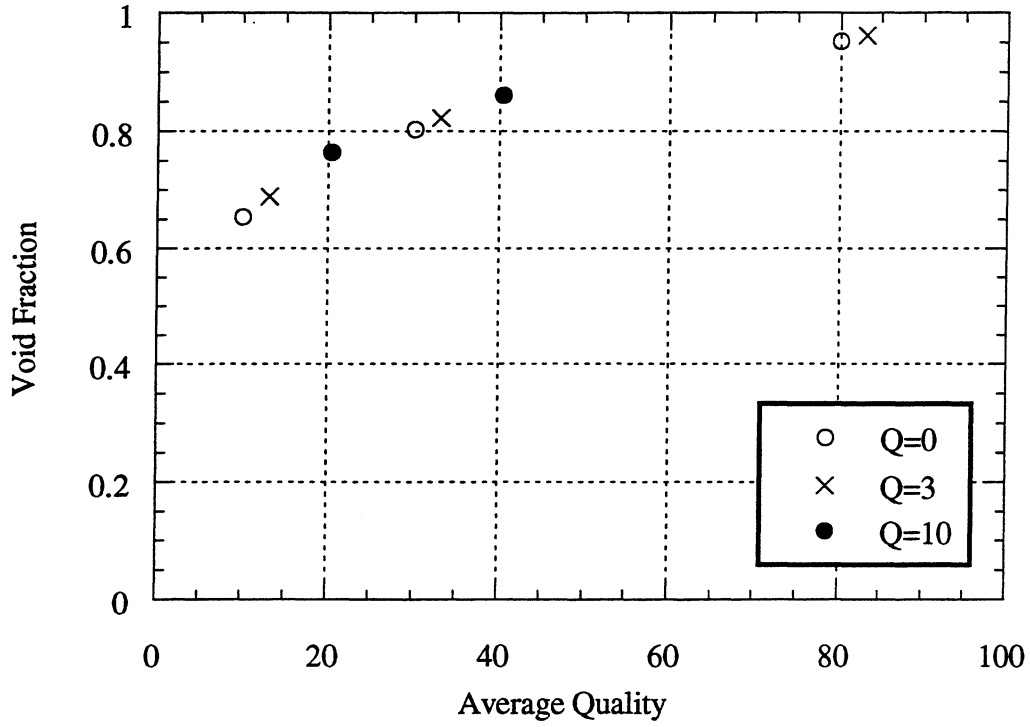

Figure C.11 Void fraction vs. average quality with a mass flux of 200 kg/m^{2}s using R410A in a 8.93 mm base diameter axially grooved tube. Heat flux (Q) in W/m^2.

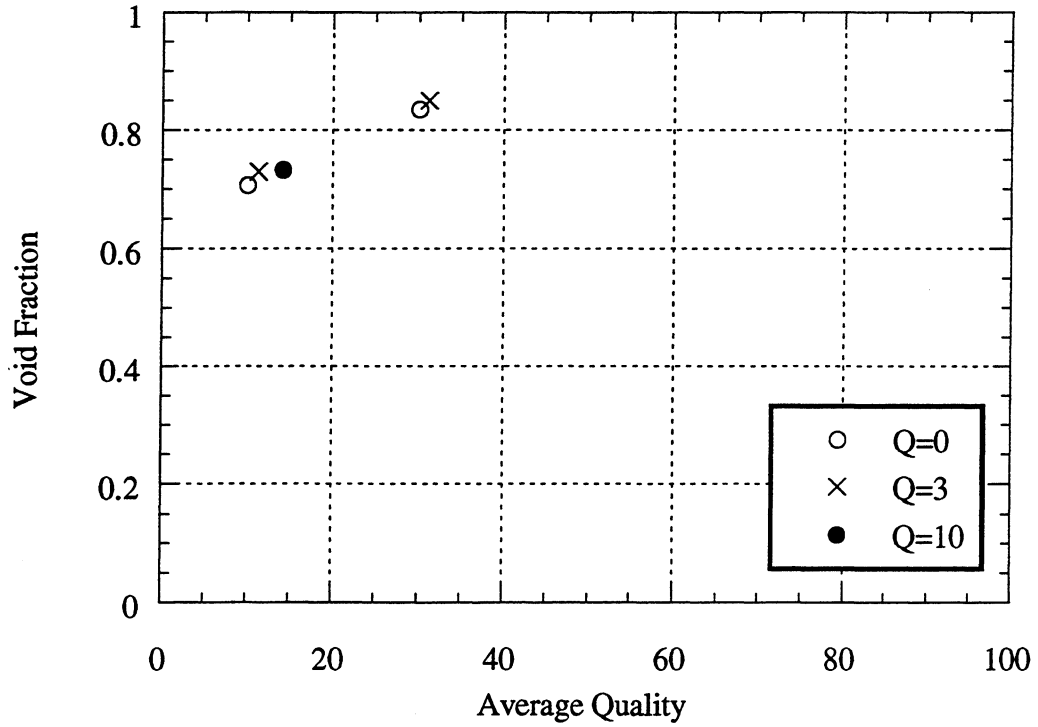

Figure C.12 Void fraction vs. average quality with a mass flux of 500 kg/m^{2}s using R410A in a 8.93 mm base diameter axially grooved tube. Heat flux (Q) in W/m^2.

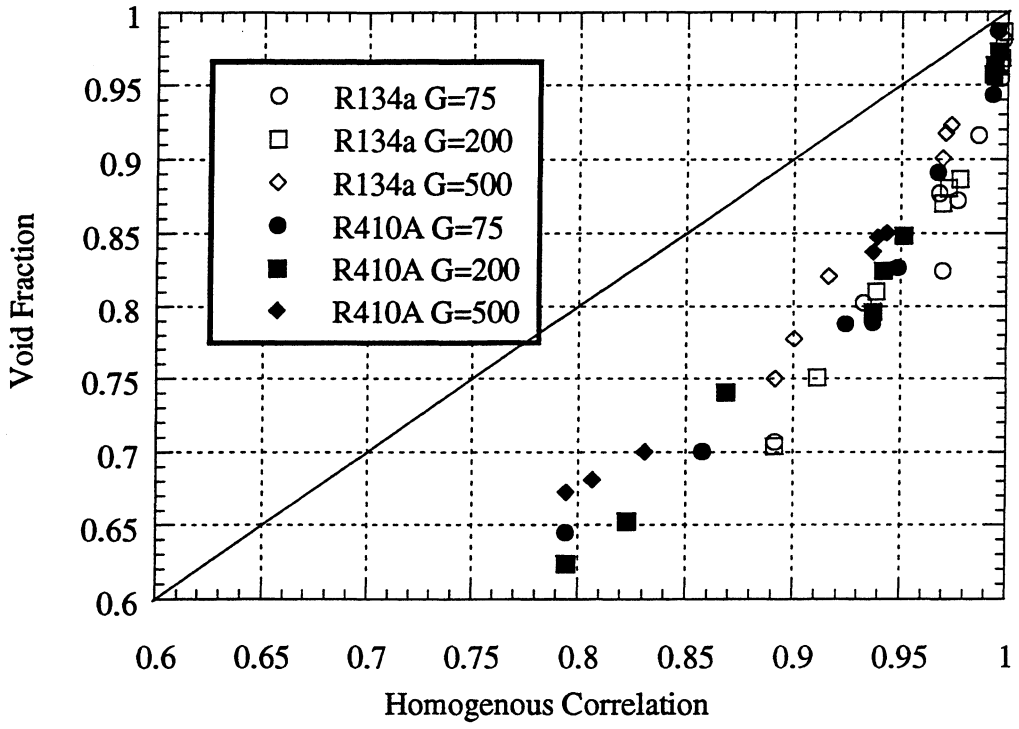

Figure C.13 Void fraction vs. homogenous correlation for 8.93 mm base diameter helically grooved tube using R134a and R410A. Mass Flux (G) given in kg/m^{2}s.

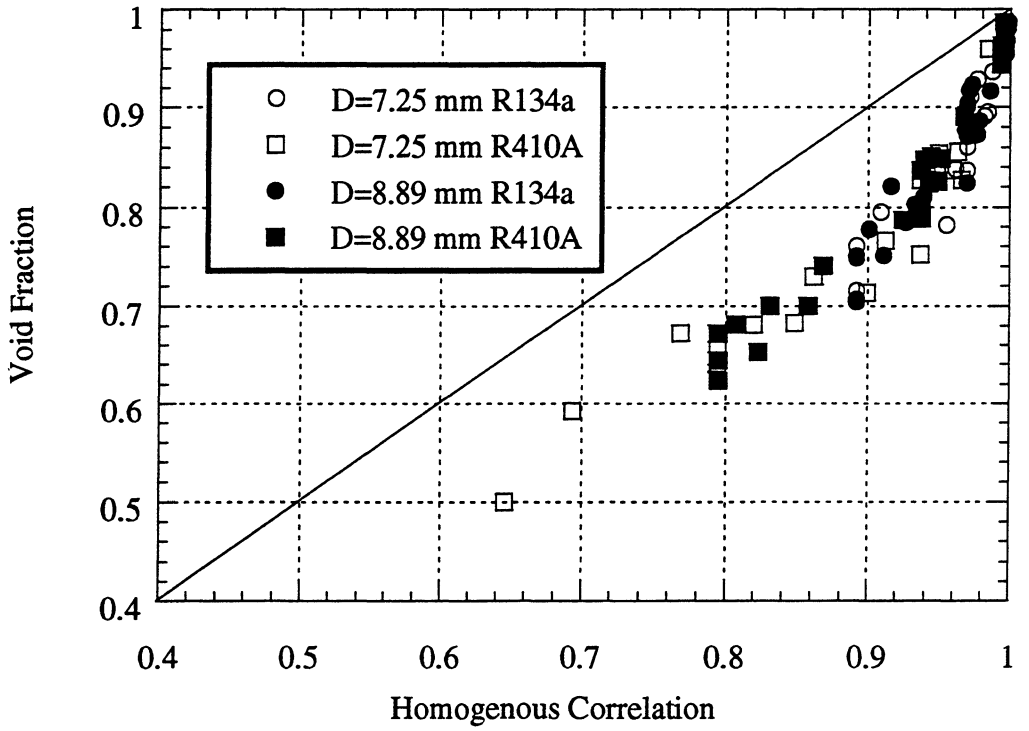

Figure C.14 Void fraction vs. homogenous correlation for 7.25 mm and 8.93 mm base diameter helically grooved tubes.

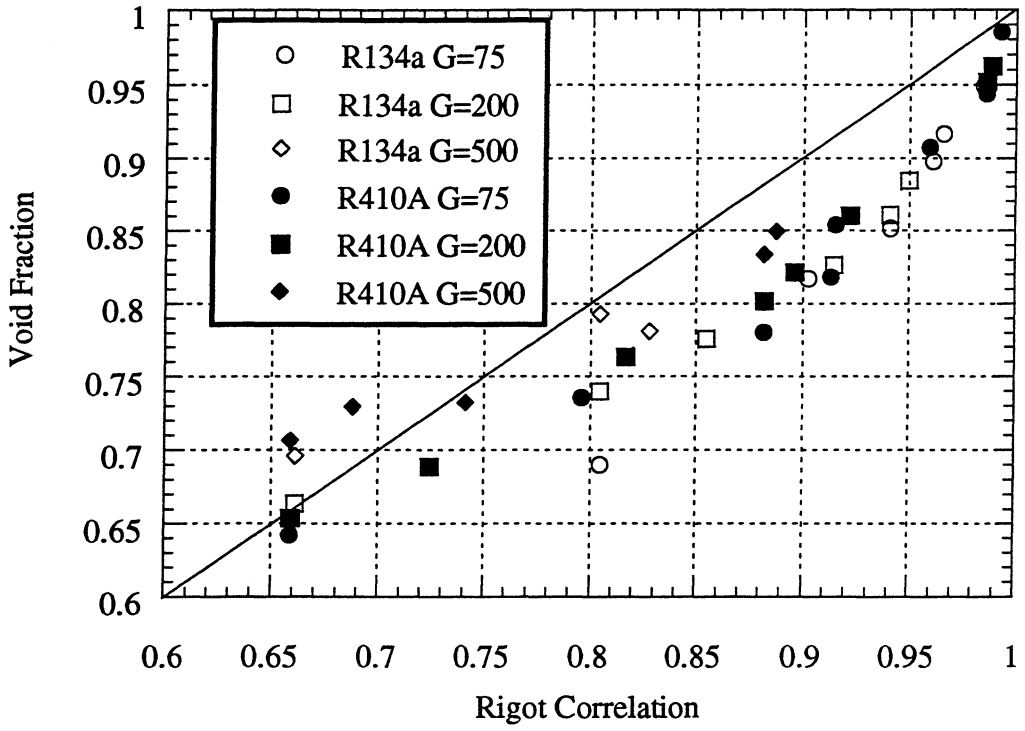

Figure C.15 Void fraction vs. Rigot correlation for 8.93 mm base diameter helically grooved tube using R134a and R410A. Mass Flux (G) given in kg/m^{2}s.

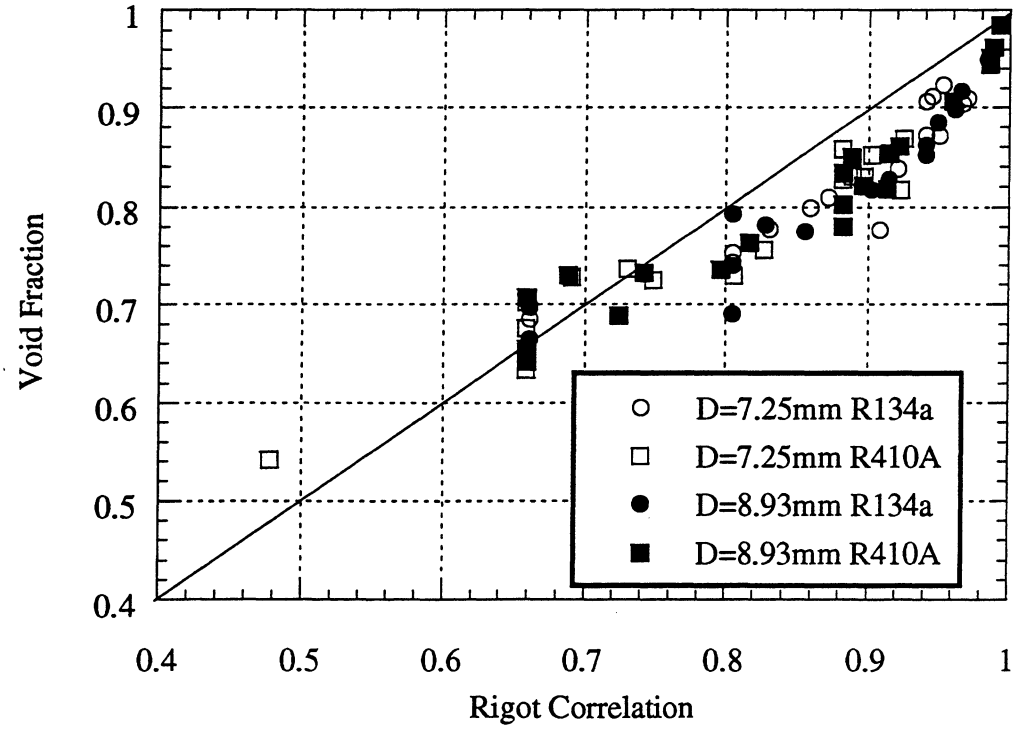

Figure C.16 Void fraction vs. Rigot correlation for 7.25 mm and 8.93 mm base diameter helically grooved tubes.

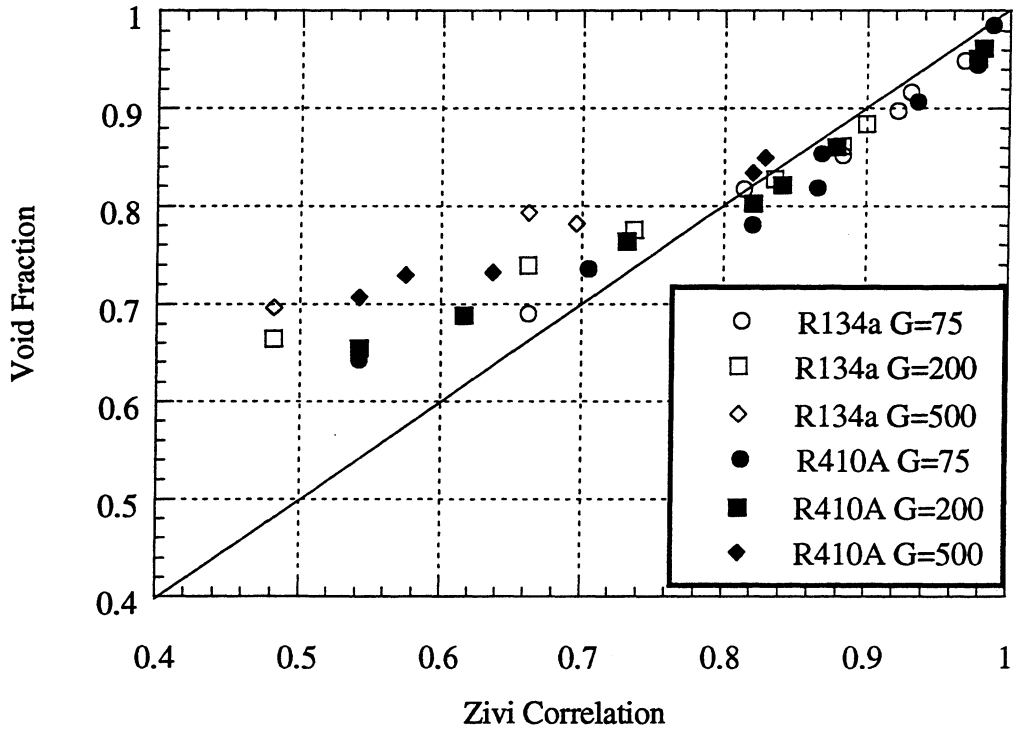

Figure C.17 Void fraction vs. Zivi correlation for 8.93 mm base diameter helically grooved tube using R134a and R410A. Mass Flux (G) given in kg/m^{2}s.

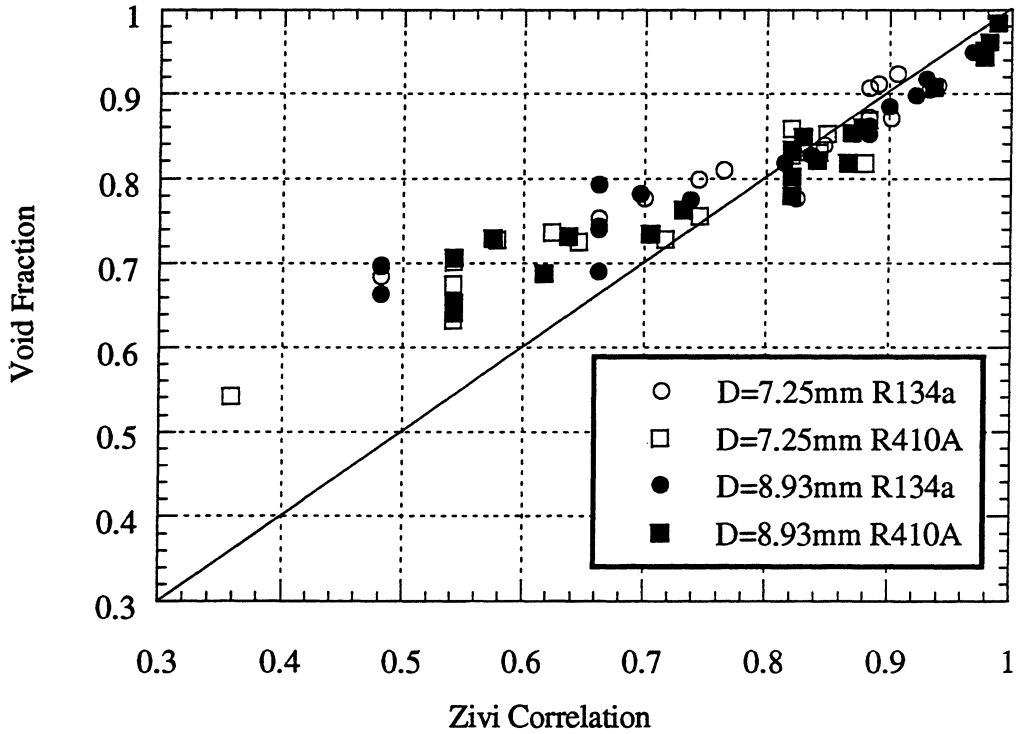

Figure C.18 Void fraction vs. Zivi correlation for 7.25 mm and 8.93 mm base diameter helically grooved tubes.

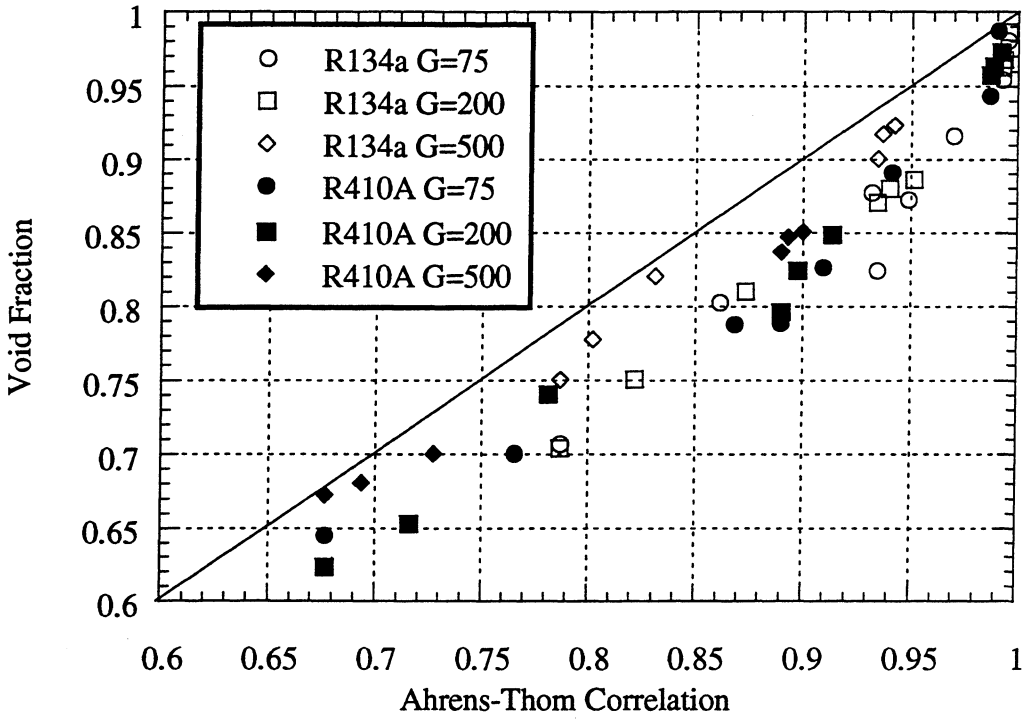

Figure C.19 Void fraction vs. Ahrens-Thom correlation for 8.93 mm base diameter helically grooved tube using R134a and R410A. Mass Flux (G) given in kg/m^{2}s.

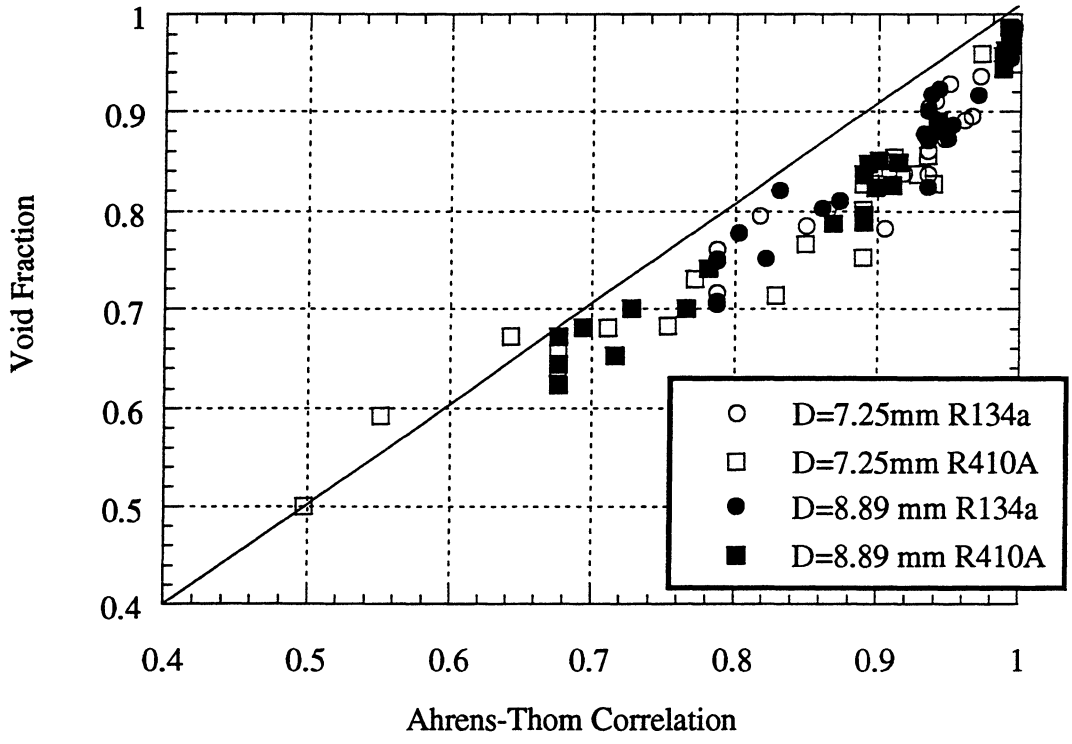

Figure C.20 Void fraction vs. Ahrens-Thom correlation for 7.25 mm and 8.93 mm base diameter helically grooved tubes.

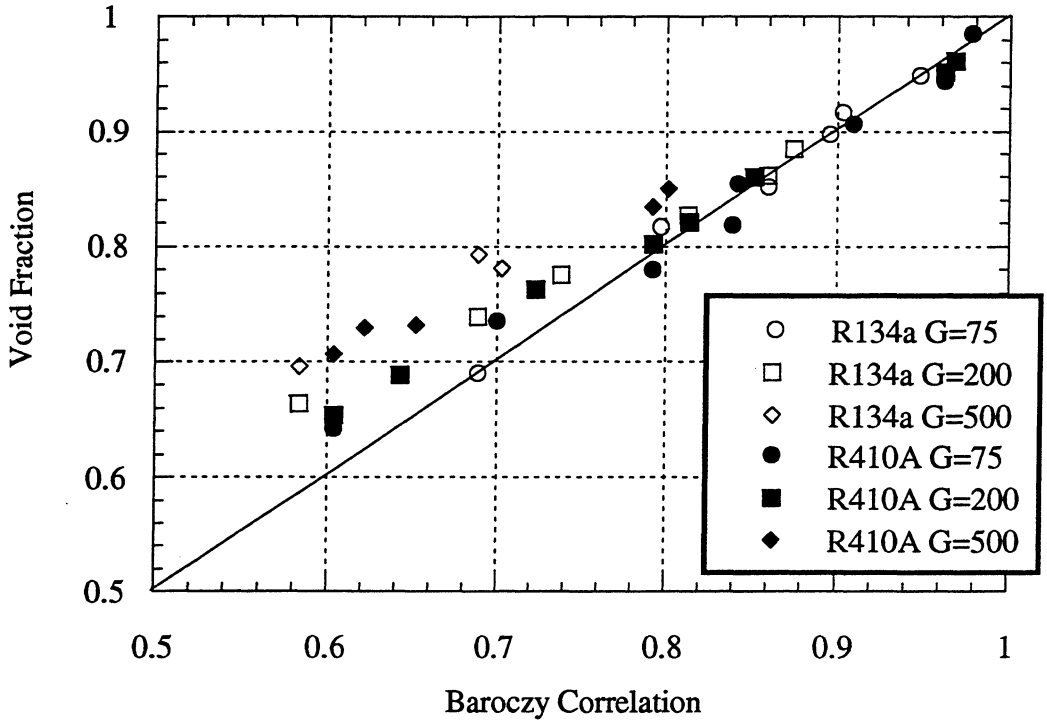

Figure C.21 Void fraction vs. Baroczy correlation for 8.93 mm base diameter helically grooved tube using R134a and R410A. Mass Flux (G) given in kg/m^{2}s.

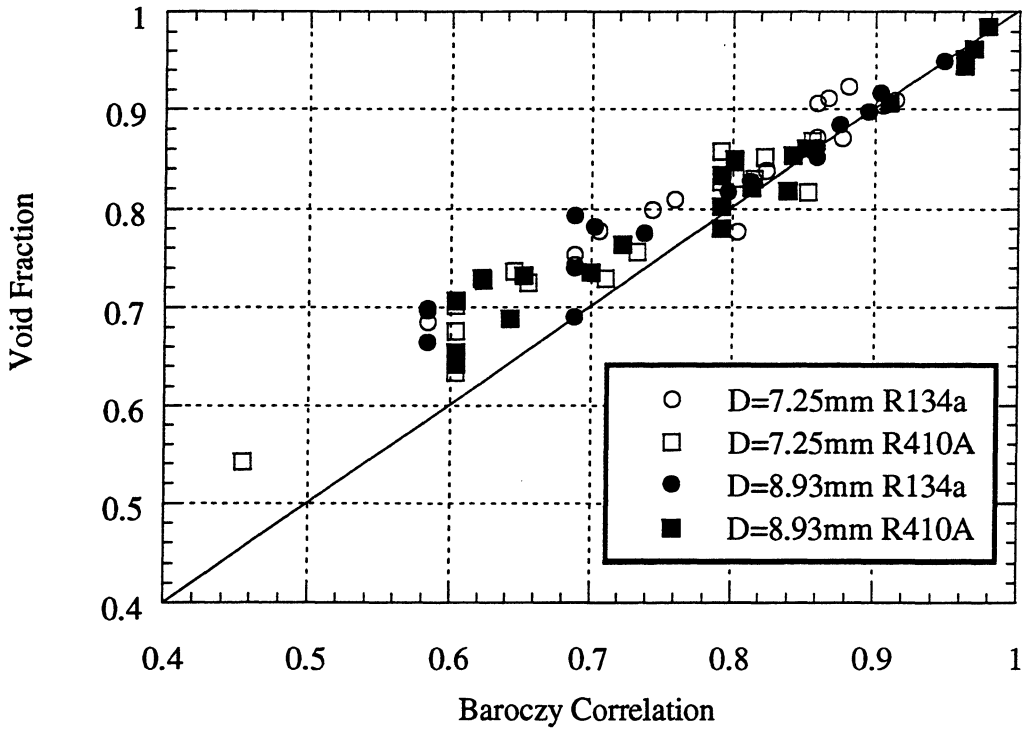

Figure C.22 Void fraction vs. Baroczy correlation for 7.25 mm and 8.93 mm base diameter helically grooved tubes.

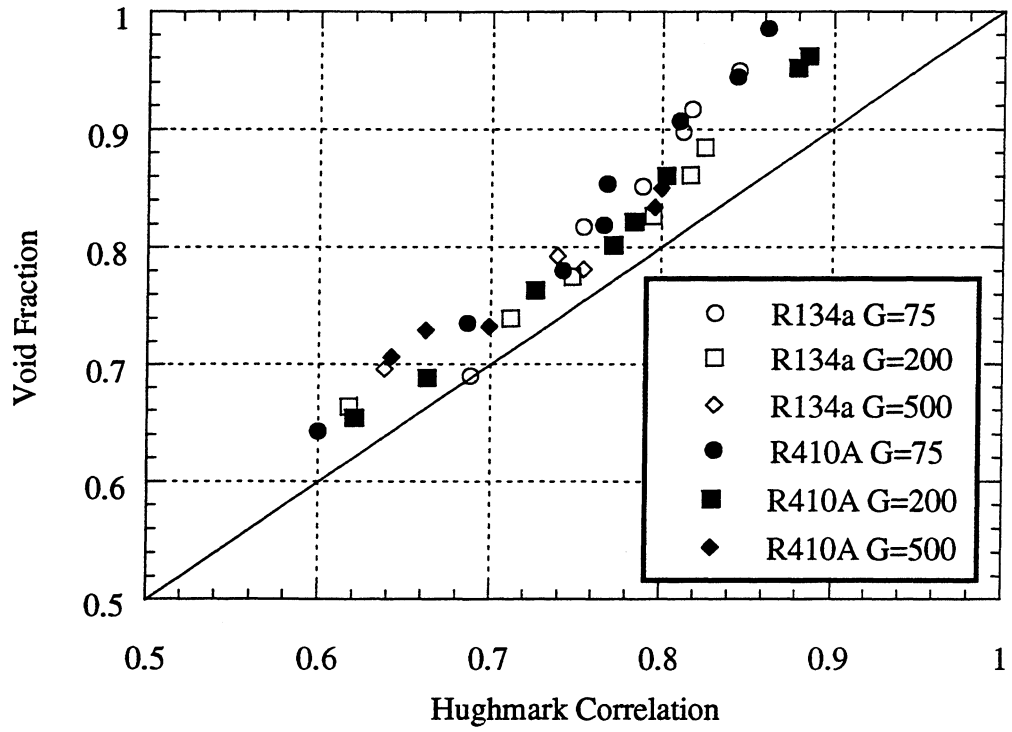

Figure C.23 Void fraction vs. Hughmark correlation for 8.93 mm base diameter helically grooved tube using R134a and R410A. Mass Flux (G) given in kg/m^{2}s.

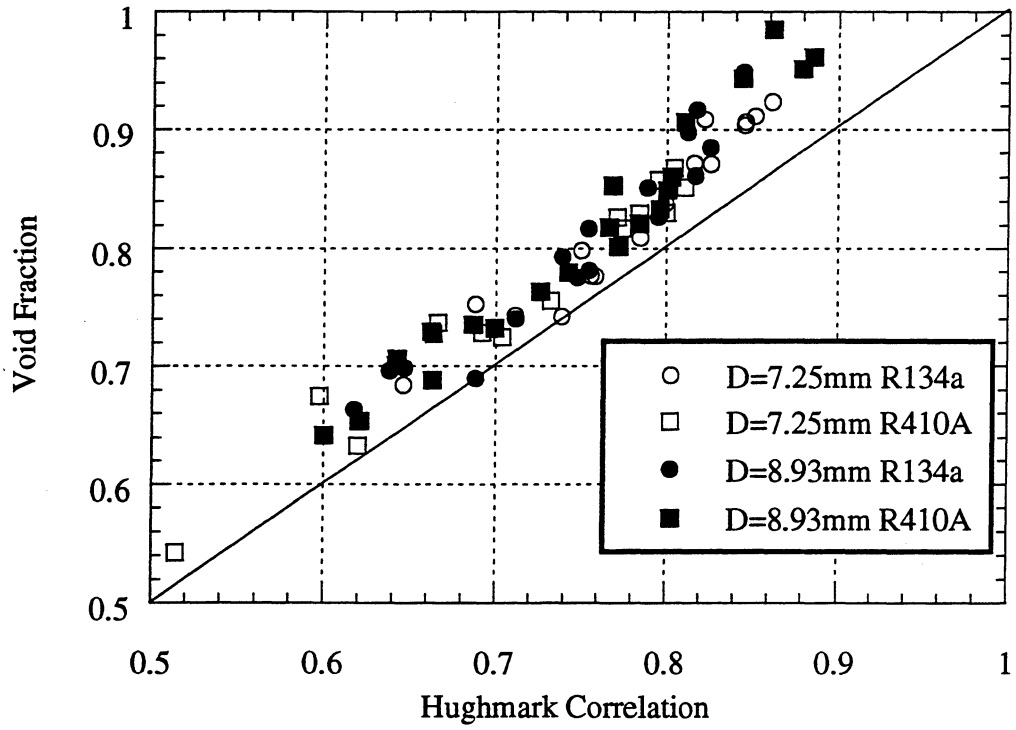

Figure C.24 Void fraction vs. Hughmark correlation for 7.25 mm and 8.93 mm base diameter helically grooved tubes.

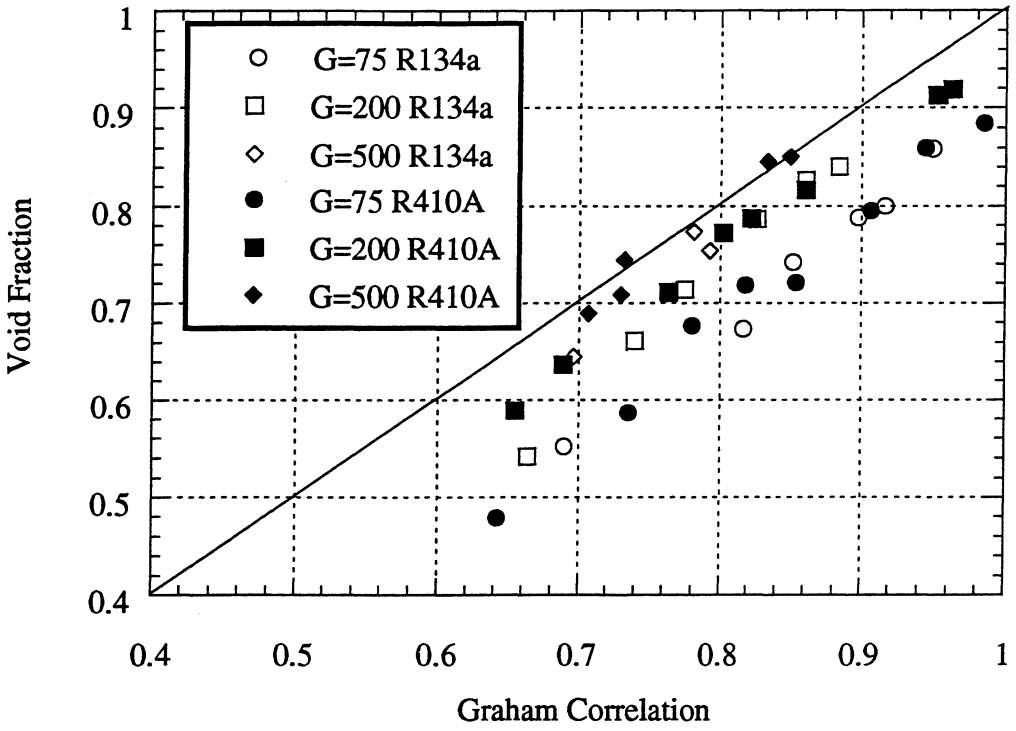

Figure C.25 Void fraction vs. Graham's condenser correlation for 8.93 mm base diameter helically grooved tube using R134a and R410A. Mass Flux (G) given in kg/m^{2}s.

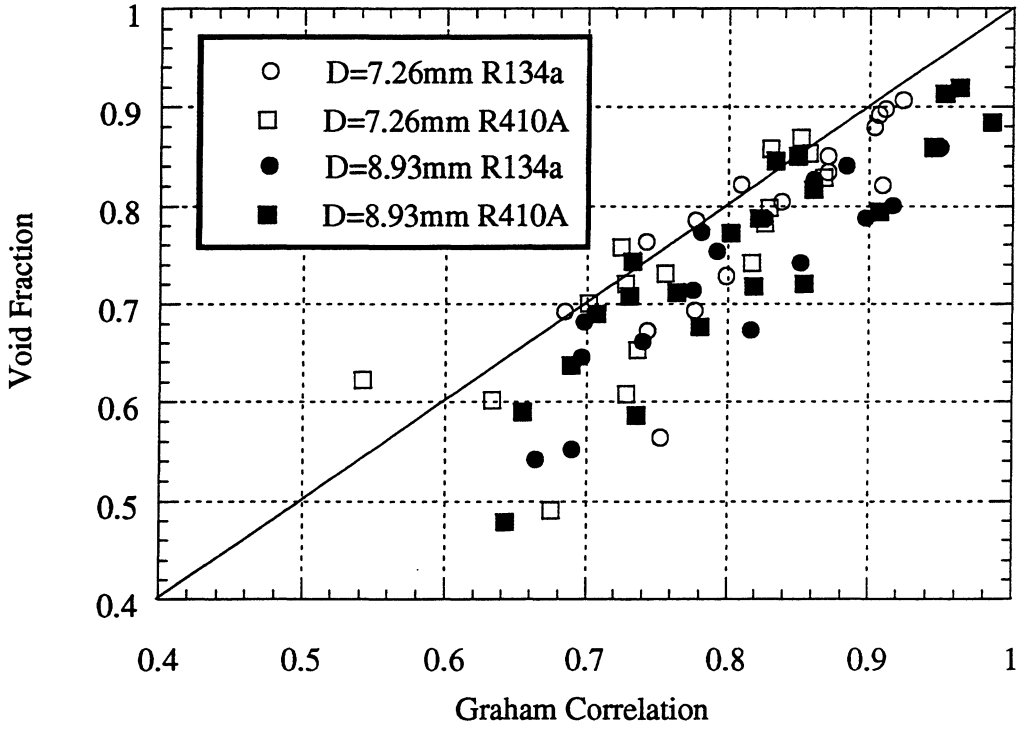

Figure C.26 Void fraction vs. Graham's condenser correlation for 7.25 mm and 8.93 mm base diameter helically grooved tubes.

Appendix D

Conclusion Plots

These plots correspond to Chapter 8 in which a number of correlations are presented to accurately predict the data.

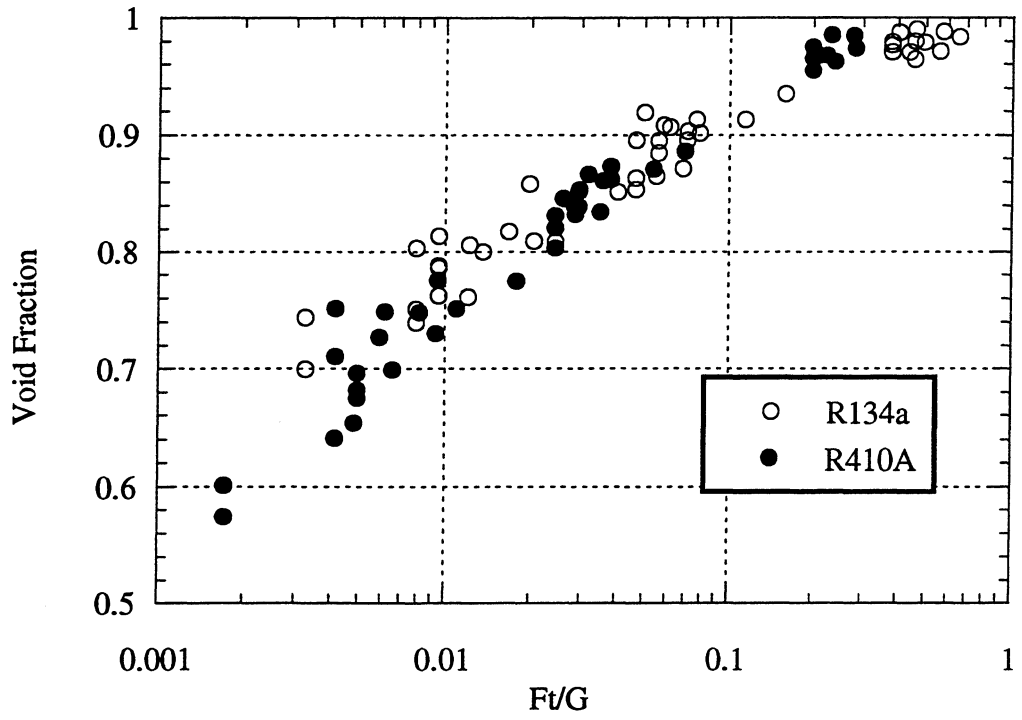

Figure D.1 Void fraction vs. Ft/G for smooth tube showing refrigerant effects.

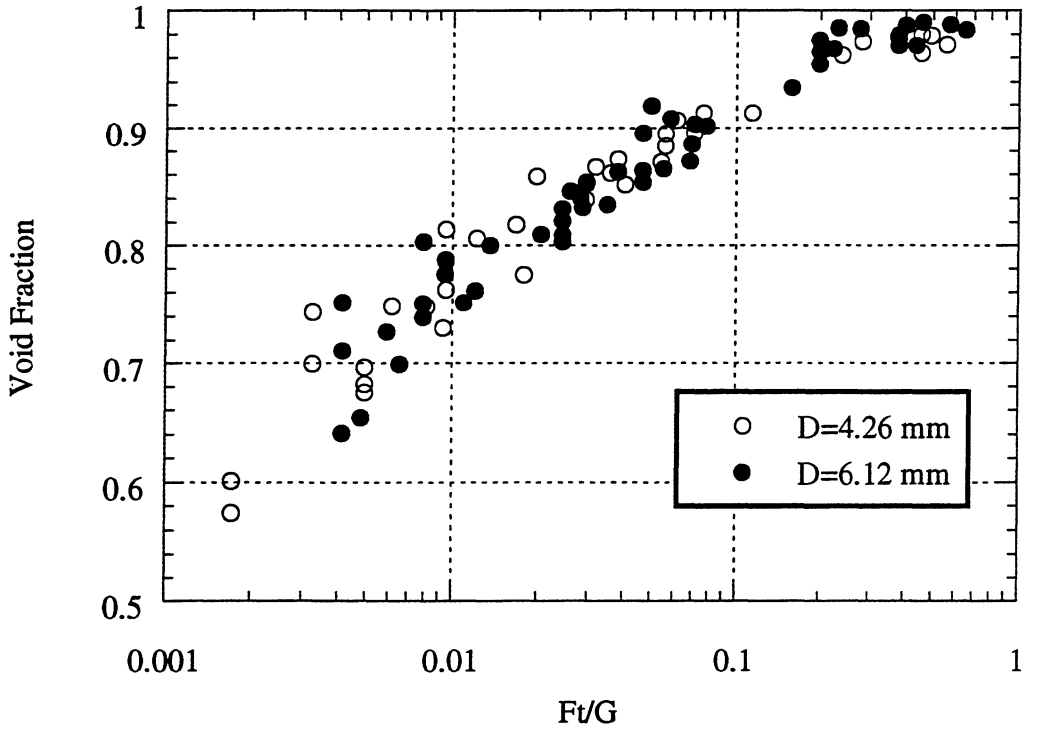

Figure D.2 Void fraction vs. Ft/G for smooth tube showing diameter effects.

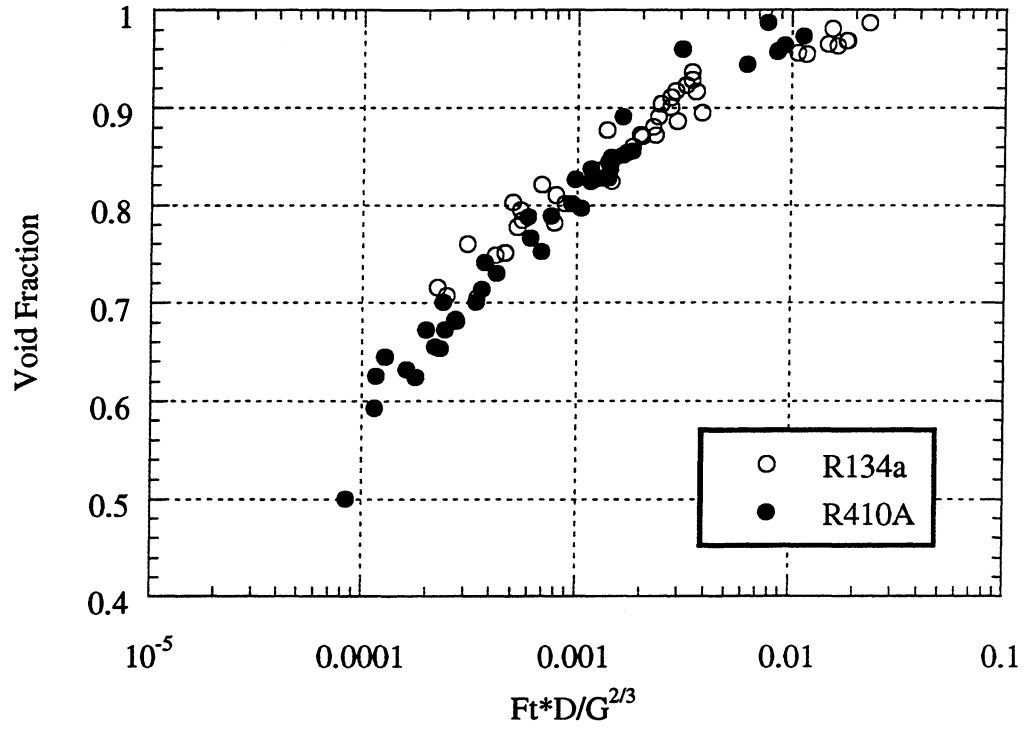

Figure D.3 Void fraction vs. $Ft*D/G^{2/3}$ for axially grooved tube showing refrigerant effects.

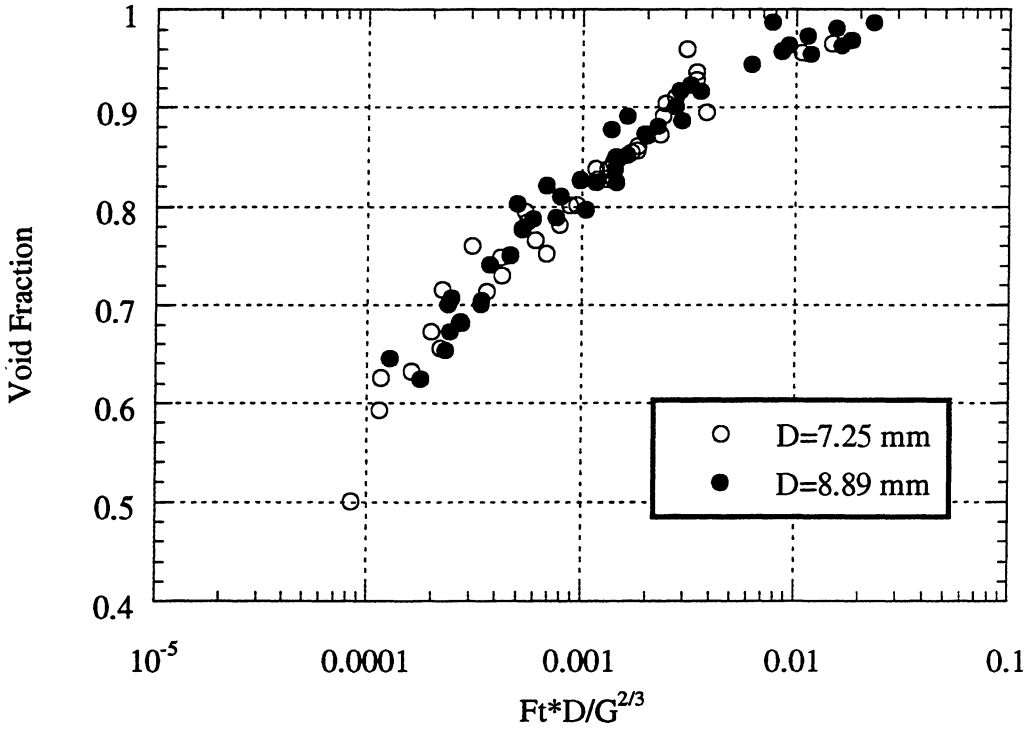

Figure D.4 Void fraction vs. $Ft*D/G^{2/3}$ for axially grooved tube showing diameter effects.

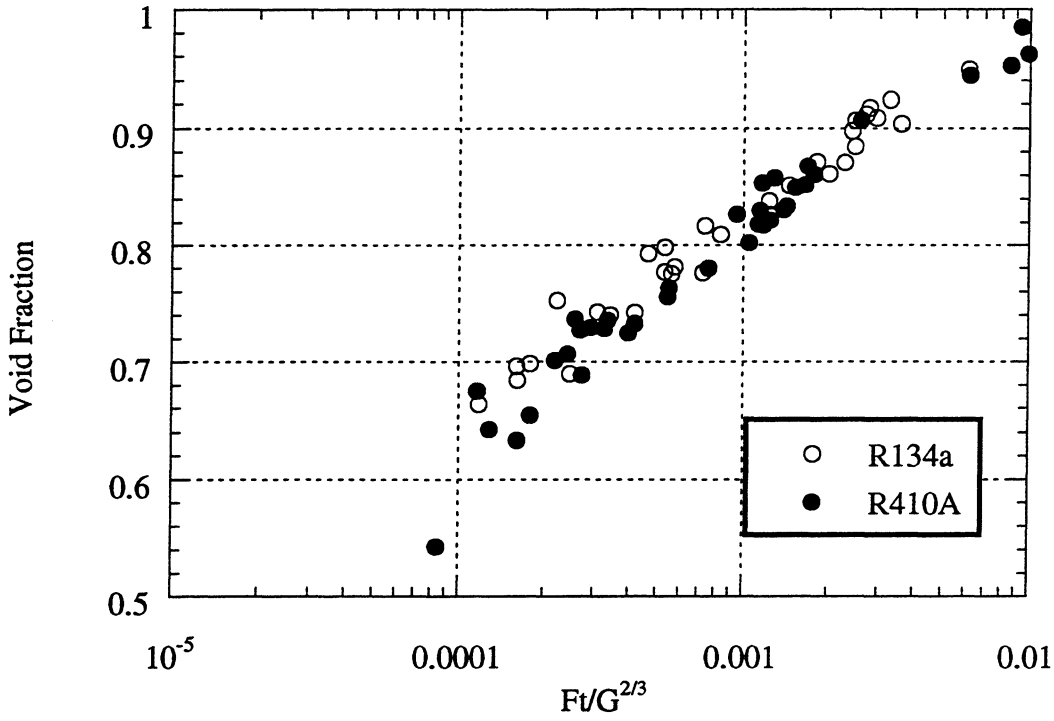

Figure D.5 Void Fraction vs. $Ft/G^{2/3}$ for helically grooved tubes showing refrigerant effects.

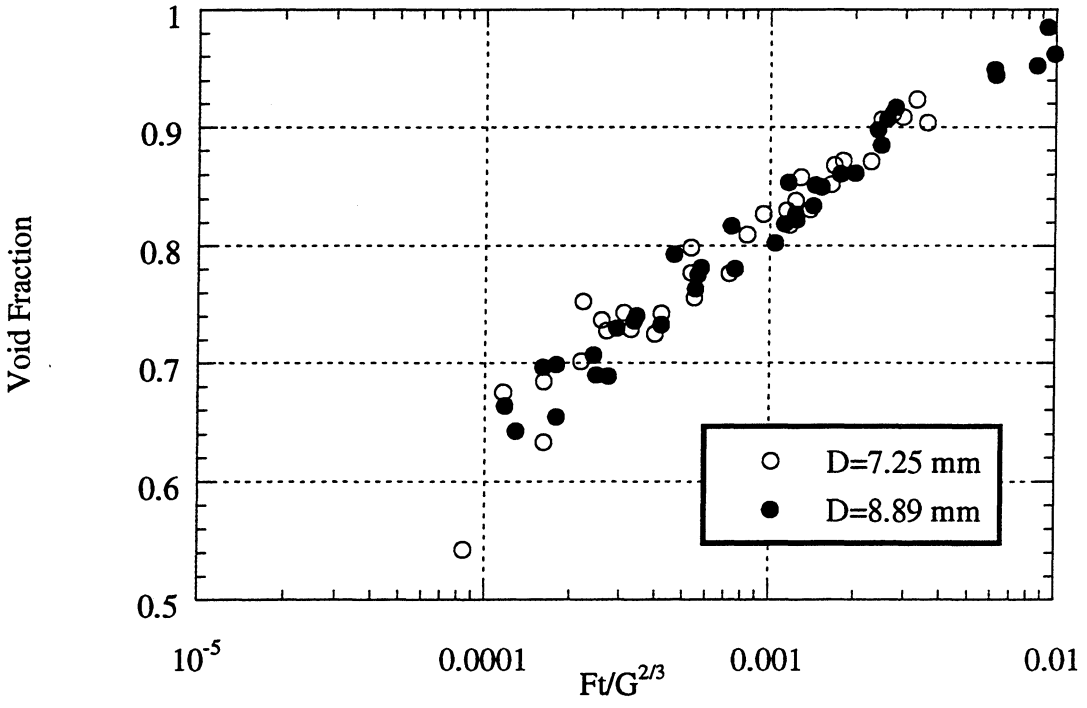

Figure D.6 Void Fraction vs. $Ft/G^{2/3}$ for helically grooved tubes showing diameter effects.